# WATER REPELLENCY EFFECT ON UNSATURATED PROPERTIES OF COMPACTED COAL COMBUSTION RESIDUALS

by

Livingstone Dumenu

A dissertation submitted to the faculty of
The University of North Carolina at Charlotte
in partial fulfillment of the requirements
for the degree of Doctor of Philosophy in
Civil Engineering

Charlotte

2019

Approved by:

_____
Dr. Vincent O. Ogunro

_____
Dr. Miguel A. Pando

_____
Dr. John L. Daniels

_____
Dr. Simon M. Hsiang

_____
Dr. Alireza Tabarraei

# ABSTRACT

LIVINGSTONE DUMENU. Water Repellency Effect on Unsaturated Properties of Compacted Coal Combustion Residuals (Under the direction of Dr. Vincent O. Ogunro and Dr. Miguel A. Pando)

The generation of electricity from coal-fired power plants continue to be a mainstream approach. It is estimated that about 107 million tons of coal combustion residuals (CCRs) were generated in 2017 in the US (ACAA 2018). This equal amount of CCRs requires safe and cost-effective management approach, including disposal and reuse. This dissertation focused on engineered water repellency of CCRs for unencapsulated beneficial reuse in civil engineering applications. Unencapsulated beneficial use of CCRs in geotechnical and geoenvironmental engineered systems such as structural fills/embankments, and liner and capping systems continue to see a downward decline with the recently implemented CCR final rule by the U. S. Environmental Protection Agency in 2015. Engineered water repellency has been identified as an alternative approach to control water infiltration and leachate generation in CCRs as it reduces water interaction with CCRs. The motivation of this study derives from the potential of engineered water repellent CCRs to contribute towards a more effective management of CCRs used in engineered systems while also serving as an infiltration control system. Specifically, this research investigates the use of organosilane (OS) chemicals towards achieving engineered water repellent compacted CCRs to be used in the aforementioned unencapsulated geotechnical and geoenvironmental applications. Additionally, the study focused on assessing any effects of the OS-based engineered water repellency on selected engineering properties of the OS-treated compacted CCRs.

This dissertation experimentally evaluated the effect of OS-based engineered water repellency on select unsaturated engineering properties of compacted CCRs. The main objectives were to correlate applicable engineering properties of CCRs to unsaturated functions of compacted untreated CCRs, study the influence of soluble salts on the engineering performance of compacted select CCR; implement a treatment protocol by understanding OS treatment of CCRs by batch sorption approach while considering practical implementation of engineered water repellency; and assess the effect of engineered water repellency on unsaturated functions of compacted CCRs. A comprehensive experimental program was developed to address each of the research objectives. The experimental program involved five CCRs, including three Class F fly ash, one lignite fly ash, and one flue gas desulphurization (FGD) gypsum, all treated with an OS water repellent chemical. The selected OS chemical was based on results from a recent dissertation of our UNCC research group. The unsaturated functions of the compacted CCRs were determined by fitting closed-form equations to laboratory-measured water retention characteristics (WRC) of the compacted CCRs using pressure plate extractor (PPE), Tempe cell (TC), and the unsaturated flow apparatus (UFA) method, and dewpoint potentiometer (WP4C). The first three methods measure matric suction, and the WP4C measures total suction. Additionally, leaching program was performed to reduce the salt contents of a select CCR and evaluated the influence of salt contents on the total suction and related osmotic suction, and on the engineering performance of compacted CCR. The batch sorption approach was used to treat the CCRs for varying degrees of water repellency while changing variables, including CCR material, OS dosage, reaction time, and drying conditions. Two OS treatment protocols,

namely pretreatment and precondition, were implemented for laboratory and practical evaluation of engineered water repellency effect on compacted CCRs, respectively. The compacted untreated CCRs were found to have high WRC defined by a wide range of suction. The estimated air entry values (AEVs) of the WRC curves were found to correlate well with the median particle sizes of the CCRs based on the pore size estimate for a cubic and tetrahedral grain packing. Osmotic suction as a function of salt content was assessed based on the independent measurement of matric and total suctions. Ionic concentration analysis performed on the CCR leachate indicates that salt-based additives from air emission control measures contribute to the osmotic activities. The pretreatment protocol was found to impact the hydrolytic stability of bond formation during the OS – CCR reaction. Further investigations indicated that the CCR chemical compositions, presence of certain soluble salts in CCRs and/or residual OS affect the hydrolytic stability. The preconditioned OS-treated CCR exhibited low surface energy resulting in less capillary and adsorptive forces resulting in a relatively lower WRC compared to the corresponding compacted untreated CCR. The unsaturated functions from the OS-treated CCR obtained indicated a wide range of suction and AEVs comparable to coarse-grained soil. However, the effect of varying degrees of water repellency was not clearly defined.

# ACKNOWLEDGEMENTS

I wish to express my sincere gratidtude to my advisors Dr. Vincent O. Ogunro and Dr. Miguel A. Pando for their guidance, encourgament, and insightful contributions throughout my time in UNC Charlotte. I would also like to thank Dr. John L. Daniels, Dr. Simon M. Hsiang, and Dr. Alireza Tabarraei for serving on my doctoral dissertation committee in addition to their valuable contributions and review of my dissertation. A special thanks to Dr. Menezes of California State University, Los Angeles for assisting with his laboratory and student (Hassan Abdullatif H Sindi) to perform experiments using the unsaturated flow apparatus. I am especially grateful to my fellow research assistants in the Infrastructural and Environmental Systems, and Civil Engineering doctoral programs at UNC Charlotte for the friendship and discussions especially Abhisek Manikonda and Rui He. My stay in UNC Charlotte would not have been a success without a good work-life balance and I would like to thank the “Wolves of EPIC” - Vona, Abhisek, Vivek, Rui, Manohar, and Tunde for creating that environment. I would like to acknowledge the financial support from the Environmental Research and Educational Foundation and American Coal Ash Association Educational Scholarship, the logistical support from the Utility companies in providing CCRs and Dow Corning for the OS chemicals. Finally but not the least, I am indebted to the Dumenu, Sarkodee-Adoo, Ohui Norgbodzi, Boateng, and Addo Families, and friends for the unmeasurable love, support, and encouragment in achieving this feat.

# DEDICATION

To all who believed in me and gave me a chance.

TABLE OF CONTENTS

LIST OF TABLES

LIST OF FIGURES

# LIST OF SYMBOLS AND ABBREVIATIONS

| | |
|---|---|
| AEV(s) | Air entry value(s) |
| BP | Breakthrough pressure |
| CCR(s) | Coal combustion residual(s) |
| $\theta^{'}$ | Contact angle |
| S | Degree of Saturation |
| DI | Deionized |
| WP4C | Denotion for dewpoint potentiometer |
| $\gamma_{dry}$ | Dry unit weight |
| σ’ | Effective stress |
| c’ | Effective stress cohesion |
| Ø’ | Effective stress friction angle |
| EC | Electrical conductivity |
| FHWA | Federal Highway Administration |
| ω | Gravimetric water content |
| HAE | High air entry |
| $\sigma_{lv}$ | Liquid-vapor interfacial tensions |
| $\psi_m$ | Matric suction |
| $\gamma_{dry,max}$ | Maximum dry unit weight |
| $\omega_{opt}$ | Optimum gravimetric water content |
| OMC | Optimum moisture content |
| OS | Organosilane |
| π | Osmotic suction |
| ppm | Part per million |
| r | Pore radius |
| pH | Potential of Hydrogen |
| PPE | Pressure plate extractor |
| $\psi_r$ | Residual suction |
| $\theta_r$ | Residual volumetric water content |
| $k_s$ | Saturated hydraulic conductivity |
| $\theta_s$ | Saturated volumetric water content |
| SDM | Sessile drop method |
| SWCC | Soil water characteristics curve |
| $\sigma_{sl}$ | Solid-liquid interfacial tensions |
| $\sigma_{sv}$ | Solid-vapor interfacial tensions |
| ψ | Suction |
| σ | Surface tension |
| TC | Tempe Cell |
| t | Time |
| $\psi_T$ | Total suction |
| USEPA | United States Environmental Protection Agency |
| $K_\psi$ | Unsaturated hydraulic conductivity |
| θ | Volumetric water content |
| WDPT | Water drop penetration time |

| | |
|---|---|
| WEP | Water entry pressure |
| WRC | Water retention characteristic |
| XRD | X-ray diffraction |
| XRF | X-ray fluorescence |
| $D_{60}$ | Particle size corresponding to 60% finer by weight in mm |

# CHAPTER 1: INTRODUCTION

This doctoral dissertation investigates the potential effect of engineered water repellency (using OS chemicals) on select engineering properties of different compacted CCRs. This introduction chapter includes the following information:

- background on CCRs,
- motivation of research,
- research objectives, and
- organization of dissertation.

## 1.1 Background

The utilization of coal combustion residuals (CCRs) continues to increase with 2017 recording a 64% utilization rate in the US for various applications with a significant increase in concrete and drywall productions. However, applications in engineered systems such as structural fill/embankment and mining reclamation, which account for a considerable portion of unencapsulated beneficial reuse, continue to see a downward trend due to concerns of associated environmental risks (ACAA 2018; USEPA 2019). In response to such concerns, the U.S. Environmental Protection Agency (EPA) developed the CCR final rule which supports beneficial applications of CCRs provided it meets the criteria of functional benefit, substitute for virgin materials, meeting product specifications and design standards, and limiting associated environmental risks (USEPA 2019).

There are limited guidelines that provide a comprehensive approach to the design and construction of structural fills in highway embankments using CCRs. One such

guideline is the Federal Highway Administration (FHWA) User Guidelines for Waste and Byproduct Materials in Pavement Constructions (FHWA 2016). The FHWA guidelines cover most of the beneficial use criteria described in the CCR final rule. In summary, it addresses design and specification requirements, including material properties, site drainage, slope stability, climate conditions, and construction practices for CCRs (mainly fly ash) utilization in structural fills/embankments. But like most other guidelines and standards, it is limited in addressing the issue of possible leachate generation when these unencapsulated systems encounter water.

In response, the US EPA, while developing the CCR final rule, identified the concept of engineered water repellency proposed by Daniels et al. (2009a) as an alternative to control infiltration and to protect groundwater for safe disposal and beneficial applications of CCRs (Federal Register 2010). Figure 1-1 illustrates the concept of water ponding on the surface of engineered water repellent CCR; thereby preventing water infiltration. The concept is well documented in the field of soil science and water resources due to its natural occurrence and how it impacts the accessibility of water for plant growth. A review of recent studies indicates a growing interest in the concept of geotechnical and geoenvironmental engineering applications. However, there is a significant knowledge gap that hinders the development of a design framework required by the beneficial application criteria for CCR applications in engineered systems such as structural fills and embankments. In addition, most of these engineered systems function in unsaturated conditions, as in many geotechnical and geoenvironmental engineering processes, such as seepage, contaminant fate, and transport, settlement, and slope failure. Therefore, the concept of engineered water repellency and CCRs in

unencapsulated applications make it appropriate to study the performance of engineered water repellent CCRs in unsaturated conditions.

Figure 1-1. Ponding of water on an engineered water repellent CCR.

In this study, a detailed laboratory experimental approach was developed to explore the WRC of compacted CCRs under the desaturation process. Selected measuring techniques were considered for the laboratory experiment. These measurement techniques operate on different principles that define unsaturated conditions in porous media, thus providing a basis of comparison. Parametric models were applied to the measured data to define unsaturated functions that describe field parameters such as hydraulic conductivity and shear strength required for analysis of such engineered systems. The understanding of the unsaturated behavior of compacted CCRs is vital for assessing their long-term performance in structural fills/embankments, liners, and capping systems. Also, the chemistry of organosilane, a water repellent chemical used in

this study, was explored in developing a factorial design experiment for a laboratory experiment for engineering practice.

## 1.2 Motivation

Management practices in the handling, disposal, and application of CCRs are undergoing a paradigm shift due to the recently implemented CCR rule by the US EPA. This rule continues to limit the beneficial use of CCRs in engineered systems due to concerns of potential leaching of trace elements into the environment, as illustrated in Figure 1-2. Recent studies have demonstrated the feasibility of engineered water repellent CCRs and soils as alternative infiltration control tools to address this concern. However, the knowledge gaps between concept and practice limit the implementation of the technique in geotechnical and geoenvironmental engineering practice. To address some of the gaps would require answering the following research questions.

1. What characterizes the hydraulic and mechanical behavior of compacted CCRs in unsaturated conditions?
2. How do CCR compositions impact its WRC?
3. Is osmotic suction significant? Can it be considered for design purposes in the long term?
4. How can OS treatment of CCRs be optimized in the laboratory while ensuring field performance are experimentally determined in the laboratory?
5. What are the implications of OS treatment on the hydraulic and mechanical behavior of compacted CCRs?

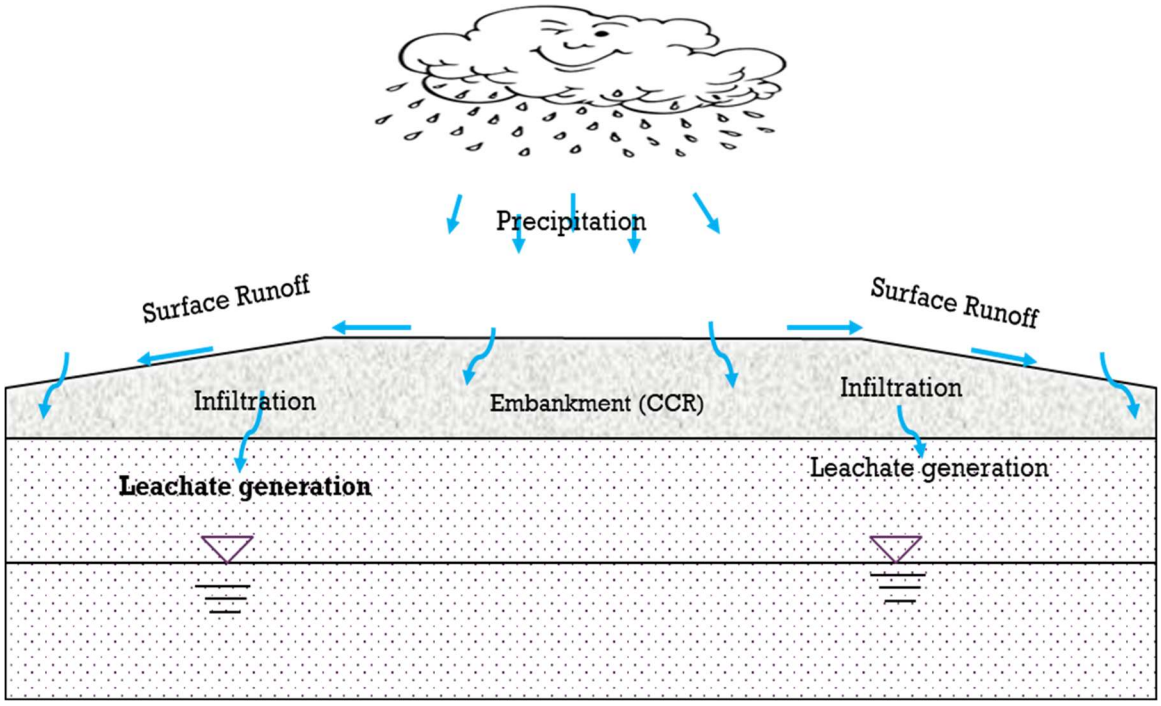


Figure 1-2. Illustration of potential environmental risks associated with CCR application in structural fill/embankment.

As such, the research motivation is derived from how the concept of engineered water repellency can be incorporated into engineered systems such as structural fill (mono fill) or liner and capping systems, as illustrated in Figure 1-3. In general, this concept allows CCRs to be effectively managed through the development of an alternative infiltration control system.

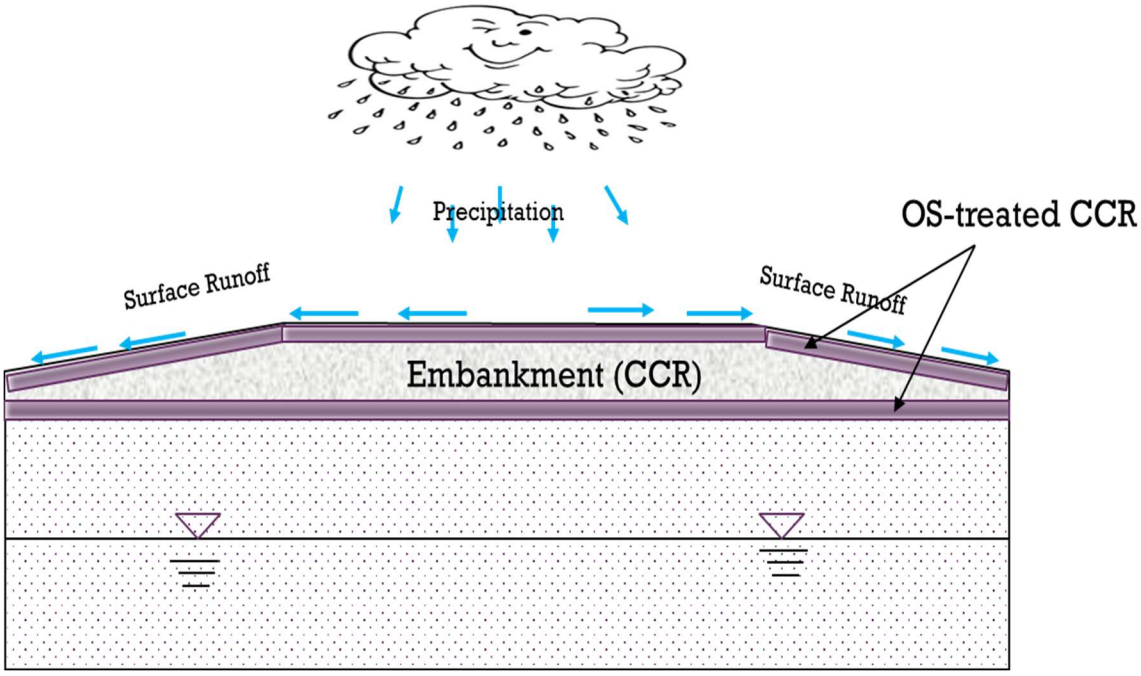


Figure 1-3. Schematic diagram showing the use of engineered water repellent CCR as liner and capping systems to control water infiltration of a CCR structural fill/embankment.

## 1.3 Research Objectives

The research goals are as follows:

1. Develop correlations among index properties, chemical and mineralogical compositions, and suction properties of untreated CCRs.
2. Characterize the influence of soluble salts on the engineering behaviors of compacted CCRs.
3. Develop a protocol to optimize OS treatment of CCRs for evaluation of engineering properties that describe field relevant parameters.
4. Evaluate the water retention behavior of compacted OS – treated CCR using selected standardized methods compatible with OS.

## 1.4 Dissertation Outline

The dissertation is divided into the following chapters including this chapter:

**Chapter 2: Background.** An overview of CCRs, the concept of unsaturated soil mechanic principles, and the concept of water repellency are presented.

**Chapter 3: Literature Review.** A review of literature relevant to the dissertation is presented. This includes geotechnical engineering characterization, WRC of CCRs, and state of research of engineered water repellency application in geotechnical and geoenvironmental engineering practice.

**Chapter 4: Materials, Methods, and Results.** This chapter describes standard test methods used to measure geotechnical engineering properties of CCRs relevant to evaluating unsaturated properties of CCRs. The test results of the properties include physical and index properties, particle size distribution, Atterberg limits, elemental and mineral compositions are presented.

**Chapter 5: Unsaturated Functions of Compacted Untreated Coal Combustion Residuals.** This chapter presents an experimental plan to investigate the WRC and unsaturated hydraulic conductivity of compacted untreated CCRs established using pressure plate extractor, Tempe cells, unsaturated flow apparatus, and the dewpoint potentiometer. The results from each measuring device are compared to each other by fitting parametric models to the measured data. In addition, a correlation between fitting parameters and engineering properties are presented.

**Chapter 6: Impact of Soluble Salt on the Engineering Performance of Coal Combustion Residuals.** This chapter details an experimental plan to vary the amount of

the soluble salts of a selected Class F fly ash. The effect of the soluble salt variability on the infiltration and strength behaviors of a Class F fly ash was investigated.

**Chapter 7: Water Repellent Treatment of Coal Combustion Residuals- A Batch Sorption Approach.** This chapter describes the batch sorption experiment as a water repellent treatment protocol for CCRs, considering a factorial design approach. Statistical analysis is performed using SAS to identify potential variables that affect water repellent treatment of CCRs.

**Chapter 8: Unsaturated Functions of Compacted Water Repellent CCR.** The chapter identifies and details the limitations associated with testing water repellent CCRs in accordance with traditional standardized test methods. This chapter presents an experimental plan to describe the WRC and unsaturated hydraulic conductivity behaviors of compacted water repellent CCRs established using Tempe cells and dewpoint potentiometer. A proposed breakthrough pressure test method using the flexible wall permeameter is presented. The results from each measuring device are compared to each other and that of corresponding untreated CCR by fitting parametric models to the measured data. Also, the correlation between fitting parameters and engineering properties is presented.

**Chapter 9: Summary, Conclusions, Contributions, and Recommendations for Future Work.** A summary of the research, overview of literature/and objectives review, research contributions, and recommendations for future research work are presented.

# CHAPTER 2: OVERVIEW OF COAL COMBUSTION RESIDUALS, UNSATURATED SOIL MECHANICS, AND WATER REPELLENCY

This chapter presents an overview of coal combustion residuals – generation, types, constituents, and its beneficial applications. Also, a brief review of unsaturated soil mechanics is presented discussing the mechanism of unsaturated conditions in soils, soil suction, measuring techniques of soil suction, and the framework of soil water characteristic curves. The final section of this chapter reviews engineered water repellency in soil science and geotechnical and geoenvironmental applications.

## 2.1 Coal Combustion Residuals

Coal combustion residuals are by-products of burning coal in power plants to generate electricity. They are the noncombustible mineral contents of coal made up primarily of silicon (Si), aluminum (Al), and iron (Fe) and trace elements such as chromium (Cr), nickel (Ni), zinc (Zn), arsenic (As), selenium (Se), cadmium (Cd), mercury (Hg), and lead (Pb) which in high concentrations could pose a potential hazards to human health and the environment. Several by-products are formed from the combustion of coal, which are mostly classified based on the sources of coal, which define the chemical compositions, collection system, storage system, and emission control systems. Figure 2-1 illustrates the processes involved in the generation of coal combustion residuals. These by-products include but are not limited to fly ash, bottom ash, ponded ash, lignite fly ash, Flue Gas Desulfurization gypsum residuals, and others.

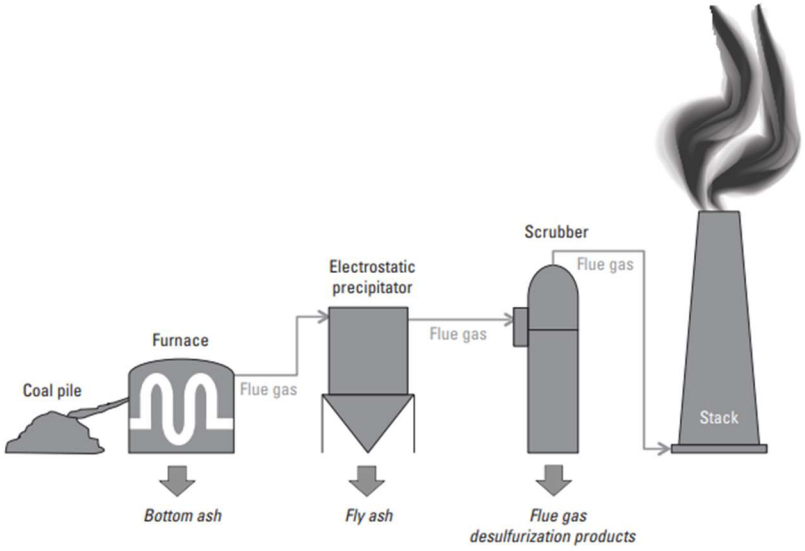


Figure 2-1. Schematic diagram of coal combustion process and generation of selected by-products. Adapted from Deonarine et al. (2015).

Fly ash is categorized into two main groups, namely class F fly ash and Class C fly ash based on their chemical compositions. Class F fly ash is generated from pulverized anthracite or bituminous coal with at least 70% combined chemical compositions of silicon dioxide ($SiO_2$), aluminum oxide ($Al_2O_3$), iron oxide ($Fe_2O_3$) plus a maximum of 18 % of calcium oxide (CaO) (ASTM 2015a; Thomas 2007). It has pozzolanic properties suitable for cement and concrete applications and others such as stabilization and solidification applications. On the other hand, Class C fly ash is generated from pulverized lignite or sub-bituminous coal with a chemical composition of at least 50% combined composition of silicon dioxide ($SiO_2$), aluminum oxide ($Al_2O_3$) and iron oxide ($Fe_2O_3$) plus a maximum of 18 % of calcium oxide (CaO)(ASTM 2015a; Thomas 2007). As a result of the higher calcium oxide content in Class C fly ash, it has

self-cementing properties with added pozzolanic properties suitable for soil amelioration (Yao et al. 2015).

Bottom ash is the coarse component of coal ash that settles at the bottom of the boiler during the combustion process. It is granular and meets the chemical compositions of Class F fly ash. Bottom ash is beneficially utilized in concrete block production as replacement aggregate and road construction as structural fill and road-base materials (Huang 1990; Jayaranjan et al. 2014).

Lignite fly ash is generated from pulverized lignite coal whose properties are intermediate to bituminous coal or peat (EPA 1995). It has a chemical composition comparable to class C fly ash (Drakonaki et al. 1998; Xenidis et al. 2002).

Flue gas desulfurization (FGD) gypsum is a by-product generated from air emission control systems that remove sulfur oxides from an FGD installed unit in a coal-fired plant to control sulfur-based gas emissions. Lime or limestone reagent reacts with sulfur and oxygen in the process of wet scrubbing, producing gypsum which is almost identical to naturally occurring gypsum (FDGProducts.org 2016). It is primarily used in the production of wallboard/drywall and other limited applications such as soil improvement, waste stabilization, and solidification.

## 2.2 Concept of Unsaturated Soil Mechanics

Saturated and dry soil systems, as presented in Figure 2-2, has been the focus of soil mechanics for decades in geotechnical and geoenvironmental engineering practices. However, real geotechnical engineered systems mostly function in unsaturated conditions (illustrated in Figure 2-2) and associated with most geotechnical engineering problems, including seepage, slope stability, and contaminant transport. When air begins to enter

the large pore spaces of saturated soil, it begins to lose water. At this point, the soil is considered partially saturated or unsaturated. In unsaturated conditions, solid-water-air interaction develops water tension stresses measured in terms of soil suction. This defines the WRC of soils.

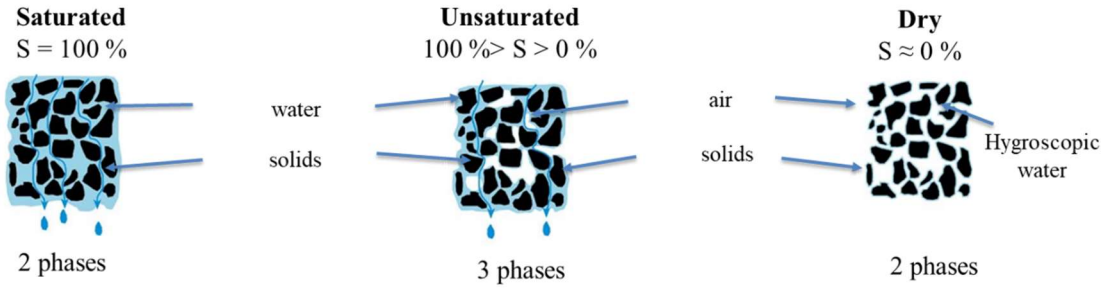


Figure 2-2. Schematic diagram of various saturation conditions in soil.

Soil suction is composed primarily of matric suction, $\psi_m$, the effect of capillary and adsorptive forces created by the interaction of the solid-liquid-air phases, and osmotic suction $\pi$, due to the dissolved solutes in pore fluids. The algebraic sum of matric and osmotic suctions gives total suction as expressed in Eq. 2-1 and illustrated in Figure 2-3. In terms of impacts on the mechanical behaviors of unsaturated soils, the matric and osmotic suctions are not additive due to the presence of solid particles and multiphase fluids (Miller 1996). Previous studies explained this concept in terms of vapor pressure, which defines total suction as controlled by hydrostatic tensions of pore water and dissolved salts in pore fluids (Krahn and Fredlund 1972). Matric suction ($u_a - u_w$; where $u_a$ = pore-air pressure and $u_w$ = pore-water pressure) is an independent stress state variable used in characterizing an unsaturated soil in the context of quantum mechanics primarily accounting for climatic effect above the ground surface (Fredlund 2006).

However, in engineering practice, osmotic suction is mostly ignored based on the assumption that solute concentrations of typical geotechnical soils are relatively small hence negligible (Miller 1996; Sreedeep and Singh 2006). However, in reviewing the roles and relevance of the suction components with regards to the volume change behavior of unsaturated soil, Miller (1996) concluded that osmotic suction can be considered as a valid independent stress state variable as it is relevant in analyzing engineering problems such as soil volume changes with high osmotic presence where matric suction boundary conditions remain constant.

$$\psi_T = \psi_m + \pi$$ Eq. 2-1

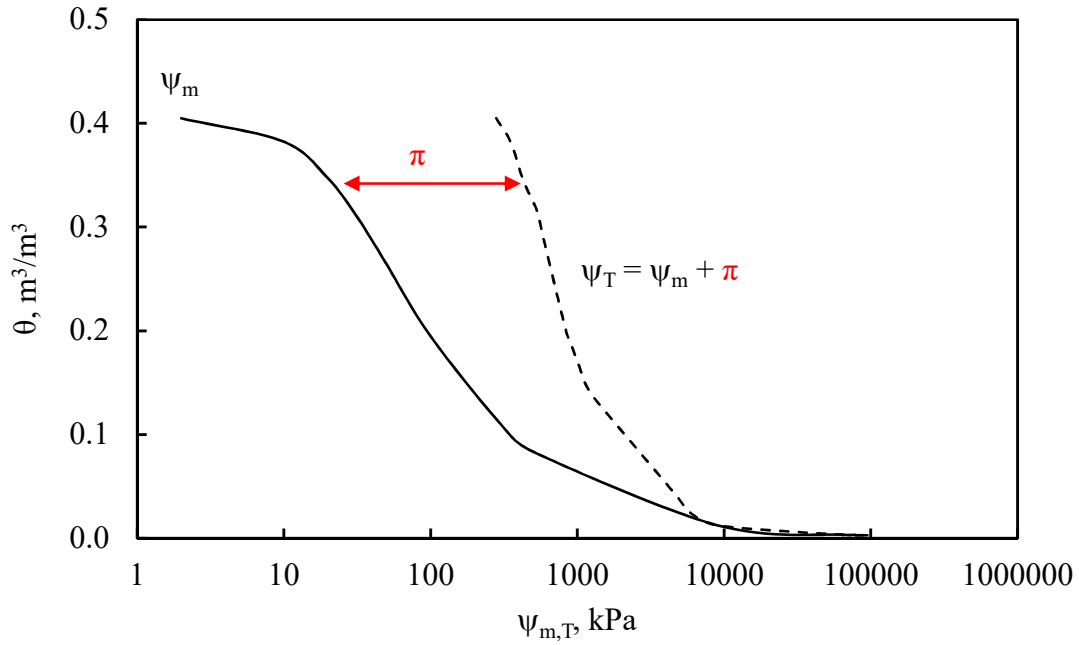


Figure 2-3. Graphical illustration of soil suction.

### 2.2.1 Suction measurement

Soil suction affects soil structure, thus impacting the hydraulic and mechanical characteristics of the porous medium (Fredlund 2006). The soil suction has a fundamental relationship with the water content of the porous medium, termed the soil water characteristics curve (SWCC), as illustrated in Figure 2-5. The SWCC provides a fundamental framework for a conceptual, interpretive, and predictive model for unsaturated soil behavior (Barbour 1998). Due to the significance of this constitutive relationship to understanding the behavior of unsaturated soils in soil science and geotechnical engineering practice, various test methods have been developed and documented on the measurement of the SWCC. Also, osmotic suction can be determined from the difference in total and matric suctions, as studies have shown a close agreement with values obtained from the squeezer method (Miller 1996; Peroni and Tarantino 2005; Sreedeep and Singh 2006).

#### 2.2.1.1 Null-type axis translation

The axis translation method measures the matric suction described by the difference in pore-air pressure and pore-water pressure. Over the decades, it has been of interest to researchers and practicing engineers in the understanding, development, and implementation of unsaturated soil mechanics (Fredlund 2006; Lu and Likos 2004). Commonly used axis translation method devices include pressure plate extractor (PPE), volumetric pressure plate extractor (VPPE), and Tempe cells (TC). The axis translation operates on the null type principle, which translates the origin of a reference to the negative pore-water pressure from atmospheric conditions. In general terms, the atmospheric pore-air pressure and the negative pore-water pressure in the unsaturated soil

are translated to conditions of atmospheric pore-water pressure and positive pore-air pressure, as illustrated in Figure 2-4.

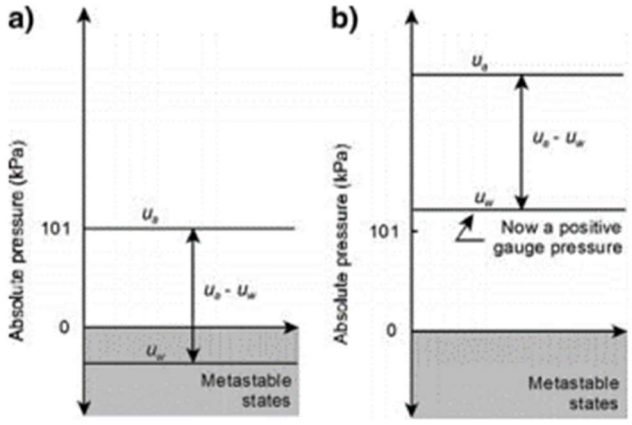


Figure 2-4. Illustration of axis translation method (a) atmospheric conditions; (b) axis translation (Marinho et al. 2009).

Despite the significant benefits derived from the use of the axis translation method in studying unsaturated soil functions, researchers (Elgabu 2013; Fredlund 2006; Lu and Likos 2004; Marinho et al. 2009; Vanapalli et al. 2009) have also documented limitations associated with the test methods which impact the interpretation of test data. Significant among the list of limitations is air diffusion. It affects water exchanges between the test specimen and the high air entry (HAE) ceramic disk potentially results in unreliable applied or measured suction. In addition, the equilibration time gets extended thus extending the testing time. Vanapalli et al. (2009) recommended the incorporation of a flushing system to periodically remove diffused air in the system. Other literature noted by Vanapalli et al. (2009) suggest the application of back air pressure to minimize air diffusion. However, Elgabu (2013) indicates these interventions have the possibility of extending the testing time. Vanapalli et al. (2009) summarized steps to account for air

dissolved in soil pores, HAE ceramic disk, and effluent lines connected to the axis-translation system.

2.2.1.2 Chilled mirror dewpoint technique

Several test methods including thermocouple psychrometer, calibrated filter paper (non-contact), Peltier thermocouple psychrometer, wet-loop psychrometer, chilled-mirror hygrometer, and the electric hygrometer have been developed for the measurement of total suction over a wide suction range. Some of these methods are time-consuming, limited on the maximum suction range, operational errors, and potential errors due to fluctuations of dependent variables (Bittelli and Flury 2009; Ebrahimi-Birang and Fredlund 2016; Gubiani et al. 2013; Leong et al. 2003).

The chilled-mirror dewpoint technique, also known as the chilled mirror hygrometer or the chilled mirror psychrometer or dewpoint potentiometer, measures the water activity of soil under isothermal conditions in a closed chamber. Using the Kelvin equation, a thermodynamic relationship, as described in Eq. 2-2, it converts the water activity to total suction.

$$\psi_T = \frac{RT}{M} ln\left(\frac{p}{p_o}\right) \qquad \text{Eq. 2-2}$$

Where R = gas constant (8.31 J/molK), p = vapor pressure of the air at dewpoint, $p_o$ = saturation vapor pressure at the air temperature, T = absolute temperature (K), and M = molecular mass of water. The dewpoint refers to the temperature at which air must be cooled for water vapor in the air to condense to liquid (Leong et al. 2003). The ratio $p/p_o$ defines the water activity or relative humidity of the specimen with $p$ measured using a chilled mirror and $p_o$ calculated from sample temperature.

The technique is rapid and covers a wide suction range from 0 MPa to 300 MPa with improved accuracy. However, it still has limited accuracy in the saturation zone due to the logarithmic nature of the Kelvin equation. For accurate total suction measurements, the water activity measurement must be to the third decimal and a dewpoint temperature maintained in ± 0.001 °C, which is challenging to achieve within the saturation zone (Bittelli and Flury 2009; Gubiani et al. 2013). Also, incomplete equilibration within the sealed chamber and operator skills introduce potential errors in the total suction measurement (Bittelli and Flury 2009; Leong et al. 2003; Patrick et al. 2007). With technological advancement, commercially available device operating the chilled-mirror technique such as the WP4C addresses most of the limitations mentioned above. The WP4C has an improved accuracy of ± 0.05 MPa from 0 to -5 MPa and 1% from -5MPa to -300 MPa compared to its predecessor WP4(T) which had an accuracy ± 0.1 MPa from 0 to -10 MPa and 1% from -10 MPa to -300 MPa (Decagon Devices Inc. 2015; Gubiani et al. 2013).

Recent studies have used the advantages associated with the technique as a reference method in assessing other test methods while determining water retention and hydraulic conductivity functions for geotechnical engineering applications (Bittelli and Flury 2009; Leong et al. 2003). Leong et al. (2003) compared total suction measurement using the chilled-mirror dew-point technique to total suction measurements from the independent measurement of matric, and osmotic suction from the null-type axis translation and pore fluid squeezer approach, respectively. The total suction measurement from the chilled-mirror dew-point technique was relatively higher than the algebraic sum of matric and osmotic suctions measured independently. Bittelli and Flury (2009)

reported a significant error in suction measurement from pressure plate for low water contents of the water retention curve leading to considerable differences in fitted hydraulic functions water retention data measured using pressure plate and chilled-mirror dew-point technique.

#### 2.2.1.3 Unsaturated flow apparatus

The unsaturated flow apparatus (UFA), also known as the centrifuge method, has proven to be relevant in the study of unsaturated properties of porous media. It measures unsaturated flow and transport parameters such as hydraulic conductivity, matric suction, diffusion coefficient, retardation factor in soils and rock under centrifugal force (Conca et al. 1997; Conca et al. 1992; Conca and Wright 1992,1998; Jirka and R. 2005; Menezes et al. 2011; Nimmo et al. 1987). It has been demonstrated to establish unsaturated flow under steady-state and transient conditions as well as test flow theories such as Darcy's law and Richards equation in a centrifugal field (Jirka and R. 2005; Menezes et al. 2011; Nimmo et al. 1987). Due to its adaptability, Menezes et al. (2011) modified and scaled the UFA test to model unsaturated flow for an anisotropic and heterogeneous porous system. Also, the UFA allows control over flux and centrifugal force, which are variables describing flow through a porous media in a centrifugal field (Conca and Wright 1998). Certain assumptions are made in the application of the UFA to flow and water retention measurement. In hydraulic conductivity measurement under steady-state conditions where flux is allowed into the sample, matric suction is relatively small compared to the driving force and hence is considered negligible (Conca and Wright 1998; Menezes et al. 2011). But in the case of water retention measurement where there is no flux into the

sample, steady-state conditions do not exist; thus, it is assumed that the matric suction gradient is equivalent and opposite to the centrifugal force (Conca and Wright 1998).

Despite its core advantages of significantly reducing time to obtain direct measurement of flow and transport parameters in unsaturated conditions, an increase in acceleration may induce compaction and affect menisci and matric suction (ASTM 2008; van den Berg et al. 2009).

### 2.2.2 Parametric and predictive models

The above-listed measurement methods generate discrete data sets provide a limited amount of information with which to describe the unsaturated soil relevant to solving geotechnical and geoenvironmental engineering problems. Also, these measurement methods are relatively demanding to operate, cost-intensive, and associated with high variability in results. The correlation between the water retention behaviors of a porous media and its pore size distribution and other properties has led to the development of several mathematical models. These models are fitted to measured data to generate parameters that are relevant in describing field parameters such as hydraulic conductivity and shear strength of unsaturated porous media. These models are easy to use, applicable to numerical simulation, and relatively accurate in predictions, thus leading to growing demand in solving engineering problems associated with seepage, slope stability, and contaminant fate and transport (Kosugi et al. 2002; Sillers and Fredlund 2001). Examples of widely used mathematical models in engineering practice are the Brooks and Corey (1964) model, the van Genuchten (1980) model, and the Fredlund and Xing (1994) model.

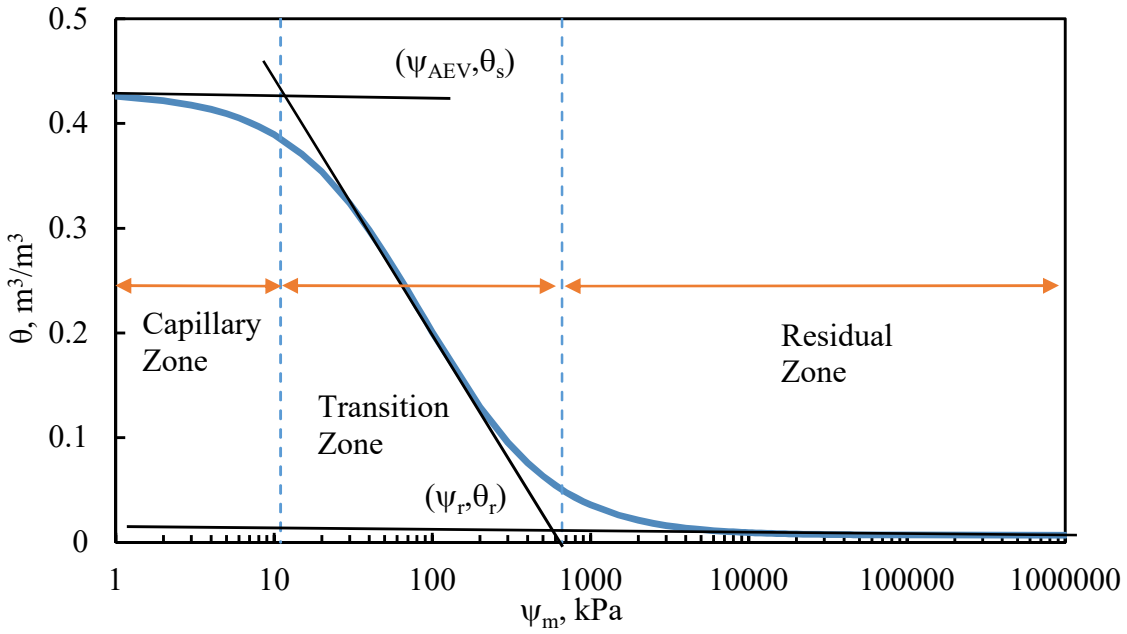


Figure 2-5. Graphical illustration of a typical soil water characteristic curve.

The van Genuchten (1980) model and its variants as presented in Eq. 2-3 through Eq. 2-5 were considered for this study due to the applicability of its fitting parameters to predict unsaturated hydraulic conductivity when combined with the pore size distribution models described by Burdine (1953) and Mualem (1976). Also, it is flexible in fitting a wide range of soils, the fitting parameters correlate with a soil property, and the effects of soil parameters are distinguishable (Elgabu 2013).

- van Genuchten (1980) model (vG)

$$\theta = \theta_r + (\theta_s - \theta_r)\left[\frac{1}{1+(\alpha\psi)^n}\right]^m \qquad m > 0 \qquad \text{Eq. 2-3}$$

- van Genuchten (1980) -Mualem (1976) model (vGM)

$$\theta = \theta_r + (\theta_s - \theta_r)\left[\frac{1}{1+(\alpha\psi)^n}\right]^m \qquad m = 1 - \left(\frac{1}{n}\right) \qquad \text{Eq. 2-4}$$

- van Genuchten (1980) - Burdine (1953) model (vGB)

$$\theta = \theta_r + (\theta_s - \theta_r)\left[\frac{1}{1+(\alpha\psi)^n}\right]^m \qquad m = 1 - \left(\frac{2}{n}\right) \qquad \text{Eq. 2-5}$$

Where $\theta_s$ and $\theta_r$ are the saturated and residual water contents ($m^3/m^3$), respectively, $\psi$ is suction (kPa), and $\alpha$, $n$, and $m$ = are dimensionless fitting parameters which are functions of AEV, rate of water desaturation describing the pore size distribution of the soil, and the asymmetry of the SWCC about the AEV.

Also, the Fredlund and Xing (1994) model (FX), as expressed in Eq. 2-6 and Eq. 2-7, were considered for this study. Fredlund and Xing (1994) developed the model on the assumption that the desaturation of a saturated porous media is a function of the pore size distribution. It covers the entire suction range and a good fit for various types of soils. Eq. 2-7 describes the WRC of soils considering the maximum attainable suction.

$$\theta = \theta_r + \frac{\theta_s - \theta_r}{\left\{ln\left[e + \left(\frac{\psi}{a}\right)^n\right]\right\}^m} \qquad \text{Eq. 2-6}$$

$$\theta = C(\psi)\frac{\theta_s}{\left\{ln\left[e + \left(\frac{\psi}{a}\right)^n\right]\right\}^m} \qquad C(\psi) = 1 - \frac{\ln\left(1 + \frac{\psi}{\psi_r}\right)}{ln\left[1 + \left(\frac{1000000}{\psi_r}\right)\right]} \qquad \text{Eq. 2-7}$$

Where $\theta_s$ and $\theta_r$ are the saturated and residual water contents ($m^3/m^3$), respectively, $\psi$ is the suction (kPa), $\psi_r$ = suction corresponding to $\theta_r$; $\alpha$, $m$, and $n$ = are dimensionless fitting parameters, and $C(\psi)$ is a correction function.

Using Eq. 2-7, Zapata et al. (2000) developed a predictive model based on soil index properties, namely Atterberg limits and particle size distribution. The model considers plastic and non-plastic soils. Results compared favorably to measured data exhibiting minimal variability. Houston et al. (2006) predicted the WRC of soils using a

one-point suction and the index property base model developed by Zapata et al. (2000). Eq. 2-8 through Eq. 2-11 apply to soils with a plastic index equal to zero.

$$\alpha = 0.8627(D_{60})^{-0.75} \quad \text{Eq. 2-8}$$

$$n = 7.5 \quad \text{Eq. 2-9}$$

$$m = 0.1772ln(D_{60}) + 0.7734 \quad \text{Eq. 2-10}$$

$$\frac{\psi_r}{\alpha} = \frac{1}{D_{60} + 9.7e^{-4}} \quad \text{Eq. 2-11}$$

Where $\psi_r$ = suction corresponding to residual volumetric water content, $\alpha$, $m$, and $n$ = are dimensionless fitting parameters as describe in Eq. 2-6, and $D_{60}$ = particle size corresponding to 60% finer on the cumulative particle size distribution in mm.

2.2.3 Unsaturated hydraulic conductivity

Unsaturated hydraulic conductivity of a porous media can be measured directly or indirectly. There are several direct methods of measurement; however, the selection is based on several factors, including the type of porous media, testing time, stress control requirement, and the replication of the flow process as it occurs in the field (ASTM 2010). The UFA test method as discussed in section 2.2.1.3, was considered due to its associated advantages of being a rapid and direct test.

Alternatively, unsaturated hydraulic conductivity can be estimated using unsaturated functions obtained from parametric models fitted to water retention characteristic measurements, as discussed in section 2.2.2. The widely used predictive models are the van Genuchten expressions described in Eq. 2-12 and Eq. 2-13 (van Genuchten 1980). These models, similar in nature, were developed based on the pore size

distribution theories but differed in terms of how the effective pore radii are estimated (Dourado Neto et al. 2011)

- van Genuchten (1980) -Mualem (1976) model

$$K_{\psi} = K_s \frac{\{1 - (a\psi)^{n-1}[1 + (a\psi)^n]^{-m}\}^2}{[1 + (a\psi)^n]^{\frac{m}{2}}} \quad \text{Eq. 2-12}$$

- van Genuchten (1980) - Burdine (1953) model

$$K_{\psi} = K_s \frac{1 - (a\psi)^{n-2}[1 + (a\psi)^n]^{-m}}{[1 + (a\psi)^n]^{2m}} \quad \text{Eq. 2-13}$$

Where $K_{\psi}$ = hydraulic conductivity at a specific matric suction $\psi$; $K_s$ = hydraulic conductivity at saturation; and $\alpha$, $m$, and $n$ = are dimensionless fitting parameters derived from the WRC or SWCC.

## 2.3 Engineered Water Repellency

Water repellency, a resistance of a surface to water (fluid) interaction, is a phenomenon that occurs naturally and can also be engineered. Natural occurrence of soil water repellency can be attributed to an organic compound including living or decomposing plants or microorganisms, and non-biological factors including temperature and fire, and soil texture and clay content (Doerr et al. 2000). It has significant repercussions for plant growth, surface and subsurface hydrology, and soil erosion (Doerr et al. 2000), leading to several decades of extensive studies in soil science. However, significant benefits have been derived from its application in engineering by utilizing water repellent chemicals including but not limited to organosilicon compounds (silanes), organosilicone compounds (siloxanes), and silicates as infiltration resistance technique in surface treatment of concrete and masonry products (Basheer et al. 1997; Dai et al. 2010; Khanzadeh Moradllo et al. 2016; Ley et al. 2012; Ley and Moradllo 2015).

There is a growing interest in engineered water repellency in geotechnical and geoenvironmental engineering practice, which is governed by surface chemistry, nonwetting fluid flow in porous media, and unsaturated fluid dynamics (Keatts et al. 2018). The adhesive and cohesive forces govern liquid interaction behavior with a solid surface. For a solid-liquid interaction, when the adhesive forces between the solid surface and liquid are greater than cohesive force in the liquid, then the solid surface is wettable (hydrophilic). In the case where the adhesive forces between the solid and liquid is less than the cohesive forces in the liquid, then the solid surface is water repellent (hydrophobic).

A direct approach to classify these categories of liquid interaction with solid surfaces is the contact angle, which is described by Young's equations given in Eq. 2-14 and graphically illustrated in Figure 2-6.

$$\sigma_{lv}\cos(\theta') = \sigma_{sv} - \sigma_{sl} \qquad \text{Eq. 2-14}$$

Where $\sigma_{lv}$ = liquid-vapor interfacial tensions; $\sigma_{sv}$ = solid-vapor interfacial tensions; $\sigma_{sl}$ = solid-liquid interfacial tensions, and $\theta'$ = contact angle. Solid-liquid interaction with contact angle < 90° is termed hydrophilic (water interaction) and > 90° is hydrophobic (water repellent interaction)

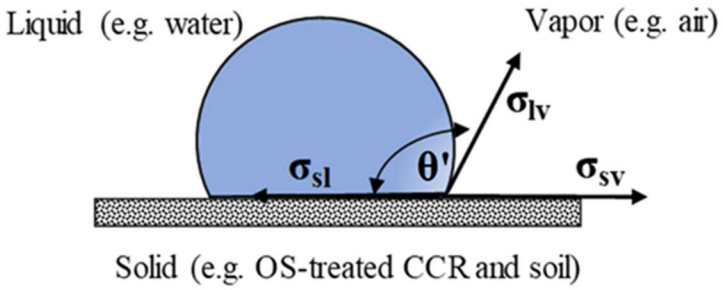


Figure 2-6. Graphical illustration of Young's equation describing contact angle.

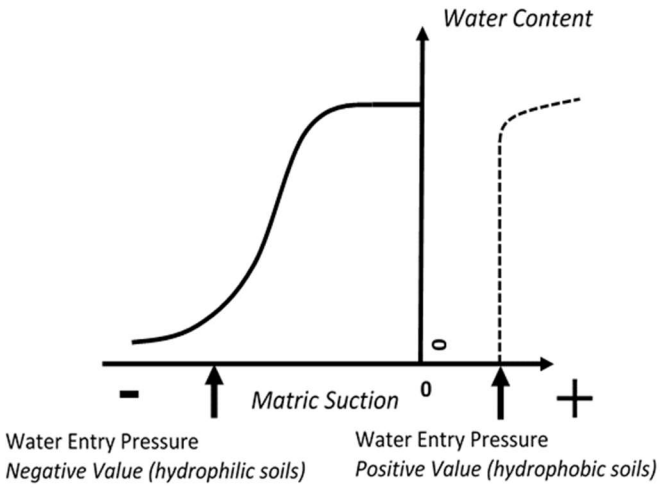


Figure 2-7. Conceptual representation of breakthrough pressure for hydrophilic and hydrophobic soils (Keatts et al. 2018).

However, several other methods are considered indirect approaches to quantify the degree of water repellent interaction of granular material. These include water entry pressure (WEP), also known as breakthrough pressure (BP), water drop penetration time (WDPT) test, molarity of ethanol droplet (MED) test, biliquid capillary rise, ninety-degree surface tension method, infiltration, intrinsic sorptivity and diffusivity, and thermal analysis. For geotechnical and geoenvironmental engineering considerations, contact angle and water entry pressure have been used (Keatts et al. 2018). Water entry pressure also known as breakthrough pressure, quantifies the amount of pressure, higher than atmospheric pressure, to infiltrate a water repellent granular material. The Washburn equation given in Eq. 2-15 and illustrated in Figure 2-6 describes the relationship.

$$H = \frac{2\sigma cos\theta'}{r\rho g} \qquad \text{Eq. 2-15}$$

Where $\theta'$ = contact angle of liquid-solid interaction inside a capillary tube of radius $r$, $\sigma$ = liquid-air surface tension, $\rho$ = liquid density, $g$ = acceleration due to gravity, H = capillary rise for $\theta' > 90°$.

# CHAPTER 3: LITERATURE REVIEW

## 3.1 Introduction

This chapter provides an overview on the state of research pertaining to the studies undertaken. Presented is a brief review of the engineering characteristics of CCRs in geotechnical and geoenvironmental engineering applications. This review is followed by a presentation of selected measuring techniques for WRC of soils that were adopted for CCRs. The limitations associated with each test method are presented. This chapter also discusses the characteristics of chemicals responsible for water repellent interactions. The section further explores factors that affect the chemistry of interaction between substrate and water repellent compounds for geotechnical and geoenvironmental engineering applications. A summary of the state of research on water repellency in geotechnical and geoenvironmental engineering practice is presented.

## 3.2 Geotechnical Engineering Characterization of CCRs

CCRs are unique geomaterials with significant heterogeneity in physical and index properties, elemental and mineral composition, and morphology due to the source of coal and the adopted combustion process (Das and Yudhbir 2005; Dillon 2015). Hence for decades, numerous studies have been conducted to characterize the various types of CCRs for technological development in utilizing CCRs in applications including concrete and building materials, road constructions, oil well construction, mining, and agriculture (Halow and Covey 1982; Huang 1990; Kim et al. 2005; Lee et al. 2014; Leonards and Bailey 1982; Martin et al. 1990; Mishra and Karanam 2006; Santos et al. 2011; Toth et al. 1988; Young 1993). Notable among the various types of CCRs for geotechnical and geoenvironmental environmental engineering-related applications are fly ash, bottom ash,

FGD gypsum, and FGD material from dry scrubbers, with fly ash having the highest rate of utilization (ACAA 2018).

### 3.2.1 Morphology of CCR particles

The combustion process in coal-powered plants dictates the particle formation of CCRs particles, as illustrated in Figure 2-1. The scanning electron electronic microscopy (SEM) method is extensively used to observe the morphological characteristics of CCR particles. High-temperature combustion of coal results in complete melting generating fly ash particles that are spherical with smooth surfaces [Figure 3-1 (b)] (Xu et al. 2011). With low-temperature conditions, incomplete melting occurs generating fly ash particles that are mostly agglomerated [Figure 3-1 (a)] and fine individual particles with irregular (sinter) shapes (Xu et al. 2011). Sintered size fly ash particles are common (Bachus et al. 2019). Other particles such as cenospheres – hollow spheres [Figure 3-1 (c)] and plerospheres are also produced as a result of combustion conditions (Trivedi and Sud 2002).

FGD gypsum is a byproduct of sulfur oxides (SOx) recovered from burning coal bypassing exhaust gas generated through a scrubber containing chemical absorbents. Its characteristics are comparable to naturally occurring gypsum. SEM images of FGD gypsum reveal varying morphological characteristics, agglomerated (Caillahua and Moura 2018), or crystalized (Bachus et al. 2019; Hao and Guo 2012; Pflughoeft-Hassett et al. 2007; Taha 1993). But predominantly crystallized. The agglomerated form has an irregular spherical shape with variable diameter and smooth surface, as presented in Figure 3-2 (a) whereas crystallized form has tubular particles, as shown in Figure 3-1 (d) but similar to naturally occurring gypsum as presented in Figure 3-2 (b).

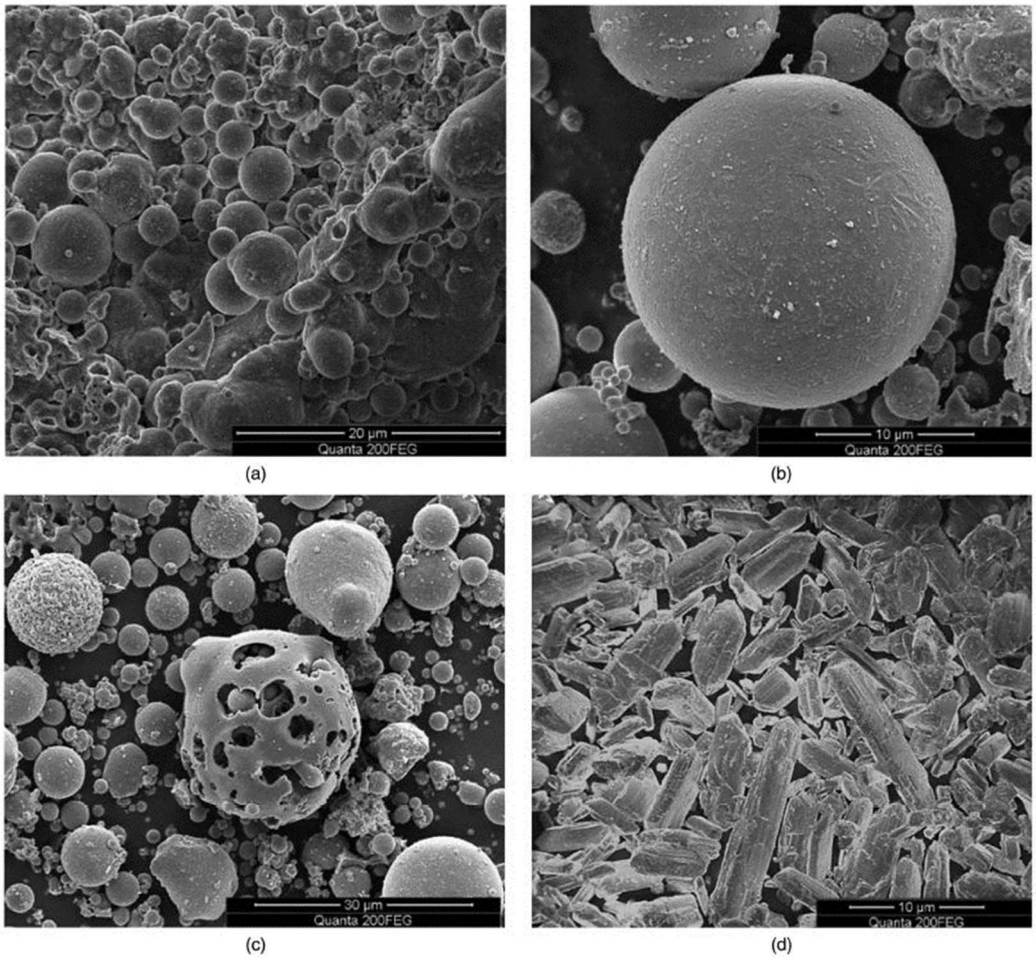


Figure 3-1. Scanning electron micrograph images of (a) a mixture of spherical and agglomerated fly ash particles; (b) spherical fly ash particle; (c) cenosphere; and (d) FDG gypsum crystals (Bachus et al. 2019).

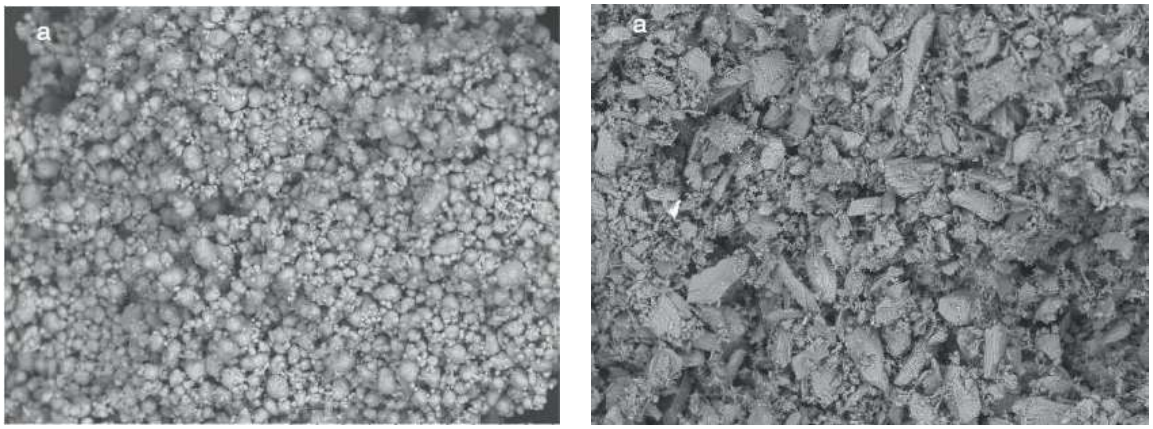


Figure 3-2. SEM images showing agglomerated (a) FGD gypsum particles and (b) naturally occurring gypsum (Caillahua and Moura 2018).

### 3.2.2 Elemental and mineral composition

The chemical constituent of the noncombustible components of coal, conditions during combustion, and emissions control processes defines the chemical composition of CCRs, subsequently influencing properties including pH, electrical resistivity, EC, and oxidation.

The elemental characteristics analyses of CCRs based on X-ray fluorescence (XRF) studies quantify the oxidized compounds and loss on ignition (LOI) in percentage by weights and trace elements in parts per million. Silica ($SiO_2$), Alumina ($Al_2O_3$), and FerroOxide ($Fe_2O_3$) constitute the significant oxides present in fly ash, including lignite fly ash with a combined percentage by weight ($SiO_2 + Al_2O_3 + Fe_2O_3$) > 50% as defined in ASTM C618 (ASTM 2015a). In the case of FGD gypsum, Calcium Oxide (CaO) and Sulphur Oxide ($SO_3$) constitute the significant oxide with the combined percentage by weight ($CaO + SO_3$) > 75% (Caillahua and Moura 2018; Hao and Guo 2012).

The mineral composition analysis of CCRs is based on X-ray diffraction (XRD) analyses, which categorize the phase constituents of CCRs. The mineral phases of fly have been extensively investigated, indicating fly ash exists in two main phases, namely amorphous and crystalline phases formed from major and minor elements in fly ash including O, Si, Al, Fe, Ca, Mg, and S (Tishmack and Burns 2004). However, it is mostly constituted in the amorphous phase (Tishmack and Burns 2004; Twardowska and Szczepanska 2002). Typical phases of minerals identified in fly ash include quartz, aluminosilicate, hematite, magnetite, mullite, tricalcium aluminate, alite, belite, hematite, lime, anhydrite, calcite, periclase, melilite, merwinite, thenardite, ettringite, albite, esperite, nepoutite, tenorite (Asokan et al. 2005; Dumenu et al. 2017; Tishmack and

Burns 2004; Twardowska and Szczepanska 2002). The major amorphous components are relics of clay minerals and glaze whereas the significant components of the crystalline phase are mullite, hematite/maghemite and quartz (Tishmack and Burns 2004; Twardowska and Szczepanska 2002).

The mineral characteristics of FGD gypsum, a product of sulfur-scrubbers, vary primarily due to its dependence on the variables defining operations of the scrubbers (Tishmack and Burns 2004). Caillahua and Moura (2018) reported basanite and hannebachite as predominate minerals with low traces of anhydrite and other compost from FGD sourced from Brazil. Kairies et al. (2006) reported quartz and dolomite with average amounts of calcite and trace amounts of clay minerals post-leached gypsum. Sun et al. (2014) reported calcium sulfate as the predominate phase with minor minerals including calcite and quartz for multiple FGD gypsum samples sourced from selected plants across China.

### 3.2.3 Physical and index properties

Bachus et al. (2019) presented comprehensive data trends on fly ash properties published in reports from around the world including North America, Europe, and Asia. The compilation focused on fundamental geotechnical engineering properties namely physical, index, chemical, mechanical and hydraulic properties. Analysis of the data, as presented in Table 3-1 , revealed significant variations in test data such as specific gravity, porosity, hydraulic conductivity, liquid limit, strength parameter, and pH. Chemical composition and morphology account for the wide variations in specific gravity and related properties (Kim and Prezzi 2008a,2008b; Trivedi and Sud 2002). Fly ash with high iron content ($Fe_2O_3$) have high specific gravity (Das and Yudhbir 2005; Trivedi and

Sud 2002). The data shows the fly ash reported had gradations comparable to well-graded silt. Bachus et al. (2019) further discussed results of new test procedures that cover general characteristics, depositional characteristics, mechanical response and diagenetic cementation of dry and ponded class F fly ash as presented in Table 3-2.

Table 3-1. Data trends of fly ash properties from around the world (Bachus et al. 2019)

| Property | Symbol | Reported cases | Unit | Range[a] | | Statistics[b] | |
|---|---|---|---|---|---|---|---|
| | | | | Minimum | Maximum | $\mu$ | $\sigma$ |
| Chemical composition | $SiO_2$ | 47 | % by weight | 27 | 64 | 47.7 | 11.0 |
| | $Al_2O_3$ | | % by weight | 7.0 | 38 | 23.6 | 7.5 |
| | $Fe_2O_3$ | | % by weight | 1.7 | 33 | 10.4 | 7.5 |
| | CaO | | % by weight | 0.5 | 27 | 7.0 | 7.5 |
| Basicity | pH[c] | 9 | — | 7.2 | 12.6 | 9.4 | 2.1 |
| Grain-size distribution | $D_{100}$ | 68 | $\mu$m | 60 | 1,960 | 442 | 464 |
| | $D_{60}$ | | $\mu$m | 8.0 | 120 | 32 | 22.6 |
| | $D_{30}$ | | $\mu$m | 2.5 | 50 | 13.6 | 9.8 |
| | $D_{10}$ | | $\mu$m | 0.4 | 15 | 5.0 | 3.8 |
| | $C_u$ | | — | 2.1 | 25 | 7.8 | 5.5 |
| | $C_c$ | | — | 0.6 | 3.9 | 1.4 | 0.8 |
| Specific surface | $S_s$ | 18 | $m^2/g$ | 0.09 | 1.3 | 0.45 | 0.39 |
| Liquid limit | LL | 11 | % | 30 | 62 | 44.1 | 10.4 |
| Specific gravity | $G_s$ | 76 | — | 1.50 | 3.02 | 2.27 | 0.3 |
| Porosity | $n$ | 26 | — | 0.36 | 0.64 | 0.50 | 0.08 |
| Hydraulic conductivity | $K$[d] | 172 | cm/s | $4 \times 10^{-7}$ | $4 \times 10^{-4}$ | $3.8 \times 10^{-5}$ | $3.3 \times 10^{-4}$ |
| Friction angle | $\phi$ | 95 | Degrees | 26 | 43 | 36.7 | 4.9 |
| Compressibility | $C_c$[d] | 92 | — | 0.04 | 0.37 | 0.11 | 0.08 |
| | $C_v$ | Range | $m^2/s$ | $2.20 \times 10^{-8}$ | $9.50 \times 10^{-5}$ | N/A | N/A |

Table 3-2. Summary of new and advance tests on selected dry and ponded fly ash (Bachus et al. 2019).

| Test category | Test | Number of tests | Typical results |
|---|---|---|---|
| Imaging | SEM | 45 | Cenospheres (some show gypsum crystals) |
| | X-ray (Shelby tube) | 14 | Layered stratigraphy |
| Index | Specific gravity $G_s$ | 32 | 1.96–2.66 |
| | Liquid limit | 9 | 26%–62% |
| | Plastic limit | 9 | 22%–55% |
| | Electrical sensitivity | 4 | Low electrical sensitivity to pore fluid chemistry |
| | Grain-size distribution | 24 | $D_{50}$ = 0.01–0.04 mm<br>$C_u$ = 2.3–4.2[a] |
| | pH | 31 | 6–12 |
| New index tests | Realizable unit weight | 68 | Minimum = 5.5 kN/m$^3$; maximum = 15.1 kN/m$^3$ |
| | Formation effects | 9 | Segregation and layering developed in all sedimentations tests |
| | Ferromagnetism | 29 | Some present in all specimens. Up to 20% by weight |
| | Contact angle | 6 | Nonwetting (water) |
| Advanced tests | Oedometer and diagenesis | 9 | High-pH specimens are prone to early diagenetic cementation |
| | Oedometer and shear-wave velocity | 17 | Undisturbed: $\alpha$ = 21.8–244 m/s; $\beta$ = 0.06–0.36<br>Remolded: $\alpha$ = 12–79 m/s; $\beta$ = 0.22–0.37[b] |
| | Hydraulic conductivity | 15 | $6.7 \times 10^{-5}$ to $1.8 \times 10^{-4}$ cm/s |
| | Constant-volume shear in AC triaxial[c] | 44 | CD: $\phi'_{peak}$ = 31°–38°<br>$\phi'_{cv}$ = 29°–36°<br>CU: $\phi'_{max}$ = 28°–36° |
| | Cyclic triaxial | 7 | Response depends on relative realizable density |

CCRs are generally non-plastic materials but may exhibit the high liquid limit values comparable to soils due to fabric (i.e., structure and arrangement of particles) and not as plasticity characteristics (Sridharan et al. 2001).

### 3.2.4 Mechanical characteristics

CCRs though not naturally occurring, possess distinct engineering qualities comparable to typical geotechnical soils such as light unit weight, good shear strength characteristics, and self-cementing properties suitable for use in engineered systems such as structural fills, embankments, road base/sub-base, and soil modification and stabilization. Rana (1996) and Chesner et al. (1998) provided a list of engineered systems across the United States that utilized CCRs as construction materials. Many researchers continue to investigate the mechanical characteristics, including compaction characteristics, shear strength characteristics, consolidation, compressibility, and liquefaction of CCRs due to the heterogeneity of CCR materials.

#### 3.2.4.1 Compaction

Sridharan et al. (2001) reported that the compaction characteristics of selected Indian CCRs – fly ash, bottom ash, and ponded ash – are similar to those of cohesionless sands or sandy gravels, however, are insensitive to variation in water content (Sridharan et al. 2001). The study further compared the volume-based representation of compaction, a function of void ratio (e), and volume water content (ωG) to the weight-based representation of compaction, a function of specific gravity. The volume-based approach was found to give a realistic representation of the CCR compaction characteristics compared to the weight-based approach by addressing the impact of significant variations in specific gravities of CCRs, although it is not practically adopted. However, using

normalized parameters preserved the advantages of the volume-based approach for geotechnical engineering practice. Kim and Prezzi (2008a) investigated the impact of gradation compaction properties of CCRS by considering a matrix of class F fly ash-bottom ash mixture. With increasing fly ash content, the maximum dry unit weight decreased while the optimum water content increases. Similar to the observation made in fly ash-soil mixture (Das and Yudhbir 2005). For selected Indian fly ashes, Das and Yudhbir (2005) reported the calcium content influence the compaction behavior of fly ash. Fly ash with high calcium content fly ash showed higher density with lower water content compared to low calcium content fly.

Contrary to the general trend of CCRs, the high calcium content fly ash was sensitive to variations in water content due to the presence of lime resulting in a narrow range of water content. However, the low calcium content fly ash had a wide range of water content and was insensitive to water content variation. The study further presented correlations between LOI and maximum dry density and optimum water.

3.2.4.2 Shear strength

In soil mechanics, the shear strength of a soil system is described by cohesion and friction, as expressed by the Mohr-Coulomb failure envelop in Eq. 3-1.

$$\tau = c + \sigma tan\emptyset \qquad \text{Eq. 3-1}$$

Where $\tau$ = shear strength, $\sigma$ = normal stress, and $\emptyset$ = internal frictional angle. The cohesion component measures the degree of soil resistance to no compressive stress. Cohesion primarily accounts for shear strength in clays and fine silt. In clays this can be attributed to the electrostatic forces present in clay particles. However, soils without significant clay content do experience apparent cohesion a phenomenon explained by soil

suction. The normal stress and internal frictional angle constitute the frictional component, which is described by the soil state variables such as relative density, effective stress state, and fabric and intrinsic variables such as particle shape, gradation, particle surface characteristics, and mineralogy (Kim 2003). CCRs can be classified as frictional and cohesive materials with class F fly ash, bottom ash, and boiler slag considered as frictional material and class C fly ash considered as a cohesive material due to the self-cementing properties which account for the significant cohesive strength (Kim 2003).

The strength characteristics of soil systems are mostly defined by the unconfined compressive strength, the direct shear strength, and the triaxial shear strength parameters determined using standardized testing methods. These tests provide details on the stress-strain behavior in addition to the strength-water content behavior. Das and Yudhbir (2005), in an unconfined compressive test, noted that the curing conditions influenced strength and stress-strain behavior of the tested fly ashes which showed brittle rapture after attaining peak. An implication of possible crack development in compacted fly ash considered for load-bearing structures in engineering practice. The study further indicated that the unconfined compressive strength with water content compared well to very fine sand.

Kim and Prezzi (2008b) examined the influence of compaction water and saturation on the shear strength using the direct shear method. Results showed a marginal difference in shear strength between samples compacted on dry and wet of optimum. With dry of optimum samples exhibit relatively higher shear strength compared to samples on the wet of optimum. Fly ash is considered frictional materials. However, the

samples experienced apparent cohesion due to capillary stresses. The study further examined the stress-strain and volume change relationship considering varying relative compaction. The compaction levels influenced the shear parameters of the test samples. However, both compaction levels behaved similarly to dilative and contractive sands.

### 3.2.5 Saturated hydraulic conductivity

The infiltration behavior of a porous media in the saturated or unsaturated zone is defined by the hydraulic conductivity. Hydraulic conductivity functions are primarily dependent on the structure or pore geometry of the porous media, which is correlated to the media gradation, particle shape and size and, mineral composition (Burdine 1953; Cabalar and Akbulut 2016; Durner 1994). Other factors include molding water content, degree of saturation, compaction energy, hydraulic gradient and void ratio (Palmer et al. 2000; Pandian 2013). In addressing geotechnical and geoenvironmental engineering problems such as seepage, drainage, groundwater flow, and contaminant fate and transport, research and industry applications primarily depend on hydraulic conductivity functions. These functions can be determined experimentally in the laboratory or field using standardized test methods and predicted using empirical models, capillary models, statistical models, and hydraulic radius theories. Examples of some laboratory or field methods used in measuring the hydraulic conductivity of CCRs are falling head test using Casagrande type consolidometer (Kaniraj and Gayathri 2004), infiltrometer (Daniels and Hourani 2009), constant head method (Young 1993), and transient water and release and imbibition method (TRIM) and modified falling head permeameter (Keatts et al. 2018).

According to Chapuis and Aubertin (2003), the best models include at least three parameters that account for flow rate and pore space properties such as pore sizes,

tortuosity and connectivity. Jaafar and Likos (2014) noted that the predictive methods that consider pore size distribution are more realistic and show better model results for saturated hydraulic conductivity most notable for cohesionless materials such as sands. However, in the development of a regression-based model to predict the saturated hydraulic conductivity of compacted soils from the grain size distribution, Boadu (2000) moved away from the traditional representation of the grain size distribution such as fractional grain size ($d_{10}$ and $d_{50}$) to an alternative representation such as the fractional dimension and entropy of the distribution as well as porosity, soil density and fines content. The study established weak correlations between the predictor variables such as the relation between hydraulic conductivity and the fractional dimension and entropy of the distributions. Therefore, a multivariate regression analysis was considered to account for the interdependencies between the predictor variables to improve the accuracy of the prediction by reducing the errors in the estimates. The study further established the fines content of the soil influences its hydraulic properties evaluating the correlations between fines content and hydraulic conductivity, porosity, entropy, and fractional dimension. The developed models performed relatively better than the Kozeny-Carmen and Hazen models.

CCRs are considered uniformly graded and cohesionless material thus enables the use of predictive models developed for such soils to compare estimated data to measured data. Young (1993) using particle size distribution data, evaluated the performance of selected empirical models. The study found the Sieler and the modified Hazen equations predicted saturated hydraulic conductivity of selected CCRs comparable to the measured data. Cabalar and Akbulut (2016) documented several other models in

the evaluation of predicted hydraulic conductivity of sands with different gradation and shape

In general, hydraulic conductivity of CCRs are comparable to typical geotechnical soils with known values ranging between $10^{-7}$ to $10^{-1}$ cm/s (Bachus et al. 2019; Kaniraj and Gayathri 2004; Keatts et al. 2018; Palmer et al. 2000). Comparing CCRs, fly ash material record the lowest values compared to bottom ash and boiler slag (Kim 2003). According to Palmer et al. (2000), the hydraulic conductivity of class F fly ash decreases with permeant containing methanol and acetic acid, long-term curing, high bentonite content in bentonite-fly ash mixtures. However, bentonite content had negligible effect on samples tested with permeant containing methanol and acetic acid. In the case of class, C fly ash, self-cementing properties, and freeze thaw cycles had significantly reduced the hydraulic conductivity.

## 3.3 Unsaturated Functions of CCRs

### 3.3.1 WRC measurement

Several test methods have been developed through extensive research to determine the unsaturated soil property functions from laboratory and field measurements. However, the introduction of these measurement techniques remain one of several challenges to engineering practice (Fredlund 2006). These test methods range from direct and indirect laboratory methods to indirect methods based on estimations from particle size distribution and knowledge-based systems. Direct laboratory methods such as the null-type axis translation, tensiometers, and suction probe, measure matric suction by observing pore-water pressure when pore-air pressure is introduced into the chamber. The indirect laboratory test methods account for soil properties such as water

content, relative humidity, temperature, and resistivity that correlate suction in measuring the main components of suction – total, matric and osmotic. Pan et al. (2010) and Elgabu (2013) provided a critical evaluation of applicability and limitations measuring methods reviewing working principles, measurement procedures, and engineering practice applications. For this study, the focus is on the application of the measuring method to CCRs. Table 3-3 presents a summary of suction measurement application to CCRs detailing specific CCRs and suction type. For this study, the suction measurement will be limited to null type axis translation methods – pressure plate and Tempe cell, dew point potentiometer, and steady-state unsaturated flow apparatus (centrifuge).

Table 3-3. Summary of suction measurement application to CCRs.

| Reference | Suction Method | Suction | Fitting Model | CCR |
|---|---|---|---|---|
| Young (1993) | Hanging column | Matric | vGM | Fly ash, flue gas desulfurization, Atmospheric fluidized bed combustion |
| | Pressure plate | Matric | | |
| Malaya and Sreedeep (2010) | Tensiometer | Matric | vGM | Fly ash |
| Malaya and Sreedeep (2014) | Tensiometer | Matric | vG and FX | Fly ash/Sand mixture |
| | Volumetric water content sensor | Matric | | |
| Abhijit and Sreedeep (2014) | Tensiometer | | vGM and FX | Fly ash |
| Web et al (2014) | Hanging column | Matric | vGM | Fly ash and Bottom ash |
| | Pressure plate | Matric | | |
| | Dew point potentiometer | Total | | |
| | relative humidity | Total | | |
| Pease et al (2017) | Hanging column | Matric | vG | Flue Gas Desulfurization Gypsum |
| | Pressure plate | Matric | | |
| | relative humidity | Total | | |
| Keatts et al. (2018) | Transient water release and imbibition method (TRIM) | Matric | not defined | Class F Fly Ash |

Young (1993) reviewed the hanging column and pressure plate method to establish the moisture retention curves of selected CCRs. Using numerical modeling, the unsaturated hydraulic conductivity functions were estimated using the saturated hydraulic conductivity, moisture retention curve, and diffusivity. Results were validated with measured unsaturated hydraulic conductivity. The study reported the physical and hydraulic properties of the selected CCRs comparable to typical geotechnical soils.

Mudd et al. (2007) reviewed the unsaturated hydraulic properties of several leached coal ashes based on several laboratory tests, including the SWCC, established using multiple devices including TC, PPE, and a salt desiccator to complement the suction range of the leached ash. The study classified the leached ashes into elastic silt and silty sand. The study found these classifications to influence the unsaturated hydraulic properties of the leached ashes. The elastic silt exhibited a wide range of suction with a 30 kPa AEV and residual suction value of 2000 kPa resulting in an adequate storage capacity. However, the silty sand had a lower storage capacity in addition to high hydraulic conductivity.

Malaya and Sreedeep (2010) compared the measured SWCC of fly ash using tensiometers to SWCC predicted using ROSETTA. The results found a significant difference in the predicted to the measured characteristics curve, an indication that estimates based on soil properties do not apply to CCRs.

Abhijit and Sreedeep (2014) evaluated the performance of a low range and high tensiometers in characterizing the water retention properties of various types of fly ash. The study found that the low range tensiometer was limited in the saturation zone of the SWCC, whereas the high range tensiometer performed relatively well in the residual zone

of the samples. The class of fly ash was found to influence the performance of the tensiometers as the low range tensiometer failed with the class C fly ash.

Malaya and Sreedeep (2014) investigated the WRC of fly ash – soil mixtures. The fly ash addition influenced the compaction characteristics with varying portion of fly ash. With an increase in the fly ash portion, the dry unit weight decreased, and the water content increased. The soil water characteristics were measured using tensiometers. Results indicate that the addition of fly ash improved the WRCof soil. The fitting models had a good fit to the measured data.

Webb et al. (2014) evaluated the unsaturated hydraulic characteristics of fly ash and bottom ash as a function of density. The study developed compressibility curves that defined the densities of samples for establishing the SWCC using multiple test methods, including hanging column, PPE, WP4C, and relative humidity. Results found variability in the unsaturated hydraulic functions obtained from the SWCC of samples compacted at different densities showing that the variability in the unsaturated hydraulic functions decreased with an increase in density. However, the study as limited in estimating the unsaturated hydraulic conductivity due to the unavailability of experimental data to validate estimate unsaturated hydraulic conductivity.

Pease et al. (2017b) compared the SWCC of FGD scrubber material established using multiple methods including hanging column, PPE, and relative humidity box to SWCC of clay, silt, and sand. The SWCC of the FGD residue was found to compare relatively well with silt in the transition zone but has relatively high saturated and low residual water content. A similar observation was made with the predicted unsaturated hydraulic conductivity which compared relatively well with silt.

Keatts et al. (2018) demonstrated the use of TRIM to establish the wetting and drying SWCC of compacted fly ash. The results found the unsaturated hydraulic functions corresponding to the SWCC compared well with the transient flow. However, the test method was limited in establishing the SWCC of water repellent fly ash due to challenges to ensure consistent flow regime in a water repellent material.

### 3.3.2 Parametric models

Table 3-3 presents a summary of the various parametric models used in fitting the measurement of WRC of CCRs. A review of the studies indicates vG, vGM, and FX models as the widely used parametric models in CCR applications. These models were found to have a good fit to measured data.

### 3.3.3 Unsaturated hydraulic conductivity measurement

Young (1993) measured diffusivity, an indirect approach of estimating the unsaturated hydraulic conductivity function of selected CCRs. The measured diffusivity of the CCRs was fitted to the van Genuchten model using Mualem's coefficients. The results indicate the predicted diffusivity of the CCRs were influenced by water content than the measured diffusivity, as predicted values were an order of magnitude lower than measured at a given water content.

Sindi (2019) investigated the effect of hysteresis on the unsaturated hydraulic conductivity of selected CCRs using the UFA, considering steady-state conditions. The study involved multiple cycles of desaturation and saturation. Results suggest that no hysteresis had negligible to no effect on the unsaturated hydraulic conductivity of the CCRs. The study further measured the matric potential of the CCRs in steady-state conditions, but only after the hysteresis tests were completed. Results compared

relatively well with typical soil such as loam and sandy soil. However, the steady was limited in comparing the measured unsaturated hydraulic conductivity with the predicted unsaturated hydraulic conductivity using the fitting parameters obtained from the water retention curves of the CCRs.

## 3.4 Ash Leaching

Mudd (2001), in the modeling of solute transport through ash disposal sites, presented a detailed overview of the mechanics of leaching in ash, the types of leaching tests and the associated advantages and limitations. The study considered the column leaching test to allow for soil water content monitoring using a Time Domain Reflectometry during the leaching process. The study developed leaching curves for Na, $SO_4$, Cl, K, and B. Results found the concentration of all but B decreased as pore volume increased with a significant solute concentration in the initial leachate.

Deka (2015) evaluated the suction measurement performance of WP4C and multiple tensiometers on repeatedly leached fly ashes using DId. The study made no mention of the leaching process considered, and no chemical analysis was performed on the leachate to test for any solute. However, total suction measurement, a function of fluid chemistry, were comparable to the original fly ashes. This observation indicated no solute present in the pore fluid under natural pH conditions.

## 3.5 Engineered Water Repellency

### 3.5.1 State of research – geotechnical/geoenvironmental engineering practice

The past decade has seen a growing interest in the use of organic compounds to modify the surfaces of the inorganic substrate to synthesize water repellent interaction for applications in geotechnical and geoenvironmental engineering practice. These

applications range from but not limited to improving the performance of clay-based barriers with respect to sorption and hydraulic conductivity (Daniels et al. 2009b), developing preventive solutions to road infrastructure failures (Ugwu et al. 2013), and developing alternative infiltration control systems for coal ash containment (Daniels et al. 2018).

#### 3.5.1.1 Water repellent chemicals and granular materials

Table 3-4 summarizes literature on engineered water repellency of typical soils for geotechnical and geoenvironmental engineering applications. Also, Table 3-4 details the active ingredient responsible for water repellent interactions, the granular material treated, the material treatment protocol – the type of solvent and mixing ratios, and the standardized test performed to assess fundamental engineering properties of the materials. The literature reveals a wide range of granular materials have been considered in these studies from standardized materials such as glass beads and Ottawa sand to non-traditional materials such as coal ash and kaolin clay. Widely used organic compounds are silanes, siliconate, and siloxanes. Others include stearic acid and octadecane which simulates the chemistry of natural water repellent substances (Lourenço et al. 2015b), stearamine, Oleic and stearic acid. The active ingredients in these organic compounds define the material treatment protocols. As discussed in section 3.5.5.1, a solvent is required to initiate hydrolysis and condensation reactions. The widely used solvent includes alcohol and water, and others such as chloroform and diethyl ether. Some of the commercially available brands have alcohol as part of the ingredients hence requiring water as solvents to prepare the water repellent solution for treatment. The chemical-solvent solution is mostly expressed as a ratio of the organic compound to the solvent in

terms of weight to weight, volume to volume, or weight to volume. In some cases, the weight of the solvent is relative to the weight of the solids. Also, the chemical-solvent solution has been expressed as a function of the specific surface area of the soil samples (Liu et al. 2012) as well as the soil texture (Bachmann and van der Ploeg 2002).

Table 3-4. Selected literature on synthesized water repellency for geotechnical and geoenvironmental engineering practice.

| References | Active ingredient | Material | Solvent | Treatment | Test |
|---|---|---|---|---|---|
| Bachmann and van der Ploeg (2002) | Dichlorodimethylsilane | Quartz sand and Silt | Not defined | $V_{Chemical} : W_{solids}$ | Temperature dependent water retention curves |
| Daniels and Hourani (2009) | 3-(trimethoxysilyl)propyl diamethyloctadecyl ammonium chlorid and ethylene glycol | Elastic silt | Water | $W_{chemical} : W_{Solvent}$ | Compaction characteristics, leaching, hydraulic conductivity, California bearing ratio, expansion index |
| Daniels et al. (2009b) | 3-(trimethoxysilyl)propyl diamethyloctadecyl ammonium chlorid and ethylene glycol | Coal Fly ash | DI water | $W_{chemical} : W_{Solvent}$ | Compaction characteristics, leaching, hydraulic conductivity, California bearing ratio, expansion index |
| Czachor et al. (2010) | Octadecyloamine | Quartz glass | Propanol | $V_{chemical} : V_{Solvent}$ | WRC |
| Truong et al. (2011) | n - octyltriethoxysilane | Glass beads | Isopropyl alcohol | $W_{chemical} : W_{Solvent}$ | Small - Strain Stiffness |
| Byun et al. (2012) | n - octyltriethoxysilane | Glass beads | Isopropyl alcohol | $W_{chemical} : W_{Solvent}$ | Strength and stiffness of unsaturated granular media |
| Liu et al. (2012) | Dichlorodimethylsilane | Sand, loam silt loam | DI water | Function of specific surface area of soil | Contact angle, Water drop penetration time, Soil water desaturation test |
| Subedi et al. (2012b) | Oleic acid and stearic acid | Sand | Diethyl ether | $W_{Chemical} : W_{solids : solvent}$ | Time dependency of contact angle |
| Ugwu et al. (2013) | Nano-z (alkyl and trialkoxy) | Silty sand, | Water | $V_{chemical} : V_{Solvent}$ | Compaction characteristics, Atterberg limits, California bearing ratio |

Table 3-4. Selected literature on synthesized water repellency for geotechnical and geoenvironmental engineering practice continued.

| References | Active Ingredient | Material | Solvent | Treatment | Test |
|---|---|---|---|---|---|
| Jordan et al. (2015) | Hydroxyalkyl-alkoxy-alkylsilyl compounds | Sand & Coal fly ash | DI water | $W_{Chemical}$ : $W_{Solvent : solids}$ | Water entry pressure as function of temperature |
| | potassium methyl siliconate | | | | |
| Lourenço et al. (2015b) | Stearic acid and Octadecane | Sand - Clay mixture | Chloroform | $W_{chemical}$ : $V_{Solvent}$ | Soil water retention curve hysteresis |
| Lee et al. (2015) | n-octyltriethoxysilane | Silt | DI water | $W_{chemical}$ : $W_{Solvent}$ | Water droplet penetration time, Water - entry pressure, and Peak friction angle |
| Choi et al. (2016) | 3-(trimethoxysilyl)propyl diamethyloctadecyl ammonium chlorid and ethylene glycol | Kaolin clay | Water | $W_{chemical}$ : $W_{Solvent}$ | Contact angel, water infiltraion time, infilrtration rate, compaction characteristics, compressibility, small strain shear modulus |
| Feyyisa et al. (2017) | Triethoxy(octyl)silane | Coal fly ash | DI water | $W_{Chemical}$ : $W_{Solids : solvent}$ | Contact angle and Breakthrough pressure |
| | Triethoxy(octyl)silane and polydimethylsiloxane | | DI water | $W_{Chemical}$ : $W_{solids : solvent}$ | |
| Keatts et al. (2018) | potassium methyl siliconate | Ottawa Sand & coal fly ash | DI water | $W_{Chemical}$ : $W_{Solvent : solids}$ | Contact angle and water entry pressure and SWCC |
| Karim et al. (2018) | n - octyltriethoxysilane | Ottawa Sand | Isopropyl alcohol | $W_{chemical}$ : $W_{Solvent}$ | Shear Strength |

3.5.1.2 Material treatment procedures

Two distinct material treatment protocols for water repellent treatment were identified in literature, namely pretreatment and molding moisture approach. The pretreatment approach involves adding a water repellent solution to the granular material, allow the mixture to sit, rotate, or stirred for a specified period. During this period, the reaction process allows the organic compounds responsible for water repellent interaction to sorb onto the substrates thus modifying the surface of the granular material. Beyond this point, there exist variants to the pretreatment approach. After the specified period, 1) the excess solution can be washed off using DI water before drying (Truong et al. 2011); 2) oven-dry or air-dry at room conditions for the excess solution to evaporate. Others after mixing the water repellent solution with the granular material, oven-dry the mixture until there is no significant change in mass of the treated sample (Feyyisa et al. 2017; Keatts et al. 2018). Another variant was treating with the concentrated water repellent solution. Daniels et al. (2009b) pretreated fly ash with OS solution, oven-dried to a specified water content for compaction and sequential treatment.

For the molding moisture approach, the water repellent chemical was added to the molding moisture content to prepare samples for engineering tests such as compaction, hydraulic conductivity, and CBR (Daniels et al. 2009b; Ugwu et al. 2013). Comparing the two methods, the molding moisture approach is applicable to field practice as mentioned by Daniels et al. (2009b) and Ugwu et al. (2013).

3.5.1.3 Water repellency assessment

The SDM, WEP/BP, and WDPT methods were considered in assessing the water repellent interaction behavior of the treated samples in the selected literature presented in

Table 3-5. The characteristics of the material widely influence test methods selection. Lourenço et al. (2015b) reported small pore sized samples significantly increase penetration time for the WDPT test due to the relatively low hydraulic conductivity, a function of pore size distribution. The water droplet tends to spread laterally instead of infiltrating. Tested samples were either planar monolayer or compacted for the SDM but compacted for the other test methods. Contact angle measurement using the SDM was widely used. Feyyisa and Daniels (2016) and Feyyisa et al. (2017), using the SDM and a drop image analysis software, described a dynamic approach to improve the repeatability of contact angle measurement for selected coal fly ash. Several studies found a positive correlation between contact angle (Feyyisa et al. 2017; Keatts et al. 2018; Lee et al. 2015), WEP (Feyyisa 2017; Keatts et al. 2018; Lee et al. 2015), and WDPT (Lee et al. 2015; Liu et al. 2012) and the dosage/concentration of the water repellent chemical/solution.

Table 3-5. Water repellent assessment methods.

| Author | Method | Test Sample |
|---|---|---|
| Bachman et al. (2002) | SDM | Compacted Sample |
| Czachor et al. (2010) | SDM | Planar Surface |
| Truong et al. (2011) | SDM | Planar Surface |
| Byun et al. (2012) | SDM | Planar Surface |
| Liu et al. (2012) | SDM and WDPT | Compacted Sample |
| Subedi et al. (2012) | WDPT, MED, SDM | Planar Surface & Compacted Sample |
| Jordan et al (2015) | WEP | Compacted Sample |
| Lourenço et al. (2015) | SDM | Compacted Sample |
| Lee et al. (2015) | WDPT, WEP | Compacted Sample |
| Choi et al .(2016) | SDM, WIT, and WP | Planar Surface |
| Feyissa (2017) | SDM and WEP/BP | Planar Surface |
| Keats et al. (2018) | SDM | Planar Surface |
| Karim et al. (2018) | SDM | Planar Surface |

3.5.1.4 Engineering properties of water repellent materials

In addition to assessing the degree of water repellent interaction, these methods can identify a correlation between water repellent interaction and some engineering properties such as index and physical, mechanical, and hydraulic/hydrological parameters. Lee et al. (2015) found an inverse relationship between WDPT and porosity with the water repellent solution concentration having a negligible effect. A similar observation was made using the WEP test. Also, the WDPT increased with an increase in the fraction of water repellent soil. Keatts et al. (2018) established a positive correlation between WEP and contact angle as a function of dry density of Ottawa sand and coal fly ash. The study made use of the Washburn equation described in Eq. 2-15 as a function of

pore radius and measured contact angle to predict the WEP for a tetrahedral and cubic packing. With the tetrahedral packing serving as the upper bound (high density) and the cubic packing as the lower bound (low density).

3.5.1.5 WRC of water repellent granular materials

Previous studies (Bauters et al. 2000; Liu et al. 2012; Lourenço et al. 2015b; Nieber et al. 2000) have reported that water repellent granular materials have lower water retention compared to corresponding wettable granular material with Liu et al. (2012) adding that the desaturation rate is a function of suction considering pore geometry. For the drainage cycle, Nieber et al. (2000) reported no significant change in WRCof hydrophobic sands with an increasing degree of water repellency, however, for the wetting cycle, pronounced variation in WRCwere observed with increasing degree of water repellency. Also, the hydrophilic sands recorded AEV of about one-half of the hydrophobic sands. In contrast, the study found a decreasing WEP with an increasing degree of water repellency in the hydrophobic sands.

Daniels and Hourani (2009) reported for saturated conditions, hydraulic conductivity decreased for a uniformly treated hydrophobic elastic silt. whereas Nieber et al. (2000) reported the same hydraulic conductivity for both hydrophilic and hydrophobic sands. Nieber et al. (2000) further demonstrated that water repellency influences drainage in unsaturated conditions using Eq. 3-2 given by Parker (1989) with hydrophobic sands predicted to have higher hydraulic conductivity compared to hydrophilic sands.

$$K_\psi = K_s(S_e)^{0.5}\left[1-(1-S_e)^{\frac{1}{m}}\right]^{2m} \qquad m = 1-\left(\frac{1}{n}\right) \qquad \text{Eq. 3-2}$$

Where $S_e$ = effective saturation.

Kim et al. (2013) evaluated the hydraulic properties of hydrophobic Jumunjin and Ottawa sands using a rigid wall permeameter. Results found no significant variation between hydrophilic and hydrophobic specimens with hydraulic conductivity increasing with porosity. Also, the results were comparable to estimated values using the Kozeny-Carman equation (Young 1993).

3.5.1.6 Mechanical characteristics

The general chemistry of OS demonstrated in Figure 3-3 indicates a transformation in the surface of substrates, which will most likely influence the mechanical behavior including strength and stiffness of the substrates. Several studies have demonstrated water repellency influences the strength parameters of various granular material. Byun et al. (2012), Lee et al. (2015), and Karim et al. (2018), at 0% degree of saturation, reported lower shear strength for hydrophobic treated materials (glass beads, silt, and Ottawa sand, respectively) compared to corresponding hydrophilic materials. Though the studies reported a further decrease in shear strength with an increase in the degree of saturation, Lee et al. (2015) reported the hydrophobic silt maintained a quasi-constant peak friction angle. Also, the peak friction angle decreased with increasing hydrophobicity. However, in the case of coal fly ash, it is not clear. Daniels et al. (2018) reported a marginal difference in peak friction angles for water repellent treated and untreated coal fly ash with 0% degree of saturation. Also, water repellency influences the shear stiffness behavior of water repellent granular material. Truong et al. (2011), under unsaturated conditions, reported a peak shear stiffness in hydrophilic glass beads compared with hydrophobically treated glass beads. However, the hydrophobic specimen maintained a quasi-constant small strain stiffness.

### 3.5.2 Characteristics of silanes

Silanes contain carbon-silicon bonds (CH3-Si-) structure termed organosilanes (OS). The carbon-silicon bonds are very stable, very non-polar and give rise to low surface energy, non-polar, water repellent interactions. The silicon hydride (–Si-H) structure is very reactive. It reacts with water to yield reactive silanol (-Si-OH). These silanols then react with other silanols to form a siloxane bond (-Si-O-Si-), a very stable structure. Also, in the presence of metal hydroxyl groups on the surface of glass, minerals, or metals, silanols will form very stable –Si-O-metal bonds to the surface. These reactions are critical for silanes to function as valuable surface-treating and coupling agents. Alkoxysilanes are the silanes that are used to couple organic polymers to inorganic materials, to improve adhesion and surface modification of substrates (Arkles et al. 1992; Xiameter 2009).

### 3.5.3 Characteristics of siloxanes

Siloxanes have silicon-oxygen-silicon bond (Si–O–Si) structure bonds termed silicones or silicone polymer. Siloxanes are oligomeric, chained molecular structures, alkylalkoxysiloxanes that have similar benefits as silanes considering reactivity and water repellency but have a low vapor pressure. Under dry conditions, they exhibit slightly less penetration than silanes. Whereas silanes have only one silicon atom, siloxanes have more than one silicon atom. Siloxanes exhibit significant resistance to oxidation, ozone, UV exposure and have significant thermal stability with virtually no biodegradation. Also, they are characterized by high compressibility and shear resistance, good dielectric properties (Buser 2013; Global Silicon Council 2019).

### 3.5.4 Chemistry of silanes and siloxanes

The general formula of organosilanes generally represented as $R'Si(OR)_3$ consists of two types of functional groups namely alkoxy group (OR) and organic functionality R'. The R group reacts with an organic polymer. During the coupling reaction, the OR group hydrolyzes and reacts with inorganic substrates (soils and CCRs) to form siloxane bonds and metal hydroxyl groups to form -Si-O-metal bonds. These reactions characterize the performance of silanes as surface treating and coupling agents. The general chemistry of organosilane is defined by four distinct processes including hydrolysis, condensation, hydrogen bonding, and bond formation, as illustrated in Figure 3-3. However, hydrolysis and condensation describe the kinetics of silane formation and reaction though very complex. Due to the complexity of the hydrolysis and condensation process several studies (Arkles et al. 1992; Brinker 1988; Brochier Salon and Belgacem 2011; Brzoska et al. 1994; Deetz and Faller 2015; Jiang et al. 2006; Krasnoslobodtsev and Smirnov 2002; Pantoja et al. 2010) have been conducted to explain general trends of which some are discussed in the following section.

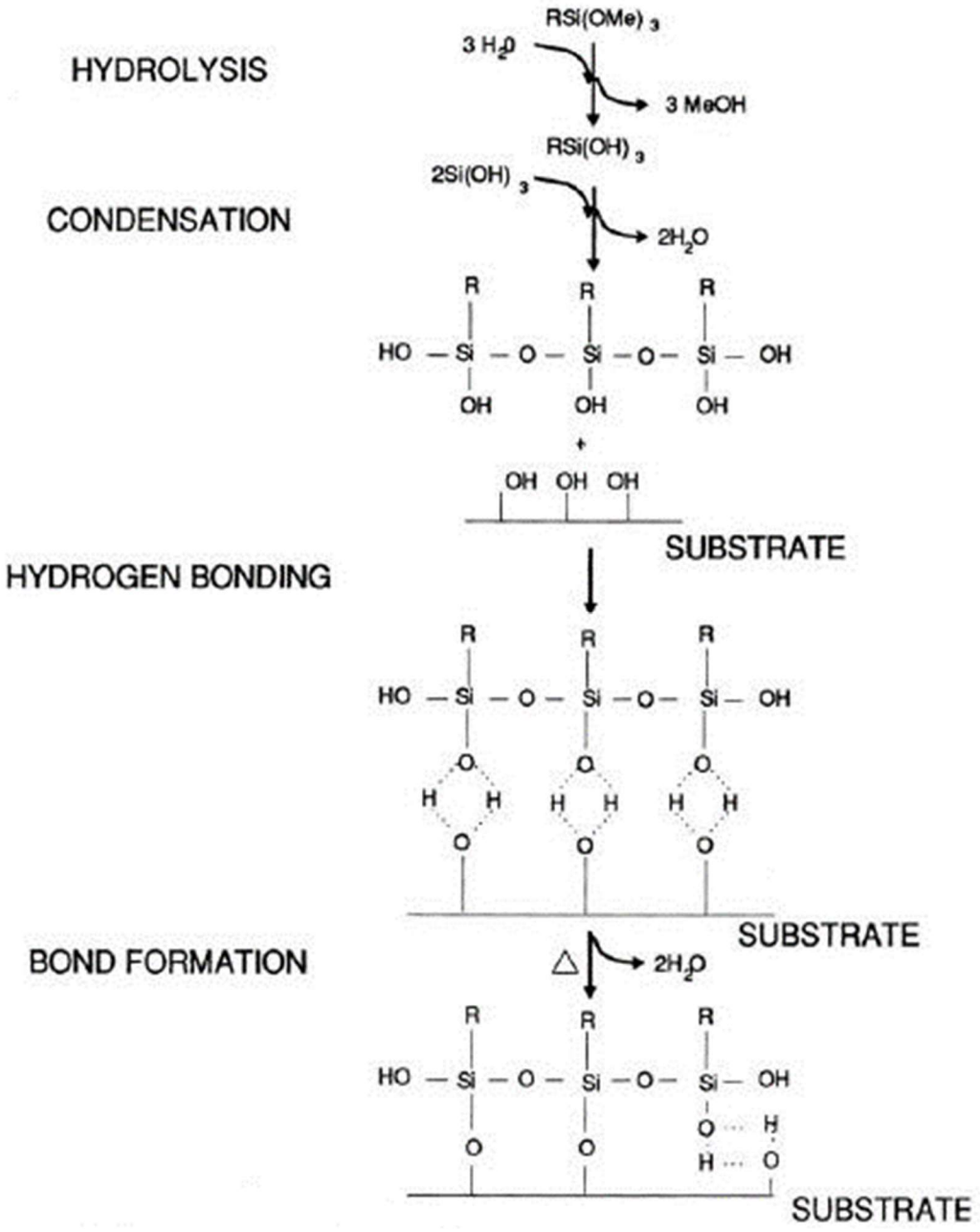


Figure 3-3. The general mechanism for silane reaction and bonding (Arkles et al. 1992).

### 3.5.5 Factors influencing organosilanes chemistry

#### 3.5.5.1 Effect of water and active ingredient.

For the hydrolysis process to be initiated, an interaction between an alkoxysilane molecule and water is required. The water is mostly added water; however, it can be present on the substrate or present in the atmosphere (Arkles 1977). The interaction results in the replacement of the alkoxy group on the silicon atom with a hydroxyl group. To completely replace all alkoxy molecules adequate reaction time is needed as the replacement usually does not occur at the same time (Jiang et al. 2006). The amount of water and active ingredient impacts the degree of polymerization of the silanes (Arkles 1977). Also, the concentration on the siloxane solution determines the thickness of a polysiloxane layer, which alters the surface energy of the substrate (Arkles 1977). Krasnoslobodtsev and Smirnov (2002), in the study of the effect of water on the salinization process of silica by trimethoxysilanes, reported that the surface concentration of coumarin dye improved 1.3 times higher than that without water treatment.

#### 3.5.5.2 Effect of pH.

Optimum hydrolysis and condensation reactions are dependent on the pH condition of the aqueous solution formed. Alkaline conditions lead to condensation of partially hydrolyzed molecules before complete hydrolysis, whereas, for acidic medium, hydrolysis in most cases is faster than condensation reaction(Jiang et al. 2006). Jiang et al. (2006), in the study of the effects of temperature and solvent on the hydrolysis of alkoxysilane under alkaline conditions, reported that the condensation reaction takes place faster compared to the hydrolysis reaction which was rate-limiting for the overall reaction. Pantoja et al. (2010), in the study of the influence of pH on the hydrolysis

process of γ-Methacryloxypropyltrimethoxysilane, reported that neutral pH conditions lead to longer hydrolysis times for a complete hydrolysis process with decreased hydrolysis times for acid and basic solutions.

3.5.5.3 Effect of temperature and solvent.

Solvents significantly affect the hydrolysis and condensation of the kinetics of silane formation and reactions. Hydrolysis of alkoxysilane in basic condition is greatly influenced by organic solvents with the potential of altering the existing state of water, and subsequently, the hydrolysis rate (Jiang et al. 2006). The repellent interaction of a silanized surface is attributed to the influence of organic solvents on the structure of water (Jiang et al. 2006). Alcohol, a special solvent for alkoxysilane hydrolysis, allows for the exchange reaction of alkoxy groups to occur when used with an alkoxy group different from the alkoxy groups of the silane (Jiang et al. 2006). The formation of a siloxane bond during polymerization can occur by an alcohol condensation reaction (Brinker 1988). Jiang et al. (2006), in the study of the effects of temperature and solvent on the hydrolysis of alkoxysilane under alkaline conditions, reported that different reaction rates were observed with varied reaction temperatures and solvents. An indication of dependence of alkoxysilane hydrolysis on temperature and solvents.

Arkles (2006) detailed factors that impact the maximization of silane reactions in the surface modification process. These factors include concentration and type of surface hydroxyl groups, hydrolytic stability of the bond formed which has to do with absorbed water interfering with the silane coupling process, and physical dimensions of the substrate or substrate features.

## 3.6 Summary

This chapter presented a review on the state of research regarding the engineering properties of CCRs and its impact on defining the WRCof CCRs. Selected methods of measuring the WRCand unsaturated hydraulic conductivity were presented. Also, the current state of engineered water repellency research in geotechnical and geoenvironmental engineering practice was reviewed with a focus on water repellency assessment, standardized geotechnical tests, and water retention characteristic measurement. Also, general information on the chemistry and factors that influence the process of engineering water repellency using OS chemical were discussed.

In conclusion, the summary of the review related to the topic under study is presented below.

1. The engineering properties of CCRs have been extensively explored and can significantly influence the WRC of CCRs.
2. Some traditional methods used in the suction measurement of typical Geotech soils apply to CCRs and most likely exhibit similar advantages and limitations.
3. The WRC in terms of laboratory measurement, use of parametric, and predictive models have not been fully explored.
4. There is a significant knowledge gap in engineering water repellency of CCRs and geotechnical soils in general for both laboratory and field evaluation.

# CHAPTER 4: EXPERIMENTAL METHODS

## 4.1 Introduction

This chapter describes the experimental methods adopted to address the objectives of this study. The experimental methods are designed to characterize the physical and index property test which includes specific gravity, particle size distribution, and Atterberg limit test; chemical composition tests which include XRD and XRF analyses for elemental and mineral compositions, respectively; saturated hydraulic conductivity test using the falling head method; the mechanical test which include compaction characteristics test, direct shear test, and triaxial shear test. Various methods were identified to describe the WRC of the compacted CCRs. However, the study was limited to the axis-translational technique – pressure plate extractor (PPE) and Tempe cells (TC), dewpoint potentiometer (WP4C), and the steady-state unsaturated flow apparatus (UFA).

In addition, selected standardized test methods were considered and modified, in some cases, to perform engineering characterization of the water repellent CCR. Detailed experimental designs to investigate potential factors influence engineered water repellent treatment of CCRs for practical applications are presented.

## 4.2 Testing Materials

### 4.2.1 CCRs

In all, five CCRs, which include fly ash, lignite fly ash, and flue gas desulfurization residues from three utilities, were considered in this study. The material designation, type, and utility are presented in Table 4-1.

Table 4-1. Details of CCRs.

| Designation | Type | *Utility |
|---|---|---|
| CCR 1 | Fly ash class F | A |
| CCR 2 | Fly ash class F | B |
| CCR 3 | Fly ash class F | C |
| CCR 6 | Lignite fly ash | B |
| CCR 7 | FGD Gypsum | B |

* The utility names are not disclosed to respect client confidentiality and non-disclosure agreements.

4.2.2 Water repellent chemical

The water repellent chemical for synthesizing water repellency of the selected CCRs is a commercially available product from Dow Corning called IE-6683 water repellent emulsion. It is a water-based silane-siloxane emulsion blend with 40% weight active ingredients. The active ingredients are alkoxysilane and polydimethylsiloxane. When diluted in water, it generates volatile organic content < 200 g/l requiring the use of personal protective equipment.

4.3 CCR Engineering Characterization

As reported by Dumenu et al. (2017), Table 4-2 presents details of the physical and index properties on the CCRs considered for this study. The specific gravity of the CCRs was found to range from 2.28 to 2.67 as presented in Table 4-2. The particle size distribution was determined in accordance with ASTM D422 (ASTM 2007). Figure 4-1 shows that the fly ash and gypsum samples are predominantly silty sized particles as more than 80% passed through sieve size 75 □m. However, Lignite fly ash comprised a significantly equal amount of sand and silt particles, with approximately 46% retained on sieve size

75μm. Table 4-2 shows a summary of the percentages of the CCRs, as illustrated in Figure 4-1. The Atterberg limits tests, plastic limit (PL), and liquid limit (LL), which describes the consistency boundaries that define the plastic states of the CCRS were performed in accordance with ASTM D4318 (ASTM 2017). All but CCR 3 and 6 showed liquid limit between 20 % and 24%, but none of the samples showed plastic limit. Therefore, the plasticity index was determined as the difference between the liquid limit and the plastic limit the CCRs were classified as nonplastic (NP) as presented in Table 4-2.

Table 4-2. Summary of engineering characteristics of CCRs (Dumenu et al. 2017).

| Property | CCR | | | | |
|---|---|---|---|---|---|
| | 1 | 2 | 3 | 6 | 7 |
| | Class F Fly Ash | | | Lignite Coal Ash | FGD Gypsum |
| Specific Gravity | 2.36 | 2.67 | 2.31 | 2.56 | 2.28 |
| Particle Size Characteristics, % | | | | | |
| Sand (4.75-0.075mm) | 8 | 11 | 14 | 46 | 4 |
| Silt (0.075-0.005 mm) | 74 | 82 | 83 | 43 | 85 |
| Clay (<0.005 mm) | 18 | 7 | 4 | 11 | 11 |
| USCS classification | ML | ML | ML | SM | ML |
| Standard Proctor Compaction: | | | | | |
| Maximum dry unit weight, $kN/m^3$ | 15 | 16 | 14 | 15 | 15 |
| Optimum water content, % | 20 | 18 | 22 | 18 | 12 |
| Saturated Hydraulic Conductivity, cm/s* | 2E-05 | 9E-05 | 1E-04 | 5E-05 | 6E-05 |
| Atterberg Limit | | | | | |
| Liquid limit, % | 24 | 23 | NP | NP | 24 |
| Plastic limit, % | NP | NP | NP | NP | NP |

**Not published*

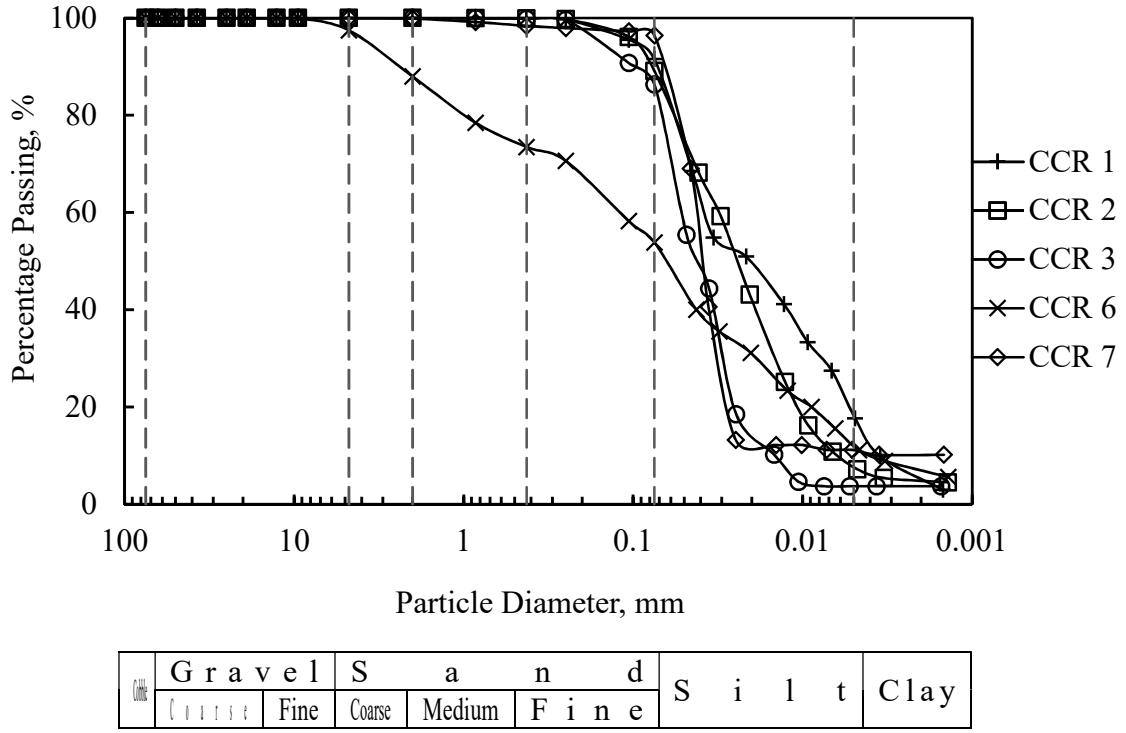


Figure 4-1. Particle size distribution of CCRs.

4.3.1 Compaction characteristics

The compaction characteristics of the CCRs were determined in accordance with ASTM D698 (ASTM 2012) using the compaction energy of 600 kN-m/m$^3$. The samples were mellowed for 24 hours prior to compaction due to the influence of the morphology of CCR particles. Also, the class C fly ash which has self-cementing reactivity when in contact with water, was immediately compacted to prevent flash setting as presented in Figure 4-2. The compaction characteristics of the CCRs are shown in Figure 4-3

Figure 4-2. Flash setting of Class C fly when mellowed for compaction characteristics test.

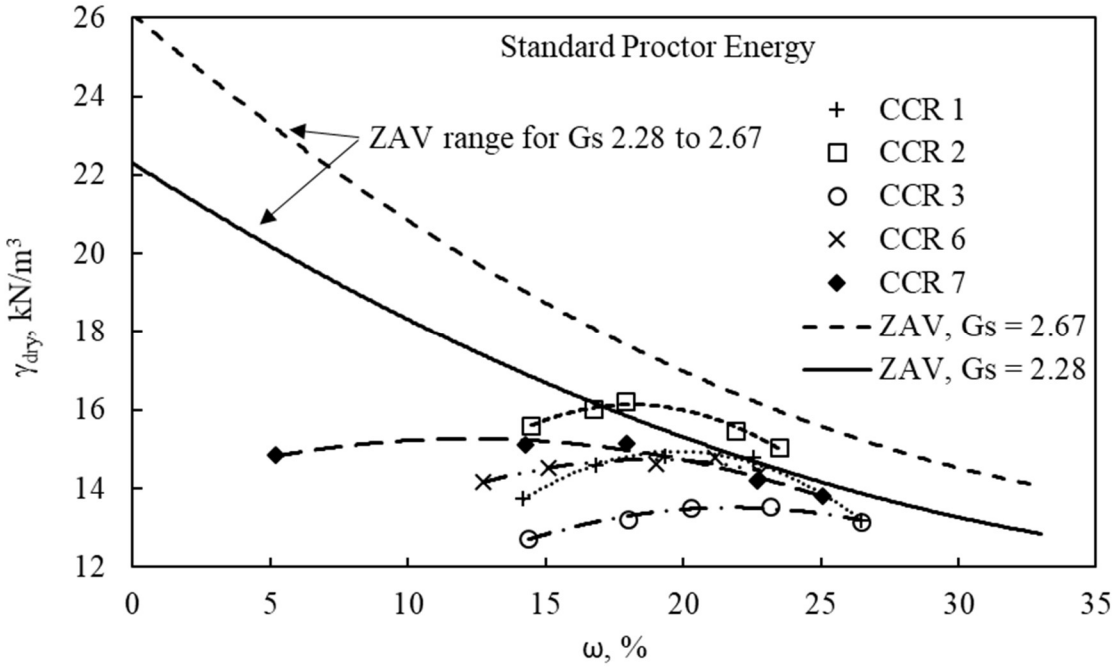


Figure 4-3. Compaction characteristics of CCRs using Standard Proctor Energy as per ASTM D698.

### 4.3.2 Maximum and minimum density

The maximum and minimum dry unit weights were performed in accordance with ASTM D4253 (ASTM 2016a) and ASTM D4254 (ASTM 2016c), respectively, on selected CCRs, namely CCR1, CCR 2, and CCR 3. However, some modification was made to the procedure in line with recommendations by Kim et al. (2006) to address dusting that will result from the vibratory motion. Table 4-3 presents the maximum and minimum dry unit weights of the untreated and OS-treated CCR compared to Kim et al. (2006). As reported in Daniels et al. (2018), the maximum dry unit weights are relatively low compared to those obtained using standard Proctor energy at optimum water content. The OS-treated CCR samples slightly increased in weight presumably as a result of the OS grafting reducing the repulsive charges of the particles hence decreasing the resistance that encourages sliding allowing more mass in unit space.

Table 4-3. Maximum and minimum dry unit weights of untreated and OS-treated CCRs (Daniels et al. 2018).

| Reference | Dry Unit Weight, kN/m$^3$ | |
|---|---|---|
| | Minimum | Maximum |
| CCR | | |
| 1 | 10.46 | 13.14 |
| 2 | 11.43 | 14.65 |
| 3 | 10.29 | 13.05 |
| OS-treated CCR | | |
| 1 | 11.84 | 13.75 |
| 2 | 11.43 | 14.65 |
| 3 | 11.11 | 13.23 |
| Kim et al. (2006) | | |
| Wabash River | 10.99 | 14.64 |
| AB Brown | 12.10 | 15.69 |
| FB Culley | 12.30 | 15.49 |

### 4.3.3 Elemental and mineral compositions

As reported by Dumenu et al. (2017) and Daniels et al. (2018), the elemental and mineral compositions of selected CCRs were analyzed using X-ray diffraction (XRD) and X-ray fluorescence (XRF), respectively. The elemental composition analysis as presented in Table 4-4 indicates the presence of oxides (%) including silica (SiO2), ferric oxide (Fe2O3), aluminum oxide (Al2O3) and calcium oxide (CaO), trace elements (ppm) including arsenic (As), barium (Ba), bromine (Br), copper (Cu), lead (Pb), antimony (Sb), selenium (Se), strontium (Sr), and zinc (Zn), and loss on ignition (%). The mineral composition analysis, as presented in qualitatively indicates the presence of quartz, hematite, magnetite, mullite, gypsum, hannebachite, lime, calcite, periclase and ettringite.

Quantitative analysis of the mineral compositions was also performed on selected CCRs (CCR 2 and 5), as presented in Table 4-6. The test samples have a high amorphous phase resulting in the XRF analysis, not fitting the XRD analysis (Dumenu et al 2017). Both samples show high content of SiO2; however, CCR 5 has significant amount of CaO element compared to negligible amount in CCR 2 as presented in Table 4-4. The results further confirm the classification of CCR 2 as class F fly ash and CCR 5 as class C fly ash in accordance with ASTM C618 (ASTM 2015a).

Table 4-4.Quantitative analysis of the elemental composition of select CCRs based on XRF analysis (Dumenu et al. 2017).

| Compounds | CCR 2 (%) | CCR 5 (%) |
|---|---|---|
| $Al_2O_3$ | 14.8 | 8.5 |
| BaO | 0.07 | 0.77 |
| CaO | 1.29 | 27.28 |
| $Cr_2O_3$ | 0.02 | <0.01 |
| $Fe_2O_3$ | 19.24 | 3.8 |
| $K_2O$ | 1.76 | 0.43 |
| MgO | 0.59 | 3.17 |
| MnO | 0.03 | 0.01 |
| $Na_2O$ | 0.88 | 1.12 |
| $P_2O_5$ | 0.23 | 1.54 |
| $SiO_2$ | 53.77 | 49.15 |
| SrO | 0.05 | 0.32 |
| $TiO_2$ | 0.86 | 0.98 |
| $V_2O_5$ | 0.03 | 0.02 |
| C | 1.712 | 0.221 |
| S | 0.939 | 0.666 |
| LOI | 3.62 | 1.53 |

Table 4-5. Qualitative analysis of the mineral compositions of selected CCRs using XRF (Daniels et al. 2018).

| Mineral Composition | CCR | | | | |
|---|---|---|---|---|---|
| | 1 | 2 | 3 | 5 | 6 |
| Quartz | x | x | x | x | x |
| Hematite | x | x | x | x | |
| Magnetite | | x | | | |
| Mullite | x | x | x | | x |
| Gypsum | | | | | x |
| Hannebachite | | | | | x |
| Lime | | | | x | |
| Calcite | | | | x | x |
| Periclase | | | | x | |
| Ettringite | | | | x | |

Table 4-6. Quantitative analysis of the mineral composition of select CCRs based on XRD analysis (Dumenu et al. 2017).

| Compounds | CCR 2 (%) | CCR 5 (%) |
|---|---|---|
| $Al_2O_3$ | 14.8 | 8.5 |
| BaO | 0.07 | 0.77 |
| CaO | 1.29 | 27.28 |
| $Cr_2O_3$ | 0.02 | <0.01 |
| $Fe_2O_3$ | 19.24 | 3.8 |
| $K_2O$ | 1.76 | 0.43 |
| MgO | 0.59 | 3.17 |
| MnO | 0.03 | 0.01 |
| $Na_2O$ | 0.88 | 1.12 |
| $P_2O_5$ | 0.23 | 1.54 |
| $SiO_2$ | 53.77 | 49.15 |
| SrO | 0.05 | 0.32 |
| $TiO_2$ | 0.86 | 0.98 |
| $V_2O_5$ | 0.03 | 0.02 |
| C | 1.712 | 0.221 |
| S | 0.939 | 0.666 |
| LOI | 3.62 | 1.53 |

### 4.3.4 Saturated hydraulic conductivity

The saturated hydraulic conductivity ($k_s$) of the compacted CCRs were measure using the falling head (increasing tailwater) method, as described in ASTM D5084 (ASTM 2016b). The setup used in this study is shown in Figure 4-4. Duplicate test samples were subcored from a standard Proctor compacted sample using a Shelby tube of equal diameter to the flexible wall permeameter of 1.4” diameter. The samples were fully

saturated using a backpressure approach. The hydraulic conductivity was measured as a function of effective stresses (σ') including 7 kPa, 35 kPa, 100 kPa, and 500 kPa. For each effective stress the burette reading was logged at every 5 mins for 50 minutes. The average saturated hydraulic conductivity at varying effective stresses as presented in Figure 4-5 range between the orders of magnitude from $10^{-4}$ to $10^{-5}$ cm/s, consistent with values reported in previous studies for CCRs (Bachus et al. 2019; Butalia and Wolfe 1999; Kaniraj and Gayathri 2004; Pease et al. 2017a) . In general, there was a decreasing trend in the average saturated hydraulic conductivity as the effective stresses increased. Thus, liners or structural fill/embankment that mostly experience high effective stresses would experience similar hydraulic conductivity with depth. Kaniraj and Gayathri (2004) reported a similar trend of hydraulic conductivity with varying vertical effective stresses for selected fly ash.

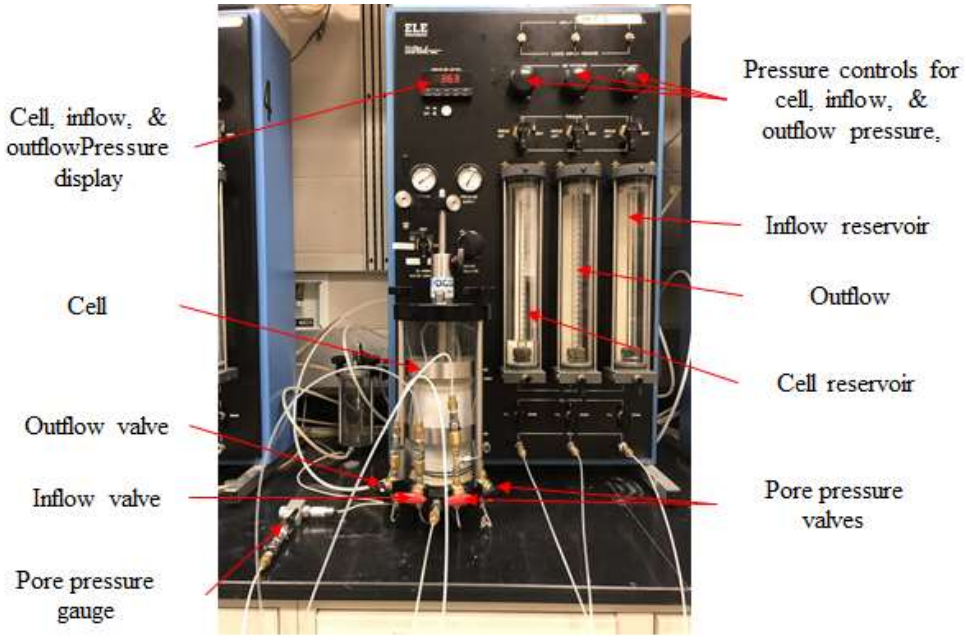


Figure 4-4. Flexible wall permeameter setup consisting of triaxial cell and pressure control panels used in measuring the saturated hydraulic conductivity of CCRs.

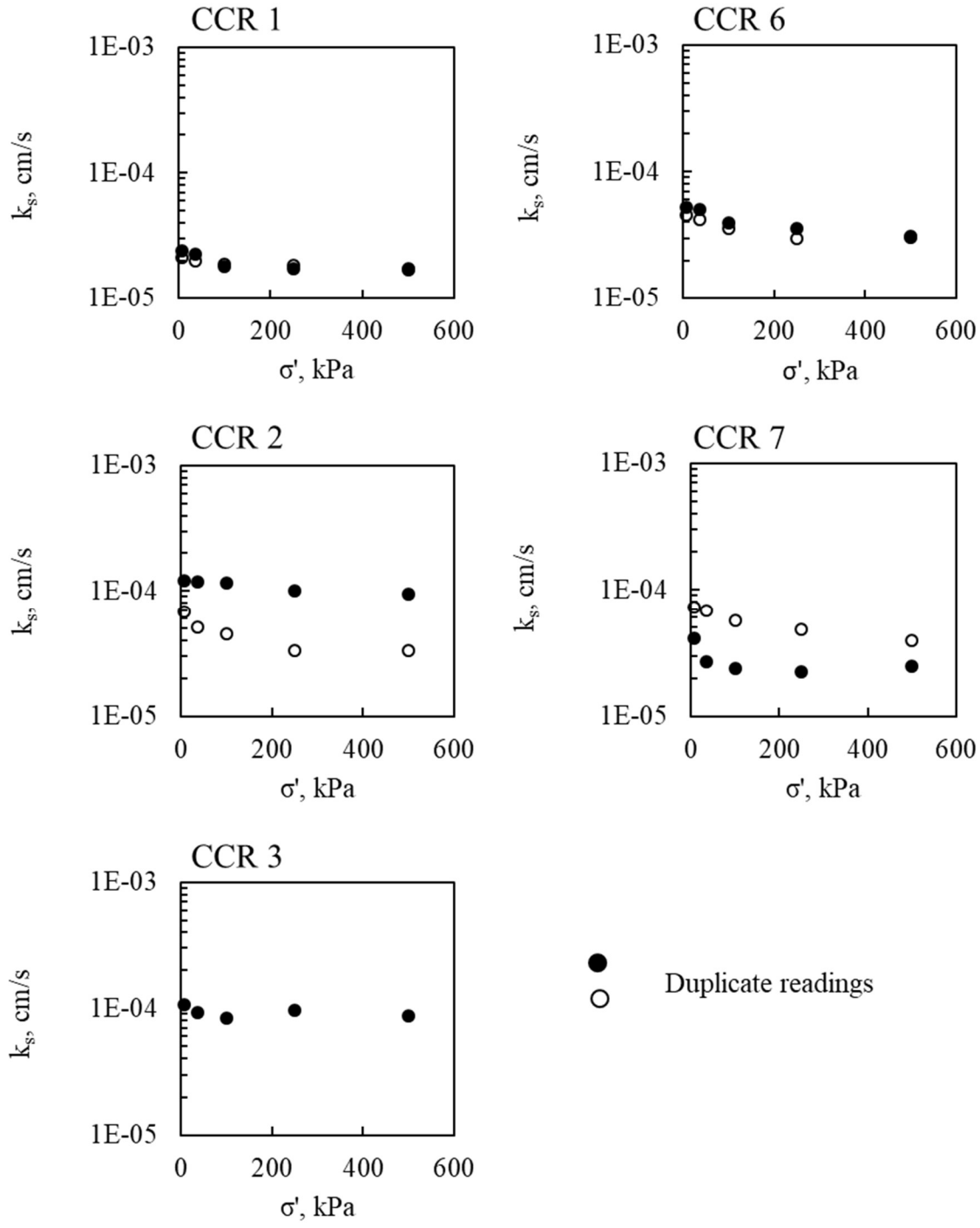


Figure 4-5. Saturated hydraulic conductivity as a function of the effective stress of CCRs.

### 4.3.5 Strength characteristics

#### 4.3.5.1 Direct shear test

The direct shear strength test was performed in accordance with ASTM D3080 (ASTM 2011b) using a Geojac Digishear device with a circular shear box of diameter 63.5 mm and height 36.5 mm. The samples were tested at normal stresses of 50 kPa, 150 kPa, 300 kPa, and 600 kPa. The tests were performed as displacement controlled for 8mm displacement (approximately 12.6% of shear box diameter) while maintaining a constant shearing rate of 1mm/min. Samples were tested in two different preparation conditions – dry CCR and standard Proctor compacted CCR at OMC to investigate the effect of mode of compaction of CCRs. The OS-treated CCRs were treated following the treatment protocol described by Feyyisa and Daniels (2016) and Feyyisa et al. (2017)

As presented in Table 4-7, Both dry CCRs and OS treated CCRs recorded cohesion values with CCR 1of 5.8 kPa and 8.5 kPa, respectively, with dry CCR 2 recording the maximum of 13 kPa and dry OS-CCR 3 recording a maximum value of 10 kPa. This observation could be a result of the apparent attractive forces present in the CCRs. The OS treatment of 8g/kg had an insignificant effect on the CCRs as both samples recorded relatively similar values of peak and residual angles contrary to previous studies (Byun et al. 2012; Lee et al. 2015). For dry and OMC compacted CCRs, the results indicate the OMC compacted sample is marginally lower than the dry compacted samples. However, the overall differences are negligible. The OMC compacted samples recorded very high cohesion values. Presumably, due to capillary forces resulting from suction activities, draw particles together, giving the OMC compacted specimens apparent cohesion as recorded. For details on the shear stress

displacement relationship and the Mohr-Coulomb failure, envelope refer to Daniels et al. (2018)

Table 4-7. A summary of direct shear strength parameters of dry CCR and OS-treated CCR and OMC compacted CCR (Daniels et al. 2018).

| | Peak | | | Residual | | |
|---|---|---|---|---|---|---|
| | C' = 0 | Cohesion | | C' = 0 | Cohesion | |
| | ø', ° | ø', ° | C', kPa | ø', ° | ø', ° | C', kPa |
| CCR | | | | | | |
| 1 | 30.2 | 29.7 | 5.8 | 30.2 | 29.7 | 5.8 |
| 2 | 31.7 | 30.6 | 13.1 | 31.1 | 30.6 | 6.9 |
| 3 | 30.9 | 30.4 | 6.6 | 30.7 | 30.7 | 0.0 |
| OS-CCR | | | | | | |
| 1 | 31.0 | 30.4 | 7.1 | 30.8 | 30.6 | 1.8 |
| 2 | 30.4 | 29.8 | 7.4 | 30.4 | 29.8 | 7.3 |
| 3 | 29.8 | 28.9 | 10.2 | 29.7 | 29.1 | 6.9 |
| OMC CCR | | | | | | |
| 1 | 33.1 | 28.7 | 53.6 | 32.1 | 30.1 | 24.2 |
| 2 | 32.8 | 28.4 | 53.0 | 32.2 | 28.8 | 41.1 |
| 3 | 34.5 | 31.4 | 37.0 | 31.9 | 30.2 | 20.4 |

4.3.5.2 Unconsolidated undrained triaxial test

The unconsolidated undrained (UU) shear strength of standard Proctor compacted CCRs were determined in accordance with ASTM D2850 (ASTM 2015b). The samples were tested at confining stress of 25 kPa, 50 kPa, and 100 kPa. The tests were performed, maintaining a constant shearing rate of 1mm/min. Results presented in Table 4-8 are

comparable to previous studies (Kaniraj and Gayathri 2003; Kaniraj and Havanagi 2001; Pal and Ghosh 2009). Figure 4-6 show the p-q plots for the UU test of CCRs

Table 4-8. A summary of unconsolidated undrained shear strength parameters of standard Proctor compacted CCRs.

| CCR | Shear Strength Parameters | |
|---|---|---|
| | ø, ° | c, kPa |
| 1 | 49.60 | 60.46 |
| 2 | 32.11 | 27.46 |
| 3 | 34.62 | 31.12 |
| 6 | 28.65 | 69.78 |
| 7 | 31.48 | 28.67 |

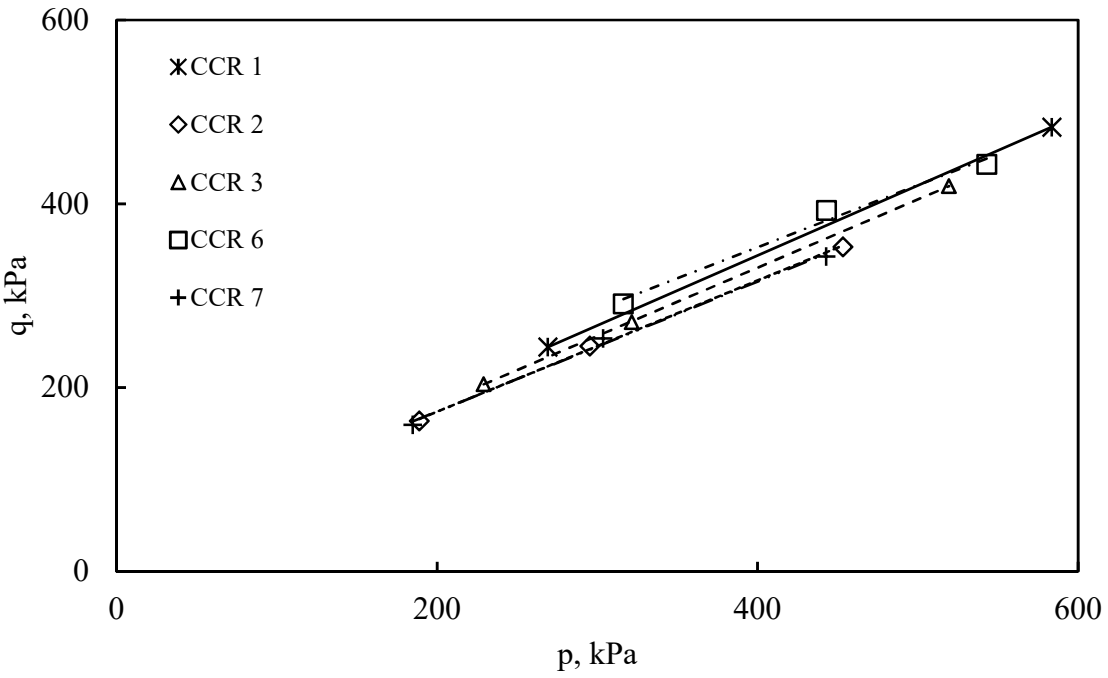


Figure 4-6. Combined p-q plot of CCRs

## 4.4 Physio-chemical Analysis

### 4.4.1 Thermogravimetric analysis

The thermogravimetric analysis (TGA) of the CCRs was performed using the SDT Q600 (TA Instruments, Delaware). At a constant rate of heating, 20°C/min, the test specimens were heated room temperature to 1000°C in a nitrogen atmosphere. Detailed TGA results of the CCRs showing the percentage mass as a function of temperature are presented in Daniels et al. (2018). The results showed that CCR 7 had significant weight loss with temperature > 85°C. As a result, the oven temperature was set to 60 °C in the determination of the geotechnical properties of the CCRs.

### 4.4.2 EC and pH

The pore fluids of the CCRs at saturation were analyzed by measuring the EC and pH. The pore fluid was extracted as described by Gartley (2011). However, the liquid to solid ratio was based on the saturation water content of a compacted CCR at maximum dry density. Thus, corresponding to a liquid to solid of approximately 0.5 as presented in Table 4-9. The measured DI water was added to dry samples of untreated CCR and mixed thoroughly until saturation is achieved where the matrix glistens and flows slightly. The pore fluid was extracted after a 24-hour equilibration period using a 0.45μm filter paper, Bucher funnel, and suction. The Mettler Toledo probe shown in Figure 4-7 was used to measure the EC and pH of the pore fluid extract.

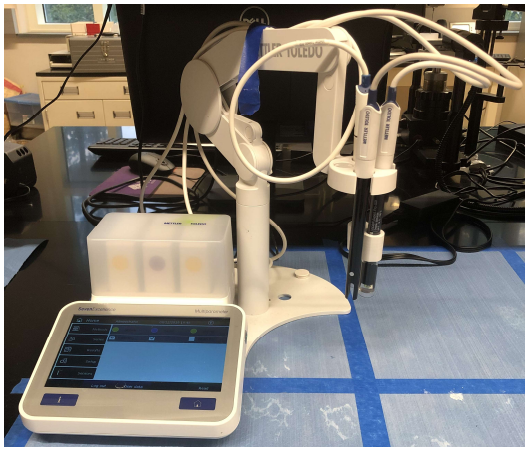

Figure 4-7. The Mettler Toledo probe used to measure the EC and pH of the saturated CCR extract.

Table 4-9. EC and pH measurement of saturation pore fluid of CCRs.

| | Water | | CCR | | | | |
|---|---|---|---|---|---|---|---|
| | Tap | DI | 1 | 2 | 3 | 6 | 7 |
| Liquid to Solid ratio | | | 0.5 | 0.5 | 0.6 | 0.6 | 0.4 |
| EC, µS/cm | 97 | 8 | 5588 | 34689 | 3240 | 8397 | 17656 |
| pH | 9.2 | 8.2 | 9.7 | 9.0 | 9.2 | 8.6 | 8.5 |

The EC values of the CCR pore fluids were significantly higher compared to the reference fluids, tap water, and DI water, presumably due to the unique chemical composition of CCRs. The pH can be classified as basic as the pH values are greater than 7. Most CCRs are classified as basic due to the presence of lime or CaO (Mudd 2001).

## 4.5 Unsaturated Property Measurements of Untreated CCRs

### 4.5.1 WRC measurement

The axis translation methods, PPE and TC, UFA, and WP4C were selected to establish the WRC of the compacted CCRs in a desaturation process. The tests were done in accordance with ASTM D6836 (ASTM 2002) and device operational guides (Decagon

Devices Inc. 2015; Soilmoisture Equipment Corp. 2015). The axis translation method and UFA accounted for the matric suction-water content relationship, whereas the WP4C also known as the chill-mirror dew point, accounted for the total suction-water content relationship. The WP4C complimented the axis translation methods and UFA in the residual zones as presented in Figure 2-5. Thus, a complete suction range was established.

The PPE comes in 5-bar and 15-bar configuration for suction range 0 – 500 kPa and 0 – 1500 kPa, respectively, as shown in Figure 4-8. A typical configuration consists of a high air entry (HAE) ceramic disk, PPE with accessories to support the HAE ceramic disk, and pressure supply system. The HAE ceramic disk can be described as extremely porous to moderately porous with hydraulic conductivity ranging in the order of $10^{-5}$ cm/s to $10^{-9}$ cm/s, and it is chemically inactive to most fluids (Padilla et al. 2006). The pressure plate extractor is fitted with accessories to allow multiple installments of HAE disk.

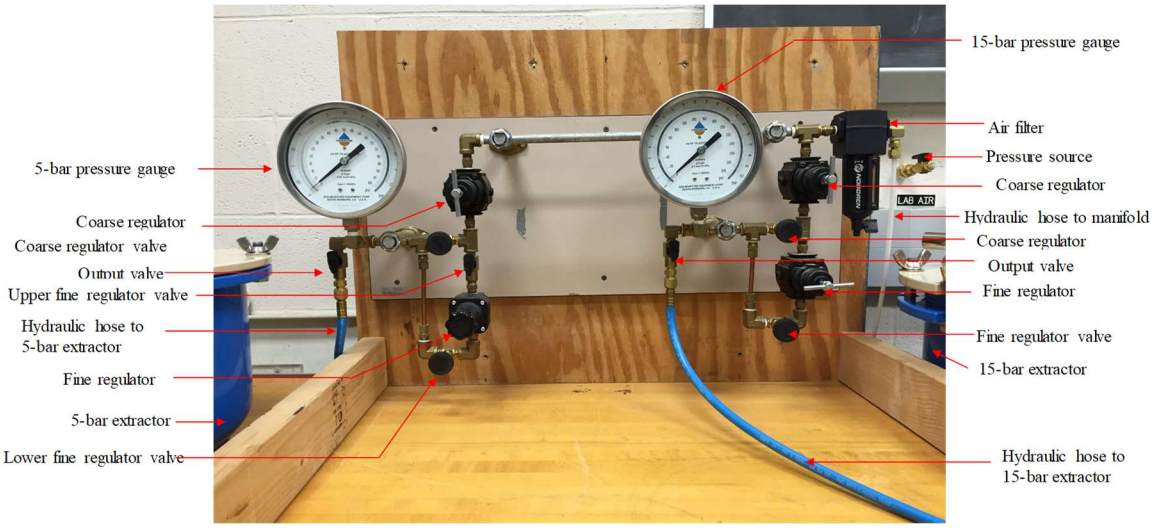


Figure 4-8. Pressure plate extractor assembly in a UNC Charlotte laboratory.

The TC consists of a top and base cap, a brass cylinder of approximate dimension 30 mm x 85 mm, and a 2-bar HAE ceramic disk for suction range 0 kPa – 200 kPa. Unlike the PPE, the TC allows one test specimen per cell; however, multiple cells can be used in an experiment, as demonstrated in Figure 4-9. The test specimen is less likely disturbed during the logging of mass as compared to the PPE test procedure. During air pressure application, extracted pore fluid can be collected for further analysis.

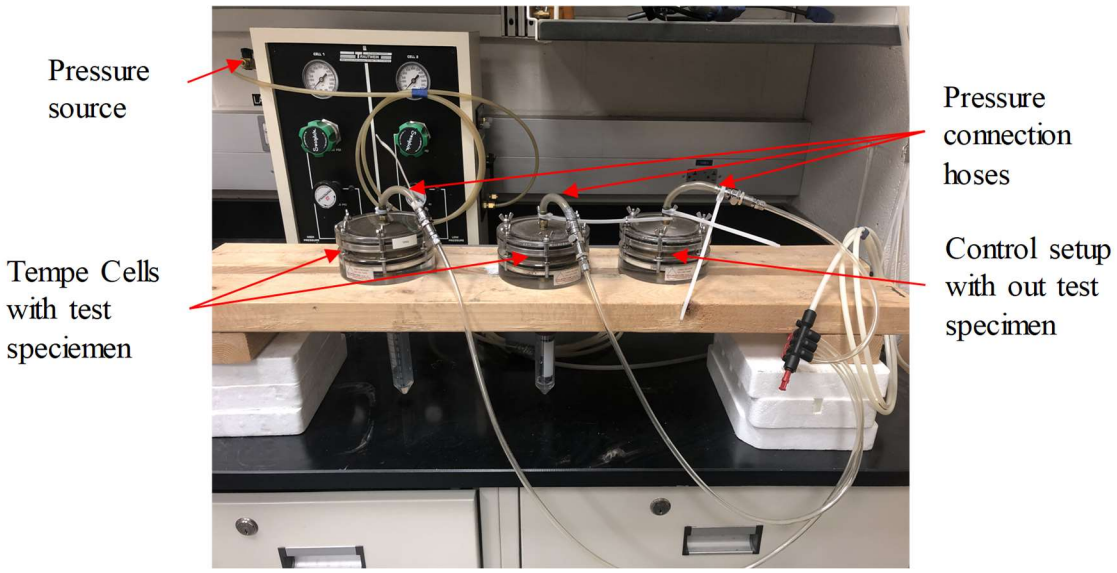


Figure 4-9. Tempe cell test assembly.

The UFA measures the matric suction of a porous media under centrifugal force is governed by Eq. 4-1.

$$\psi_m = \frac{\rho\omega^2}{2g}(r_1^2 - r_2^2) \qquad \text{Eq. 4-1}$$

Where $\psi_m$ = matric suction, $g$ = acceleration due to gravity, $r_1$ = radial distance to the top of the test specimen, $r_2$ = radial distance to the bottom of the test specimen, ω = angular speed, ρ = density of sample fluid. For the given geometry of the UFA rotor and sample

holder assembly of the UFA presented in Figure 4-10, which are constant, the matric suction applied to the test specimens were predetermined and summarized in Table 4-10 as a function of rotational speed.

Table 4-10. UFA matric suction chart used for this study.

| Speed, rmp | Suction, kPa |
|---|---|
| 300 | 4 |
| 600 | 17 |
| 800 | 30 |
| 1000 | 47 |
| 1200 | 68 |
| 1800 | 153 |
| 2100 | 208 |
| 2500 | 295 |
| 3000 | 425 |

The unsaturated flow apparatus consists of an ultracentrifuge with a constant flow micro infusion pump and rotating seal assembly, as shown in Figure 4-10. Mounted on the rotating seal assembly is the sample cup containing the sample holder which contains the test specimens. The sample cup has an effluent collection chamber that collects effluent as water is pumped into the sample during rotation. As discussed in section 2.2.1.3, there is no flow into the sample during the suction measurement; therefore, steady-state condition does not exist. Equilibrium condition was attained when no fluid drained from the test specimen. The centrifuge chamber was maintained at room temperature of 25 °C ± 1. Duplicate test specimens were subcored from a standard Proctor compacted sample and trimmed to fit specimen cups with the initial masses

logged. Prior to subcoring, a saturated filter paper was installed at the bottom of the specimen cup to prevent the loss of CCR particles. Saturation can be achieved by allowing the flow of water under relatively low rotation speed or by using capillary action when placed in a water bath. For this study, matric suction measurements were performed after the wetting cycle of the unsaturated hydraulic conductivity was conducted which resulted in the test specimens being saturated at the end of the wetting cycle.

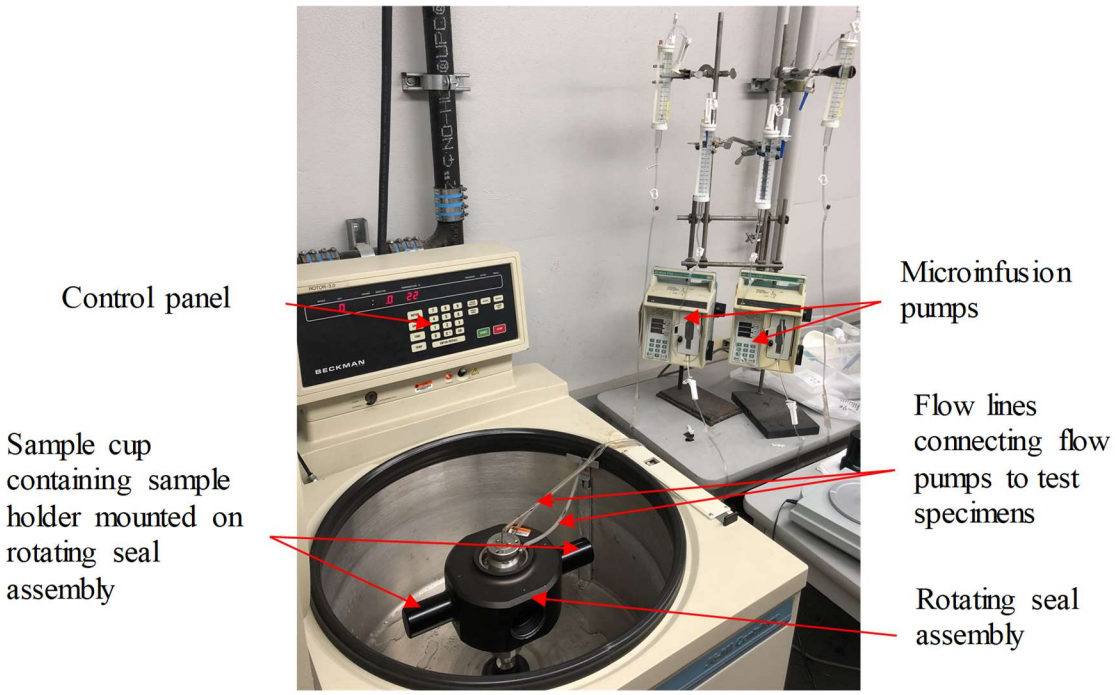


Figure 4-10. Unsaturated Flow Apparatus (Centrifuge) with microinfusion pumps setup located in Dr. Menezes' lab in Cal State LA.

The Dewpoint Potentiometer (WP4C) device, as shown in Figure 4-11, operates on the principle of the dewpoint technique. It has a fan, a mirror, a photodetector cell, and an infrared thermometer used to measure the thermodynamic conditions of the air in a sealed chamber, as presented in Figure 4-11(b). The test specimen can be subcored, compacted or slurry but fills at least half the stainless steel or plastic cup

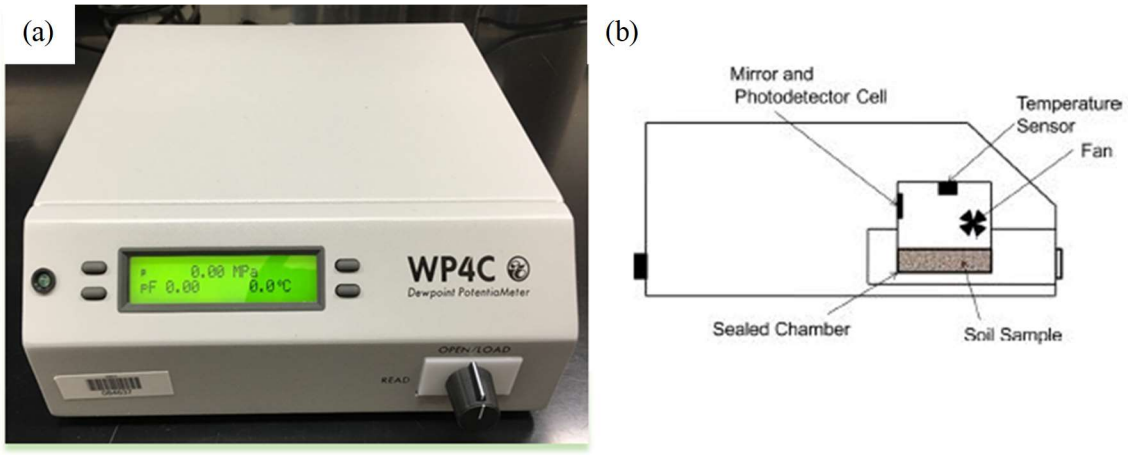


Figure 4-11. (a) Dewpoint potentiometer; (b) schematic diagram of dewpoint potentiometer (Ebrahimi-Birang and Fredlund 2016).

4.5.2 Unsaturated hydraulic conductivity measurement.

The unsaturated flow apparatus was adopted to measure the unsaturated hydraulic conductivity of the compacted CCRs in accordance with ASTM D6836 (ASTM 2002). The test procedure is similar to the WRC measurement as detailed in section 4.5.1 except for the flux through the sample during rotation.

4.6 Water Repellency Treatment of CCRs

4.6.1 Batch sorption procedure

The batch-type procedure, as described in Roy et al. (1992), was adopted in the treatment of CCRs for water repellency by the sorption approach due to its applicability to non-ionic solutes such as OS. The supernatant of the CCR-OS solution matrix was evaluated for EC and pH levels as described in section 4.4.2 for the 24 hours reaction time. Figure 4-12 illustrates a conceptual diagram developed for the sorption treatment. Table 4-11 presents independent variables and their levels that could potentially influence the sorption of OS compounds on CCR substrates. The contact angle measured by SDM

was defined as the dependent variable. Contact angle data were analyzed using SAS, a statistical tool, to identify the independent variables considered to influence OS treatment by sorption.

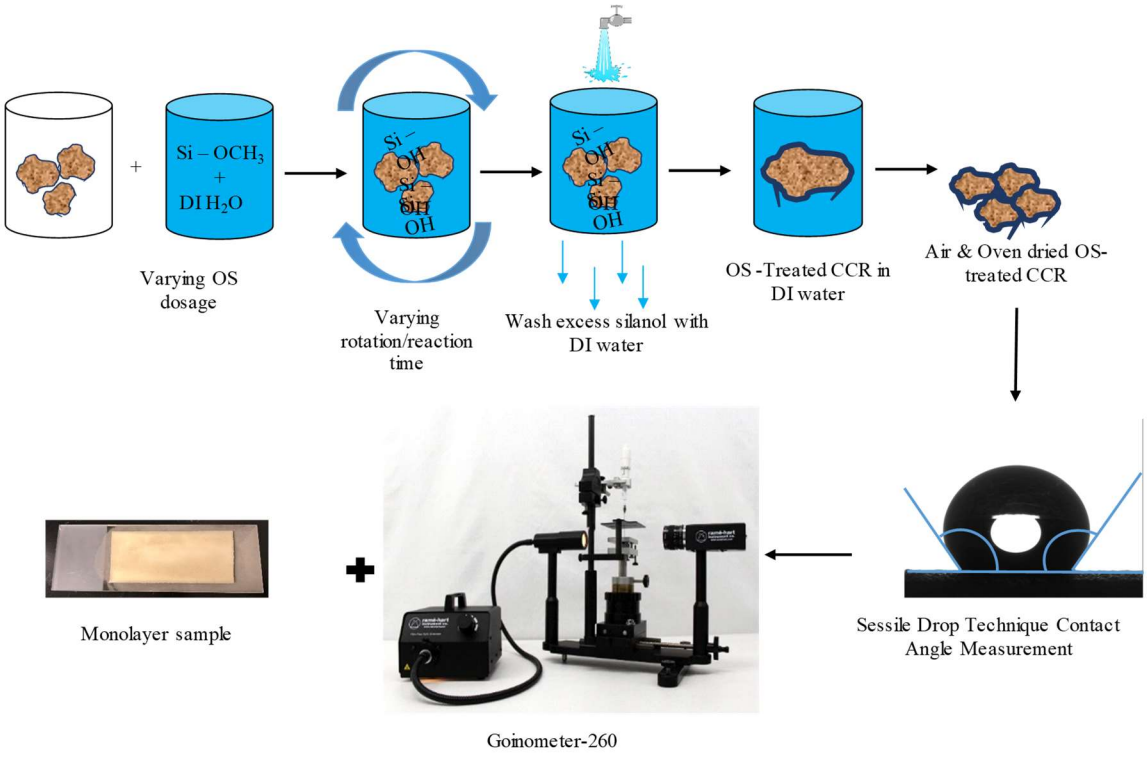


Figure 4-12. Conceptual diagram of OS treatment based on batching (sorption) test.

Table 4-11. Independent variables for sorption water repellency treatment of CCRs

| Independent Variables | Levels |
|---|---|
| Materials | CCR 1, 2, 3 & 6 |
| Dosage, g (OS)/ kg (CCR) | 2, 4, 6, & 8 |
| Reaction time, hr | 1/4, 6, 12, & 24 |
| Drying conditions | lab conditions and oven |

### 4.6.2 Pretreatment and precondition

Standard geotechnical laboratory experiments mostly require remolded, undisturbed, or slurry test specimens. In the case of OS-treated CCR, the treatment protocol described in literature limits the remolding of OS-treated due to the high degree of water repellent interaction. Therefore, following the concept of OS treatment by sorption, two treatment protocols were adopted, namely precondition and pretreatment.

Pretreatment protocol, as described in Daniels et al. (2009b), involves forming a matrix of CCR with OS solution and oven-drying to specified water content before remodeling. In the case of precondition protocol, a matrix of CCR and OS solution was formed, and oven-drying to a specific water content then thoroughly was to remove excess OS. The residue was then oven-dried to the particular content of water prior to remolding.

## 4.7 Selected Engineering Characterization of OS-treated CCR

### 4.7.1 Standard Proctor compaction characteristics

The precondition protocol was adopted to evaluated the compaction characteristics of OS-treated CCR using the standard Proctor compaction effort, as described in ASTM D698 (ASTM 2012). The duplicate test was performed to ascertain any form of variability in sample preparation. For each compaction point, samples were oven-dried to assess the water repellent interaction of the OS-treated samples using the sessile drop method and drop image analysis, as discussed.

### 4.7.2 Breakthrough pressure and saturated hydraulic conductivity of OS-treated CCR

Figure 4-13 illustrates the flexible wall permeameter setup as described in ASTM D5084 (ASTM 2016b) to assess the breakthrough pressure and saturated hydraulic

conductivity of the OS-treated CCR, with operational concept as the rigid wall permeameter approach reported in previous studies (Carrillo et al. 1999; Feyyisa et al. 2019; Fink 1970; Jordan et al. 2015; Lee et al. 2015; Wang et al. 2000).

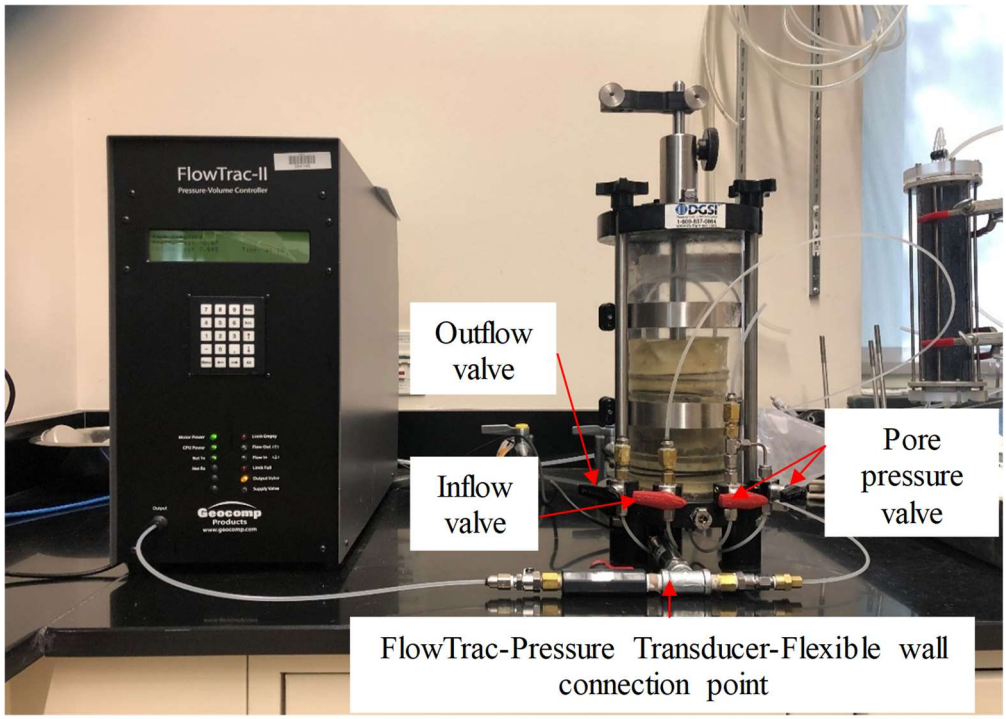


Figure 4-13. Breakthrough pressure assembly using the flexible wall permeameter.

### 4.7.3 Water repellency assessment of compacted OS-treated CCR

The Water drop penetration test and SDM, as described in Liu et al. (2012) and Feyyisa et al. (2017), were adopted to assess the water repellency of compacted OS-treated CCR as a function of water content. Table 4-12 presents a classification to describe the water repellency of compacted OS-treated CCR based on water penetration time with water content.

Table 4-12. Water repellent classification chart for water drop penetration test as described in Liu et al. (2012).

| Water Drop Penetration, s | Classification |
|---|---|
| < 5 | Completely wettable |
| 5 – 60 | slightly repellent |
| 60 – 600 | Strongly repellent |
| 600 – 3600 | Severely repellent |
| > 3600 | Extremely repellent |

## 4.8 Summary

This chapter discussed the experimental design detailing the materials, the experimental methods and results that characterize the engineering properties of CCRs and OS-treated CCRs. Also, modifications made to some standardized test methods to adopt to the workability of OS-treated CCRs were discussed. Also, non-traditional test method to assess these modifications were discussed.

# CHAPTER 5: UNSATURATED FUNCTIONS OF COMPACTED UNTREATED COAL COMBUSTION RESIDUALS

## 5.1 Introduction

Coal combustion residual applications in geotechnical/geoenvironmental engineered systems continues to witness a decline due to the potential of CCRs to release its constituent of concerns into the environment when it interacts with water. This chapter focused on characterizing the unsaturated functions of compacted CCRs to gain insights into the engineering performance, such as infiltration in unsaturated conditions as part of efforts to address the concern and aid in the effective management of CCRs through disposal or beneficial reuse. A comprehensive experimental designed was developed to describe the water retention behavior of compacted CCRs by suction measurement and unsaturated hydraulic conductivity. An overview of the chapter is as follows:

- Multiple samples for selected test methods were subcored from standard Proctor compacted CCRs involving at least duplicate samples for TC, UFA, and WP4C, and triplicates for PPE.
- Suction measurements were performed in accordance with standardized test methods. For UFA, the same test specimens were used for unsaturated hydraulic conductivity followed by suction measurement.
- Selected parametric models were fitted to the measured data to generate unsaturated functions to predict unsaturated hydraulic conductivity. Parametric model based on index properties was considered to evaluate the relationship between index properties and WRC of the CCRs.

## 5.2 Experimental Design

### 5.2.1 Materials

Five CCRs made up of 3 types of class F fly ash, 1 lignite coal ash, and 1 FGD gypsum were considered for this study. DI water was used as the molding water to ensure the chemical compositions of the CCRs defined the pore water chemistry, which controls osmotic suction.

### 5.2.2 Test methods

Four suction measurement methods, namely PPE, TC, and UFA matric suction and WP4C for total suction, were considered with the UFA used to measure the unsaturated hydraulic conductivity. The test specimens for these methods were subcored from standard Proctor compacted CCR using DI water as molding water. However, the process of subcoring was unique to each test method due to the different features of the specimen cup or rings. To cover the complete suction range of the compacted CCRs, the test specimens were saturated in deaired DI water bath for at least 24 hours. The PPE consisted of 5 bar and 15 bar chambers with 1 bar and 5 bar HAE disks, respectively. The 1 bar HAE disk for suction range 10 kPa – 50 kPa and the 5 bar HAE disk for 100 kPa – 500 kPa. Both disks were saturated prior to testing. The TC consisted of two cells using 2 bar HAE disk for suction range 10 kPa – 100 kPa with HAE disk saturated prior to testing. The setup of the UFA was completely different, as it does not utilize HAE disk. In addition, the unsaturated hydraulic conductivity was conducted for a desaturation and saturation cycle prior to the suction measurement that ranged from 4 kPa – 424 kPa. The WP4C covered a wide range but was based on the degree of saturation before testing and the climatic conditions in the laboratory which was monitored using a HOBO

temperature and humidity sensor. The PPE and TC test specimens were checked for attainment of equilibration at each pressure application by logging the gravimetric water content with time. At the end of the test, test specimens were oven dried. APPENDIX A details a comprehensive suction measurements for the aforementioned test methods.

## 5.3 Results and Discussions

### 5.3.1 Compaction conditions for WRC measurements

The WRC test specimens were subcored from a standard Proctor compaction. In general, all the WRC test specimens were prepared to within close range of dry unit weight and water content. The initial compaction conditions were estimated using the water – density relationship whereas the final compaction was estimated using the mass – volume relationship of the oven-dry solids. Figure 5-1 through Figure 5-5 shows the compaction conditions of the test specimens in relation to the maximum dry unit weight and optimum water content.

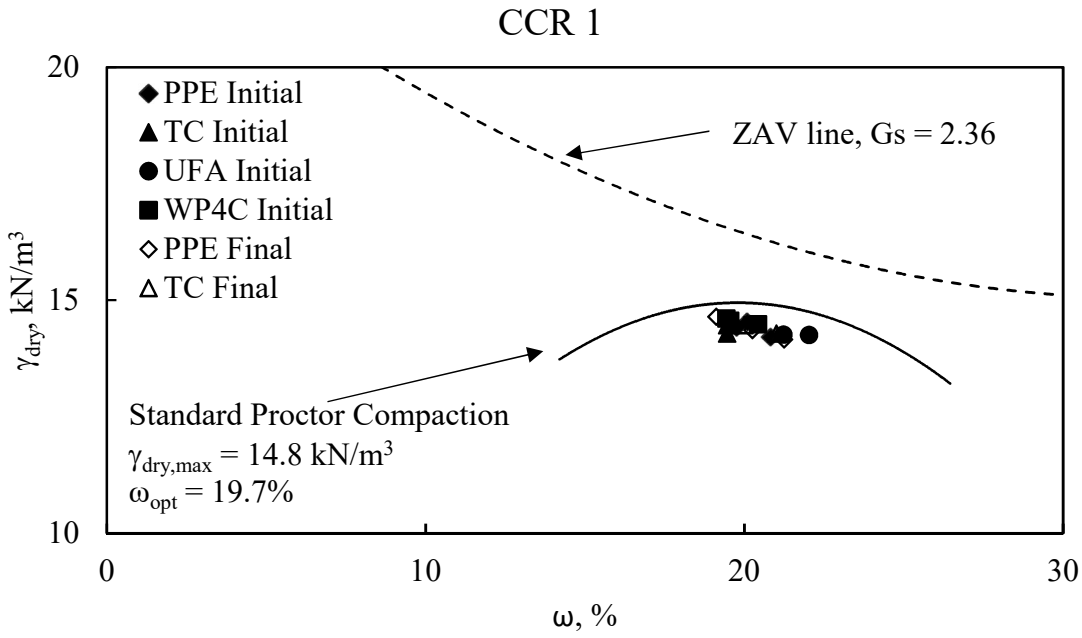


Figure 5-1. Compaction conditions of test specimens for CCR 1 WRC measurements.

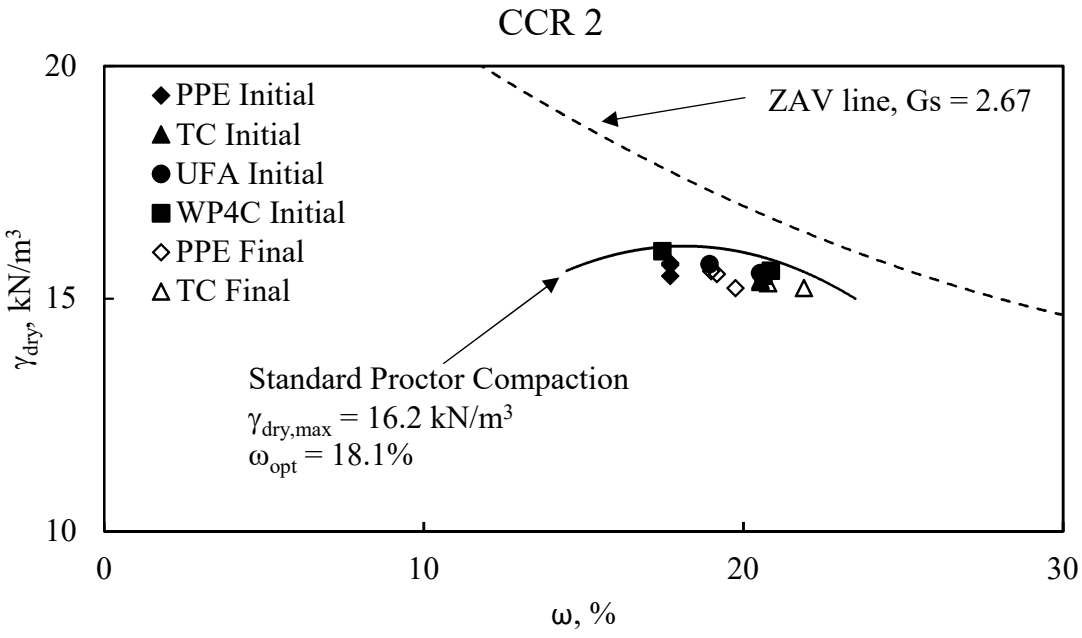


Figure 5-2. Compaction conditions of test specimens for CCR 2 WRC measurements.

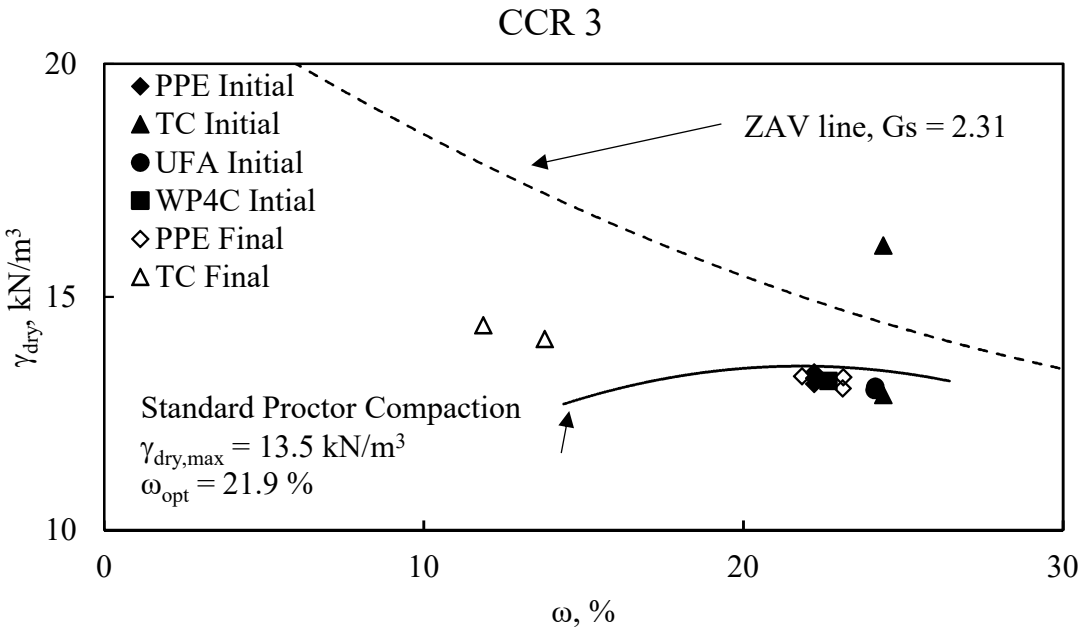


Figure 5-3. Compaction conditions of test specimens for CCR 3 WRC measurements.

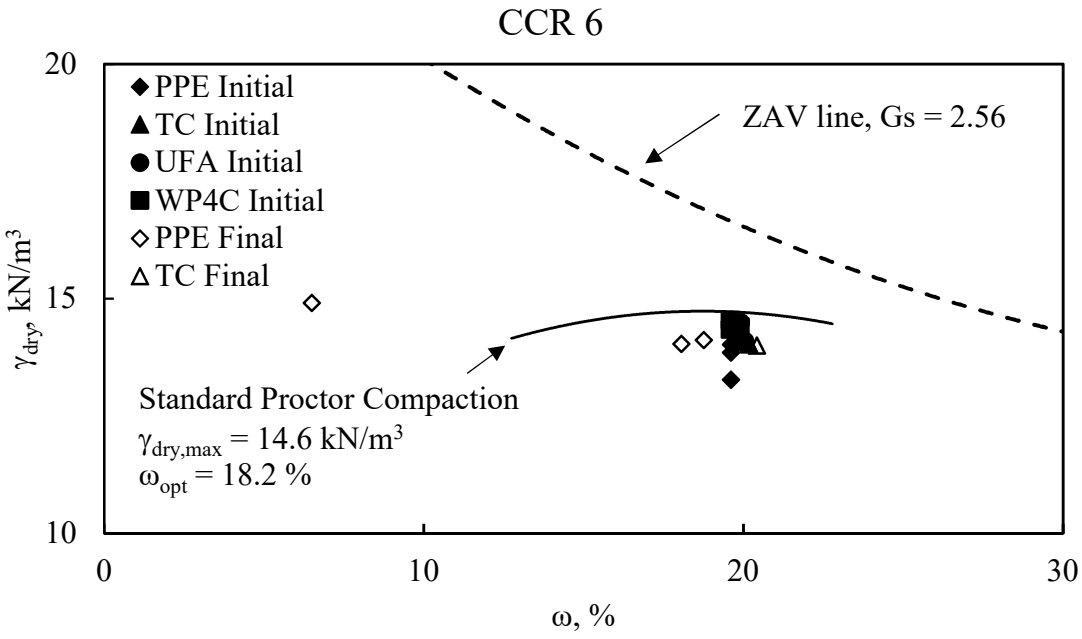


Figure 5-4. Compaction conditions of test specimens for CCR 6 WRC measurements.

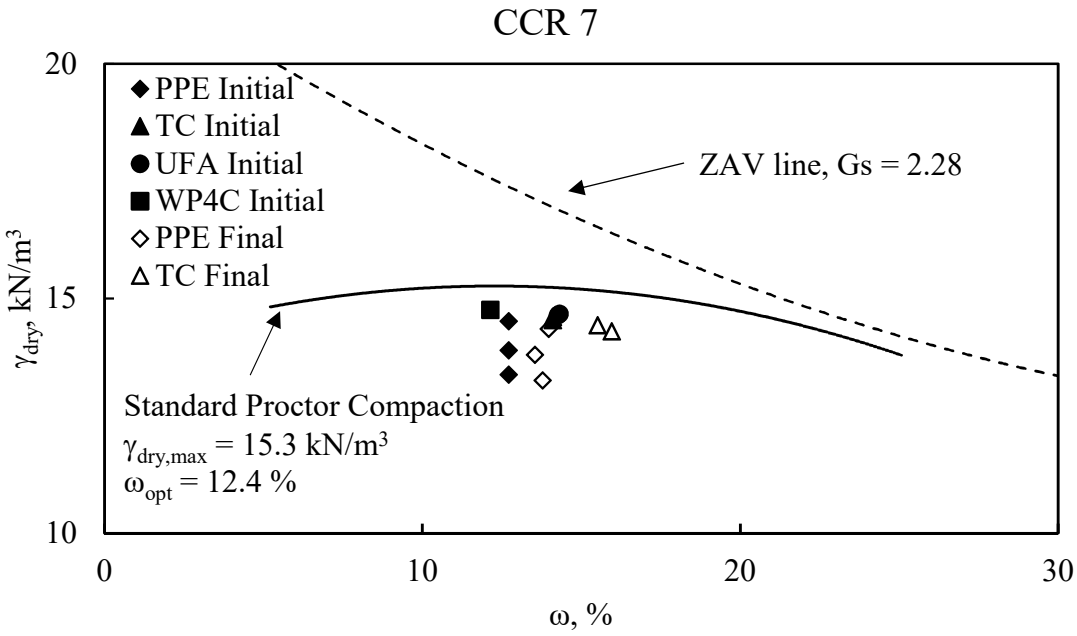


Figure 5-5. Compaction conditions of test specimens for CCR 7 WRC measurements.

5.3.2 Suction equilibration time

The time it takes for the axis translation methods, PPE and TC, test specimens to attain equilibration for an applied pressure was monitored by measuring the gravimetric water content with time. APPENDIX B and APPENDIX C show the equilibration time plots for all CCRs in TC and PPE, respectively. At equilibration, the applied pressure becomes equal to matric suction, which results in no change in water content. The masses of test specimens were logged every hour for the first 6 hours of pressure application. All samples had a relatively similar pattern of equilibration and desaturation, but there was some exception, for example, in TC for CCR 6, one of the duplicate test specimens experience rapid desaturation. Presumably, due to leakage in the TC set up as the pressure increases. There was rapid desaturation in the first 6 hours of initial pressure

applications within the saturation and initial section of the transition zone. After the AEV had been attained subsequent pressure application saw no significant desaturation in the first 6 hours of applications.

At pressure applications > 100 kPa for both PPE and TC, the desaturation rate in all the CCRs considered was observed to increase, remaining constant without converging to equilibrium, hence leading to a long equilibration time. Vanapalli et al. (2009) noted that great care should be taken in the interpretation of results of test specimens with long equilibration time observation. As a result, to avoid the introduction of errors, the PPE measurements were terminated at 300 kPa. Similarly, in the case of TC, the suction measurements were terminated at 100 kPa. The long equilibration time observed in PPE and TC could be associated with air diffusion through the ceramic disk, discontinuity of the air-water phase due to occluded air in the test specimen, and loss in hydraulic contact between the test specimens and the ceramic disk as reported in literature (Elgabu 2013; Vanapalli et al. 2009).

Table 5-1 presents a summary of the time required to complete the suction measurement tests. Time required to complete a test is dependent on the number of suction values considered and the equilibration time. The PPE had eight pressure applications and long equilibration time resulting in a minimum and maximum test run of 42 days and 64 days, respectively, followed by TC, which had 28 days for minimum and 49 days for maximum test runs. The fasters methods were UFA and WP4C test methods with at least seven days for a test run.

Table 5-1. Completion time for each test method.

| CCR | Test Run, day | | | |
|---|---|---|---|---|
| | PPE | TC | UFA | WP4C |
| 1 | 64 | 39 | 7 | 7 |
| 2 | 51 | 28 | 7 | 7 |
| 3 | 58 | 40 | 7 | 7 |
| 6 | 49 | 49 | 7 | 7 |
| 7 | 42 | 31 | 7 | 7 |

5.3.3 Unsaturated functions of compacted CCRs

5.3.3.1 WRC

The final compaction conditions was used in the WRC analysis as it provided the true representation of the test specimen. Figure 5-6 through Figure 5-10 show the WRC of compacted CCRs 1, 2, 3, 6, and 7, respectively measured with PPE, TC, and UFA for matric suction, and WP4C for total suction. In general, all the CCRs had unique WRC defined by the water content – suction relationship. Studies have shown that soil type, compaction characteristics, stress conditions, influence the WRC of soils (Elgabu 2013; Miller et al. 2002). It was observed that there were variations in duplicate/triplicate test specimens and the test methods for matric suction measurement for each CCR considered. Nevertheless, comparable trends in the desaturation of the test specimens for each CCR were observed. CCR 6 showed significant variations in multiple measurements for both matric and total suction, as presented in Figure 5-9.

In this study, the compaction energy was limited to standard Proctor energy eliminating the potential effect compaction energy might have on the unsaturated CCR functions. As shown in Figure 5-1 through Figure 5-5, there are variations in the dry unit

weights of the multiple test specimen for each test method. Test specimens with lower dry unit weights will have higher porosity thus higher degrees of saturation. Such test specimens tend to desaturate quickly resulting in lower water compared to test specimen with a higher dry unit weight under the same suction application. The variations in total suction measurements of CCR 6 could be a result of varying pore water chemistry, which influences total suction measurement.

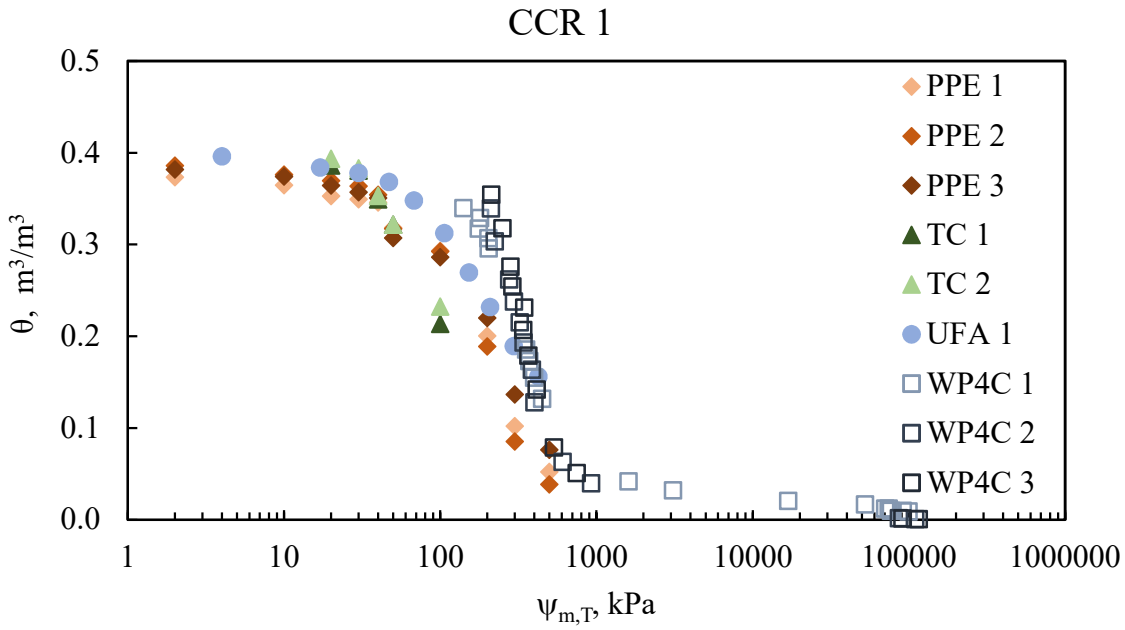


Figure 5-6. Water content - suction relationship of compacted CCR 1.

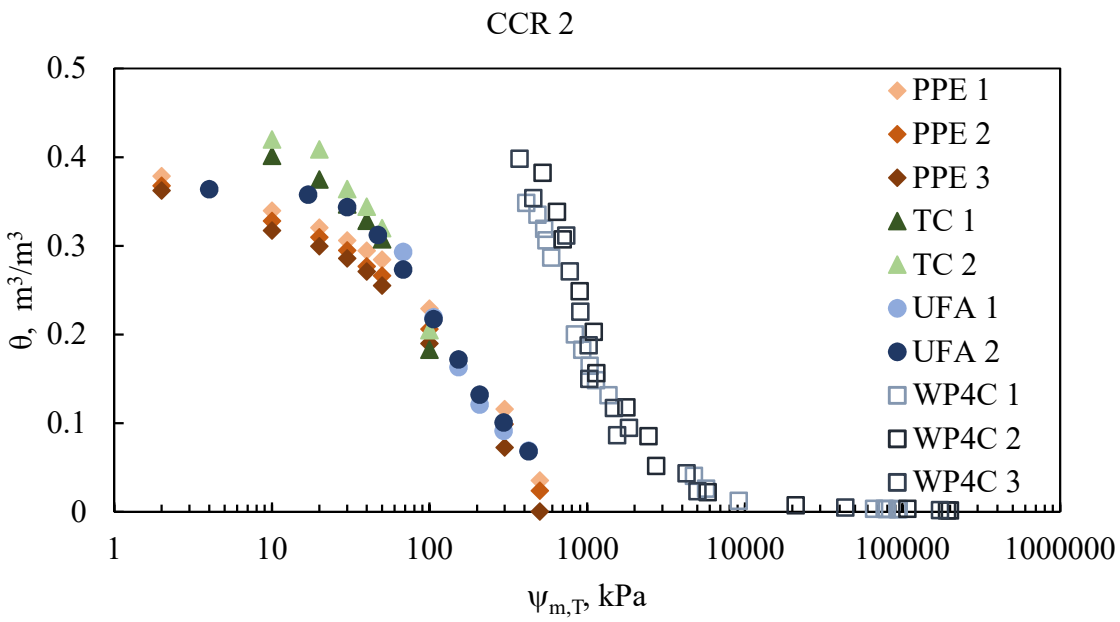


Figure 5-7. Water content - suction relationship of compacted CCR 2.

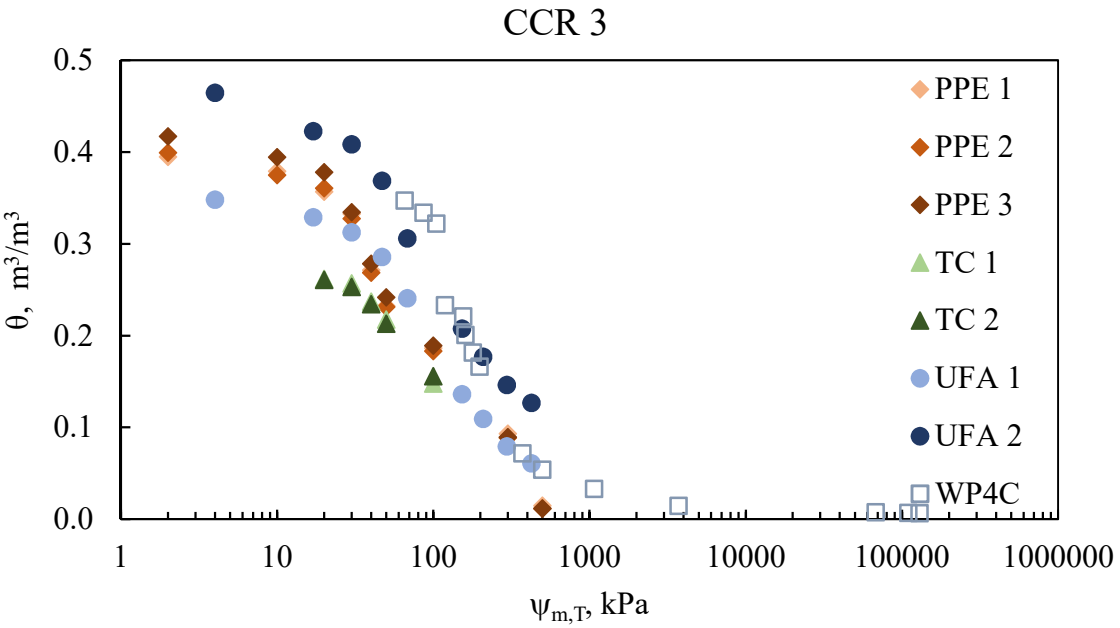


Figure 5-8. Water content - suction relationship of compacted CCR 3.

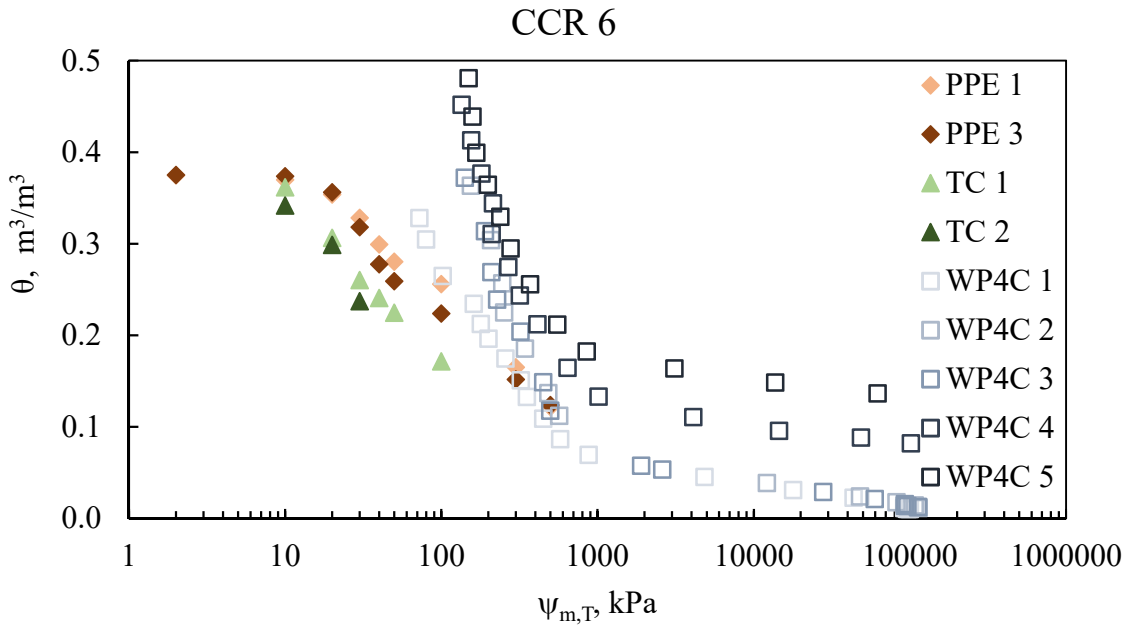


Figure 5-9. Water content - suction relationship of compacted CCR 6.

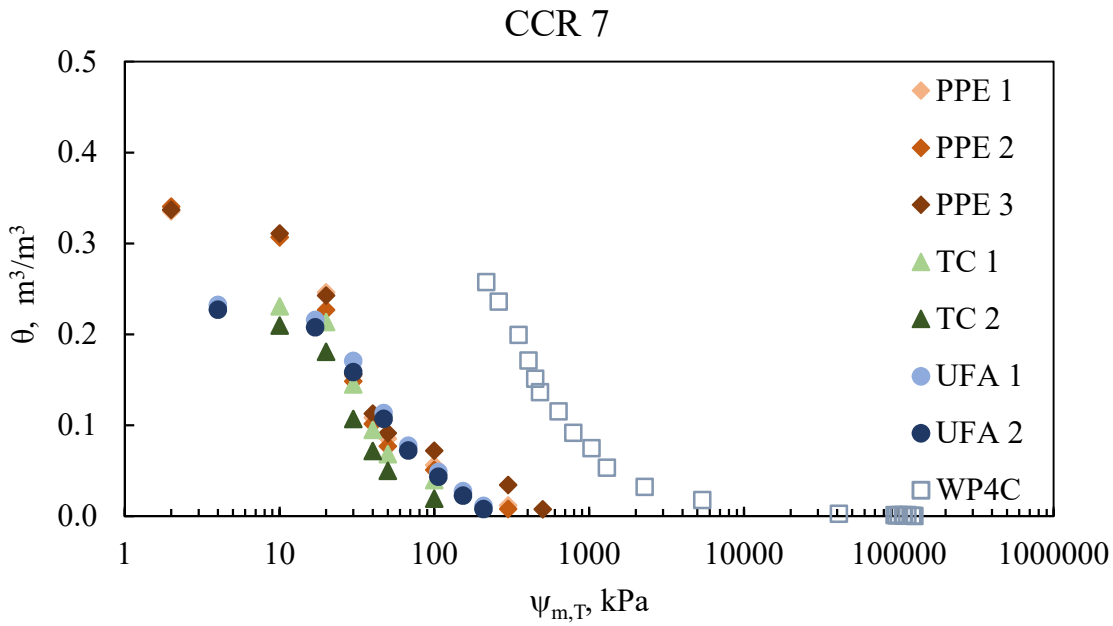


Figure 5-10. Water content - suction relationship of compacted CCR 7.

In addition, osmotic suction, the component of total suction dependent on soluble salts in the pore fluid, activity was assessed based on the ionic activity of all CCRs tested

and was found to be significantly high in CCR 2 and CCR 7, which are class F fly ash and FGD gypsum, respectively. These observations match the high EC values presented in Table 4-9 for CCR 2 and CCR 6. Previous studies (Pflughoeft-Hassett et al. 2009; Renew et al. 2015) indicated that emission control measures such as calcium bromide additives, brominated powdered activated carbon injection, sodium-based reagent (Trona) injection could account for a significant amount of salts in CCRs. These salts enhance the mobility of heavy metals, but its impact on the performance of an engineered system such as structural fill/embankment has not been fully explored in CCRs. The relativity of osmotic suction was discussed in section 2.2.

5.3.3.2 Parametric model fitting

The parametric models, vG, vGM, vGB, and FX, as detailed in Eq. 2-3 through Eq. 2-7, respectively, were fitted to the measured data to provide a continuous characterization of the water retention behavior of the compacted CCRs. The fitting process was done using EXCEL Solver, a least square regression built-in function, to minimize the sum of square deviation by optimizing the model parameters. The WP4C data set in the residual zone was used to complement data sets from PPE, TC, and UFA. Each test specimen of a duplicates/triplicates was considered an independent measurement to ascertain the variability and repeatability of the test method. In addition, data set from duplicates/triplicates were combined for an average estimate of the model parameters for each test method. Subsequently, matric suction measurements from all test methods were combined to represent each CCR. Figure 5-11 through Figure 5-15 presents fitted models to measured data for each CCR with Table 5-2 through Table 5-6 detailing the corresponding model parameters.

In general, the parametric models had a good fit to the measured data considering the R – squared valued generated from the least square regression analysis. However, the R – squared values were marginally higher for the independent measurement analysis than for the combined measurement analysis. The saturation volumetric water content, $\theta_s$, was taken as the average of all test specimens for matric suction and total suction. Hence variations were observed, a result of different dry unit weights of each test specimen. The residual water content was fitted to the data thus adding to the number of fitting parameters for each parametric model with relatively low values and in some cases, zero values. Overlapping of fitting models was observed in the saturation zone for CCR 1, 6, and 7 and in the transition zone for all CCRs due to the difference in volumetric water content a result of varying drying unit weights of each test specimen. The difference in matric and total suction was clearly defined in CCR 2 and 7 than in CCR 1, 3, and 6. The AEV of total suction measurements were higher than matric suction measurements with CCRs having osmotic suction activity recording significant AEV as presented in Table 5-2 through Table 5-6. The AEVs of the matric suction were in a narrow range of magnitude $10^{-1}$ and $10^{-2}$ MPa. The estimated residual suction varied over a wide range with the minimum value as 11 MPa and a maximum > 1000 MPa exceeding the measurable range of the WP4C, 300 MPa. However, the measured values obtained ranged between 62 MPa and 130 MPa. Therefore, the compacted CCRs have a measurable suction range between 0.01 MPa – 130 MPa indicating high WRC. The *n* and *m* parameters that describe the pore size distribution and the asymmetry of the SWCC about the AEV, respectively, were found to vary in the range 0.66 – 2.56 and 0.17 – 3.58 for the matric suction characteristics of the CCRs. These values compare relatively well

with those reported in literature for CCRs (Abhijit and Sreedeep 2014; Deka 2015; Keatts et al. 2018; Malaya and Sreedeep 2010; Malaya and Sreedeep 2014; Sindi 2019; Young 1993).

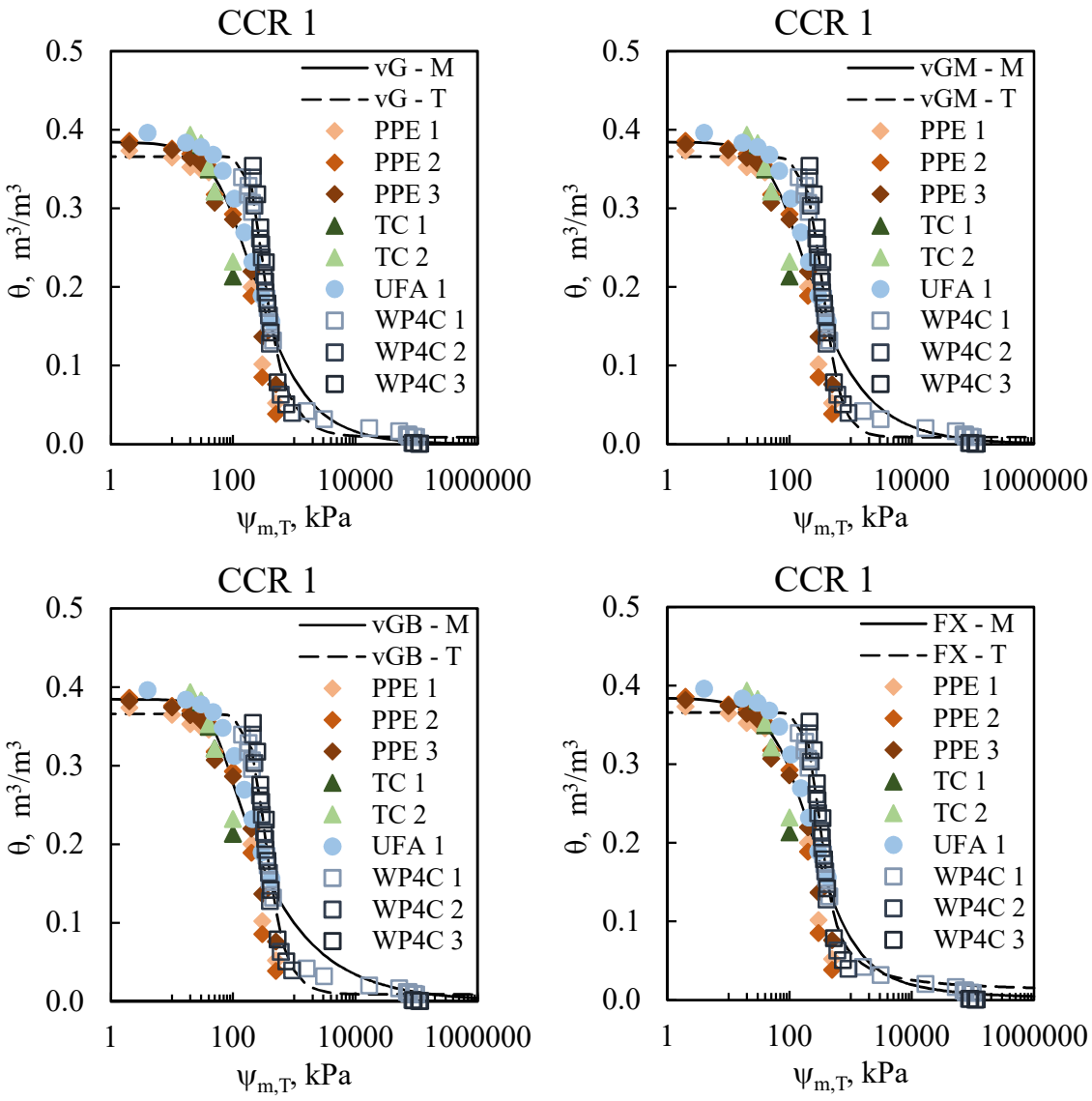


Figure 5-11. Parametric models from top left to right vG, vGM, vGB, and FX fitting to CCR 1 measured data.

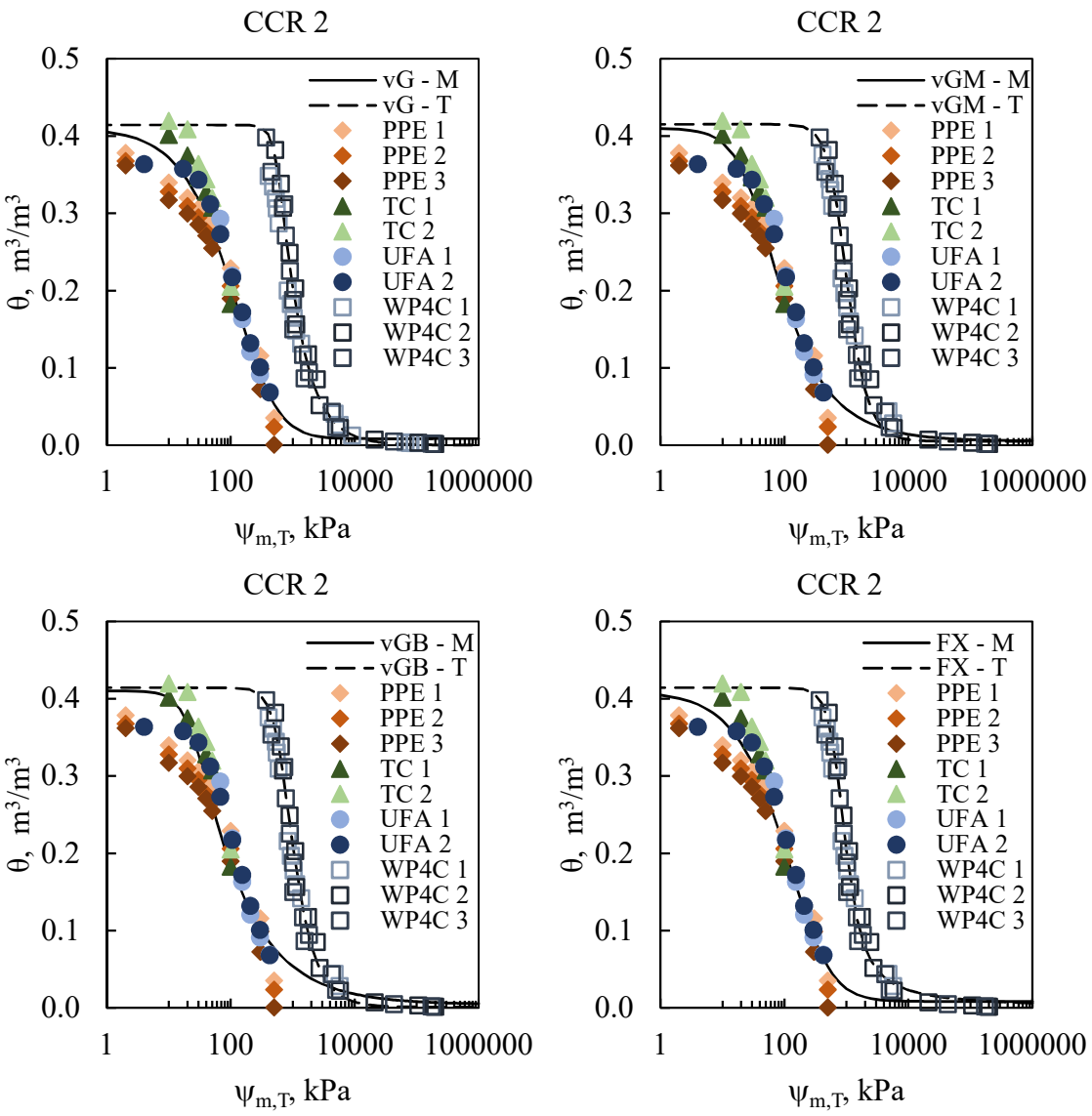


Figure 5-12. Parametric models from top left to right vG, vGM, vGB, and FX fitting to CCR 2 measured data.

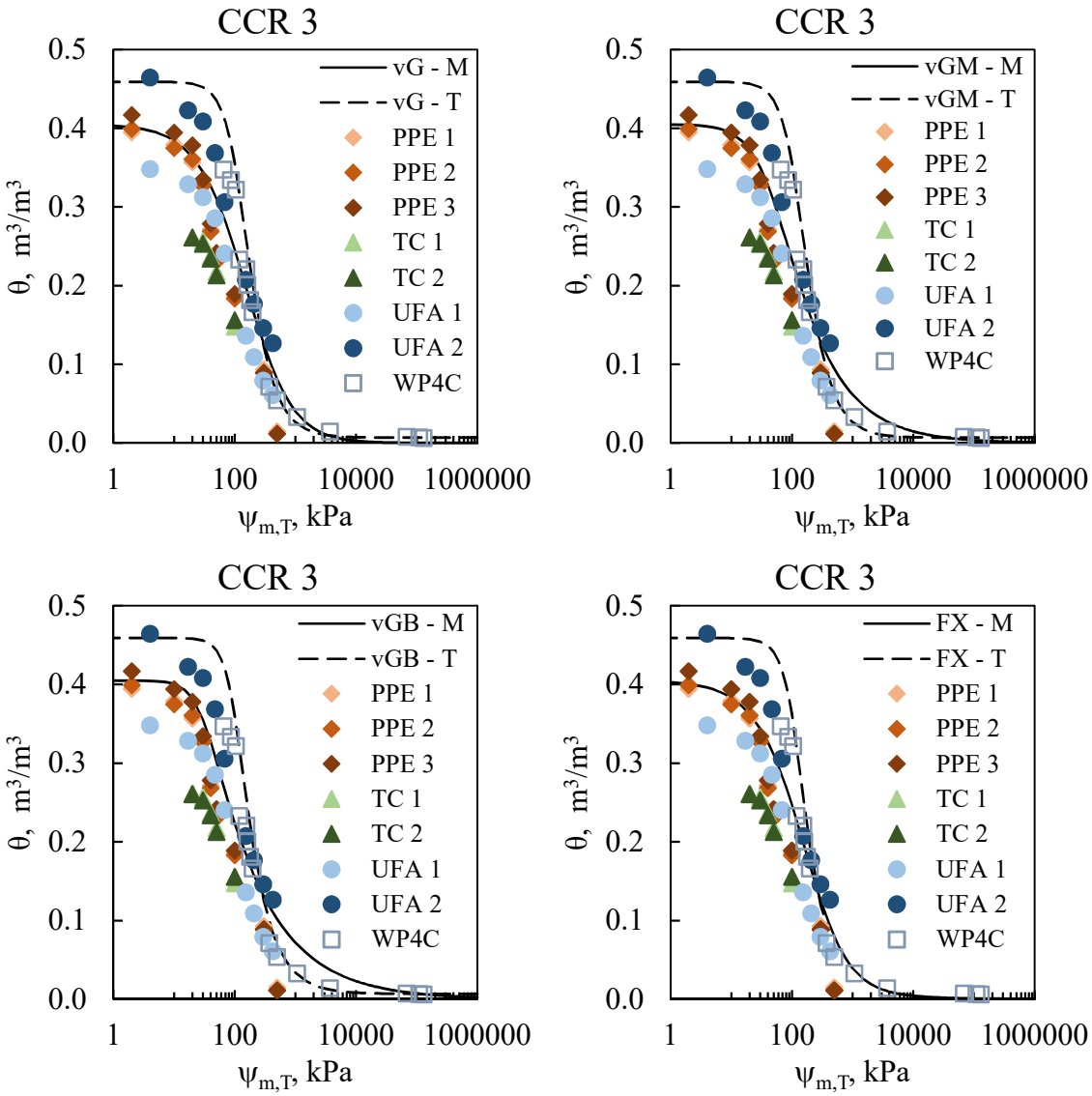


Figure 5-13. Parametric models from top left to right vG, vGM, vGB, and FX fitting to CCR 3 measured data

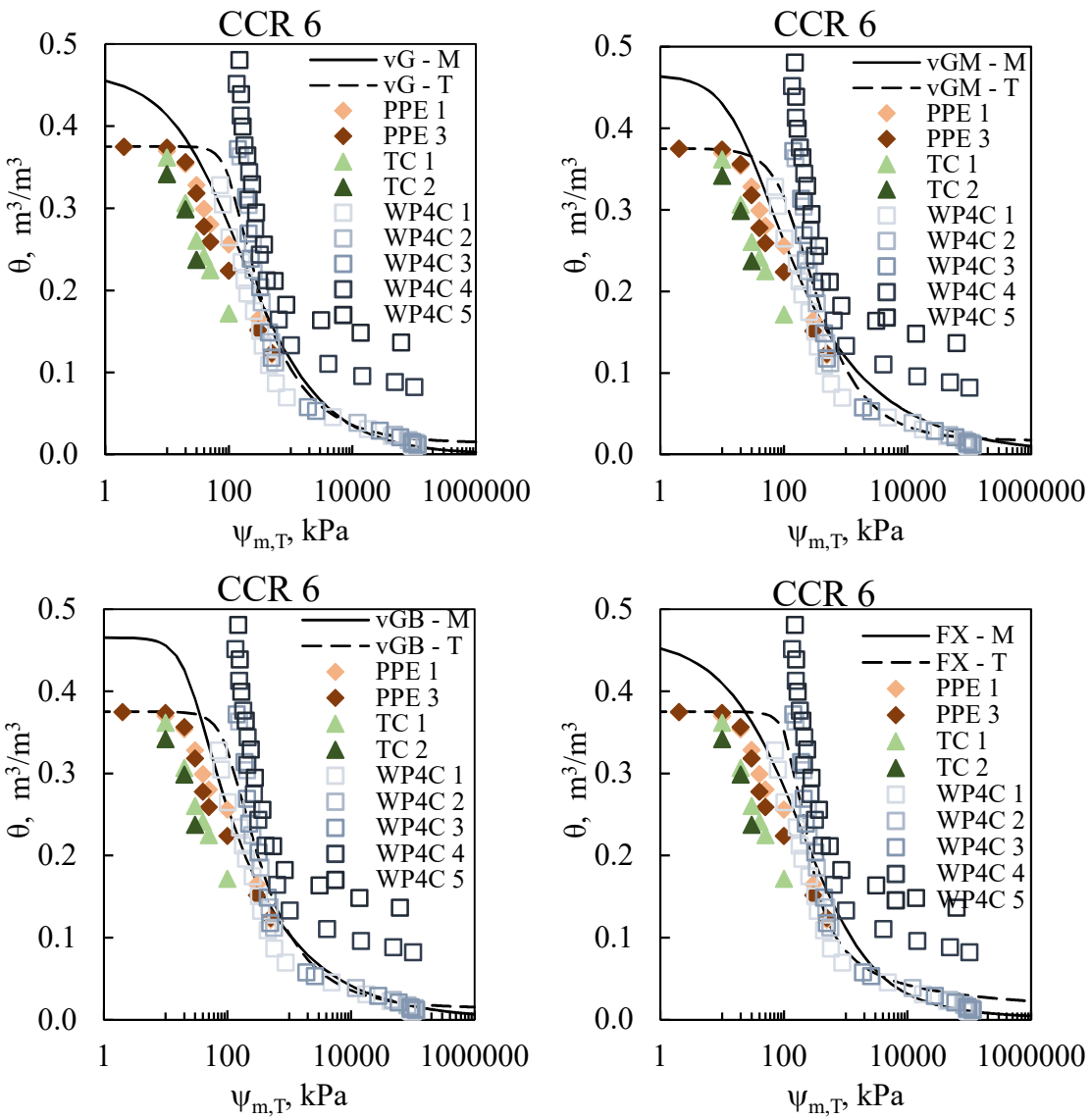


Figure 5-14. Parametric models from top left to right vG, vGM, vGB, and FX fitting to CCR 6 measured data.

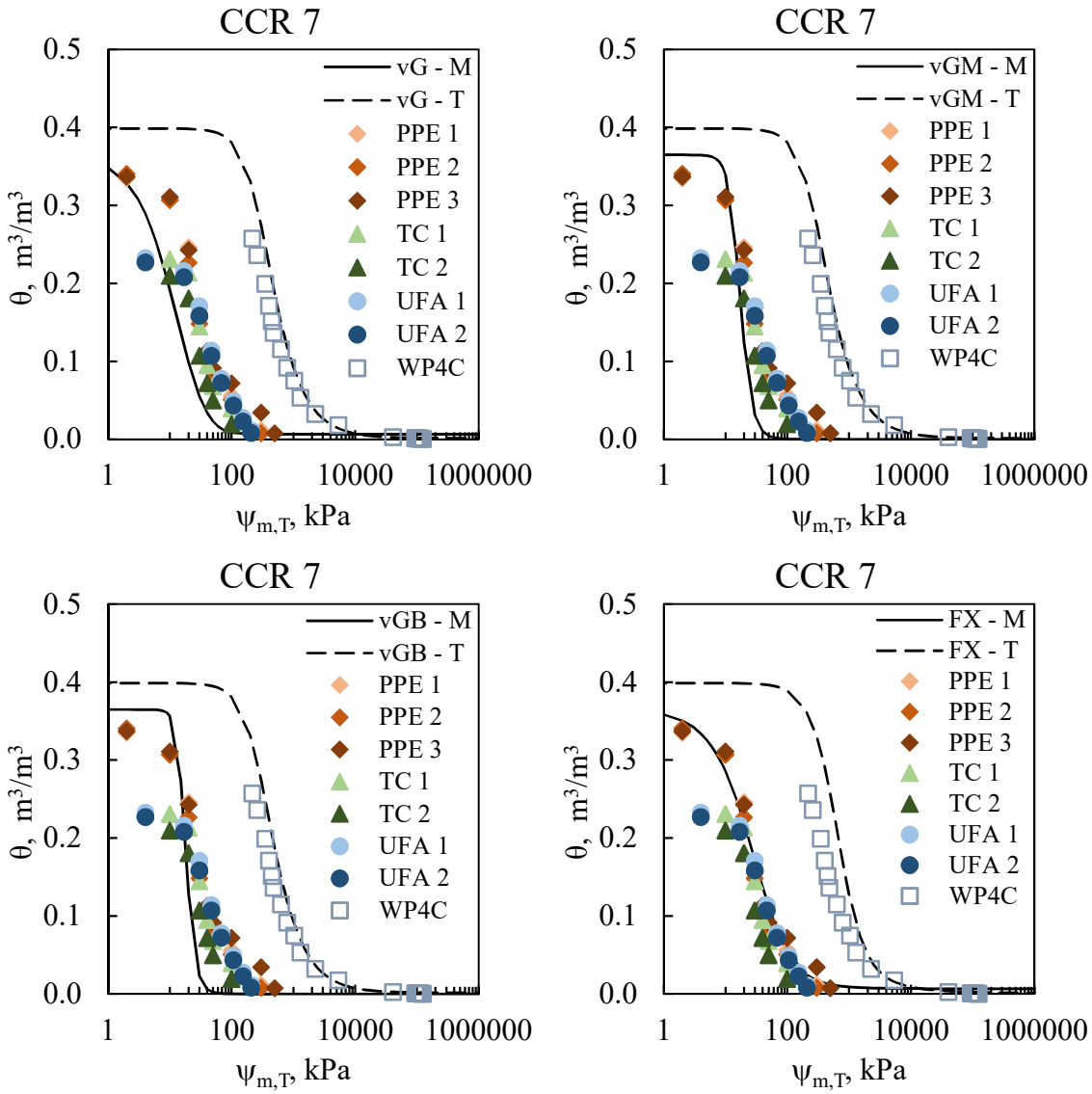


Figure 5-15. Parametric models from top left to right vG, vGM, vGB, and FX fitting to CCR 7 measured data.

Table 5-2. Summary of model parameters for CCR 1.

| Method | Model | Model Parameters | | | | | | |
|---|---|---|---|---|---|---|---|---|
| | | $\theta_s$ | $\theta_r$ | $\psi_{AEV}$ | $\psi_r$ | n | m | $R^2$ |
| | | $m^3/m^3$ | $m^3/m^3$ | MPa | MPa | | | |
| Matric | vG | 0.3786 | 0.0044 | 0.1272 | 14 | 1.39 | 0.52 | 0.9757 |
| | vGM | 0.3786 | 0.0019 | 0.0908 | >1000 | 1.60 | 0.38 | 0.9752 |
| | VGB | 0.3786 | 0.0000 | 0.0539 | >1000 | 2.46 | 0.19 | 0.9725 |
| | FX | 0.3786 | 0.0000 | 0.1923 | 36 | 1.22 | 1.90 | 0.9759 |
| Total | vG | 0.3717 | 0.0089 | 0.2279 | 74 | 5.21 | 0.28 | 0.9655 |
| | vGM | 0.3717 | 0.0089 | 0.3141 | 11 | 3.38 | 0.70 | 0.9639 |
| | vGB | 0.3717 | 0.0089 | 0.2699 | 24 | 3.87 | 0.48 | 0.9649 |
| | FX | 0.3717 | 0.0089 | 0.2650 | >1000 | 4.27 | 1.12 | 0.9710 |

Table 5-3. Summary of model parameters for CCR 2.

| Method | Model | Model Parameters | | | | | | |
|---|---|---|---|---|---|---|---|---|
| | | $\theta_s$ | $\theta_r$ | $\psi_{AEV}$ | $\psi_r$ | n | m | $R^2$ |
| | | $m^3/m^3$ | $m^3/m^3$ | MPa | MPa | | | |
| Matric | vG | 0.4102 | 0.0084 | 0.343 | 14 | 0.90 | 2.50 | 0.9670 |
| | vGM | 0.4102 | 0.0053 | 0.034 | >1000 | 1.68 | 0.40 | 0.9562 |
| | VGB | 0.4102 | 0.0044 | 0.024 | >1000 | 2.56 | 0.22 | 0.9467 |
| | FX | 0.4102 | 0.0082 | 0.293 | 36 | 0.90 | 5.72 | 0.9670 |
| Total | vG | 0.4153 | 0.0000 | 0.569 | 820 | 5.58 | 0.22 | 0.9907 |
| | vGM | 0.4153 | 0.0049 | 0.847 | 52 | 3.07 | 0.67 | 0.9780 |
| | vGB | 0.4153 | 0.0009 | 0.685 | >1000 | 3.53 | 0.43 | 0.9884 |
| | FX | 0.4153 | 0.0000 | 0.733 | >1000 | 3.61 | 1.29 | 0.9902 |

Table 5-4. Summary of model parameters for CCR 3.

| Method | Model | Model Parameters | | | | | | |
|---|---|---|---|---|---|---|---|---|
| | | $\theta_s$ | $\theta_r$ | $\psi_{AEV}$ | $\psi_r$ | n | m | $R^2$ |
| | | $m^3/m^3$ | $m^3/m^3$ | MPa | MPa | | | |
| Matric | vG | 0.4050 | 0.0000 | 0.180 | >1000 | 1.06 | 1.17 | 0.8518 |
| | vGM | 0.4050 | 0.0000 | 0.048 | >1000 | 1.62 | 0.38 | 0.8495 |
| | VGB | 0.4050 | 0.0000 | 0.031 | >1000 | 2.50 | 0.20 | 0.8455 |
| | FX | 0.4050 | 0.0000 | 0.208 | >1000 | 1.01 | 3.30 | 0.8517 |
| Total | vG | 0.4178 | 0.0067 | 0.128 | 82 | 2.52 | 0.60 | 0.9874 |
| | vGM | 0.4178 | 0.0067 | 0.128 | 82 | 2.52 | 0.60 | 0.9874 |
| | vGB | 0.4178 | 0.0067 | 0.103 | 290 | 3.24 | 0.38 | 0.9888 |
| | FX | 0.4178 | 0.0067 | 0.124 | >1000 | 2.78 | 1.42 | 0.9895 |

Table 5-5. Summary of model parameters for CCR 6.

| Method | Model | Model Parameters | | | | | | |
|---|---|---|---|---|---|---|---|---|
| | | $\theta_s$ | $\theta_r$ | $\psi_{AEV}$ | $\psi_r$ | n | m | $R^2$ |
| | | $m^3/m^3$ | $m^3/m^3$ | MPa | MPa | | | |
| Matric | vG | 0.4655 | 0.0000 | 0.097 | >1000 | 0.76 | 0.73 | 0.8979 |
| | vGM | 0.4655 | 0.0000 | 0.022 | >1000 | 1.36 | 0.26 | 0.8951 |
| | VGB | 0.4655 | 0.0000 | 0.023 | >1000 | 2.40 | 0.17 | 0.8850 |
| | FX | 0.4655 | 0.0000 | 0.212 | >1000 | 0.66 | 2.69 | 0.8975 |
| Total | vG | 0.4288 | 0.0141 | 0.105 | >1000 | 3.44 | 0.18 | 0.7865 |
| | vGM | 0.4288 | 0.0170 | 0.142 | >1000 | 1.71 | 0.42 | 0.7798 |
| | vGB | 0.4288 | 0.0142 | 0.109 | >1000 | 2.62 | 0.24 | 0.7845 |
| | FX | 0.4288 | 0.0000 | 0.158 | >1000 | 3.22 | 0.84 | 0.8019 |

Table 5-6. Summary of model parameters for CCR 7.

| Method | Model | Model Parameters | | | | | | |
|---|---|---|---|---|---|---|---|---|
| | | $\theta_s$ $m^3/m^3$ | $\theta_r$ $m^3/m^3$ | $\psi_{AEV}$ MPa | $\psi_r$ MPa | n | m | $R^2$ |
| Matric | vG | 0.3648 | 0.0064 | 0.039 | >1000 | 1.18 | 3.58 | 0.9168 |
| | vGM | 0.3648 | 0.0000 | 0.016 | >1000 | 4.90 | 0.80 | 0.8979 |
| | VGB | 0.3648 | 0.0000 | 0.017 | >1000 | 6.64 | 0.70 | 0.8876 |
| | FX | 0.3648 | 0.0064 | 0.040 | >1000 | 1.17 | 3.69 | 0.9162 |
| Total | vG | 0.3403 | 0.0014 | 0.301 | 470 | 2.20 | 0.55 | 0.9967 |
| | vGM | 0.3403 | 0.0014 | 0.301 | 470 | 2.20 | 0.55 | 0.9967 |
| | vGB | 0.3403 | 0.0014 | 0.301 | 470 | 2.20 | 0.55 | 0.9967 |
| | FX | 0.3403 | 0.0000 | 0.618 | 270 | 1.92 | 2.26 | 0.9778 |

5.3.3.3 Osmotic suction

Osmotic suction is dependent on the presence of soluble salts in the pore fluid. As discussed in the previous section, there are various methods to estimate the osmotic suction component of total suction. Experimentally, it can be determined by analyzing the pore fluid extract for salt concentrations using EC value. The van Hoff equation can be used for pore fluid, which classifies as ideal fluids. Also, osmotic suction can be determined by finding the difference between the independent measurement of total and matric suctions. Comparing these methods, several studies reported no significant variation in the osmotic suction determined via pore fluid extract analysis and finding the difference between the independent measurement of total and matric suction. Also, the EC values of the CCR pore fluids at near saturation, as presented in Table 4-9, showed high levels of salt concentrations which do not classify them as ideal fluids, limiting the

use of the van Hoff approach. Therefore, for this study, the osmotic suction was estimated as the difference in total suction and matric suction using the fitted parametric models vG, vGM, vGB, and FX. Eq. 2-3 through Eq. 2-7 were written in terms of suction to estimate the suction at a specific volumetric water content common to both matric and total suctions. Though some level of ionic activity was observed in CCR 1, 3, and 6 in terms of EC values, the WRC curves showed insignificant osmotic suction activity hence were not considered for osmotic suction analysis. Figure 5-17 and Figure 5-17 presents the osmotic suction relative to the independent measurements of total and matric suctions for CCR 2 and 7, respectively.

The osmotic suction was observed to have the typical S-shaped curve that describes the SWCC increasing in magnitude as desaturation progressed. The high magnitude of osmotic suction can be attributed to higher salt concentrations at lower water content. CCR 2 and CCR 7 recorded osmotic suction in the range 0.3 MPa – 74 MPa and 0.009 MPa – 7 MPa, respectively, from saturation to residual water conditions. The variations in osmotic magnitude could be due to different salt contents and concentrations. The high values of suction in the saturation and transition zones suggest the total suction is dominated by the presence of soluble salts in the pore fluid. These observations are comparable to what has been reported by previous studies (Abedi-Koupai and Mehdizadeh 2007; Miller and Nelson 2006; Sreedeep and Singh 2006). The significant osmotic suctions observed have implications to the engineering performance of geotechnical and geoenvironmental engineered systems designed using CCRs. Engineered systems such as liner systems that undergo high-stress applications might experience volume changes that could impact the engineering performance of the system.

Also, osmotic suction could enhance the mobility of contaminants, such as heavy metals from a high osmotic zone to a low osmotic zone.

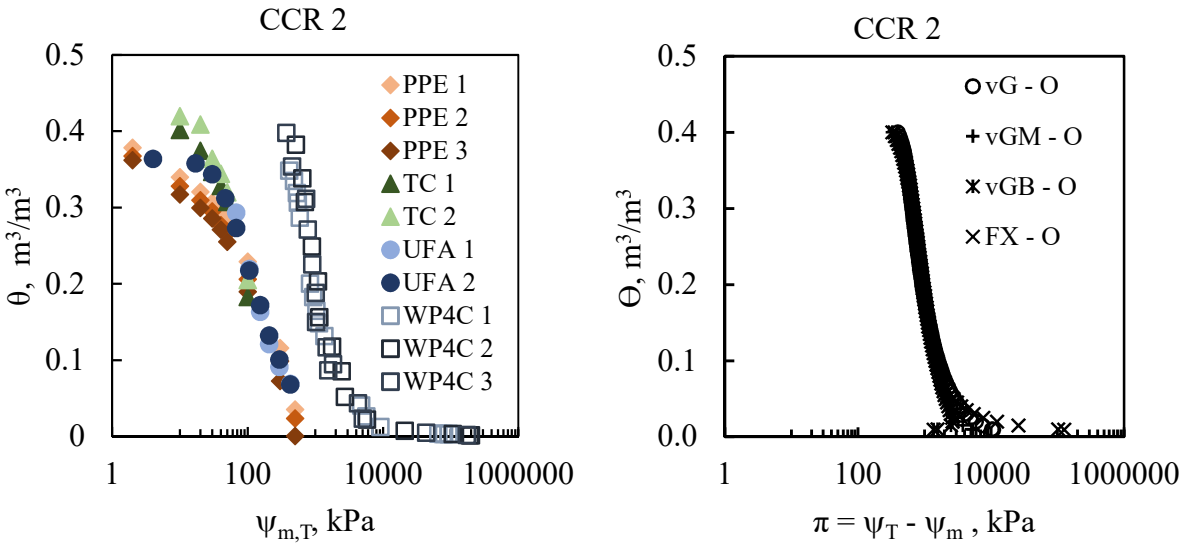


Figure 5-16. Osmotic suction relative to measured matric and total suction of CCR 2.

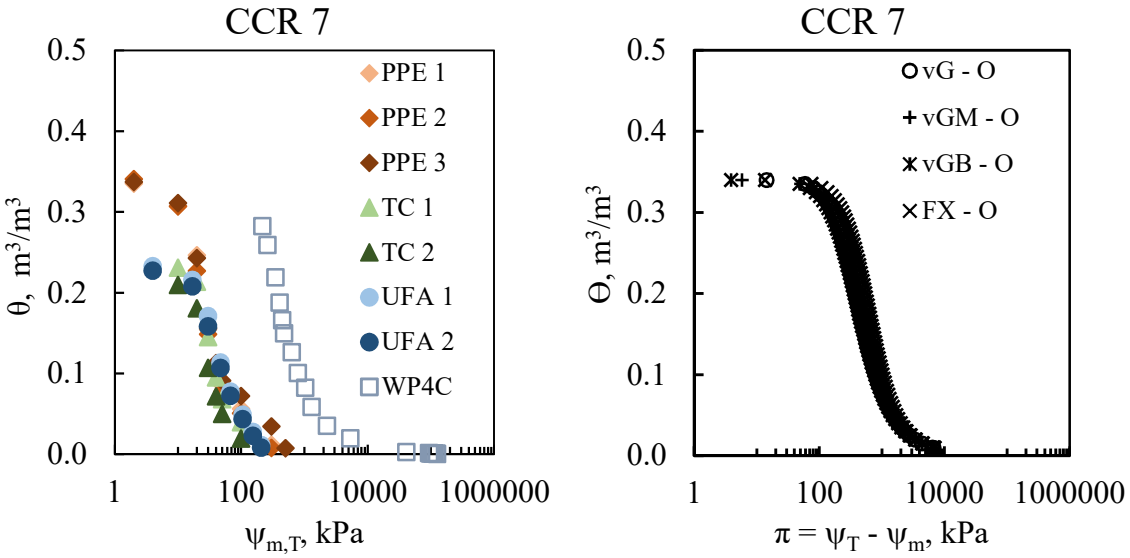


Figure 5-17. Osmotic suction relative to measured matric and total suction of CCR 7.

5.3.3.4 Unsaturated hydraulic conductivity

Using the unsaturated functions obtained from the WRC curves in section 5.3.3.2, the unsaturated hydraulic conductivity of the compacted CCRs were predicted using the vGM and vGB models described in Eq. 2-12 and Eq. 2-13, respectively. At saturation, both models predicted similar values; however, after the AEV was crossed, variations were observed with hydraulic conductivity decreasing with an increase in matric suction. The same trend was observed for the unsaturated hydraulic conductivity – water content relationship. These observations compare well with that reported in literature for soils (Menezes et al. 2011) and fly ash (Young 1993). The UFA measures the unsaturated hydraulic conductivity as a function of water content. Therefore to compare predicted values to the measured values, Eq. 2-12 and Eq. 2-13 were defined in terms of volumetric water content as described by Dourado Neto et al. (2011). Figure 5-18 through Figure 5-22 illustrate the comparison of measured unsaturated hydraulic conductivity to predicted unsaturated hydraulic conductivity using the estimated unsaturated functions from Table 5-2 through Table 5-6.

The vGM model had a better fit to the measured data compared with the vGB model. Both models predicted relatively lower values for CCRs consider except for CCR 1, where the vGM model predicted high values as matric suction increased, and water content decreased. In general, the vGB model predictions showed significant variations at lower water contents where matric suctions were higher. The variations in predictions can be attributed to the tortuosity and connectivity of the pore size distributions. Therefore, considering the good fit of vGM, which considers a tortuosity level of 0.5,

suggests the vGM provides a good representation of the pore size distribution than the vGB model, which considers a tortuosity level of 2.

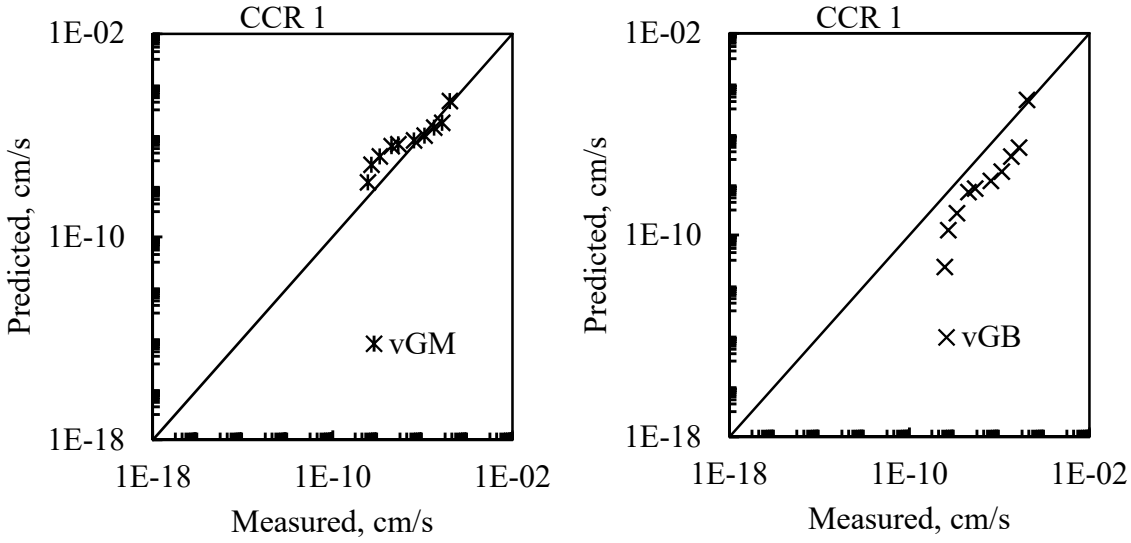


Figure 5-18. Graphical comparison of vGM and vGB unsaturated hydraulic conductivity to UFA measure data CCR 1.

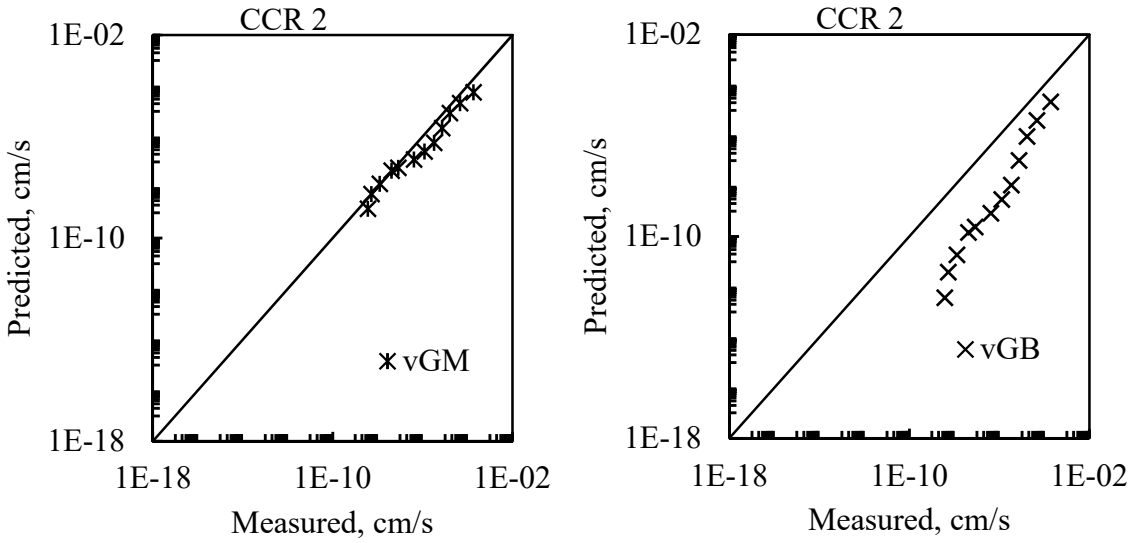


Figure 5-19. Graphical comparison of vGM and vGB unsaturated hydraulic conductivity to UFA measure data CCR 2.

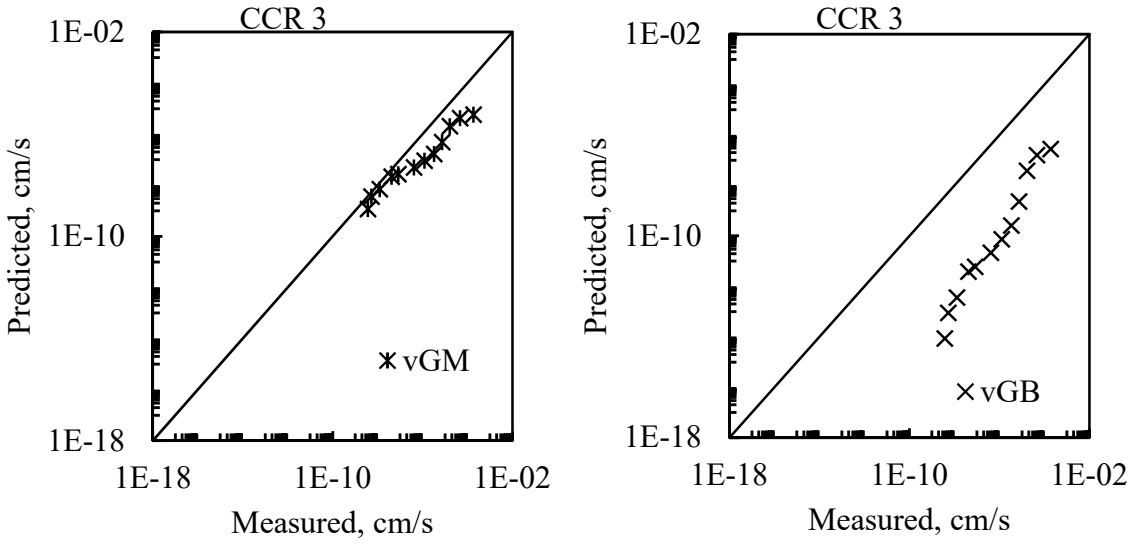


Figure 5-20. Graphical comparison of vGM and vGB unsaturated hydraulic conductivity to UFA measure data CCR 3.

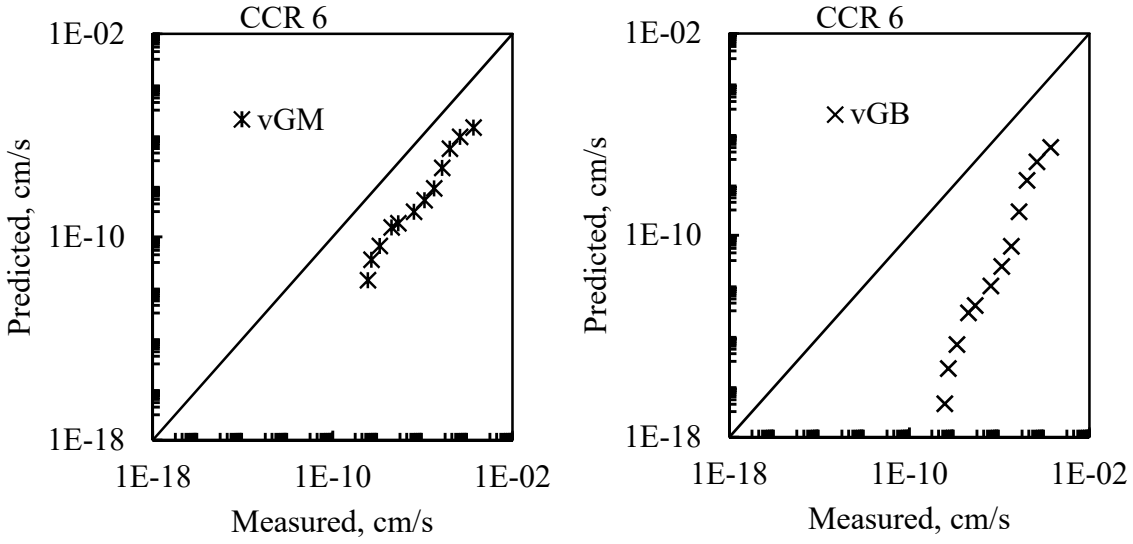


Figure 5-21. Graphical comparison of vGM and vGB unsaturated hydraulic conductivity to UFA measure data CCR 6.

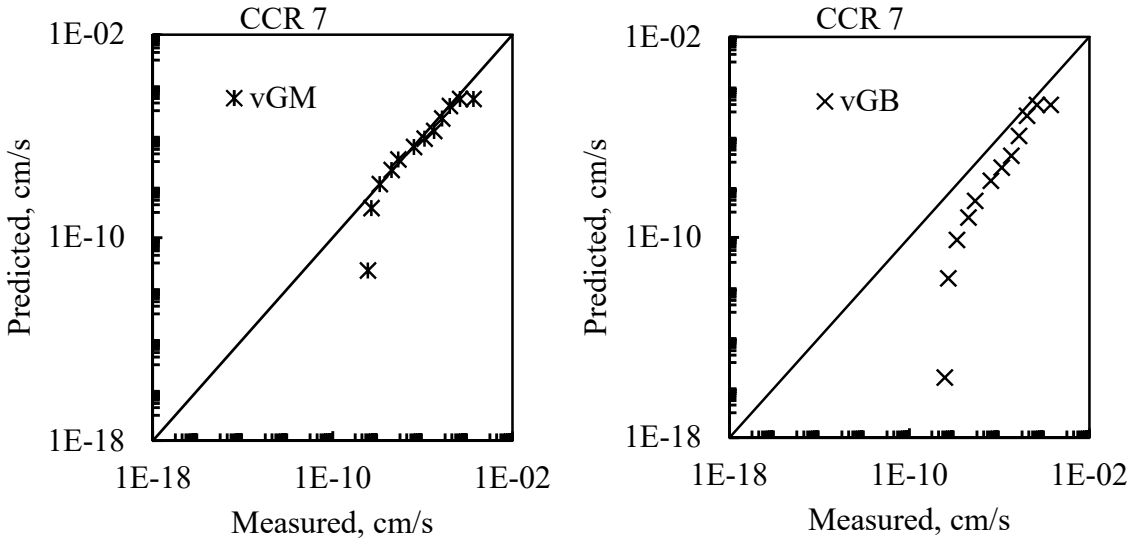


Figure 5-22. Graphical comparison of vGM and vGB unsaturated hydraulic conductivity to UFA measure data CCR 7.

5.3.3.5 Predictive model

Table 5-7 provides a summary of the model parameters estimated based on the particle size distribution parameter, $D_{60}$ of the CCRs using Eq. 2-8 through Eq. 2-11. The results were inconclusive as the predicted WRC had a poor fit to the measured WRC of the compacted CCRs. The estimated AEVs and *m* were lower compared to that presented in Table 5-1 through Table 5-6. The n parameter was assumed constant. Though the CCRs are non plastic, this observation could be attributed to the unique morphorlogy of CCRs hence require further investigation using Pedotransfer method.

Table 5-7. Summary of model fitting parameters based of $D_{60}$.

| Parameters | CCR | | | | |
|---|---|---|---|---|---|
| | 1 | 2 | 3 | 6 | 7 |
| $D_{60}$, mm | 0.038 | 0.031 | 0.051 | 0.125 | 0.041 |
| a, kPa | 10.06 | 11.72 | 8.06 | 4.11 | 9.50 |
| n | 7.5 | 7.5 | 7.5 | 7.5 | 7.5 |
| m | 0.1939 | 0.1578 | 0.2461 | 0.4049 | 0.2074 |
| $\psi_r$, kPa | 46.63 | 56.16 | 35.26 | 13.59 | 43.44 |

5.3.3.6 Pore size estimate of compacted CCRs

Considering untreated CCR, Eq. 2-15 can be written in terms of suction as described in Eq. 5-1 for pore size analysis.

$$r = -\frac{2\sigma cos\theta'}{\psi_m} \quad \text{Eq. 5-1}$$

Where r = pore radius in mm, σ = surface water tension in N/m, θ′ = contact angle in degrees, and $\psi_m$ = matric suction in kPa. The average temperature reading in the laboratory using a temperature and humidity sensor was approximately 22 °C. Therefore, the surface tension of water at 22°C was taken as 0.07025 N/m (Vargaftik et al. 1983). The CCRs were determined to by hydrophilic with contact angle assumed to be zero as drop volume of water was not sustainable for contact angle measurement. The largest pore sizes of the compacted CCRs were estimated using the AEV which has an indirect relationship with the largest pore radius as given in Eq. 5-1. These values of pore radii were compared to pore radii of standard grain packings, cubic and tetrahedral, as a function of the median diameter of the particle size distribution using Eq. 5-2 and Eq. 5-3, respectively (Keatts et al. 2018). Table 5-8 presents the largest pore size estimates of

the compacted CCRs using AEV estimated from parametric models considered in this study. Results for each test method refer of fitting to all multiple test specimens performed on each CCR sample while combined refers to all multiple test specimens of the multiple test methods all together.

$$r_{Cubic} = \frac{0.41D_{50}}{2} \quad \text{Eq. 5-2}$$

$$r_{Tetrahedral} = \frac{0.15D_{50}}{2} \quad \text{Eq. 5-3}$$

Results show that most of the pore radii estimates are in the range of cubic and tetrahedral packing with some outliers. The pore radii values greater than the cubic packing pore radius suggested a more porous CCR, which corresponds to relatively low AEVs comparable to coarse grain particles. For pore radii values less than tetrahedral packing pore radius, values indicated relatively higher AEVs for matric suction. These values corresponded to parametric models with more than two parameters that had no constraints on the upper limits, i.e. vG and FX. Nevertheless, the pore radii estimated shows a good correlation to the particle sizes of the CCRs considered.

Table 5-8. Pore size analysis of compacted CCRs.

| CCR | $D_{50}$,mm | Packing Pore Radii, mm | | Model | AEV Pore Radii, mm | | | |
|---|---|---|---|---|---|---|---|---|
| | | Cubic | Tetrahedral | | PPE | TC | UFA | Combined |
| 1 | 0.012 | 0.0025 | 0.0009 | vG | 0.0005 | 0.0041 | 0.0013 | 0.0011 |
| | | | | vGM | 0.0015 | 0.0018 | 0.0011 | 0.0016 |
| | | | | vGB | 0.0025 | 0.0029 | 0.0015 | 0.0027 |
| | | | | FX | 0.0006 | 0.0021 | 0.0006 | 0.0007 |
| 2 | 0.026 | 0.0053 | 0.0004 | vG | 0.0018 | 0.0021 | 0.0052 | 0.0004 |
| | | | | vGM | 0.0061 | 0.0030 | 0.0034 | 0.0042 |
| | | | | vGB | 0.0073 | 0.0046 | 0.0046 | 0.0061 |
| | | | | FX | 0.0000 | 0.0022 | 0.0030 | 0.0005 |
| 3 | 0.042 | 0.0086 | 0.0006 | vG | 0.0032 | 0.0018 | 0.0019 | 0.0008 |
| | | | | vGM | 0.0044 | 0.0046 | 0.0030 | 0.0030 |
| | | | | vGB | 0.0060 | 0.0063 | 0.0042 | 0.0047 |
| | | | | FX | 0.0023 | 0.0017 | 0.0016 | 0.0007 |
| 6 | 0.063 | 0.0129 | 0.0010 | vG | 0.0027 | 0.0164 | 0.0052 | 0.0015 |
| | | | | vGM | 0.0035 | 0.0165 | 0.0034 | 0.0067 |
| | | | | vGB | 0.0050 | 0.0221 | 0.0046 | 0.0063 |
| | | | | FX | 0.0009 | 0.0058 | 0.0030 | 0.0007 |
| 7 | 0.039 | 0.0080 | 0.0006 | vG | 0.0071 | 0.0074 | 0.0000 | 0.0038 |
| | | | | vGM | 0.0098 | 0.0054 | 0.0529 | 0.0090 |
| | | | | vGB | 0.0124 | 0.0064 | 0.0374 | 0.0087 |
| | | | | FX | 0.0067 | 0.0060 | 0.0001 | 0.0036 |

## 5.4 Summary

The unsaturated functions of compacted CCRs were determined by measuring the WRC and the unsaturated hydraulic conductivity. The variability and repeatability of the test methods were evaluated using multiple test specimens for each test method. The

variability and repeatability in terms of CCRs were assessed using various test methods. Parametric models were fitted to the suction measurements, and their performance evaluated. A predictive model based on the index property was evaluated in developing the WRC of compacted CCR. Measured unsaturated hydraulic conductivity values were compared to predictive values, and the fitness of the predictive models evaluated.

- The test method performed relatively well with little to no variations in multiple test specimens for each test method. Variations observed were mostly limited to varying dry unit weights of the multiple test specimens.
- Variations were observed for the various test methods considered for the CCRs primarily due to dry unit weight and due to the governing principle measuring techniques. However, measured data were comparable as similar trends of desaturation were observed for test methods considered for each CCR.
- The parametric models matched well, having a good fit to measured data and generating parameters comparable to what has been reported in literature.
- The vGM unsaturated hydraulic conductivity model predictions compared well with the UFA measured data for all CCRs providing an idea on the tortuosity and pore size distribution of the compacted CCR.
- Significant osmotic suction was observed in CCR 2 and CCR 7 due to the presence of high salt concentrations presumably from air emission control measures and not the chemical compositions of the CCR.
- The largest pore radii estimated were found to correlate with the particle size distribution of the CCRs.

- In general, the suction measurements were found to be influenced by the physical and chemical properties of the CCRs. For example, the transition zone of the WRC curve is dependent on the pore size distribution of the compacted, a fuction of particle size distribution and structure. Thereby, influencing the water storage capacity and permeability characteristics of the compacted CCRs.

# CHAPTER 6: IMPACT OF SOLUBLE SALTS ON UNSATURATED HYDRAULIC ENGINEERING PERFORMANCE OF COAL COMBUSTION RESIDUALS

## 6.1 Introduction

Coal combustion residuals have a unique chemical composition, mostly defined by the source of coal and the emission control system. However, the U.S EPA implementation of the new emission controls such as sodium-based dry sorbent injection, wet FGD additives, among others, has the potential to increase the salt content of CCRs, thus influencing the CCR chemical compositions for disposal and beneficial reuse. Studies have demonstrated that pH conditions defined by presence of salts enhance the mobility of trace elements in CCRs (Izquierdo and Querol 2012). The effect of these salts on the engineering performance of CCRs has not been fully explored.

Therefore, the motivating question for this chapter was whether the presence of soluble salts in CCRs contributes to the unsaturated hydraulic properties of CCRs and should it be considered for long term design in engineered systems. The main objective of this chapter was to assess the significance of soluble salts to field relevant parameters of CCRs such as infiltration.

This chapter is divided into four sections, namely experimental design, selected engineering properties that describe the hydraulic and mechanical behaviors of compacted CCRs, unsaturated functions of compacted leached CCR, and the concluding remarks.

## 6.2 Experimental Design

### 6.2.1 Materials

CCR 2, a class F fly ash, was considered for this study for two main reasons. First, the EC, which has a direct relationship with the amount of dissolved salt in pore fluid, was tens of thousands higher than the DI water used in this study as presented in Table 4-9, and second, fly ash make up a significant portion of unencapsulated beneficial use of CCRs in engineered systems such structural fills/embankment and mining reclamation. Thus, it is relevant to evaluate the significance of soluble salt to the performance of these engineered systems.

Unlike most salinity studies (Abedi-Koupai and Mehdizadeh 2007; Miller and Nelson 2006; Thyagaraj and Rao 2010), where known salts were added to the soil matrix in varied concentrations, this study took a reverse approach by reducing the salt content in the selected CCR. The US EPA method 1313 leaching test (USEPA 2012), was adopted to lower the soluble salt content in the CCR 2 through an extensively leaching program at apparent natural pH conditions. The variation in the soluble salt concentration provided the basis for evaluating the effect of salts on the unsaturated hydraulic behavior of a salt enriched CCR. The leached CCR was tested for selected geotechnical characterization tests, hydraulic and mechanical response at maximum dry density wet of optimum water content, and WRC for samples compacted at standard Proctor effort.

### 6.2.2 Experimental method

For a liquid to solid (L/S) ratio of 1 (L/S = 1), DI water was added to oven-dried CCR in a 1000 ml HDPE bottle and tumbled in an end-to-end fashion to form a homogeneous matrix using a tumbler machine for 2 hours. The matrix of DI water and

CCR 2 was left to settle for a period of 10 minutes. The supernatant was evaluated for EC and pH, then later decanted. Using a filtration system consisting of a 0.45 µm filter and a Buchner funnel assembly, a portion of the supernatant was filtered and stored in a 50 ml centrifugal vial for ionic concentration analysis. DI water was added to the residue at a L/S = 1, and the process repeated until there was no significant change in the EC logged. The residue was oven-dried until no change in mass was recorded. The process was repeated until sufficient quantity was produced for further geotechnical analysis. Figure 6-1 provides a conceptual diagram of the leaching process as described above.

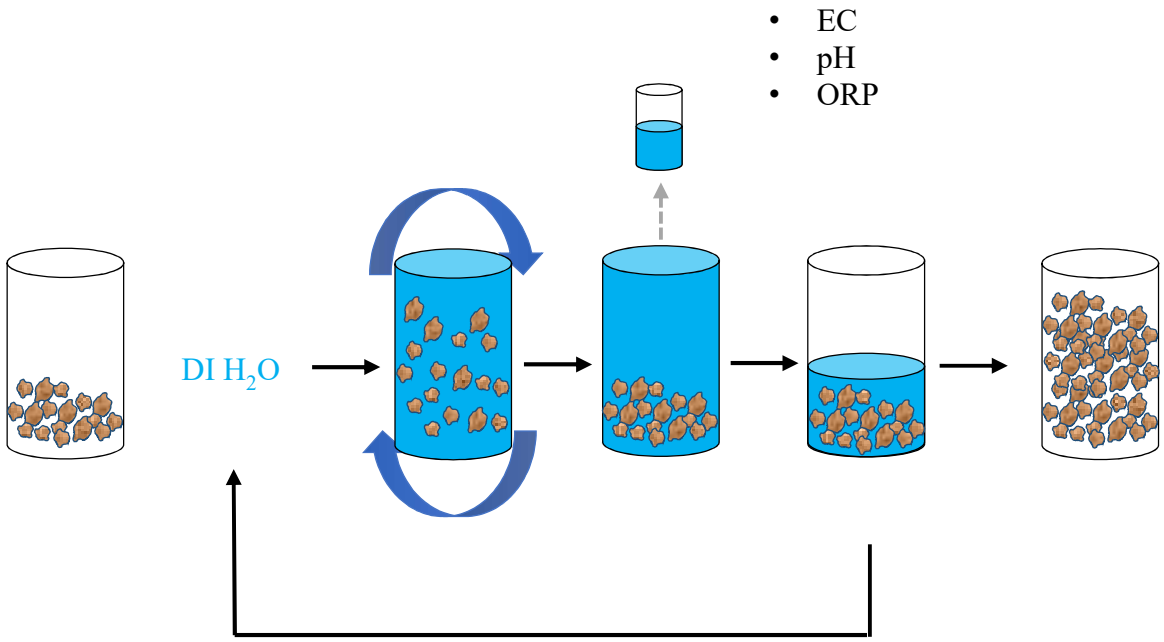


Figure 6-1. Illustration of the leaching process using the US EPA Method 1313 method to reduce the salt content of the CCR.

The supernatant chemistry was monitored for each leaching cycle by logging the EC and pH behavior. Figure 6-2 illustrates the change in EC as a function of the number of leaching cycles. This was compared to samples leached at L/S = 1 for 24 hours of

tumbling and at L/S = 20 for 24 hours of tumbling (Method 1313) as illustrated in Figure 6-2. The initial supernatant produced relatively high EC values as the soluble salts in the CCR diffused into the DI water which had relatively low EC as presented in Table 4-9. As the number of leaching cycles increased, the EC of the pore fluid decreased due to a reduction in soluble salt concentrations as shown in Figure 6-2. Although initial values were high, significant variability existed for the conditions considered. The initial EC value L/S = 1 for 2 hours was 43% and 103% more than L/S = 1 for 24 hours and L/S = 20 for 24 hours, respectively. The EC values of L/S = 1 for 2 hours reached that of tap water after the 12$^{th}$ leaching cycle. After the 3$^{rd}$ cycle of leaching, L/S = 1 for 2 hours compared relatively well to L/S = 1 for 24 hours. For L/S = 20 for 24 hours, the EC got to the levels of the laboratory tap water as presented in Table 4-9after the 3$^{rd}$ cycle of leaching.

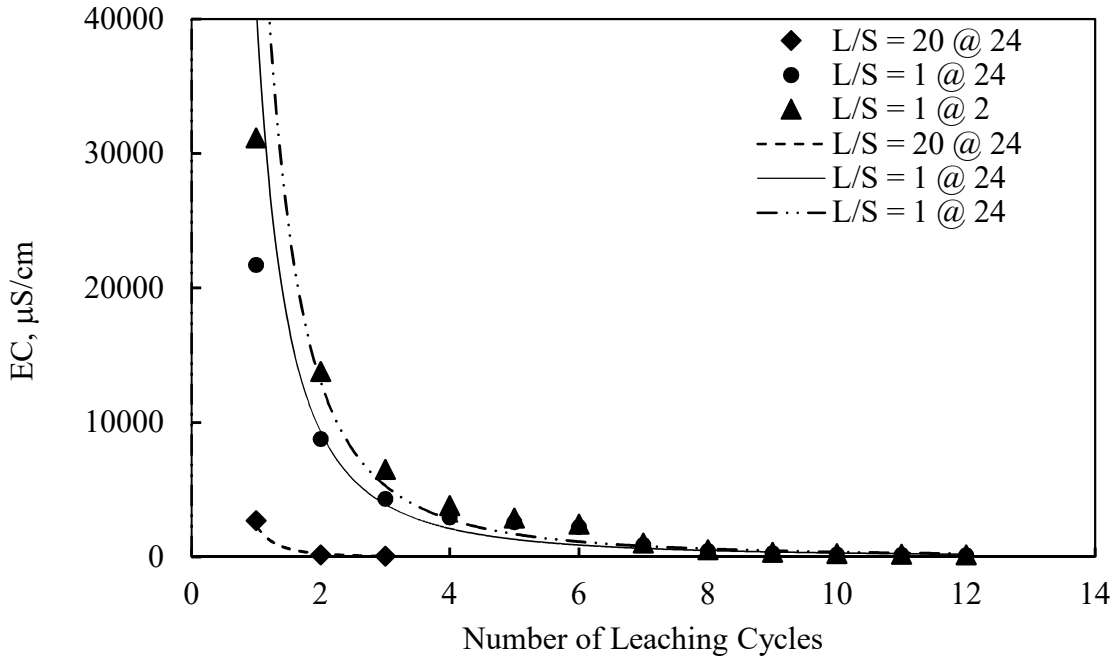


Figure 6-2. Change in soluble salt content as a function of EC with an increase in leaching cycles.

6.3 Chemical Analysis of CCR Leachate

The leachate generated after each leaching cycle was analyzed for concentrations of select cations using the inductively coupled plasma optical emission spectrometry (ICP-OES). Anions were not analyzed in this study. The test covered a wide range of metals including silicon (Si), aluminum (Al), arsenic (As), argon (Ar), boron (B), barium (Ba), calcium (Ca), chromium (Cr), potassium (K), lithium (Li), magnesium (Mg), sodium (Na), selenium (Se), silicon (Si), strontium (Sr), and vanadium (V). The results were analyzed based on the USEPA Method 200.7 (USEPA 1994). Figure 6-3 shows the concentrations in ppm of cations analyzed in the initial leachate generated in ppm.

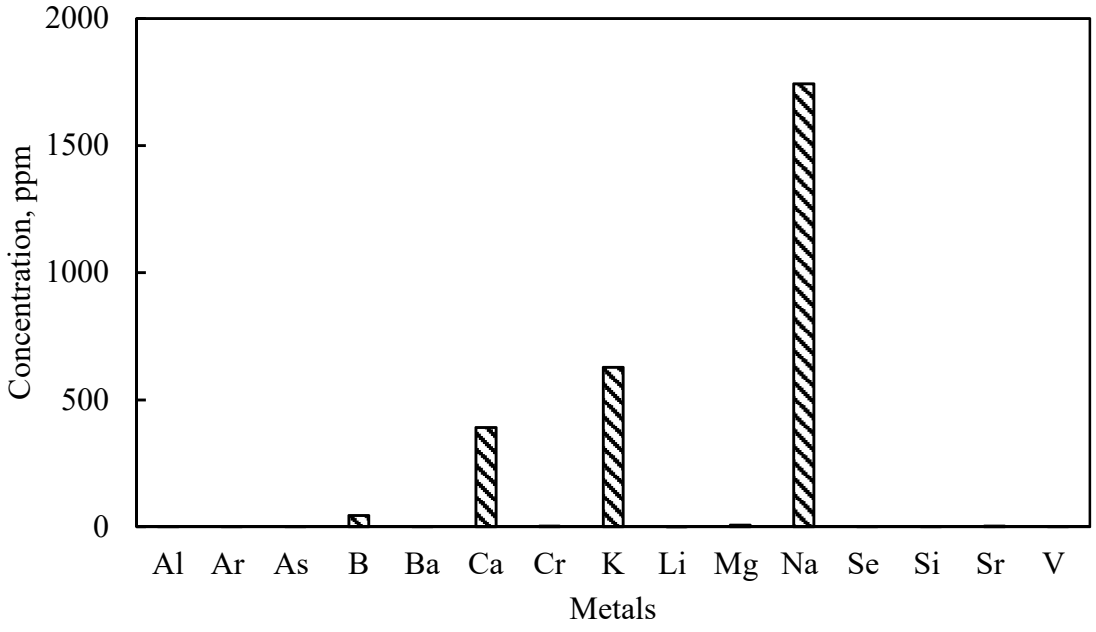


Figure 6-3. Cation concentration of metals in initial leachate generated in CCR 2 for L/S = 1 for 2 hours of tumbling.

The concentration of Ca, K, and Na constitute a total of 98% of the metals analyzed. These metals indicated the presence of Ca, K, and Na based salts in CCR 2. The presence of Ca in fly ash come in several forms including calcite, lime, anhydrite, and glassy matrix and leaches without difficulty irrespective of the extractant used (Izquierdo and Querol 2012). Potassium and Na occur in glassy matrix and have relatively low leachability under toxicity characteristics leaching procedure and water based leaching test for both acidic and alkaline fly ash (Izquierdo and Querol 2012). A large amount of Ca in CCR leachate indicates the presence of free lime, whereas leachable K and Na indicate Al-K-sulphate coating absorbed on a glassy matrix (Izquierdo and Querol 2012). Considering the leaching conditions of CCR 2, it can be assumed that the high concentrations of Na, Ca, and K are a result of emission control and zero liquid discharge policies, as discussed by Renew et al. (2015). Further analysis of subsequent leachate generated show a significant reduction in these metals as shown in Figure 6-4.

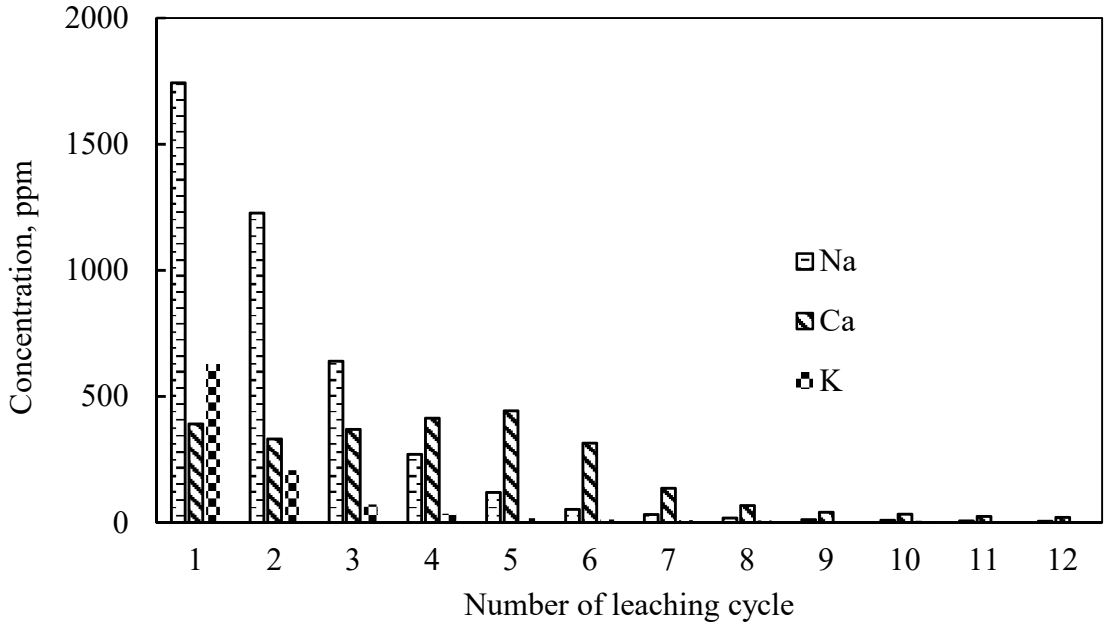


Figure 6-4. Leaching characteristics of Na, Ca, and K metals with an increasing number of leaching cycles.

6.4 Engineering Characterization of Leached CCR.

For this study, the heavily leached CCR was termed “leached CCR”. The leached CCR was thoroughly mixed to form a homogeneous material for further laboratory analysis. Selected geotechnical engineering index property tests were performed in accordance with standardized test methods, including specific gravity ASTM D854 (ASTM 2014), standard Proctor compaction ASTM D698 (ASTM 2012), and particle size distribution using a laser diffraction particle size analyzer. The results are summarized in Table 6-1 with the particle size distribution curves, and compaction curves shown in Figure 6-5 and Figure 6-6, respectively.

Table 6-1. Summary of physical properties of leached CCR.

| Property | CCR 2 | |
|---|---|---|
| | Leached | Unleached |
| | Class F Fly Ash | |
| Specific gravity | 2.66 | 2.67 |
| Particle size characteristics, % | | |
| Sand (4.75-0.075mm) | 11 | 12 |
| Silt (0.075-0.005 mm) | 84 | 85 |
| Clay (<0.005 mm) | 5 | 3 |
| % < | | |
| $D_{10}$, mm | 0.0079 | 0.0079 |
| $D_{50}$, mm | 0.0307 | 0.0307 |
| $D_{90}$, mm | 0.1085 | 0.1085 |
| USCS classification | ML | ML |
| Standard Proctor Compaction: | | |
| Maximum dry unit weight, $kN/m^3$ | 15.30 | 16.20 |
| Optimum water content, % | 18.40 | 18.10 |

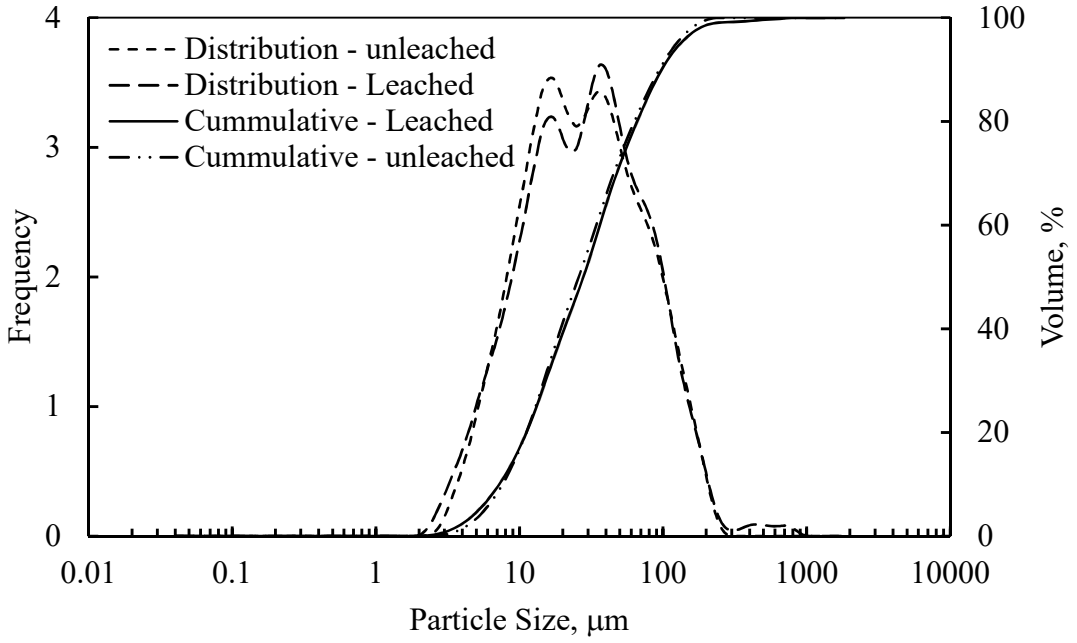


Figure 6-5. Particle size distribution curve using a laser diffraction particle size analyzer.

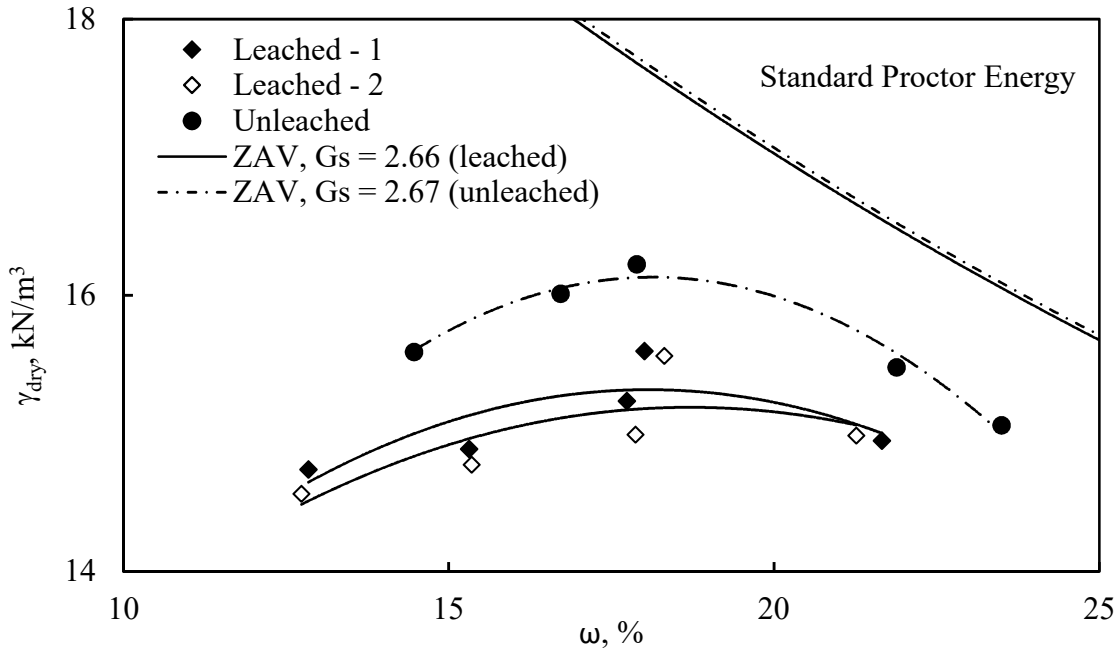


Figure 6-6. Standard Proctor compaction characteristics of leached CCR.

The measured specific gravity of the leached CCR was obtained from duplicate tests with an average value of 2.66 approximately equal to that of the unleached CCR, which had significant soluble salt contents. Dissolved salts have the potential of introducing some errors in the estimation of particle densities as it increases fluid mass than fluid volume, thus increasing the fluid density. Gorakhki and Bareither (2016) addressed this limitation considering the dissolved salt to correct the specific gravity of saline soils. The results showed a significant reduction in specific gravity values with an increase in salinity. The presence or absence of soluble salts do not significantly impact the specific gravity estimation in this research.

The particle size distribution curves were obtained from the duplicate tests with each test having triplicate runs. Both samples showed a bimodal distribution of particle sizes with no significant changes in the particle gradation, as presented in Figure 6-5. The leached CCR had a wider range of particle sizes from approximately <5 μm to 1041.0 μm as compared to the unleached CCR with a particle size range from 1.8 μm to 309.6 μm. With approximately 85% by volume of the particles within 1.5 μm to 75 μm range, both samples fall within silty sized particles thus can be classified as fine-grained with classification symbol ML according to USCS ASTM D2487 (ASTM 2011a). The laser diffraction particle size analyzer method is based on the % particle volume finer compared well with the % particle size distribution test method ASTM D422 (ASTM 2007) based on the particle mass finer.

The compaction curve of the leached CCR was determined using the standard Proctor energy. Duplicate tests were performed to ascertain any variation in the leached CCR. No significant differences were observed as the compaction curves were relatively

the same. But the compaction curves of the leached CCR were relatively lower compared to the unleached CCR for the range of water content considered as shown in Figure 6-6. The average value of the maximum dry unit weight equals 15.3 kN/m$^3$, a six per cent reduction in the maximum dry unit weight of the unleached CCR. However, the corresponding optimum water content of 18.4 % was marginally higher. The leached CCR has compaction characteristics as the unleached CCR as well as those reported in previous studies. There were no significant changes in the dry unit weight of the leached CCR with variations in water content giving it a relatively flat shape. Several studies have reported a considerable increase in compaction characteristics in salt amended soils. The reduction in dry unit weight can be attributed to the absence of the Na, Ca, and K base salts. Studies have reported that these salts undergo chemical reactions that result in binding particles together, thus improving interconnectivity, which results in the improvement of the mechanical performance of CCRs and soils. The dissolution of these salts can result in structural failure in CCRs and soils (Foncea et al. 2005; Trivedi and Sud 2004).

## 6.5 WRC Measurements of Leached CCR

### 6.5.1 Suction measurement

The Tempe cell and WP4C were selected to measure the matric and total suction of the leached CCR, respectively. The osmotic suction was analyzed by finding the difference in the total suction and matric suction. Sample preparation was similar for both tests but tailored to fit the test specimen rings and cups for TC and WP4C, respectively. Duplicate test specimens were prepared for each test device to assess the reliability and repeatability of the selected test method. The specimens were subcored from a standard

Proctor compacted sample and trimmed to fit specimen rings with the initial masses logged. The compaction conditions of the test specimens are illustrated in Figure 6-7 in relation to the standard Proctor compaction characteristics of the leached sample. The initial compaction conditions were estimated using the water – density relationship whereas the final compaction was estimated using the mass – volume relationship of the oven-dry solids. The test specimens were compacted wet of optimum water content with dry unit weight density at least 95% of maximum dry unit weight.

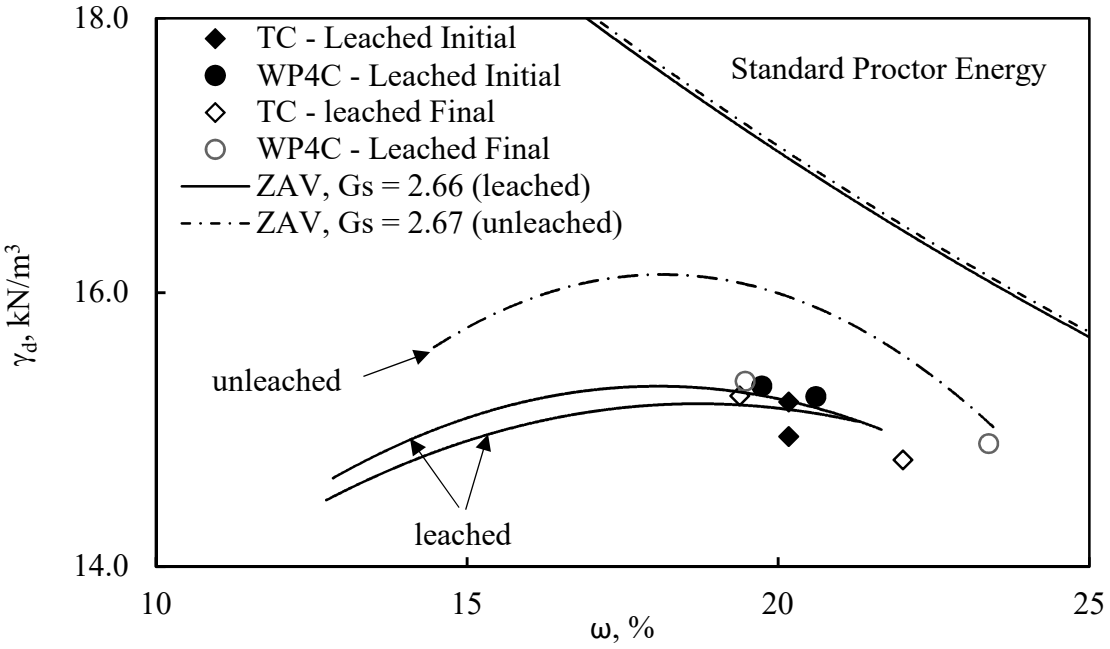


Figure 6-7. Compaction conditions of leached test specimens.

For the TC, saturated filter paper with medium permeability was installed on the saturated HAE disk to prevent the fine particles from clogging the pores of the HAE ceramic disk. Good contact was ensured with the HAE ceramic disk with a firm press and twist. Prior to saturation, the top cap was installed with the total mass logged. The

complete setup was fully submerged in a water bath of deaired DI water bath for at least 24 hours but with the top cap partly loose to prevent entrapped air from resisting the capillary rise of water during saturation. The degree of saturation was checked using measured parameters including bulk unit weight, dry unit weight, and specific gravity. The process of saturation continued until at least a 95% degree of saturation is achieved. Using the air pressure assembly in Figure 4-9, the specified air pressure was applied with the TC tightly sealed to prevent leakage. The test began with air pressures 10 kPa, 20 kPa, 30 kPa, 40 kPa, 50 kPa, and 100 kPa. For each air pressure applied to start from the lowest, the masses of the test specimens were logged at a specific time interval until no apparent change in the masses of the test specimens, wherein equilibration was attained. The next air pressure was applied until equilibration was achieved. At the end of the last air pressure application, the TC set up was disassembled, and test specimens were oven dried. The gravimetric water contents were back calculated for the saturation water content at each equilibrated mass. The mass of the HAE ceramic disk and the filter paper placed between the test specimens and the HAE ceramic disk was corrected using a TC setup without a test specimen.

In the case of the WP4C test specimens, the test specimens were saturated in a deaired DI water bath for at least 24 hours. The close bottom of the cup limits the flow of water during saturation due to the presence of entrapped air. The saturated test specimens were trimmed to almost half cup depth with initial moisture content measured. Due to limitations associated with saturation, few drops of deaired DI water was added to increase the saturation level. The sample cup with the trimmed sample was sealed with a plastic cap and Pama film and left for 24 hours to equilibrate. Prior to suction reading, the

WP4C was calibrated every 24 hours using a 0.5M KCl solution provided by Decagon and subsequently prepared in the UNC Charlotte Environmental Engineering research labs. Readings were taken for an hour using the continuous mode for suction range 0 MPa – 2 MPa and an average value was determined. For suction ranges 2MPa – 40 MPa and 40 MPa – 300 MPa, single readings are taken in precise and fast mode, respectively. Moisture content was measured before and after each reading over a period of 10 days.

### 6.5.2 Suction equilibration time

Following the same criteria for suction equilibration defined for Tempe cell, the rate of change in the gravimetric water content of the test specimen was logged and presented in Figure 6-8. The total test run was approximately 24 days. The shortest of 2 days occurred with a 10 kPa pressure application, which was observed to have occurred around the saturation and transition zone boundaries. For pressure application of 30 kPa through 100 kPa, it was found that the rate of change remained constant with a downward decline occurring within the transition zone of the test specimen.

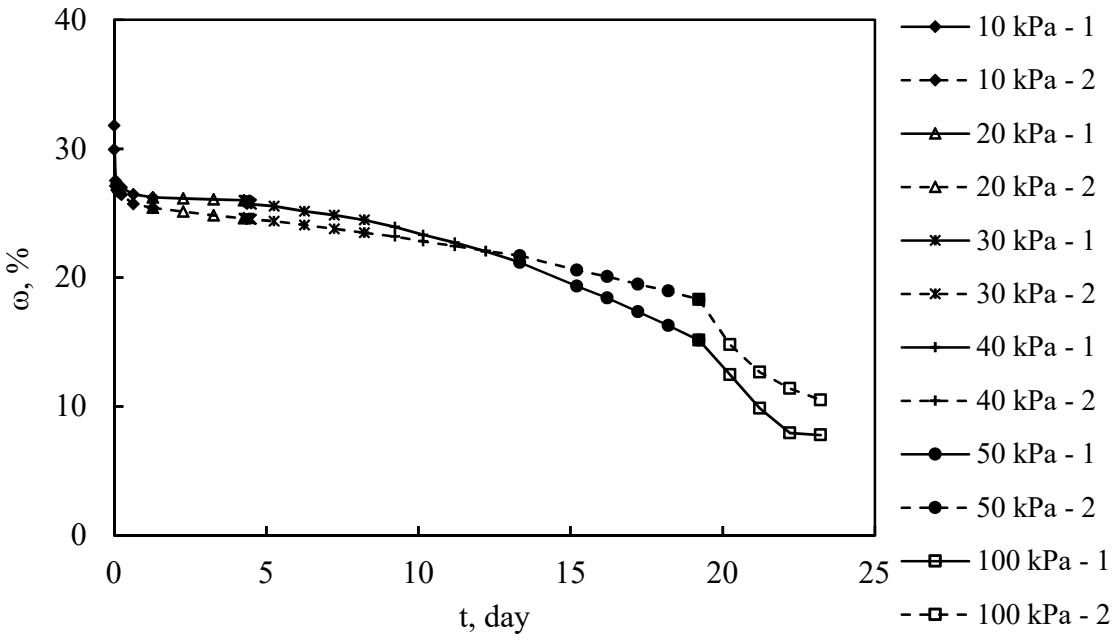


Figure 6-8. Suction equilibration time for leached CCR using TC.

### 6.5.3 WRC of leached CCR

The final compaction conditions was used in the WRC analysis as it provided the true representation of the test specimen. Figure 6-9 shows the volumetric water content-suction relationship of the leached CCR determined using the TC and WP4C for matric and total suctions, respectively. The Tempe cell had a short range of suction measurements from 10 kPa to 100 kPa due to the limit of the AEV of the HAE ceramic disk used. The WP4C covered a wide range of suction from 20 kPa to 100,000 kPa with suction relatively higher than that of TC. The high suction values in Figure 6-9 could be attributed to the presence of remnant dissolved salts within the hydroscopic moisture of fine particles of the test specimen, which accounts for osmotic suction or decrease in accuracy due to the sensitivity of the WP4C in the saturation zone. The difference in total

and matric suction, the osmotic suction is marginal and decreased in value with decreasing water content. However, both the matric and total suction increased with decreasing water content. Thus total suction was assumed to be equal to matric suction in the residual zone, where water content is low due to the negligible difference between the two (Sreedeep and Singh 2006). The total suction measurement seems to have a much higher desaturation rate than the matric suction measurement. This observation is related to the pore space distribution within the test specimen and is measurable using a parametric model to fit the measured data.

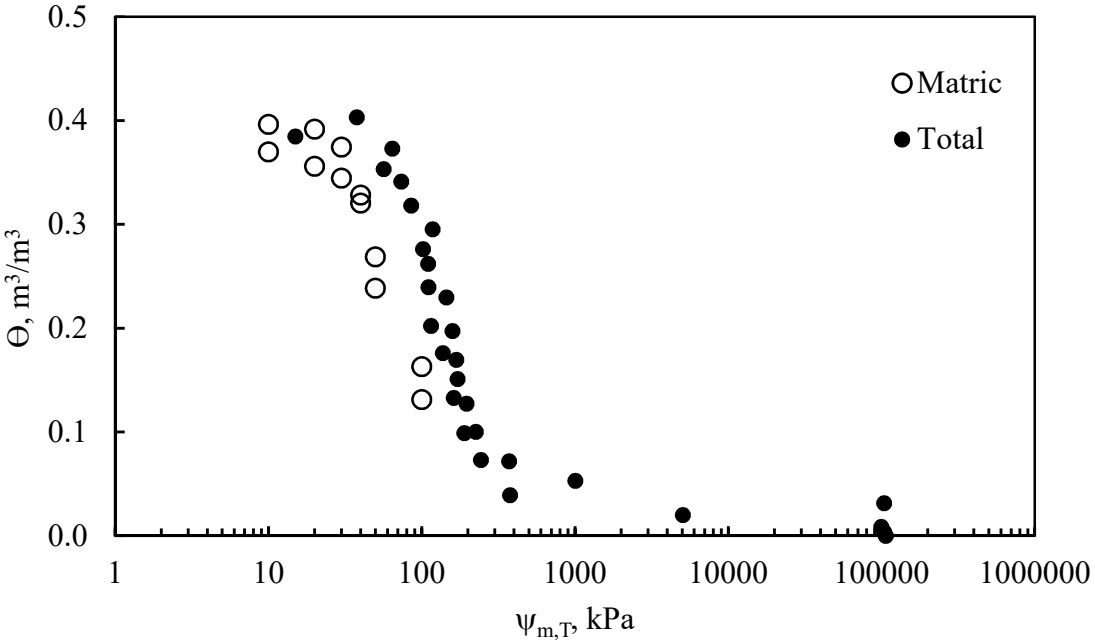


Figure 6-9. WRC of leached CCR using TC and WP4C.

6.5.4 Parametric model fitting

The parametric models, vGM, vGB, and FX, were fitted to the measured data to provide a continuous characterization of the water retention behavior of the leached CCR as explained in section 5.3.3.2. For clarity, only model fitting to combine data set are

shown in Figure 6-10 with a summary of corresponding model parameters presented in Table 6-2.

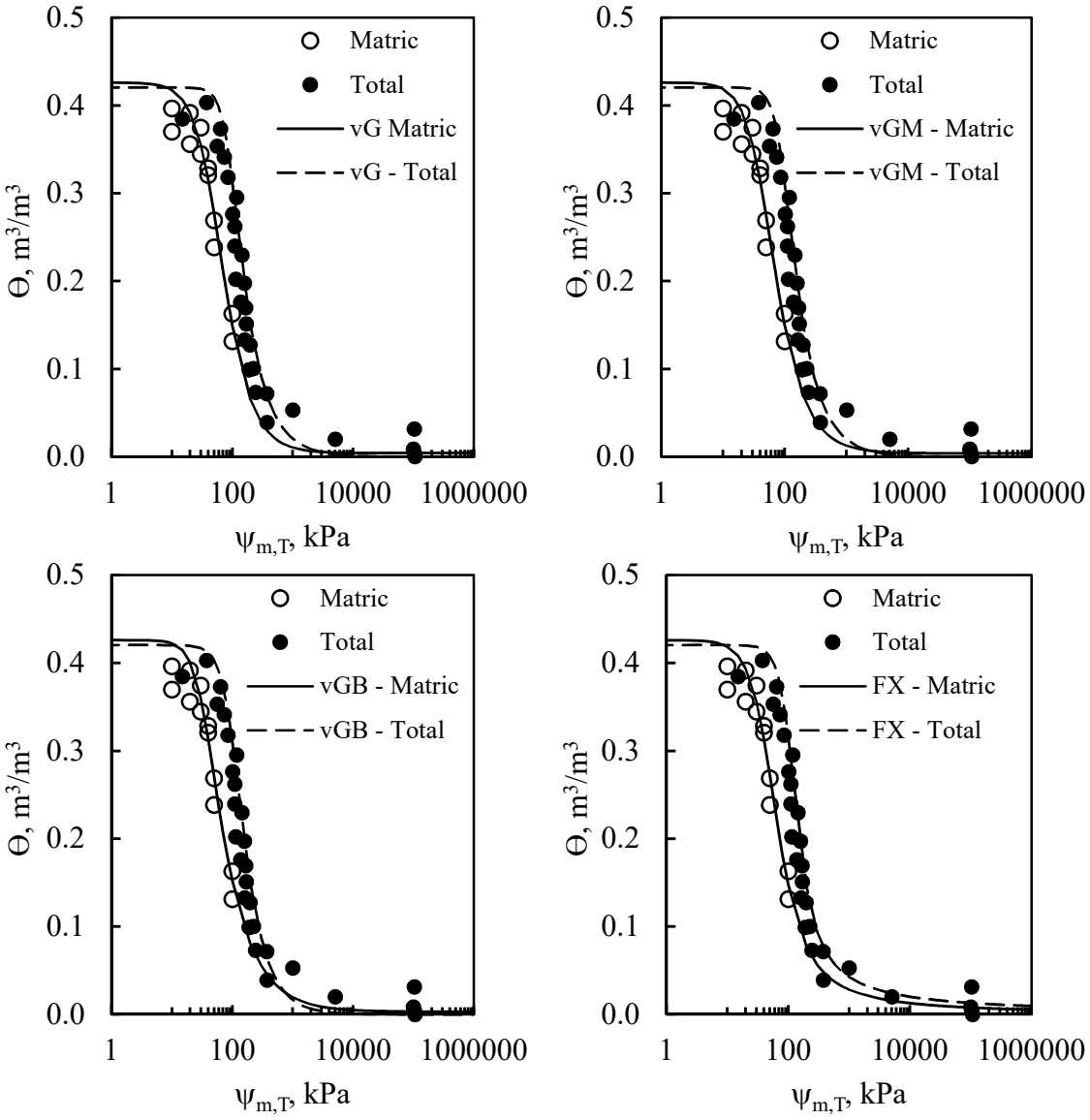


Figure 6-10. Parametric model fitting to combined data of matric and total suctions of the leached CCR measured using TC and WP4C, respectively.

Volumetric water content is a function of dry unit weight implying the lower the dry unit weight, the higher the porosity, which results in a more saturated sample. This

was the case of the TC test specimen, which had higher saturation volumetric water content compared to the WP4C test specimen due to the low dry unit weight of the test specimen, as illustrated in Figure 6-7. The selected parametric models fitted well to the measured data with marginal variations in the generated unsaturated functions. The AEVs, which correlates with the largest pore sizes, were found to be in the same order of magnitude and comparable to that of unleached CCR (Table 5-3) but an order of magnitude lower.

Table 6-2. Summary of model parameters for leached CCR.

| Suction | Model | Parameters | | | | | | |
|---|---|---|---|---|---|---|---|---|
| | | $\theta_s$, $m^3/m^3$ | $\theta_r$, $m^3/m^3$ | $\psi_{AEV}$, MPa | $\psi_r$, MPa | n | m | $R^2$ |
| Matric | vG | 0.4260 | 0.0041 | 0.053 | >1000 | 2.0878 | 0.6787 | 0.9767 |
| | vGM | 0.4260 | 0.0039 | 0.046 | >1000 | 2.2511 | 0.5558 | 0.9769 |
| | vGB | 0.4260 | 0.0031 | 0.034 | >1000 | 2.9603 | 0.3244 | 0.9771 |
| | FX | 0.4260 | 0.0000 | 0.046 | >1000 | 2.2090 | 1.4133 | 0.9773 |
| Total | vG | 0.4204 | 0.0000 | 0.087 | 140 | 4.2476 | 0.2899 | 0.9742 |
| | vGM | 0.4204 | 0.0000 | 0.088 | 130 | 4.1335 | 0.4226 | 0.9949 |
| | vGB | 0.4204 | 0.0000 | 0.097 | 68 | 3.3826 | 0.4087 | 0.9540 |
| | FX | 0.4204 | 0.0000 | 0.101 | >1000 | 3.6313 | 1.0789 | 0.9566 |

6.5.5 Pore size estimate of compacted leached CCR.

Following procedures detailed in section 5.3.3.6, the largest of pore of the test specimens were estimated and compared to the pore radii of standard grain packings, cubic and tetrahedral. Table 6-3 presents the largest pore estimates using AEVs of the matric suction WRC curve. The results show that the estimated pore radii are within the range of cubic and tetrahedral packing estimates. The pore radii estimated show a good

correlation to the particle sizes of the leached CCR and comparable to that of the unleached CCR.

Table 6-3. Largest pore radii estimate of leached and unleached CCR.

| CCR | $D_{50}$, mm | Packing Pore Radii, mm | | Model | AEV Pore Radii, mm | |
|---|---|---|---|---|---|---|
| | | | | | TC | |
| | | Cubic | Tetrahedral | | 1 | 2 |
| Leached | 0.0307 | 0.0063 | 0.0023 | vG | 0.0032 | 0.0035 |
| | | | | vGM | 0.0028 | 0.0034 |
| | | | | vGB | 0.0034 | 0.0029 |
| | | | | FX | 0.0035 | 0.0024 |
| Unleached | 0.0307 | 0.0063 | 0.0005 | vG | 0.0044 | 0.0044 |
| | | | | vGM | 0.0034 | 0.0027 |
| | | | | vGB | 0.0039 | 0.0042 |
| | | | | FX | 0.0023 | 0.0023 |

6.5.6 Effect of soluble salts on matric and total suction

For the matric suction, the leached test specimen matched reasonably well with the unleached test specimens. It was observed that the leached test specimens had relatively lower volumetric water content than the unleached test specimens. As mentioned previously, the lower the dry unit weight, the larger the pore spaces; hence, the less water to retain. In addition, the precipitation of soluble salts can increase the interparticle cohesion which then improves packing density, decreasing pore sizes therefore the more water to retain. With the leached test specimen having relatively the lower dry unit weight due to less soluble salt contents compared to the unleached test specimen as illustrated in Figure 6-7, its water retention capacity will be lower as

observed. The selected parametric models were fitted to the matric suction data set complimented by the corresponding total suction data set in the residual zone. The matric suction results indicate comparative model parameters to unleached CCRR (CCR 2) as presented in Table 5-3 but with marginal variations. The parametric models had a good fit for both measured data sets but with a better fit for the unleached test specimen. The rate of desaturation, estinmated through model parameter *n* (matric suction), was marginally higher in the leached test specimen compared to the unleached test specimen. An indication that the leached test specimen has large pore sizes indicating low capillary effect compared to the unleached test specimen, which was denser hence has small pore sizes; therefore, lower water drainage rate. It was also observed that AEV of the leached test specimen was marginally lower than that of the unleached test specimen a result of variations in dry unit weight as reported by (Elgabu 2013).

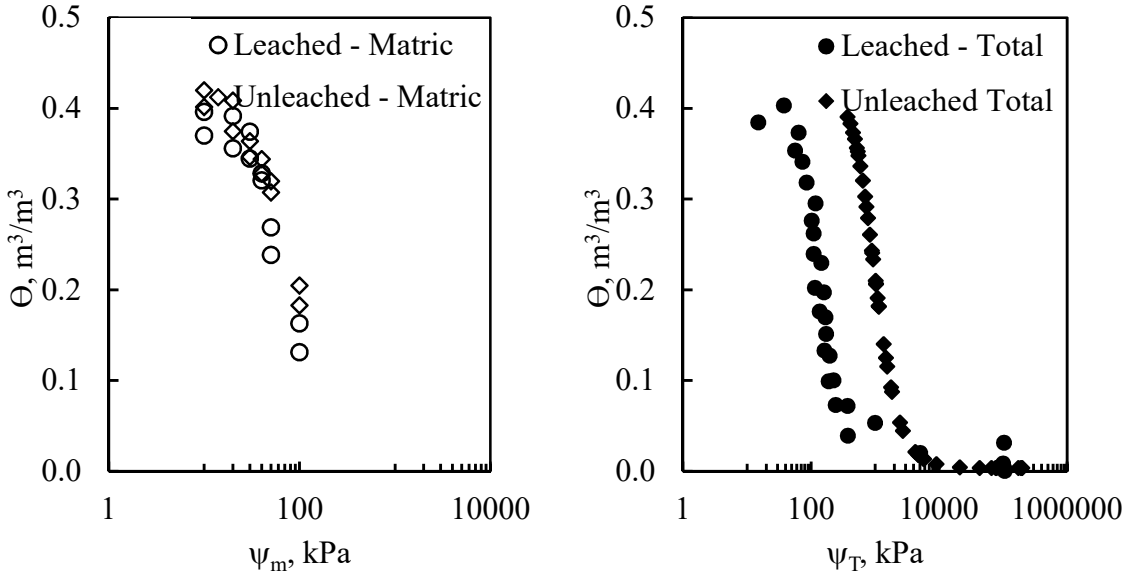


Figure 6-11. Comparison of (a) matric suction measurement for leached and unleached CCR and (b) total suction measurement for leached and unleached CCR.

For total suction, as shown in Figure 6-11(b), there is a significant difference in the leached and unleached test specimens. The total suction decreased with a decrease in soluble salt contents similar to observations made by Miller and Nelson (2006) where the addition of a moderate amount of known salt resulted in a significant increase in total suction measurements. The total suction of the unleached test specimen reduced by approximately 42% on the average. As shown in Figure 6-12, the osmotic suction range from approximately 200 kPa to 200 MPa increasing with a decrease in volumetric water content.

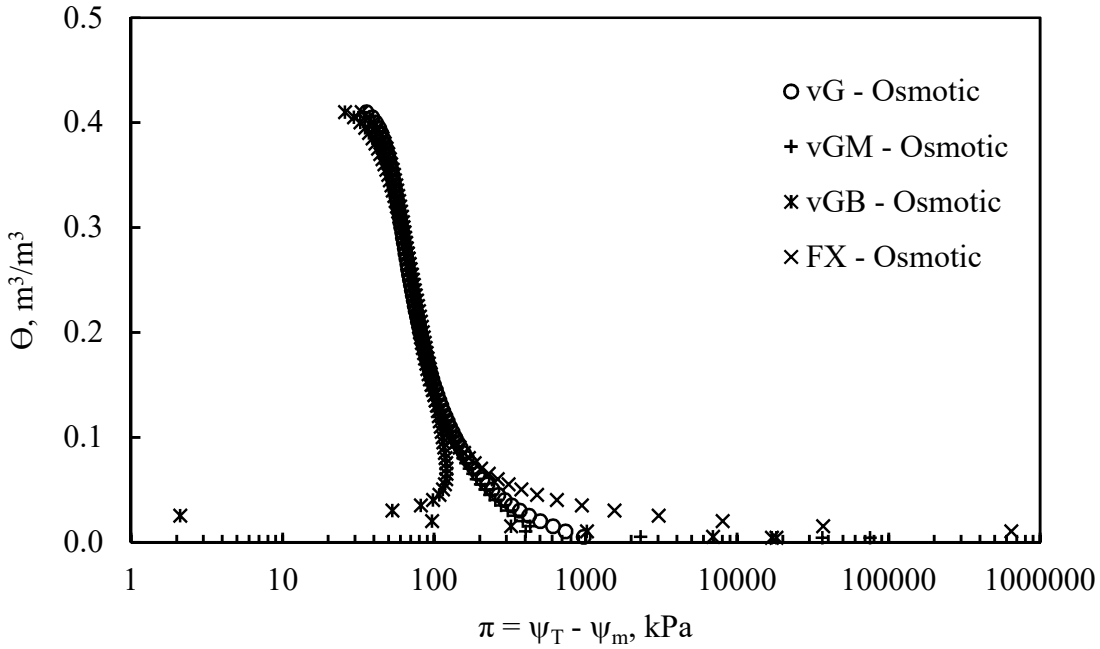


Figure 6-12. Osmotic suction of unleached CCR.

## 6.6 Summary

This chapter evaluated the impact of soluble salts present in the CCR on the selected engineering properties. The CCR was heavily leached and tested for engineering properties, including specific gravity, particle size distribution, compaction

characteristics, and WRC. The TC and WP4C were selected to measure the WRC, which were fitted with selected parametric models.

- The main soluble salts present in the selected CCR were found to be Na, K, and Ca implying they are presumably from the implementation of air emission control measures.
- The presence of the NA, K, and Ca base salts contribute to the compaction characteristics of the CCR, thus motivating the study on the potential impacts on the unsaturated hydraulic behaviors.
- The presence of the Na, K, and Ca salts have little to no effect on the unsaturated hydraulic functions of the selected CCR, which is mostly governed by matric suction, a function of capillary and adsorptive forces. However, the salt content significantly impacts the osmotic suction which can lead to volume changes and contaminant transport, as reported in literature.
- The WRC of the compacted CCR with extreme levels of soluble salts, which resulted in different dry unit weights, showed a marginal impact on AEV.
- The residual suction of CCRs is influenced by the morphology of the CCR particles and not particle pore space.
- The selected parametric models fitted well to the experimentally measured data of the leached and unleached CCR.
- Assuming the total suction of CCRs to be equal to matric suction for engineering design analysis without further tests would lead to errors in design parameters.

# CHAPTER 7: WATER REPELLENT TREATMENT OF COAL COMBUSTION RESIDUAL – A BATCH SORPTION APPROACH

## 7.1 Introduction

One of the objectives of this research was to gain better insights into the CCR surface modification process through OS sorption and to develop treatment method more suitable to standard geotechnical experimental evaluation of OS-treated CCRs. Recent studies have shown that there are multiple treatment protocols to achieve water repellency in soils and CCRs. However, these methods limit the remolding of OS-treated CCRs for geotechnical experimental evaluation. To contribute to the current knowledge of engineered water repellency treatment for typical geotechnical soils and CCRs, a batch sorption test protocol was developed as a fundamental approach to understand factors that influence water repellency of OS-treated CCRs.

Specifically, a factorial experiment was designed and implemented in this chapter to study the influence of the variables including material, OS dosage, reaction time, and drying conditions based on the batch sorption test. An overview of the testing protocol is as follows:

- Batch samples were prepared at varying OS dosages with constant L/S value detailed in Table 4-11.
- The OS solution-CCR matrix were batched in a tumbler for specified reaction period.
- The batched samples were allowed to settle and the supernatant decanted. The residual OS solution was rinsed off using DI water at L/S = 20 for multiple times until OS concentration is negligible.

- The residue was split into two specimens to oven dry and air-dry.
- The degree of water repellency was measured using SDM and drop image analysis software.

The decanted supernatant of the sample batched for 24 hours was analyzed for EC and pH to establish qualitatively the reactivity and sensitivity of the OS sorption process.

7.2 Sorption Test Procedure

Four different dosages were considered for surface modification test and evaluated for varying degrees of water repellency. The dosages were determined by weight using the ratio of 2, 4, 6, and 8 g OS to 1000 g CCR as defined by Feyyisa et al. (2017). The CCR samples were oven-dried for 24 hours prior to the surface modification process. To ensure complete saturation of the CCR sample during the batching process, a liquid to solid ratio (L/S) of 5 was considered. Therefore, for a 50g of CCR sample, 250 ml of DI water was used to dilute the OS quantity. To initiate the water repellent treatment, the measured OS chemical was systematically diluted and washed into a 250 ml HDPE bottle containing the CCR sample. The matrix of OS-CCR-DI water was installed in a rotary tumbler to run for reaction times of 0.25, 6, 12, 18, and 24 hours. At the end of the specific reaction times, the batch matrix was allowed to settle for 10 mins then decanted. Approximately 75% of the supernatant was decanted. The residues were subsequently washed using DI water corresponding to L/S = 20 multiple times until the OS concentration in the supernatant was negligible. This was carried in a 1000 ml HDPE with 1000ml of DI water. The sealed bottle was gently agitated for 1 min in an end-to-end pattern then allowed to settle for 10 mins and decanted. This process was repeated at least five times by which the OS chemical has been sufficiently washed out. The

minimum number of repeated rinses was determined based on a trial using the maximum dosage and minimum reaction time of 15 mins. The level of OS concentration was determined using the chemical oxygen demand (COD) test on the supernatant. The residue was then split into two parts, one for air-drying and the other for oven-drying for 48-72 hours. The air-drying was done in an air-conditioned lab, with the climatic conditions monitored using a HOBO temperature and humidity sensor, at an approximate temperature of 22 °C and relative humidity of 40 %. The oven-drying was done using an electric oven at 60 °C. The experimental design process for the above procedure is conceptualized in Figure 4-12.

### 7.3 Water Repellency Assessment of OS-CCRs Treated by Sorption

The degree of water repellent interaction of the OS-treated CCRs was assessed by contact angle using the SDM and the drop image analysis software. The oven-dried and air-dried samples were crushed using light force applied to a wooden pestle to break up any agglomerations formed during the drying process while maintaining the integrity of the CCR particle sizes. In some reported studies, prior to treatment, the materials were passed through specified sieves (Choi et al. 2016; Feyyisa et al. 2017), providing a uniform range andshape surface, thus eliminating variations due to gradation. With one side of a double-sided adhesive tape fixed to a slide glass, the OS-treated CCR was gently applied and pressed to the other side using a spatula. The process was repeated until full coverage, and the consistent monolayer was formed. The slide was subsequently tapped carefully to remove particles that are unattached to the adhesive tape. This part of the process of ensuring full coverage and adherence was important because studies have

shown that the liquid-solid-gas interface influences the drop shape. Feyyisa et al. (2017) reported an inconsistent monolayer surface generated highly variable results.

The monolayer surface, as shown in Figure 4-12, was installed in the Goniometer-260 setup. An initial drop of at least 14mm$^3$ DI water was metered on to the monolayer OS-treated surface using a FlowTrac-II at a predetermined flow rate of 0.00095 l/s. Time-series images of the water droplet were captured at 1s interval for 10s using the drop image analysis software, ASDA. The software analyzed the interaction of the solid-liquid-air phases to estimate the contact angle of the drop size. To investigate the OS-treated surfaces for consistency, the initial angle formed was advanced, as described in Feyyisa et al. (2017), by increasing the sessile drop volume with time. This was achieved in increment of approximately 10 mm$^3$ until the contact radius reached equilibrium resulting in a constant contact angle measured or maximum allowable drop size due to contact radius not attaining equilibrium. The images of the newly formed drop volume were captured and analyzed. Two additional monolayer specimens were tested for the same OS-treated sample to access the variability associated with the treated sample and the monolayer preparation process.

## 7.4 Results and Discussion

The batch sorption method was adopted to treat four different CCRs for varying degrees of water repellency using a commercially available OS chemical by varying the OS dosage, reaction time, and drying conditions. The SDM, together with a drop image analysis software, was used to characterize the surface modification of the CCRs from the OS treatment by measuring the contact angle. Due to the gradation of the CCRs, the initial contact angle was advanced by increasing the drop volume with time to assess the

influence of roughness and heterogeneity from gradation effect on the wettability of the OS-treated CCR. The subsequent sections discuss the observed results.

### 7.4.1 Chemical analysis of OS sorption solution

Roy et al. (1992) recommended and detailed a hydrolysis screening test to study the degradation path for nonionic solutes such as OS might influence the interpretation of the sorption test results if significant. Therefore, prior to testing, the hydrolysis behavior of the OS chemical was evaluated using OS dosage 8 g OS/kg CCR (equal to 0.4 g OS for 50 g of CCR), in a solution volume of 250 ml, which corresponds to L/S = 5 and batched at specified reaction time the reaction times specified. The high reactivity of OS compounds with glass components that have mostly silica ($SiO_2$) required the test method described by Roy et al. (1992) to be modified. In place of hypovials, HDPE centrifuge vials were used. The COD test was selected to evaluate any degradation of the OS compound in solution. 50 ml HDPE centrifuge vials were filled with the OS solutions with concentration 0.001604 g/L to the brim eliminating any head space to prevent potential oxidation from taking place. The vials were subsequently sealed and placed in a water bath at room temperature for the specified reaction times. The COD test were performed on duplicates of the solutions. The results, as presented in Figure 7-1, showed no significant change in organic activity, an indication that any organic activity during the sorption process would be a result of reaction with the CCR solids. Also, the EC ranged between 5.8 μS/cm and 29.3 μS/cm, and pH ranged between 7.6 and 7.8 slightly basic.

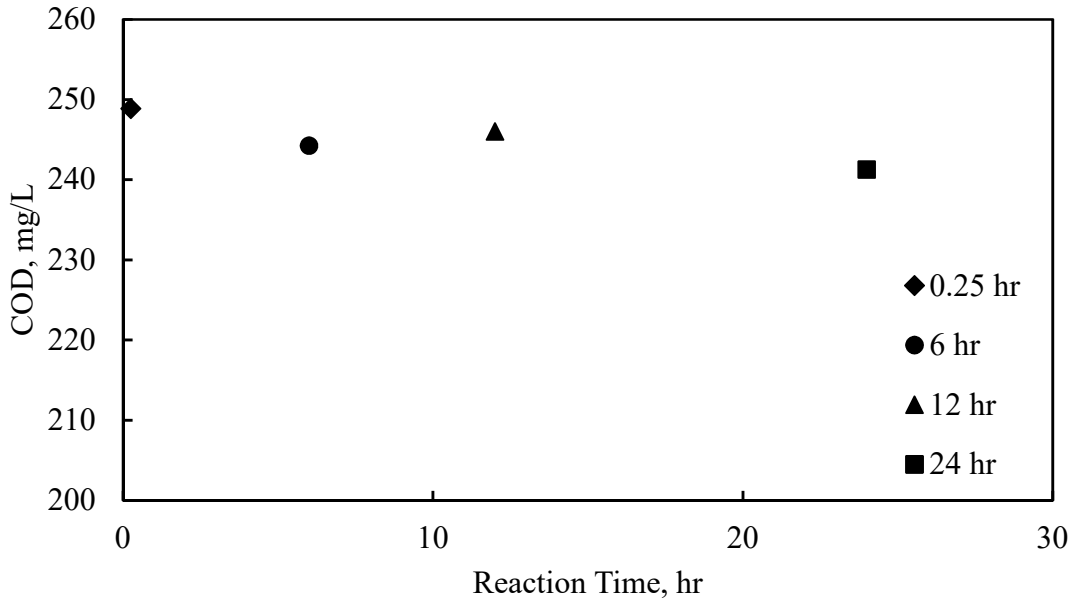


Figure 7-1. Hydrolysis of OS solution.

The solution of the batched matrix was evaluated for ionic activity by measuring the EC and pH values of the supernatant after the specified reaction times 0.25, 6, 12, and 24 hours of tumbling. A summary of the results, as presented in Figure 7-2 shows that significant ionic activity existed during the batch sorption process. This ionic activity could be attributed to the CCRs chemical reaction with DI water. The high EC compared to that of tap water and DI water may be a result of soluble salts present in the CCRs and metals that are mobile in basic conditions. In addition, it was observed that the ionic activity defined by EC and pH remaine relatively constant for the specified OS dosage and reaction times for all CCRs.

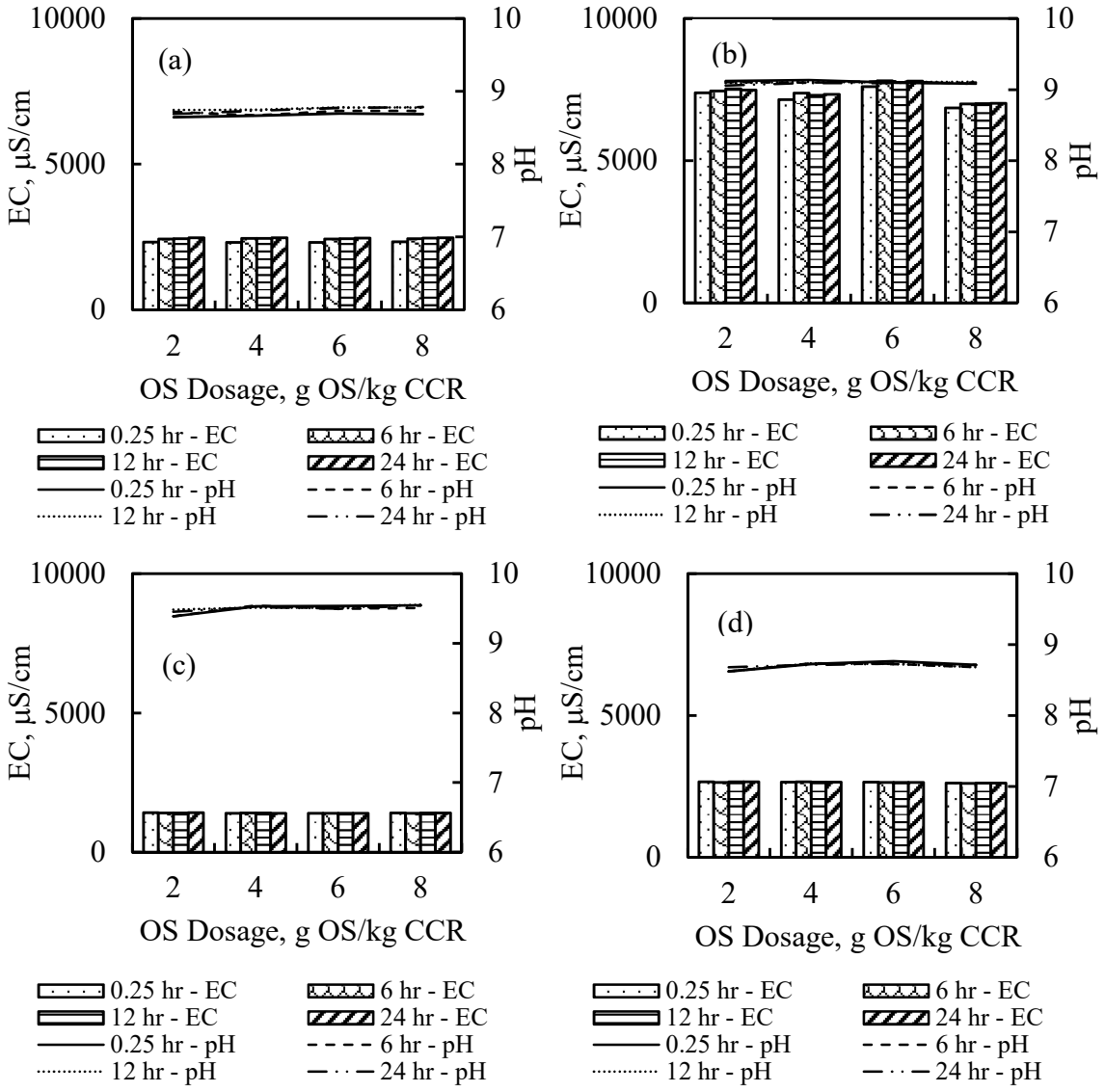


Figure 7-2. Ionic activity of OS batch solution after tumbling for specified reaction times for (a) CCR 1, (b) CCR 2, (c) CCR 3 and (d) CCR 6.

7.4.2 Contact angle – drop volume relationship

The relationship describing the advancement of contact angle with drop volume increment is presented in Figure 7-4 through Figure 7-7 for CCR 1, 2, 3, and 6, respectively. The relationship shows a general trend of contact angle increasing with drop volume increase. This trend was observed for all CCRs irrespective of the OS

dosage, reaction time, and drying conditions. However, though the general trend is observed for all CCRs, the impact of the variables on the trend is unique to the CCR which is similar to the findings of Kwok and Neumann (1999). The variation in measured contact angle decreased with an increase in OS dosage which described the degree of water repellency. Also, this was observed to correlate the contact radius to the drop volume. Kwok and Neumann (1999) noted that for a surface characterized by roughness, irregularity, and inconsistency the contact radius should be considered a geometric property.

The initial drop volume averaged 15 $mm^3$ with the peak contact angle mostly measured at drop volumes greater than initial drop volumes but less than or equal to the maximum drop which averaged approximately 90 $mm^3$. All the CCRs considered except for CCR 2, had contact angle measurement terminated < 100$mm^3$. For OS dosage of 2 g OS/kg CCR, the drop volume where found to have large contact radius which resulted in the test terminating at relatively low drop volumes averaged approximately at 60 $mm^3$ as presented in Figure 7-4 through Figure 7-7 for CCR 1, 2, 3, and 6, respectively. Feyyisa et al. (2017) detailed advancing measuring techniques for quantifying wettability of OS-treated CCRs. The study recommended minimum drop volumes for varying CCRs and OS dosage, but this was limited to CCRs sieved through sieve size 75μm (< 75μm) which produce predominantly smooth, regular, and consistent monoplanar surface. It was also observed that advancing the initial drop volume resulted in a decrease in contact angle due to a change in the contact radius presumably due to rough, irregular, and inconsistent surface. However, as the drop volume was gradually increased at a constant rate, the contact angle increased in response. In some cases, this phenomenon occurs multiple

times while advancing the contact angle. It was observed to be unique to at least OS dosage 4 g OS/kg CCR. Figure 7-3 demonstrates this phenomenon with the images of the initial drop volume and the next two drop volumes. Kwok and Neumann (1999) described this phenomenon as slipping for a drop in contact angle and sticking for a rise in contact angle and attributed it to non-inert surfaces.

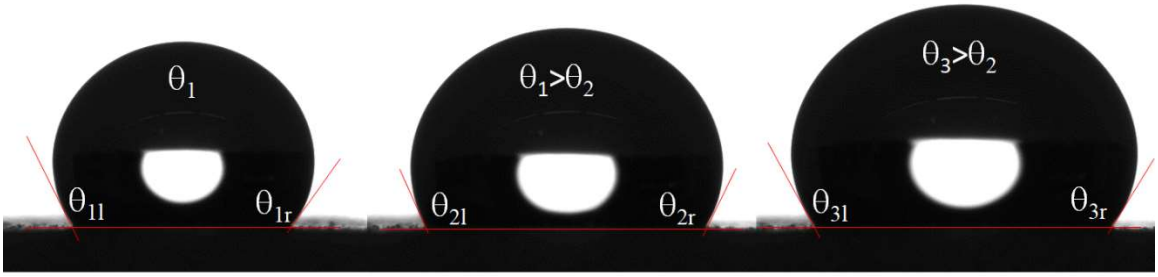


Figure 7-3. Illustration of the fall and rise in contact angle as drop volume increase for CCR 6, dosage 4, reaction time 0.25 hr, and oven-dry condition.

Three types of hydrophobicity were observed. These include contact angles < 90° which Czachor et al. (2010) and Lourenço et al. (2015b) classify as subcritical hydrophobicity, contact angle > 90° but < 150° classified as hydrophobicity, and contact angle > 150° classified as superhydrophobicity. In all, CCR 2 had relatively significant water repellent activity with OS dosage 2 g OS/kg CCR recording peak contact angles in the range 110° - 134° compared to other CCRs with peak contact angles < 100° for the same OS dosage.

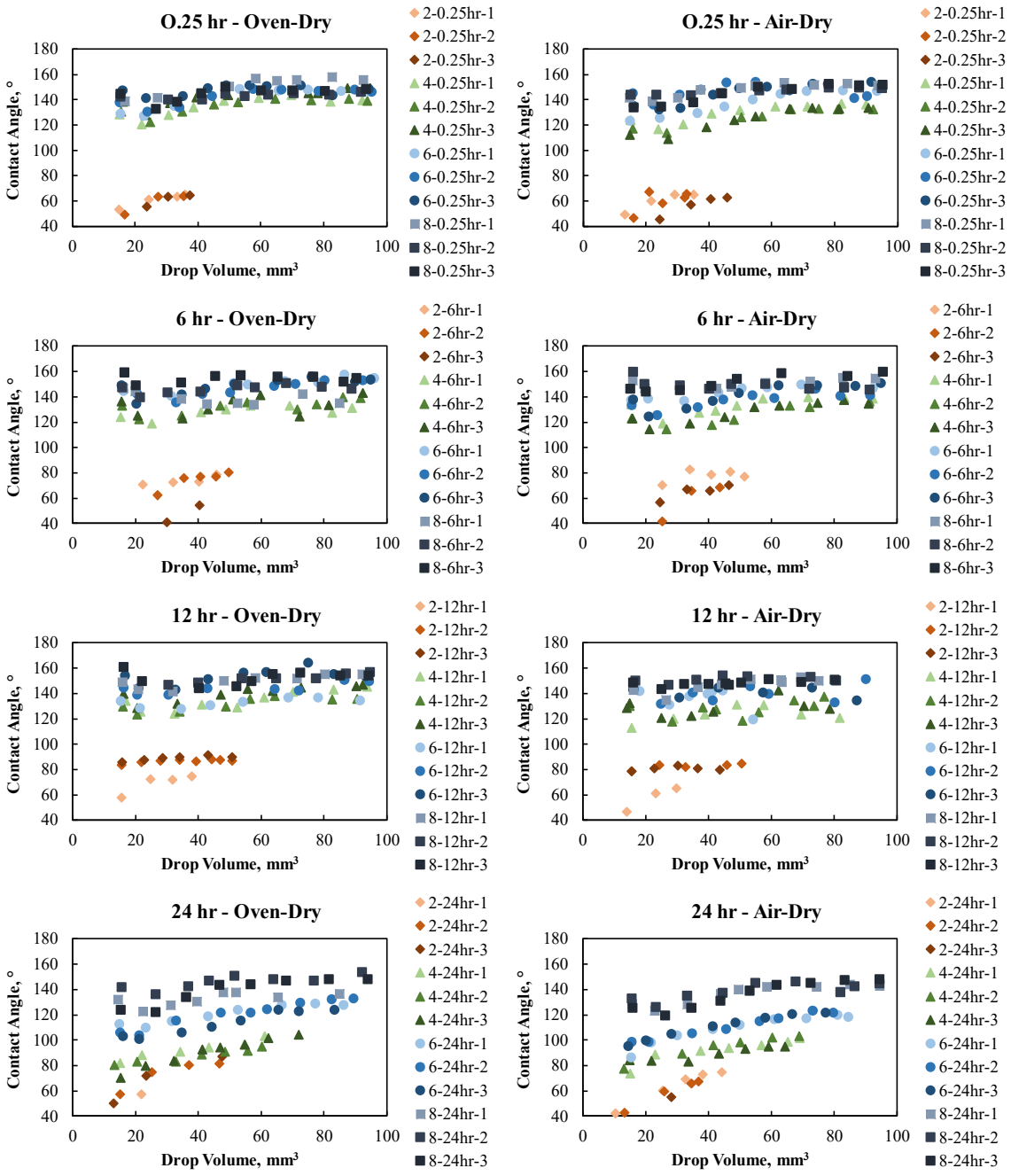


Figure 7-4. CCR 1 contact angle - drop volume relationship for varying OS dosage, reaction time, and drying conditions.

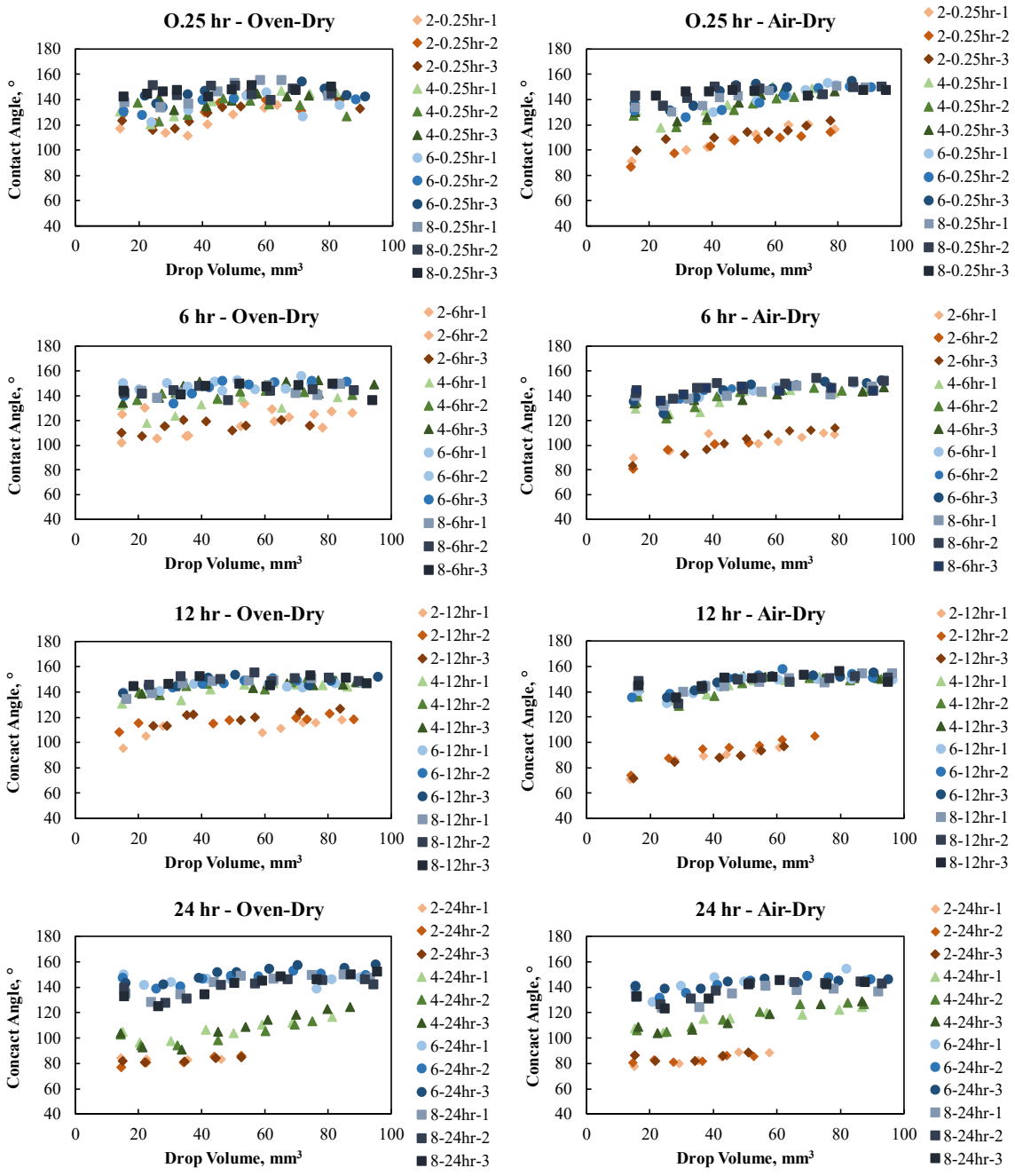


Figure 7-5. CCR 2 contact angle - drop volume relationship for varying OS dosage, reaction time, and drying conditions.

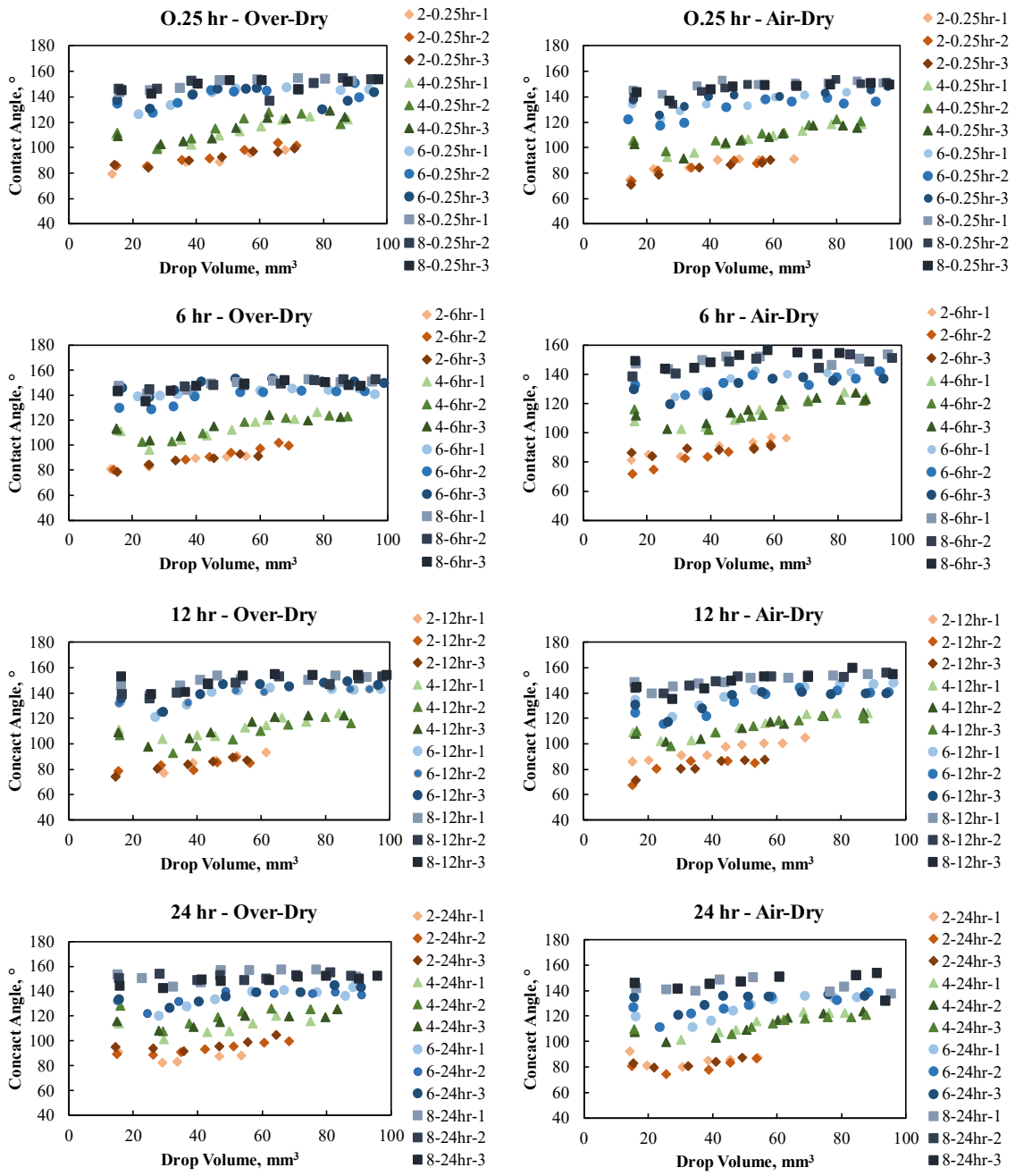


Figure 7-6. CCR 3 contact angle - drop volume relationship for varying OS dosage, reaction time, and drying conditions.

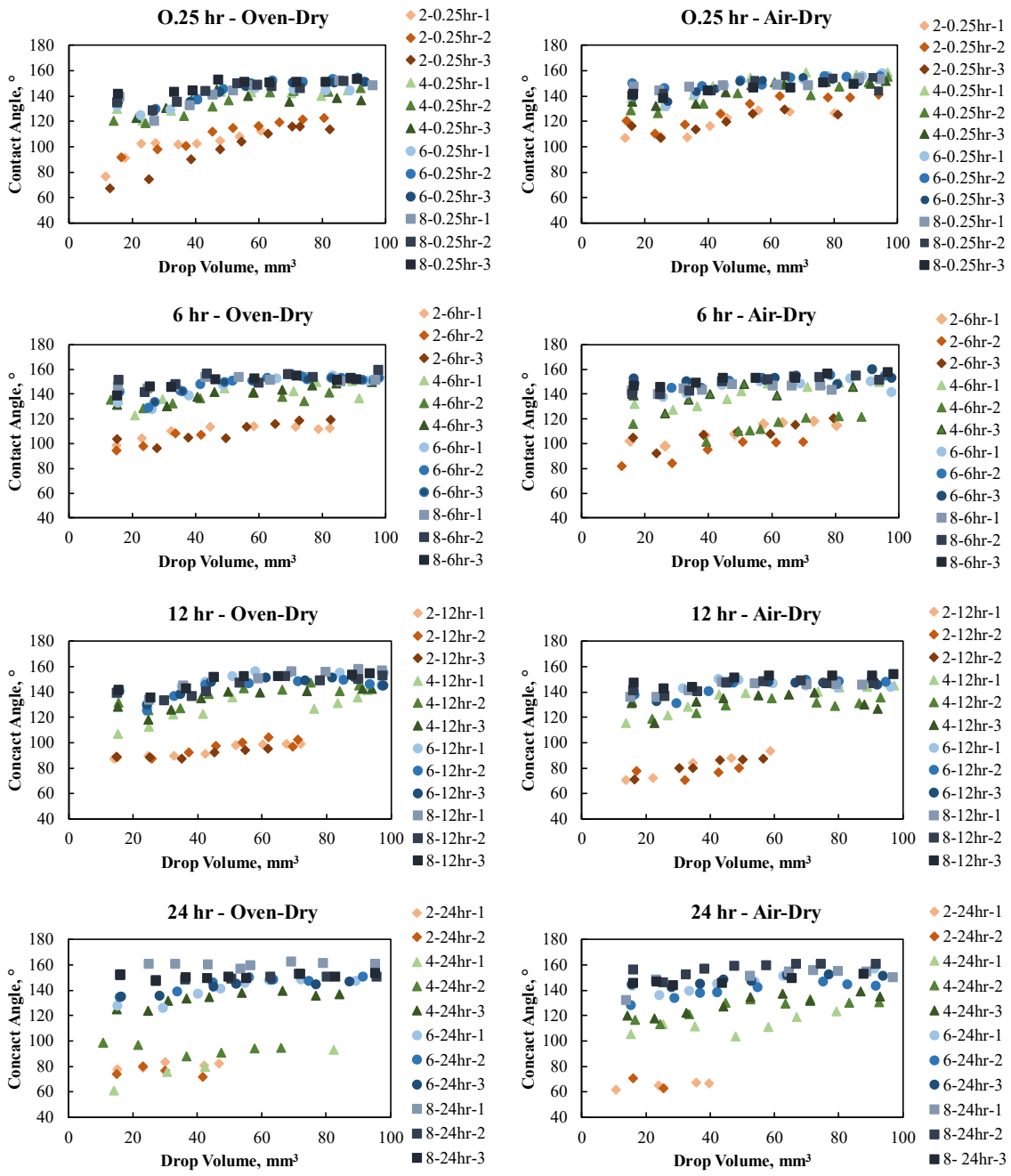


Figure 7-7. CCR 6 contact angle - drop volume relationship for varying OS dosage, reaction time, and dry conditions.

It was observed that interactions existed between variables considered. CCR – OS dosage interactions were clearly evident as this resulted in relatively varying measured

contact angles. This interaction agreed comparably well with what has been described in literature for CCRs (Feyyisa et al. 2017; Keatts et al. 2018) and soils (Choi et al. 2016; Keatts et al. 2018; Lee et al. 2015; Subedi et al. 2012a). However, other interactions were unique to the CCR type, as well as other specific conditions. An example is the CCR-drying condition interaction, which was not clearly defined for all but CCR 2. For CCR 2, dosage 2 g OS/kg CCR, the air-dry samples recored lower contact angle compared to the oven-dry samples for all reaction time observed. This could be attributed to inadequate silanol generated to bond with the silanols and metals on the substrate (CCR).

#### 7.4.3 Variable interaction analysis

As mention in the previous section, there exist multiple interactions between the variables considered in this study. The variables including material, OS dosage, reaction time, and drying conditions were classified as the independent variables with the contact angle as the dependent variable. To identify variables that are relevant to the sorption treatment of CCRs for water repellency without complicating or illogically creating an undesirable experimental condition, SAS, a statistical software, was adopted to evaluate these interactions.

##### 7.4.3.1 The PROC GLM procedure

Due to the multiple independent variables under consideration, the PROC GLM procedure was considered for analysis of variance also known as ANOVA (SAS Institute Inc 2008) . The PROC GLM procedure fits general linear models to data using the method of least squares (SAS Institute Inc 2008). The generalized linear model has the independent variable term and an error term. Considering all possible interactions could potentially result in an error term with zero value, the mean square (error) term becomes

undefined as it is the ratio of sum of square (error) to degree of freedom (error). For this analysis, the average of the maximum contact angle recorded were considered.

#### 7.4.3.2 The PROC VARCOMP procedure

The PROC VARCOMP procedure estimates the contribution of each independent variable and possible interaction of the variables, collectively termed source, to the variance of the dependent variable (SAS Institute Inc 2013). The syntax and result outputs are presented in APPENDIX E. In all 15 possible sources were generated, excluding the error term which had approximately a zero value. Considering all possible sources will result in the mean square error being undefined as explained in PROC GLM (section 7.4.3.1). The source including Dosage, Material, Material*Dosage, Reaction Time, Material*Dosage*Reaction Time, Material* Reaction Time were found to contribute significantly to the total sum of squares which defined the variance of the dependent variable. Dosage had the significant contribution with approximately 76% of the sum of squares followed by Material, Material*Time, Time, Material*Dosage*Time, and Material*Time with approximately 5%, 5%, 4%, 4%, and 2% of the sum of squares, respectively. The others were < 1% each and sum up to approximately 2% of the total sum of squares, therefore can be considered to account for the error term in performing ANOVA using PROC GLM. Figure 7-8 details the source that contribute significantly to the total sum of squares.

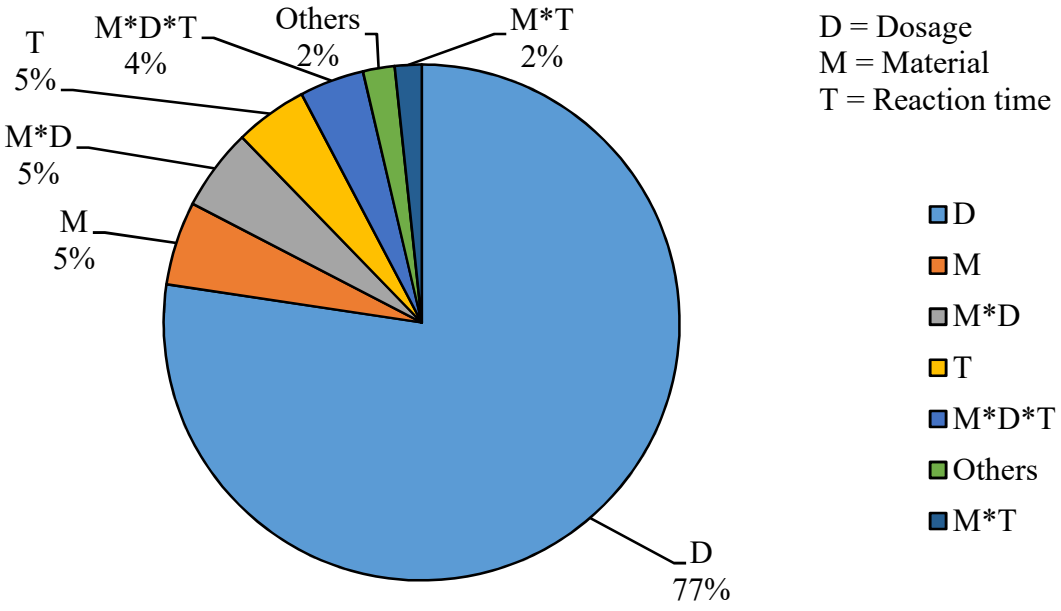


Figure 7-8. Contribution of independent variables and their interactions to the total sum of squares.

7.4.3.3 Material effect

The variance of material contribution to the total sum of squares can be attributed to the unique elemental and mineral composition of the CCRs, specifically class F fly ash and lignite coal fly ash. These CCRs constitute oxide compositions mainly $SiO_2$, $Al_2O_3$, and $Fe_2O_3$ and trace elements as presented in

Table 4-4 and varying mineral compositions, as shown in Table 4-5. These oxides and minerals constitute substrates containing silanols and metals that favor bonding with other silanols produced during the hydrolysis process of the OS treatment to form siloxane bonds (-Si-O-Si-) and metal hydroxyl groups to form -Si-O-metal bonds. This reaction chemistry defines OS as a surface treatment agent (Xiameter 2009); hence, the significant variance observed with the CCRs. In addition, the solution chemistry generated, as discussed in section 7.4.1, is basic and provides enabling conditions for an

effective OS reaction. The particle size, particle shape, and surface roughness have been documented in literature also to influence the engineered water repellency of granular materials. Saulick et al. (2018) reported a significant increase in contact angle measurements as particle size decrease and as the particles become more angular. However, surface roughness was reported to be sensitive to particle size and particle shape, with the contact angle measurement increasing with decrease in surface roughness. The inherent chemical composition and physical properties contribute to the OS treatment of CCRs during batch sorption process.

7.4.3.4 Dosage effect

The dosage levels considered were the same as reported by Feyyisa et al. (2017), but the L/S was increased from 0.4 to 5 to assess the effect the OS dilution rate on the treatment process. The L/S = 5 of DI/CCR, at high dilution rate or lower concentration, resulted in comparable degree of water repellency. It should be noted that water as a solvent is critical in activating the hydrolysis process but is limited to the maximum amount to initiate the process. In this study, for CCR 1, dosage 2 g OS/kg CCR, water repellency activity relatively low as observed for L/S = 5, but at L/S = 0.4 (Feyyisa et al. 2017) recorded significant water repellency activity. This underscores the fact that water as a solvent has an effective range to contribute to the OS reaction chemistry for surface treatment. Arkles (2006) explained the layer of siloxane is dependent on the OS concentration: thus, for multiple layers of siloxane, a recommended OS solution of 0.25% concentration is required. The study further described a correlation between particle size and OS concentration for monolayer coverage of siloxane bonds. The results showed that the contact angle measurements increased with dosage increase, though a significant

amount of residual OS must have been removed during the rinsing. It should be noted that the thickness of the siloxane and – Si – O – metal bonds formed during the surface modification was not evaluated in this study.

7.4.3.5 Reaction time effect

Reaction time accounted for approximately 5% of the total sum of squares as presented in Figure 7-8. Further analysis showed that significant part of the reaction time contribution resulted from the 24 hour reaction time as the 0.25 hr, 6 hr, and 12 hr reaction times contributed less than 1%. This observation could be presumably attributed to the batch sorption mechanism of the CCRs and the OS solution. In addition, the results indicates that a reaction time of at least 15 mins was adequate for water repellent activity to occur, provided optimal conditions for OS reaction prevailed. However, this could be limited to the type of OS chemical considered. Issa and Luyt (2019) in the review of the kinematics of alkoxysilanes and organoalkoxy silanes, indicated that the hydrolysis reaction process is a first-order reaction that requires a catalyst but also depends on the concentration, water, pH, and alcohol produced. Considering the solution chemistry discussed in section 7.4.1, the right conditions prevailed to initiate the hydrolysis reaction resulting in a faster water repellent activity. It must be noted that, though time does not contribute significantly to the variance of the dependent variable, it has interactions with other variables, which would require further analysis and interpretation for laboratory and practical applications.

7.4.3.6 Drying effects

Lee et al. (2015) noted that drying conditions influence water repellency of soils with oven-dried soils having greater water repellency than that of air-dried and field -

dried conditions. For this study, the drying conditions of air and oven contributed the least variance in the peak contact angle measurements. However, considering the behavior of contact angle advancement as illustrated in the contact angle – volume relationships in Figure 7-4 through Figure 7-7 suggest some level of variance in air-dried and oven-dried samples which could be due to error in surface preparation, contact angle measurements, and operator error.

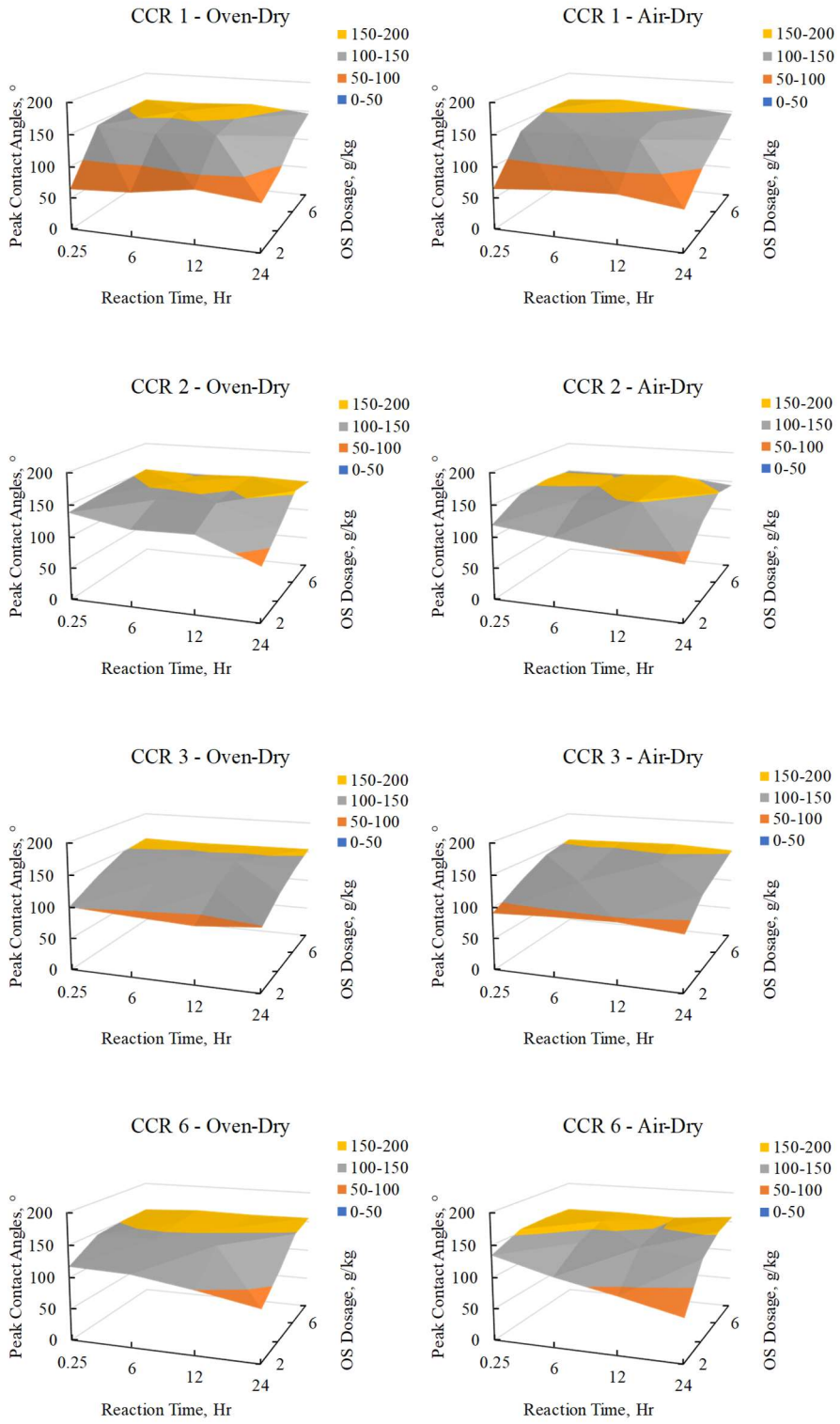


Figure 7-9. 3D representation of the peak contact angles as a function of OS dosage, reaction time for materials and drying conditions.

## 7.5 Summary

In this chapter, the concept of sorption was considered as the physical and chemical process by which silanols produced from the hydrolysis and condensation of OS bond to the silanols and metals in CCRs developing siloxane and – Si – O – metal bonds to effect water repellency. The current treatment protocols are to oven-dry the matrix of OS solution and CCRs or soils to allow OS solutions to react with soil particles for a period and washed without evaluating the potential variables of the physical and chemical process.

An experimental design based on the batch sorption test was developed to assess the effect of potential variables such as material, reaction time, dosage, and drying conditions on the OS treatment of CCRs for water repellency. The sorption test was performed in lab conditions but limited to the L/S specified and the OS chemical type. The degree of water repellency of the OS treatment of CCRs was based on contact angle measurements using the SDM and drop image analysis. Statistical analysis was performed to evaluate the variance of the contribution of each of the variables.

- The sorption test performed favorably well with the test parameters considered as potential variables for OS treatment of CCRs for laboratory and field tests.
- The contact angle advancement approach of measuring the degree of water repellency followed the trend described in literature, provided information on consistency and repeatability of the test process.
- Material and OS dosage were identified to significantly influence the OS sorption to CCRs for water repellency, with the inherent chemical and physical properties of CCRs and OS chemicals controlling the process.

- Time and drying conditions contributed to variance in contact angle measurement but were considered negligible. However, some interactions existed between time and drying conditions which can be relevant in understanding the process of sorption for field application.

# CHAPTER 8: WATER RETENTION CHARACTERISTICS OF COMPACTED OS-TREATED COAL COMBUSTION RESIDUAL

## 8.1 Introduction

The bonding of OS compounds to CCR particles transforms the surface properties of the CCR particles. The main objective was to evaluate the effect of water repellent on the WRC of compacted CCRs. The study developed an experimental design considering the practical implementation of the OS-treated that would allow the use of current geotechnical laboratory test method to evaluate the engineering properties of OS-treated CCR. Also, the study considered the possible interactions of residual OS compound with testing device components, which could potentially compromise and lead to misinterpretation of test results. Specifically, two OS treatment protocols, namely pretreatment and precondition, were considered. Pretreatment inclined towards practical implementation, whereas precondition focused on limiting the interference of residual OS with components of test devices. An overview of the study is as follows.

- Compaction characteristics of OS pretreated CCR using standard Proctor compaction energy for OS dosage 4 g OS/kg CCR and 8 g OS/kg CCR.
- Compacted preconditioned OS-treated CCR with varying degrees of water repellency were evaluated for unsaturated functions using TC and WP4C.
- Breakthrough pressure and saturated hydraulic conductivity analysis of OS-treated CCR was demonstrated using the flexible wall permeameter.
- An overview of hydrolytic stability in OS bond formation during the OS treatment process was presented.

- Water repellency was assessed as a function of water content and suction using WDPT and SDM.
- The thermal stability of the OS-treated CCR was assessed to investigate the degree of surface modification from OS treatment.

## 8.2 Materials

CCR 2 was selected as the geomaterial due to its unique chemical compositions, and their potential impact on OS treatment of CCRs. Results in 7.4.2 show that CCR 2 has two degrees of water repellency, specifically hydrophobicity and superhydrophobicity, which is attainable using dosage 4 g OS/kg CCR and 8 g OS/kg CCR, respectively. DI water was used as the solvent in activating the water repellency treatment. From this point forward, CCR 2 treated with dosage 4 g OS/kg CCR and 8 g OS/kg CCR would be referred to as OS-CCR 2-4 and OS-CCR 2-8, respectively.

## 8.3 OS Treatment Protocol

For this study, two protocols, namely pretreatment, and precondition, were implemented in the OS treatment of CCRs for geotechnical engineering tests due to 1) the practical implementation considerations, and 2) the potential interaction of the residual OS with some components of standardized test devices which could influence results interpretation, respectively. Both treatment protocols were designed to imitate the sorption treatment discussed in the previous chapter.

### 8.3.1 Pretreatment protocol

The liquid limit represents the water content at the boundary of the liquid and plastic state of soils; hence, the liquid limit of CCR 2, 23%, were considered in selecting the L/S for the pretreatment protocol. However, the L/S ratio was increased to 0.3 to

address workability issues and provide complete saturation of the solid surface in the OS solution. Using an automated mixer, a homogenous matrix was formed by adding the measured OS and DI water simultaneously to the oven dried CCR 2 and mixed for 15 minutes. Additional DI water corresponding to L/S = 0.1 is used to wash the residual matrix from the mixing bowl translating to a total L/S = 0.4 as reported in the literature (Feyyisa et al. 2017; Jordan et al. 2015; Keatts et al. 2018). The matrix was oven-dried at 60 °C to a specified water content allowing for remolding to a specific density for further standard geotechnical laboratory experiments. With the known mass of pan and CCR, the difference in water content to make up the target water content was computed and added to the matrix to form a homogenous mixture of pretreated OS-treated samples.

### 8.3.2 Precondition protocol

The preconditioned protocol is similar to the pretreatment protocol except that after oven drying to a specified water content, the matrix was thoroughly washed using DI water corresponding L/S = 20 as described in the previous chapter on the sorption treatment protocol. The resulting residue was oven-dried to a specific water content to allow for remolding. This approached is considered to be expensive and not environmentally friendly as it requires a considerable amount of water to reduce the excess OS content to the barest minimum and in the process leaches out soluble salts and heavy metals which may cause environmental concerns in CCR management.

## 8.4 Compaction Characteristics

Standard Proctor compaction was performed on OS-treated CCR 2 in accordance with ASTM D698 (ASTM 2012). The OS-treated CCR was prepared following the pretreatment protocol, as described in section 8.3.1. With the known mass of the pan and

solids, the target water contents were computed for the compaction points specified. Duplicates compaction characteristics were established for OS-CCR 2-4 to assess the variability and repeatability of the treatment process. Figure 8-1 illustrate the compaction characteristics of the OS-treated CCR using the pretreatment protocol.

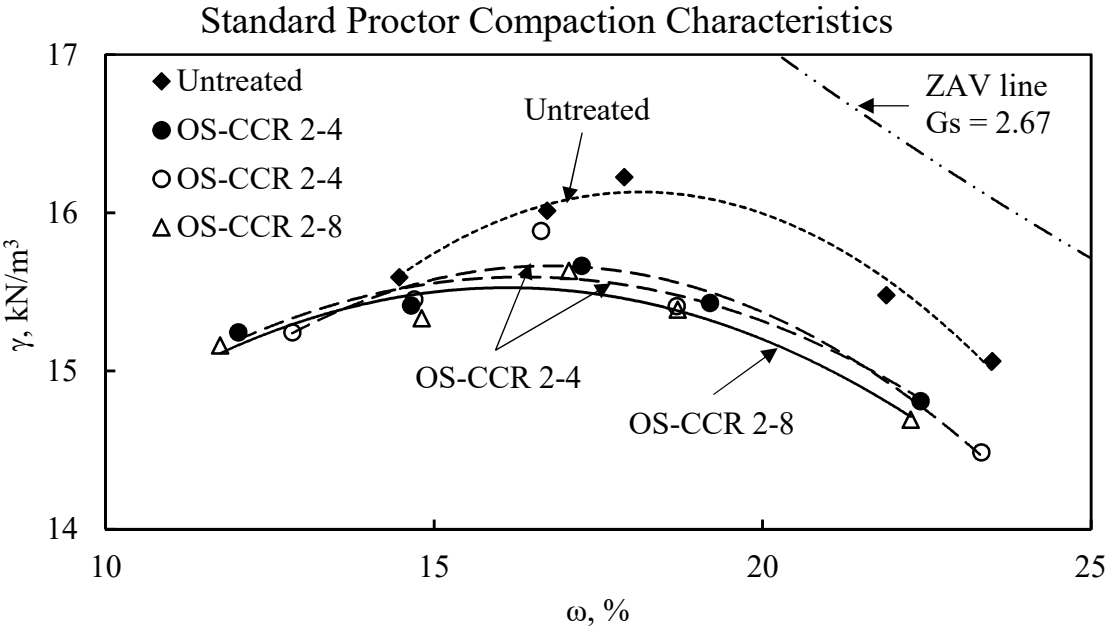


Figure 8-1. Standard Proctor compaction characteristics of OS-treated CCR using the pretreatment protocol.

Table 8-1. Summary of standard Proctor Compaction characteristics of OS-treated CCR using pretreatment protocol.

| | $\gamma_{dmax}$, kN/m$^3$ | $\omega_{opt}$, % |
|---|---|---|
| CCR 2 | 16.14 | 18.15 |
| OS-CCR 2-4 | 15.59 | 16.35 |
| OS-CCR 2-4 | 15.66 | 16.73 |
| OS-CCR 2-8 | 15.52 | 16.09 |

The compaction characteristics of the OS-treated CCR are slightly lower than the untreated CCR. The OS dosage was found to have relatively little to no effect on the water content and dry unit weight of the OS-treated CCR, thus accounting for flatter curves as shown in Figure 8-1. Sridharan et al. (2001) discussed the phenomenon of bulking, a result of capillary forces resisting the rearrangements of the particles against the external compaction energy. However, in the case of the OS pretreated CCR, it is most likely to be a combination of capillary forces and water repellent surfaces resisting the rearrangements of the particles against the external compaction energy. The duplicate tests of OS-CCR 2-4 showed relatively similar maximum dry unit weight of 15.59 $kN/m^3$ and 15.66 $kN/m^3$ but with marginal difference in optimum water content of 16.73% and 16.96% for test 1 and 2, respectively as presented in Table 8-1. This is an indication of consistency in the sample preparation procedure. In general, the degree of water repellency impacts the standard Proctor compaction characteristics of CCR 2, considering the treatment protocol. The compaction characteristics of the OS-treated CCR decreased as the OS dosage increased, recording lower dry unit weight and lower optimum water contents compared to that of untreated CCR 2. This observation compares well with literature for water repellent kaolin (Choi et al. 2016), and sand-clay mixtures (Lourenço et al. 2015a). However, Daniels et al. (2009b) observed a decrease in optimum water content, but an increase in the maximum dry unit weight of OS preconditioned coal fly ashes attributing it to particle surface charge and hydration. The variations observed in the compaction characteristics could be attributed to material preparation, engineering properties of CCR, and the water repellent chemicals. Nonetheless, the relative

compaction of the OS-treated CCRs to the untreated is 97%, arguable within range of the acceptable density for the untreated CCR 2.

The degree of water repellency of the pretreatment samples were assessed following procedures outlined in section 7.3 using SDM and drop image analysis. The average maximum contact angles for OS-CCR 2-4 and OS-CCR 2-8 are 114° and 135°, respectively, lower than obtained by sorption treatment  but comparable to Feyyisa et al. (2017) presumably to varying treatment protocol.

## 8.5 Unsaturated Functions of Compacted OS-treated CCR

The WRC of compacted CCR or soils, in general, is described by unsaturated functions obtained from fitting parametric models to measured data. The TC and WP4C, as described in previous chapters, were considered in measuring the WRC of compacted OS-treated CCR. These methods of measurement have components that can potentially react with OS. The HAE ceramic disk in the TC is made from clay or alumina, which are one of the substrates that have an excellent reaction with OS (Arkles 2006). These HAE ceramic disks are hydrophilic and must be maintained as such throughout the measuring process. The WP4C has sensors with glass components made from silica-based materials. With OS highly reactive in vapor form (Xiameter 2009), puts these sensors at high risk of being compromised. The preconditioning protocol was considered for treating the CCR for water repellency to avoid misinterpretation of data due to residual OS compromising device components.

The test specimens were subcored from compacted samples in standard Proctor compaction molds in specimen rings and cups for TC and WP4C. Figure 8-2 presents the compaction characteristics for the initial compaction conditions estimated using the water

– density relationship and the final compaction conditions estimated using the mass – volume relationship of the oven-dry solids. The test specimens for both measurement methods were wet of optimum and dry unit weight lower than maximum dry unit weight. Generally, hydraulic conductivity is reported to be dependent on water content, decreasing with increasing water content (Boynton and Daniel 1985).

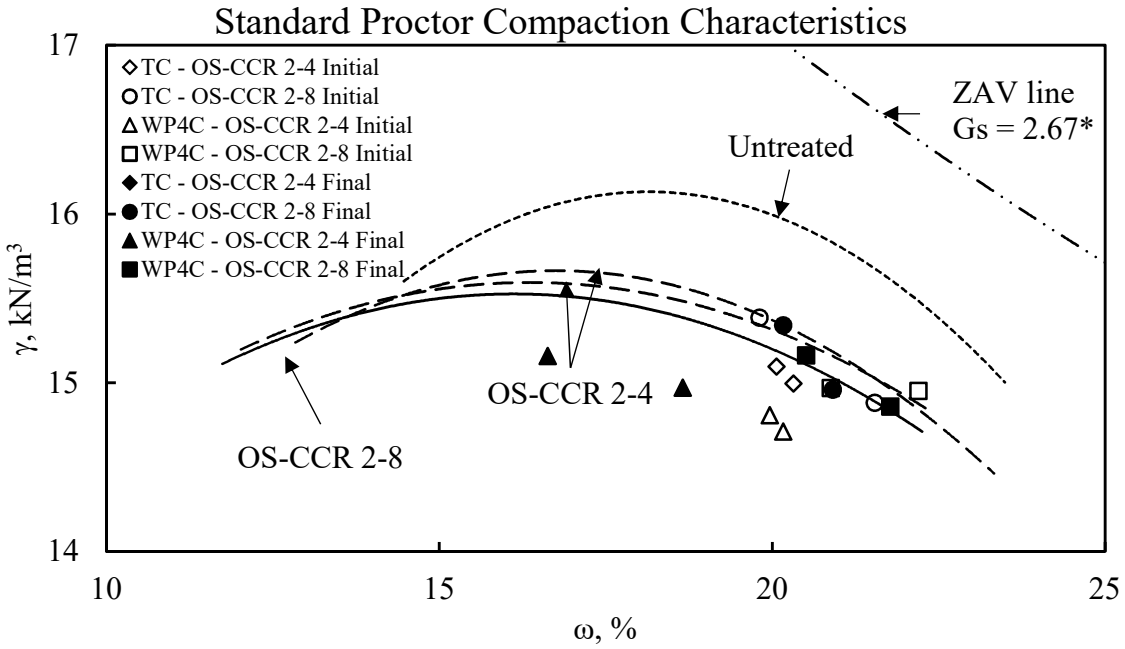


Figure 8-2. Compaction conditions of TC and WP4C test specimens for WRC measurements.

8.5.1 Suction equilibration time

The time taken for a TC test specimen to attain equilibration for an applied pressure was monitored by measuring the gravimetric water content with time. At equilibration, the applied pressure becomes equal to matric suction; hence, there is no change in water content in terms of volume or mass of water. The weight of the test specimen was logged every hour for the first 6 hours of pressure application. The TC test

took a total of approximately 29 days and 37 days for OS-CCR 2-4 and OS-CCR 2-8, respectively. Both samples had relatively similar pattern of equilibration and desaturation except for test specimen 2 of OS-CCR 2-4 which experience rapid desaturation as shown in Figure 8-3. There was rapid desaturation in the first 6 hours of pressure application for 10 kPa, 20 kPa, and 30 kPa presumably in the saturation and initial section of the transition zones. Pressure 40 kPa, 50 kPa, and 100 kPa saw no significant desaturation in the first 6 hours of applications. The rate of desaturation increased as the applied suction increases resulting in a long time of equilibration. Also, test specimen 2 of OS-CCR-2-8 had a higher rate of desaturation for the first 6 hours and stabilized after that until equilibrium compared to test specimen 1 which had a relatively lower desaturation rate but maintain a constant rate until equilibrium as illustrated in Figure 8-4.

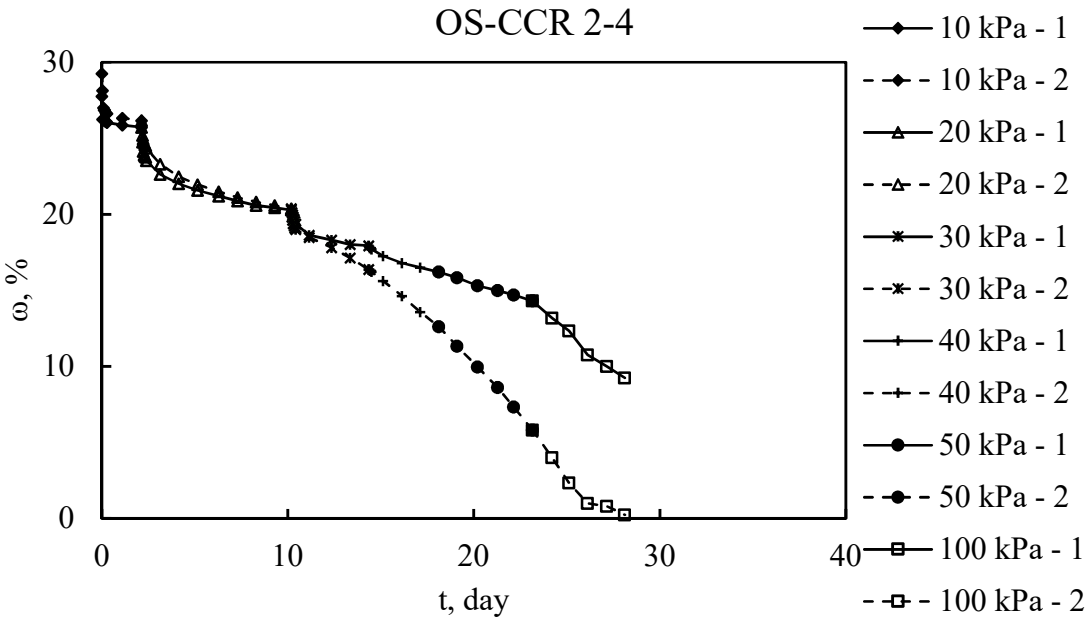


Figure 8-3. Tempe cell suction equilibration for OS-CCR 2-4.

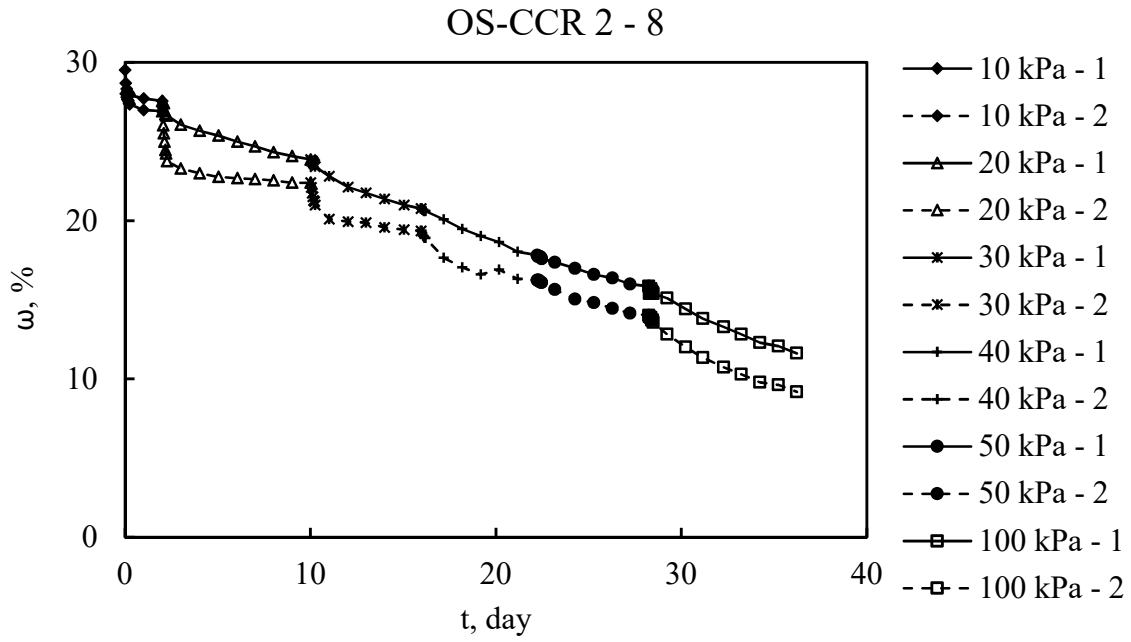


Figure 8-4. Tempe cell suction equilibration for OS-CCR 2-8.

### 8.5.2 WRC of OS-treated CCR

#### 8.5.2.1 Compaction characteristics of WRC samples

In the absence of a compaction curve to describe the compaction characteristics of the preconditioned OS-treated CCR, the compaction state presented in Table 8-2 served as a reference for the analysis. Also, the specific gravity was assumed to be the same as the untreated CCR. The final compaction conditions was used in the WRC analysis as it provided the true representation of the test specimen. Averagely, the untreated CCR recorded the highest dry unit weight and water content resulting in a higher degree of saturation and lower porosity compared to the OS-treated CCRs. The OS-treated CCRs have relatively similar compaction characteristics hence can be described as having similar texture and pore size distributions. However, contrary to previous studies reported

in the literature, dry unit weight decreases with increasing degree of water repellency. The dry unit weight of OS-CCR 2-8 was marginally higher though it was expected to be lower due to an anticipated the higher degree of water repellency.

Table 8-2. Compaction characteristics of WRC test specimens based on final compaction conditions.

| Method | Sample | Parameters | | | |
|---|---|---|---|---|---|
| | | $\gamma_{dry}$, kN/m$^3$ | ω, % | Θ, m$^3$/m$^3$ | S, % |
| Tempe Cell | CCR 2 | 15.23 | 21.89 | 0.3398 | 81.17 |
| | | 15.33 | 20.77 | 0.3245 | 78.24 |
| | OS-CCR 2-4 | 14.96 | 20.63 | 0.3145 | 73.31 |
| | | 15.09 | 20.08 | 0.3090 | 72.91 |
| | OS-CCR 2-8 | 14.96 | 20.91 | 0.3188 | 74.34 |
| | | 15.34 | 20.16 | 0.3153 | 76.09 |
| WP4C | CCR 2 | 15.95 | 18.21 | 0.2962 | 75.75 |
| | | 15.22 | 22.78 | 0.3535 | 84.39 |
| | OS-CCR 2-4 | 15.16 | 16.63 | 0.2569 | 60.97 |
| | | 14.97 | 18.66 | 0.2847 | 66.44 |
| | OS-CCR 2-8 | 15.16 | 20.51 | 0.3170 | 75.25 |
| | | 14.86 | 21.78 | 0.3298 | 76.22 |

Figure 8-5 presents both the matric and total suction measurements describing the WRC of the OS-treated CCRs with varying degrees of water repellency. The TC measured the matric suction over a short-range from 10 kPa to 100 kPa due to the HAE limitation of the ceramic disk used, whereas the total suction was measured using a WP4C covering a wide range from approximately 40 kPa to 200000 kPa. Both test specimens started in the saturation zone. The WRC of the OS-treated has the S-shaped

curve with the volumetric water content rapidly decreasing asymptotically towards the residual zone as suction increased. The duplicate test specimens showed less variability and good repeatability in the suction measurements of the OS-treated CCR.

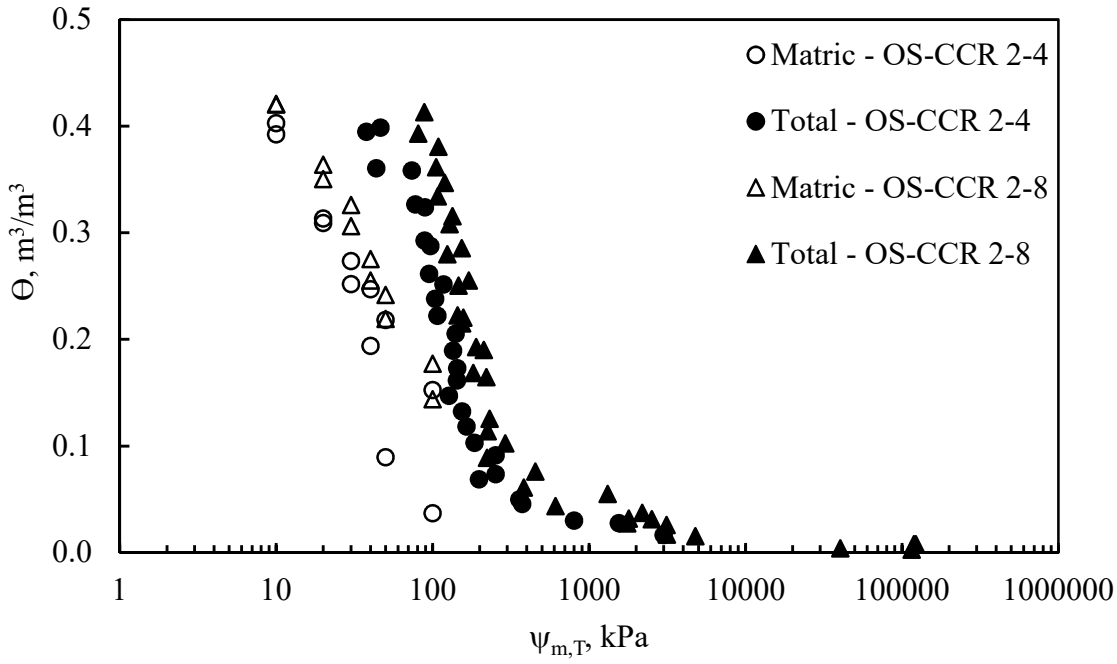


Figure 8-5. Matric and total suctions of OS-treated CCR.

Figure 8-6 shows the comparison between the OS-treated CCR and the corresponding untreated CCR in terms of matric and total suction measurements. The matric suction of the OS-treated CCR test specimen compares relatively well with the corresponding untreated CCR. However, the OS-treated CCR had lower water content compared to the untreated CCR over the suction range considered. This observation was expected as water repellent activity results in low surface energy, hence a reduction of the adsorptive and capillary forces, which describes matric suction. Therefore, the water retention of the OS-treated CCR will be lower than the untreated CCR for an applied

suction. The observation compared well with what has been reported in literature for hydrophilic and water repellent soils (Czachor et al. 2010; Liu et al. 2012; Lourenço et al. 2015b). Also, the desaturation rate of the OS-treated was higher than the untreated CCR, similar to the observation made by Nieber et al. (2000) for silica sand treated for varying degrees of water repellency. However, no consistent trend was observed for varying degrees of water repellency. For evaporation and drainage studies, Kim et al. (2015) reported an increase in the evaporation rate in water repellent Ottawa sand than wettable Ottawa sand.

The total suction measurement showed significant variation between the OS-treated CCR and the untreated CCR, with OS-treated CCR recording lower total suction values. This observation can be attributed to the precondition protocol used to treat the CCR for water repellency. The residual OS was washed out, as a result, soluble salts present in the CCR were washed out as well. Soluble salts in pore fluid contributes significantly to total suction, the absence of soluble salt means a reduction in total suction measurement as observed. The rate of desaturation was high and similar in all cases.

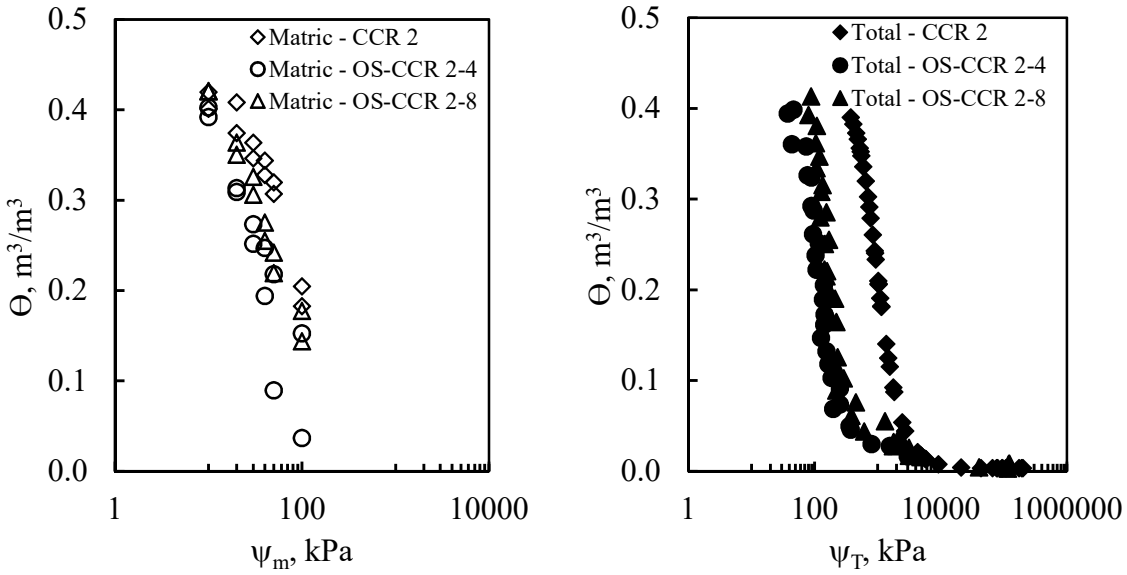


Figure 8-6. WRC of OS-treated CCR compared to corresponding untreated CCR. (a) matric suction and (b) total suction.

8.5.2.2 Parametric models fitting

The parametric models, vG, vGM, vGB, and FX, were fitted to the measured data to provide a continuous characterization of the water retention behavior of the OS-treated CCR as explained in section 5.3.3.2 . For clarity, only model fitting of combined data set are shown in Figure 8-7 and Figure 8-8 with a summary of corresponding model parameters presented in Table 8-3 and

Table 8-4 for OS-CCR 2-4 and OS-CCR 2-8, respectively.

The test specimens for both test methods showed varied saturated volumetric water contents presumabley due to differences in saturation conditions which is a function of dry unit weights and gravimetric water content. The average of the duplicate test specimens were reported for the pramateric model analysis. In general, the parametric models showed a good fit to the measured data with the models performing relatively

well with the measured data of OS-CCR 2-8. The fitting parameters compared well for the parametric models considered but with variations. The variations in the fitting parameters showed no unique trend concerning the degree of water repellency or the parametric models considered. The estimated AEVs, which correlate with the largest pore sizes, were found to vary for the degree of water repellency with OS-CCR 2-4 having lower values than OS-CCR 2-8. In general, the AEVs for the OS-treated CCR were lower than the corresponding AEVs of the corresponding untreated CCR. This could be explained by the phenomenon of surface tension. The OS-treated CCR will exhibit low surface energy meaning a decrease in surface tension leading to a reduction in capillary and adsorptive forces. Therefore, in such a condition, it will be expected that the OS-treated CCR will drain at a lower suction, making it behave as coarse graded material as discussed in literature (Nieber et al. 2000).

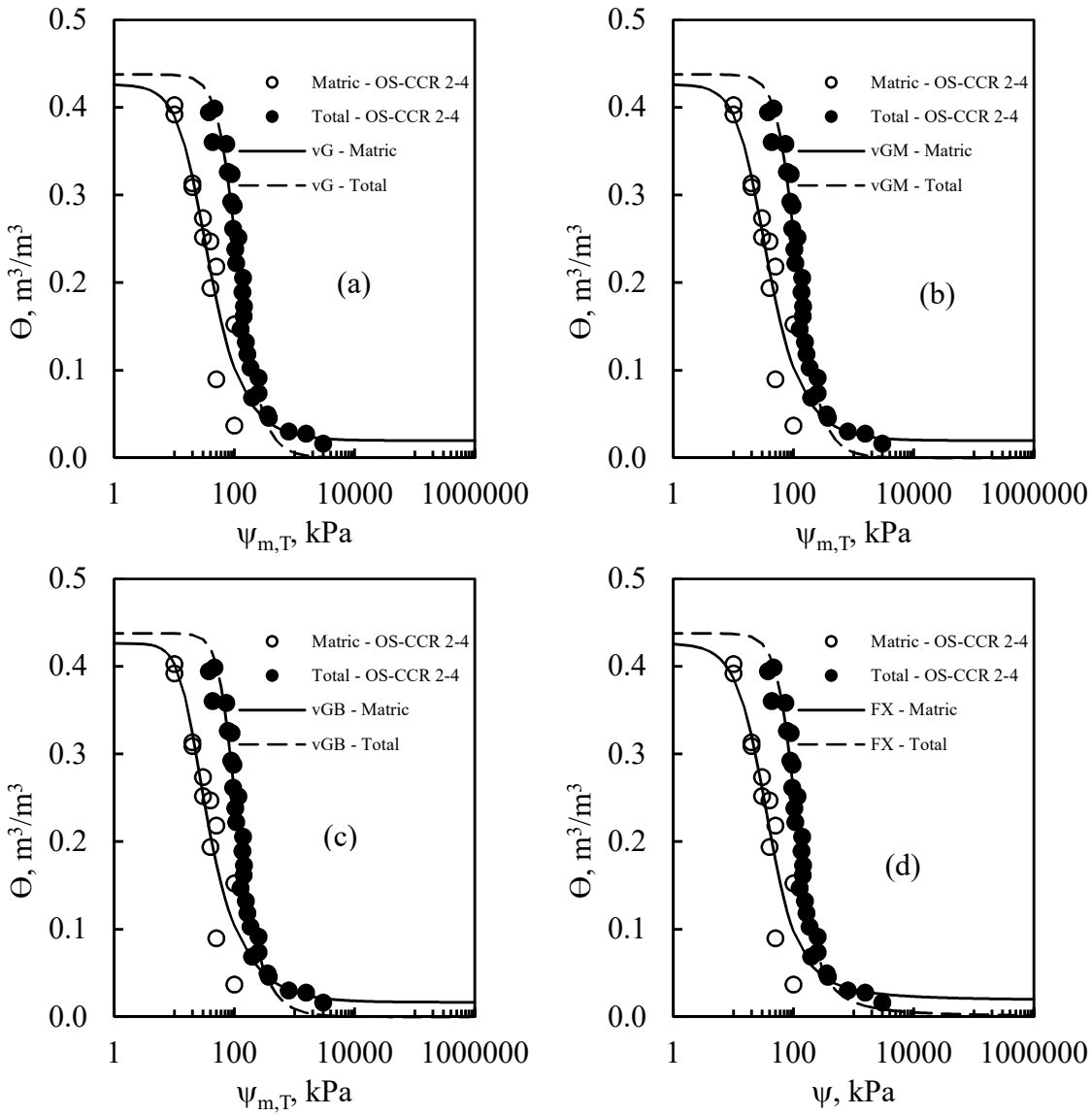


Figure 8-7. Parametric models (a) vG, (b) vGM, (c) vGB, and (d) FX fitting to OS-CCR 2-4 measured data.

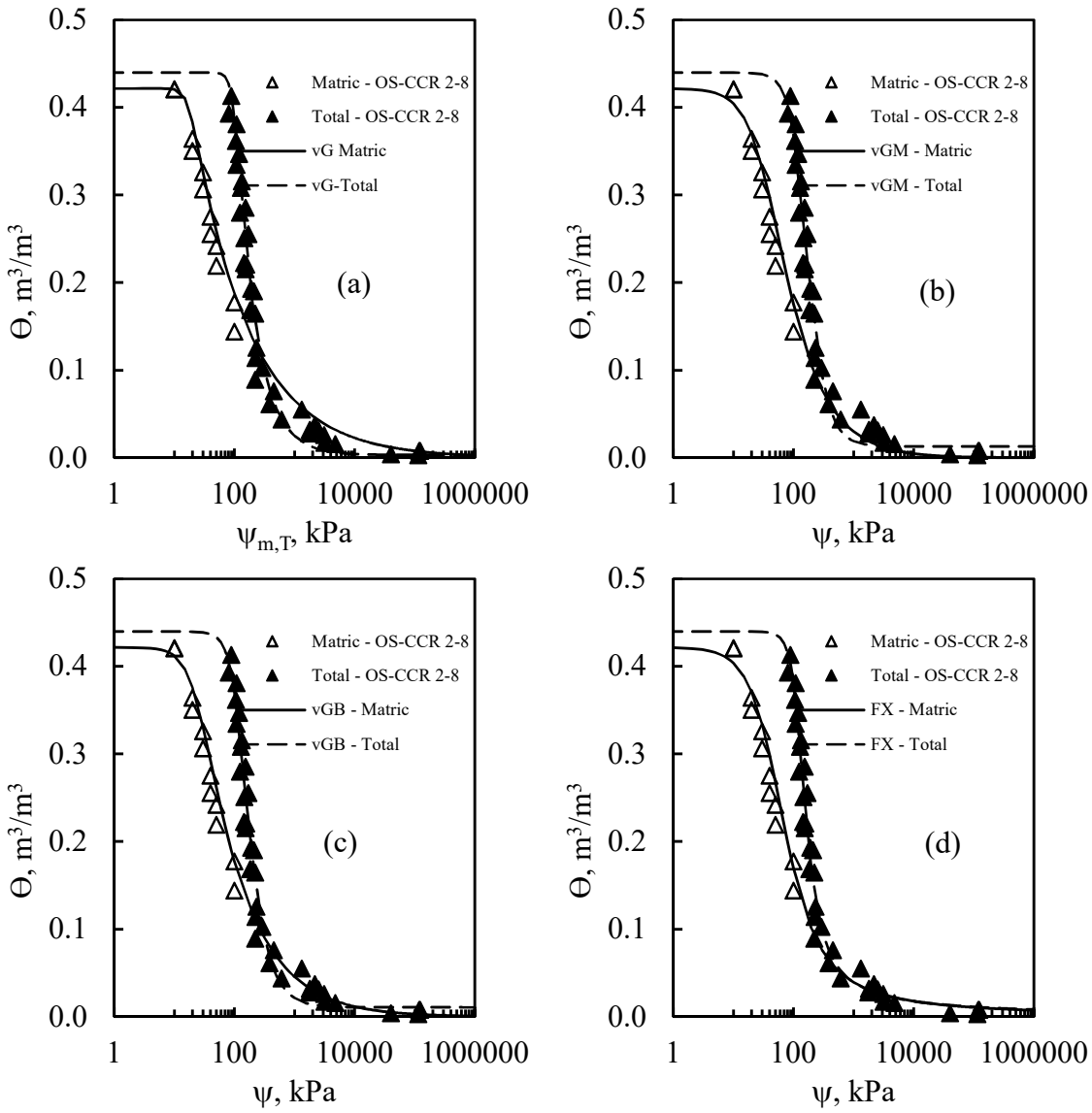


Figure 8-8. Parametric models (a) vG, (b) vGM, (c) vGB, and (d) FX fitting to OS-CCR 2-8 measured data.

Table 8-3. Parametric model functions for OS-CCR 2-4.

| Suction | Model | Parameters | | | | | | |
|---|---|---|---|---|---|---|---|---|
| | | $\theta_s$ | $\theta_r$ | $\psi_{AEV}$ | $\psi_r$ | n | m | $R^2$ |
| | | $m^3/m^3$ | $m^3/m^3$ | MPa | MPa | | | |
| Matric | vG | 0.4264 | 0.0289 | 0.023 | 0.8 | 2.8978 | 0.4820 | 0.9417 |
| | vGM | 0.4264 | 0.0197 | 0.022 | 180 | 2.0417 | 0.5102 | 0.9416 |
| | vGB | 0.4264 | 0.0166 | 0.017 | >1000 | 2.8716 | 0.3035 | 0.9390 |
| | FX | 0.4264 | 0.0185 | 0.031 | >1000 | 1.6882 | 1.9544 | 0.9415 |
| Total | vG | 0.4377 | 0.0001 | 0.094 | >1000 | 2.7225 | 0.6765 | 0.9667 |
| | vGM | 0.4377 | 0.0000 | 0.091 | >1000 | 2.7919 | 0.4594 | 0.9667 |
| | vGB | 0.4377 | 0.0000 | 0.077 | >1000 | 3.5143 | 0.4309 | 0.9661 |
| | FX | 0.4377 | 0.0000 | 0.095 | >1000 | 2.7207 | 1.7535 | 0.9693 |

Table 8-4. Parametric model functions for OS-CCR 2-8.

| Suction | Model | Parameters | | | | | | |
|---|---|---|---|---|---|---|---|---|
| | | $\theta_s$ | $\theta_r$ | $\psi_{AEV}$ | $\psi_r$ | n | m | $R^2$ |
| | | $m^3/m^3$ | $m^3/m^3$ | MPa | MPa | | | |
| Matric | vG | 0.4216 | 0.0289 | 0.017 | >1000 | 4.6353 | 0.1214 | 0.9959 |
| | vGM | 0.4216 | 0.0000 | 0.036 | >1000 | 1.7956 | 0.4431 | 0.9895 |
| | vGB | 0.4216 | 0.0000 | 0.024 | >1000 | 2.5936 | 0.2289 | 0.9936 |
| | FX | 0.4216 | 0.0000 | 0.044 | >1000 | 1.6572 | 1.4425 | 0.9878 |
| Total | vG | 0.4398 | 0.0032 | 0.098 | >1000 | 8.0388 | 0.1603 | 0.9704 |
| | vGM | 0.4398 | 0.0130 | 0.145 | >1000 | 3.2083 | 0.4594 | 0.9656 |
| | vGB | 0.4398 | 0.0107 | 0.124 | >1000 | 3.7693 | 0.4694 | 0.9675 |
| | FX | 0.4398 | 0.0000 | 0.122 | >1000 | 4.4776 | 1.0785 | 0.9746 |

## 8.6 Water Repellency Assessment of Compacted OS-Treated CCR

Duplicate test specimens for OS-CCR 2-4 and OS-CCR 2-8 were subcored from a standard Proctor compacted CCR into WP4C sample cups of 37 mm diameter and 8.5 mm in height. The test specimens were saturated in a deaired DI water bath for at least 24 hours. Following the WP4C suction measurement protocol, the test specimens were placed in an air-conditioned laboratory, monitored using a HOBO temperature and humidity sensor, with an average humidity of approximately 33 % and temperature of approximately 22 °C. The desaturation of the test specimens was monitored every hour by logging the mass of the test specimens followed by placing approximately 20 μL drop of DI water on the compacted surface using a syringe with a pipette tip. The test specimens were moved to the SDM and drop image analysis setup when penetration time greater than 5s was observed and subsequent contact angle measurements. Using the SDM, DI water of approximately 20 μL was discharged onto the surface of the test specimen. The length of time for the water drop to infiltrate the test specimens was logged. Lee et al. (2015) placed test specimens in a sealed chamber containing 26 % NaCl solution at the bottom to prevent evaporation while maintaining a relative humidity of approximately 75%. Also, Liu et al. (2012) used a sealed chamber to prevent evaporation but without NaCl solution at the bottom. However, in this study, the test specimens were exposed to the laboratory climatic condition for the WDPT test to allow for concurrent contact angle measurement using the SDM and the drop image analysis. Triplicate readings were made for each test specimen at a specific water content at random locations.

Water repellency activity was observed at volumetric water content less than 0.1 $m^3/m^3$ corresponding to the lower boundary of the transition zone of the WRC measurements in section 8.5.2 for all test specimens. Therefore, irrespective of the OS dosage, the OS-treated CCR was observed to have a wide range of wettable characteristics. The OS dosage was found to influence the infiltration behavior of water into the compacted test specimen, as presented in Figure 8-9. The higher the OS dosage, the more time required for the drop of DI water ro infiltrate the compacted OS-treated CCR. The duplicate test specimen compared well with each other indicating the test had less variability and repeatable for the WDPT of compacted OS-treated CCR as illustrated in Figure 8-9(b). In accordance with the WDPT classification detailed in Table 4-12, the OS CCR 2-4 test specimens were slightly and strongly water repellent over a relatively short transition water content whereas the OS CCR 2-8 test specimen were strongly and severely water repellent with extremely water repellent observation made in some of the triplicate readings. These observations are comparable to the findings of Liu et al. (2012). The location of the water drop was observed to impact the time taken for the water drop to infiltrate the compacted OS-treated. The WDPT variations observed were significant for increasing OS dosage and decreasing water content, as illustrated with the error bars plot in Figure 8-9 (a) and can be attributed to the packing density and water repellency of the local region of the water drop. Lee et al. (2015) found the WDPT for water repellent silty soil to decrease as porosity increased with the concentration of the water repellent chemical having less effect. In addition, the study found the WDPT increased as the fraction of water repellent soil increased in the soil matrix.

No unique trend was observed in contact angle measurement with regards to the OS dosage and water content. For slightly water repellent conditions with WDPT < 60 s, contact angle measurements could not be taken. Table 8-5 provides a summary of water repellency comparison of multiple measurement methods.The contact angle of compacted OS-treated CCR compared well with contact angle measurement using a planar monolayer surface as detailed in section 8.4 and Feyyisa et al. (2017).

Table 8-5. Summary of water repellency classification based on several methods.

| Material | Sample ID | WDPT | $\gamma_d$, kN/m$^3$ | Contact Angle, ° | |
|---|---|---|---|---|---|
| | | | | Compacted | Planar Monolayer |
| OS-CCR 2-4 | 1 | Strongly | 14.44 | 145 | 152 - 153 |
| | 2 | Strongly | 14.46 | 125 | |
| OS-CCR 2-8 | 1 | Strongly | 14.99 | 146 | 152 - 156 |
| | 2 | Strongly | 14.88 | 141 | |
| | 1 | Severely | 14.99 | 142 | |
| | 2 | Severely | 14.88 | 144 | |

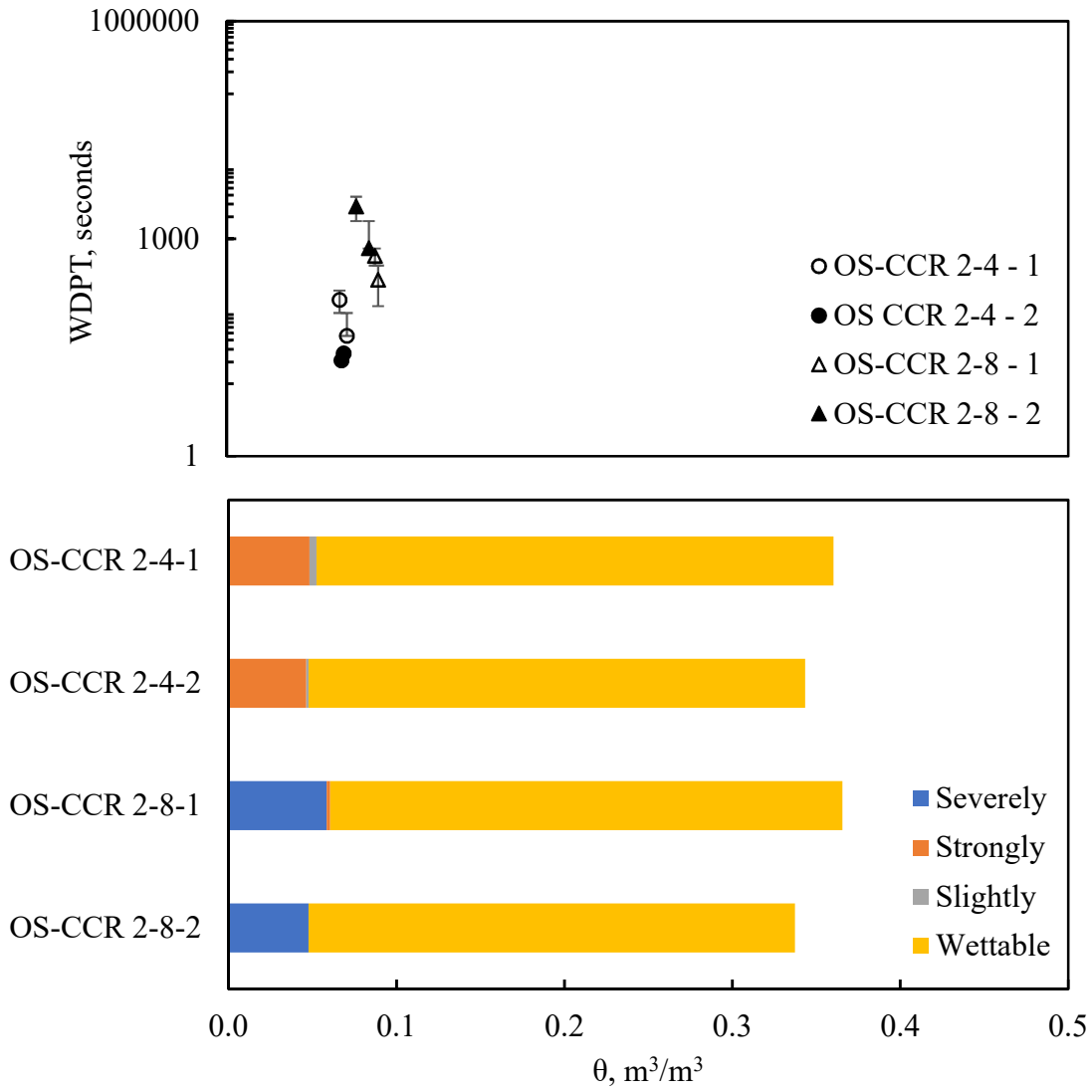


Figure 8-9. WDPT of OS-treated CCR.

## 8.7 Hydrolytic Stability Phenomenon

The pretreatment protocol was considered for the remolding of the OS-treated CCR for geotechnical laboratory tests such as hydraulic conductivity, strength analysis, and breakthrough pressure. The compacted OS-treated CCR was oven-dried for breakthrough pressure analysis. Cracks developed after 24 hours of drying, which

progressed with time. A similar observation was made for the air-drying conditions in the laboratory. Figure 8-10 shows cracks in the oven-dried and air-dried OS-treated CCR, respectively. It was noted that the compaction characteristics, wet and dry of optimum water content, did not prevent the crack development. Extensive literature review revealed that the crack development could be attributed to the hydrolytic stability of OS bond formation to substrates.

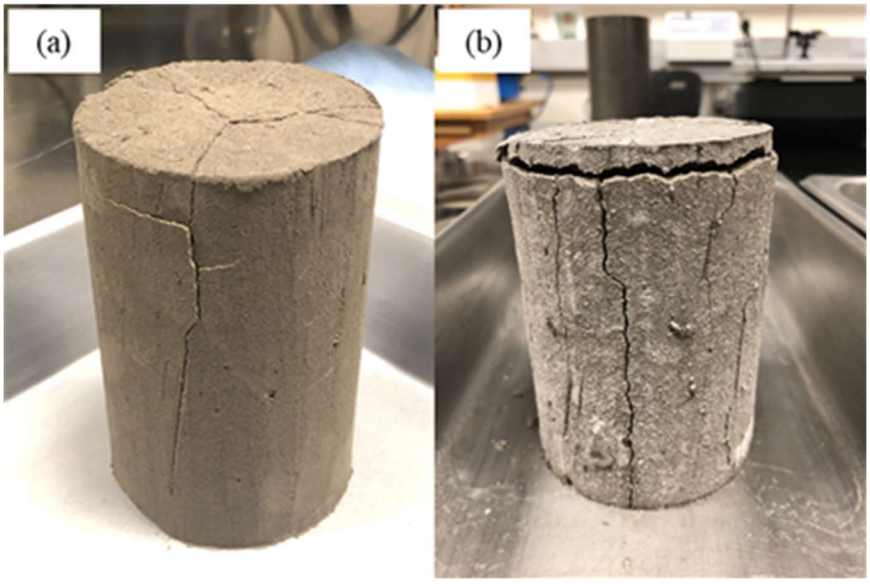


Figure 8-10. Crack development in OS-treated CCR 2. (a) oven-dried and (b) air-dried.

Licari and Swanson (2011) defined hydrolytic stability as "the resistance of a cured polymer material to reverting to a semisolid or liquid form when exposed to high humidity and temperature." In the absence of hydrolytic stability, reversibility takes place, characterized by softening, chalking, blistering, cracking, tackiness, loss of adhesion, or liquefaction of the polymer (Licari and Swanson 2011).

In the review of silane as coupling agents, Arkles (2003) discussed the potential of oxane bond (– Si – O – metal) formation reversing to a certain degree. The oxane bond consists of the metal hydroxyl on the substrate surface and silanols produced from OS reacting with water, as illustrated in Figure 3-3. Water removal takes place in a climatic condition with a temperature difference to about 120° C. During this process, there is oxane bond formation, breaking and reforming of bonds to release stress. The review noted that residual hydroxyl in a non-condensed form could interfere with the process of bond formation. Also, the review discussed substrates that are challenging to modify with OS, such as calcium carbonate, copper, ferrous alloys, and high phosphate and sodium glasses.

Therefore, considering the CCR in question which was found to contain high Na, K, and Ca as discussed in section 6.3; the pretreatment protocol which results in residual OS; and the evidence of cracks when compacted OS-treated CCR was placed in a climatic environment leads to the conclusion that hydrolytic stability in the OS-treated CCR is weak. However, further investigations are required to gain insights into this phenomenon in OS treatment of CCR for water repellency. The study considered the precondition treatment protocol to evaluate the contribution of residual OS and salt to the development of cracks as the protocol is expected to reduce the residual OS and salt to negligible levels. The compacted OS-treated CCR according to precondition protocol was oven-dried and monitored. No visible cracks were observed over at least seven days, as illustrated in Figure 8-11. In conclusion, residual OS and/or soluble salt in CCRs are concerns in understanding cracking in the OS pretremented test specimen.

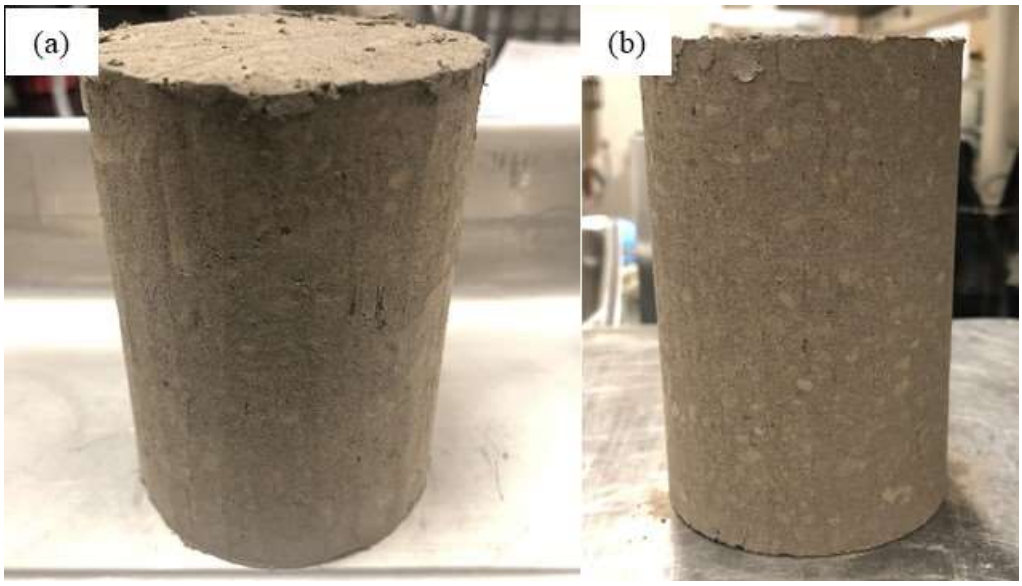


Figure 8-11. Preconditioned Oven-dried OS-treated CCR 2. (a) 4 g OS/kg CCR and (b) 8 g OS/kg CCR.

## 8.8 Breakthrough Pressure and Saturated Hydraulic Conductivity

The pretreatment protocol, as described in section 8.3.2, was followed in preparing the compacted OS-treated CCR. Prior to setting up, the bottom porous stone was saturated for 24 hours to reduce the time required to get water to the OS-treated CCR and porous stone interface. Also, it minimized the introduction of potential errors during the infiltration of the porous stone. The compacted oven-dried OS-treated CCR was mounted in the triaxial setup, as described in ASTM D5084 (ASTM 2016b). A predetermined cell pressure (limited to the maximum pressure setting on the FlowTrac, in this case 138 kPa) was applied to prevent preferential flow between the flexible membrane and the OS-treated CCR using the pressure control panel in Figure 4-4. The pressure lines and bottom porous stone were flushed with a 6.7 kPa head to remove entrapped air. The setup was connected to the FlowTrac and the pressure transducer-

computer system via the inflow valve, as shown in Figure 4-13. The outflow valve was kept opened to allow pore-air to escape during water infiltration. The pore pressure valves were closed throughout the test period. At a rate of 3.4 kPa/s, the FlowTrac supplied DI water that infiltrated the OS-treated CCR until a max of 139 kPa was reached and remained constant. The pressure response at the OS-treated CCR and porous stone interface was logged every second using a software paired with the pressure transducer. Resistance developed as the water got to the OS-treated CCR, indicated by a sudden rise in slope in the pressure-time series plot in Figure 8-12 (b), at the point the breakthrough pressure was attained. Water continued to infiltrate at the constant rate of 3.4 kPa/s until the pressure in the FlowTrac reached 139 kPa, where it remained constant. The breakthrough pressure test was terminated at the exit of water through the outflow valve. The flexible wall permeameter setup was disconnected from the system and mounted to the pressure assembly in Figure 4-4 for the saturated hydraulic conductivity test as described in ASTM D5084 (ASTM 2016b).

### 8.8.1 Breakthrough pressure

Fink and Myers (1969) identified the breakthrough pressure as the point a change in the slope of the linear section of the pressure-time series plot occurs. Feyyisa et al. (2019) identified the breakthrough pressure as the pressure corresponding to the maximum rate of change of the pressure-time data series. A careful review of these definitions shows a correlation where the peak of the rate of pressure application correspond to the point of inflection in the pressure-time series plots. Adopting the rate of change in pressure, the max peak dp/dt corresponded to a pressure of 27 kPa, as illustrated in Figure 8-12 (b), and by Fink and Myers (1969) definitions equals the

breakthrough pressure. The value compared well with the breakthrough pressure value reported Feyyisa et al. (2019) for the same material and OS dosage as presented in Table 8-6.

Table 8-6. Summary of breakthrough pressure compared to literature.

| Reference | Breakthrough Pressure | |
|---|---|---|
| | kPa | cm head of water |
| OS-CCR 2-4 | 27.00 | 275 |
| Feyyisa et al. 2019 | 26.48 | 270 |

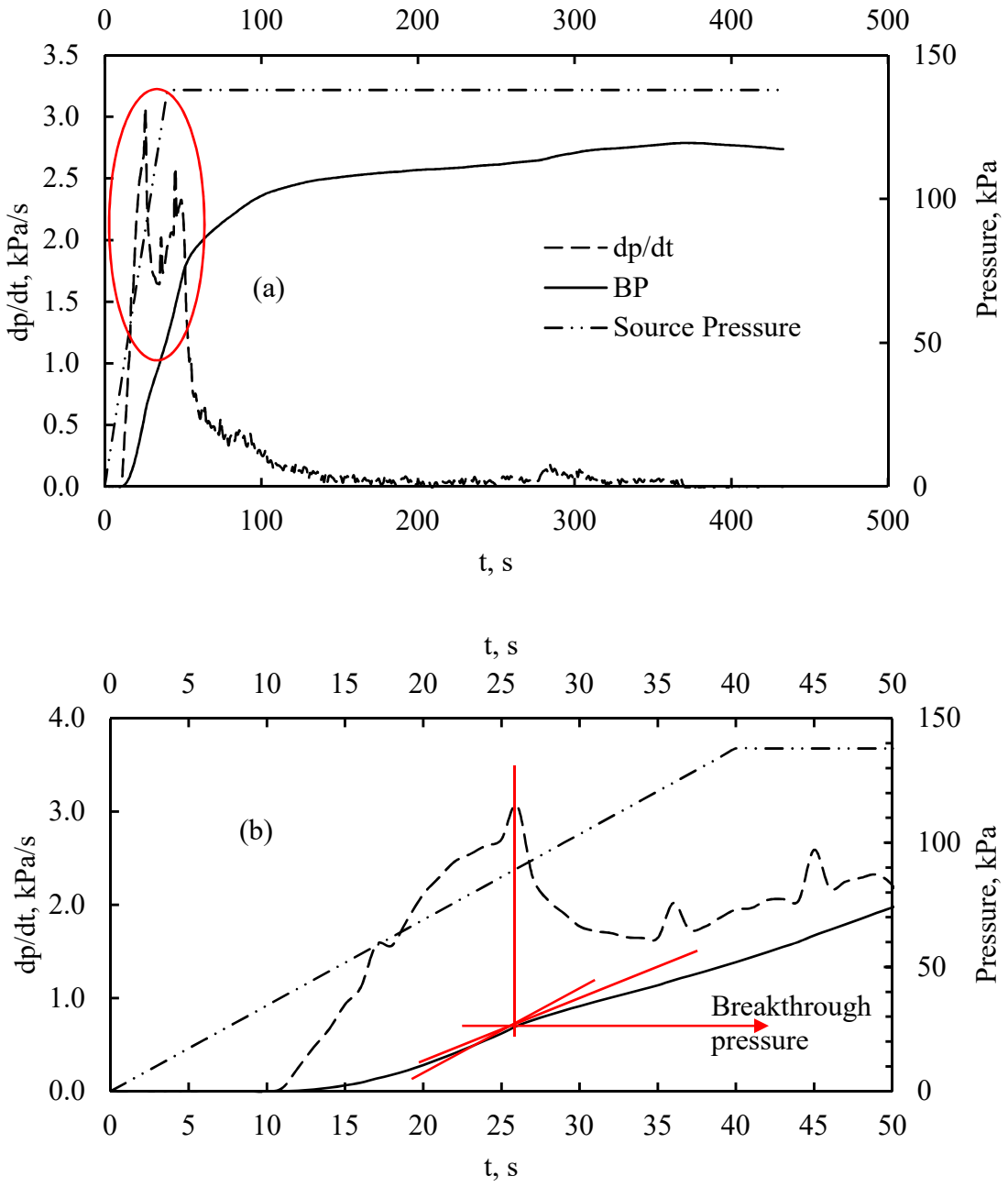


Figure 8-12. Breakthrough pressure analysis for OS-CCR 2-4 (a) Pressure – time series (b) scaled up plot to identify breakthrough pressure.

### 8.8.2 Saturated hydraulic conductivity

Figure 8-13 shows the saturated hydraulic conductivity at varying effective stresses, which range from $10^{-4}$ to $10^{-5}$ cm/s. These values are comparable to the corresponding untreated CCR presented in Figure 4-5 but marginally higher. The increase in hydraulic conductivity can be attributed to the low surface energy which leads to water repellent interaction reducing capillary and adsorptive forces. Therefore, the flow between the water repellent particles will be faster compared to untreated samples that exhibit strong adsorptive and capillary forces. In general, there was a decreasing trend in the saturated hydraulic conductivity as the effective stresses increased. However, an increase in hydraulic conductivity was observed for the effective stress of 500 kPa. This could be attributed to the development of a flow path that enhances preferential flow. Kim et al. (2013) noted that saturated hydraulic conductivity increased with porosity and may be due to a negligible effect in drag force in the water repellent sands.

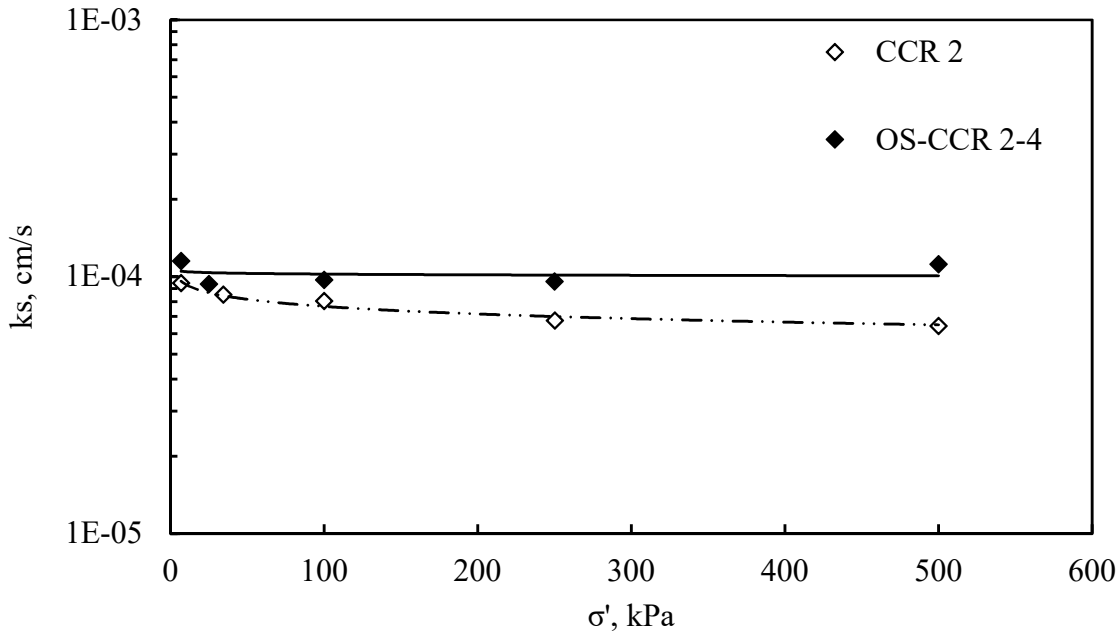


Figure 8-13. Saturated hydraulic conductivity of OS-CCR 2-4 with varying effective stresses compared to corresponding untreated CCR.

8.8.3 Unsaturated hydraulic conductivity prediction

Figure 8-14 illustrates the comparison between the unsaturated hydraulic conductivity of OS-CCR 2-4 predicted using Eq. 3-2 (Parker 1989) and that of CCR 2 predicted using Eq. 2-12 (Burdine 1953; van Genuchten 1980). At saturation, the predicted values of OS-CCR 2-4 were found to be identical to CCR 2; however, after the AEV was crossed, both samples exhibited similar trends in unsaturated hydraulic conductivity reduction as matric suction increased. The OS-CCR 2-4 predicted values were found to be higher as suction increased and, in some cases, for independent and average measurement significantly higher than CCR 2. Nevertheless, these observations were comparable to those reported by Parker (1989) and Nieber et al. (2000).

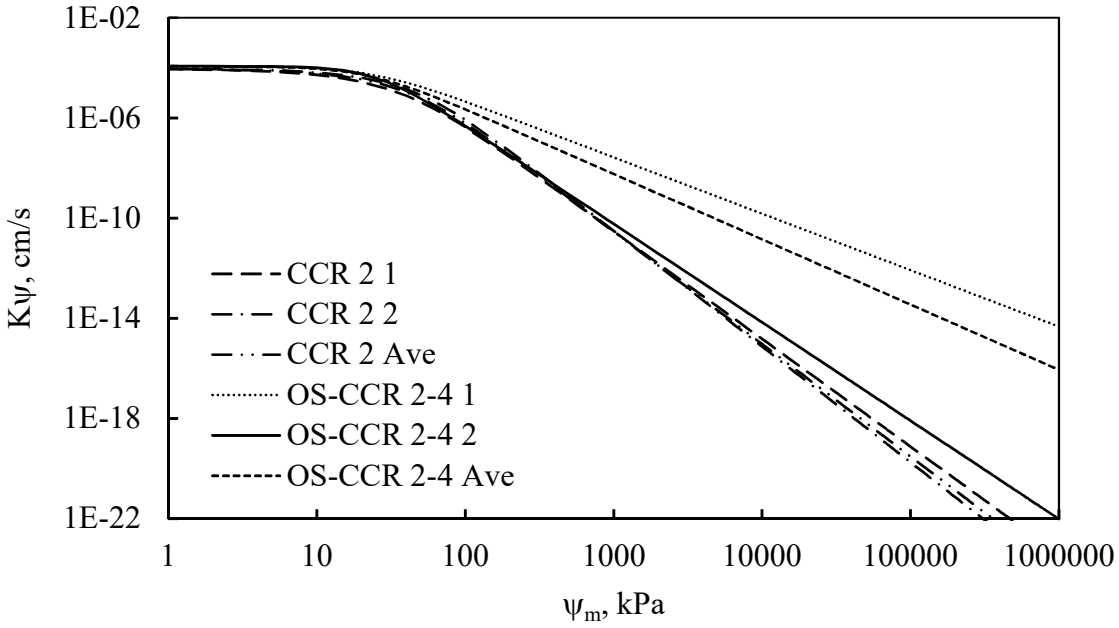


Figure 8-14. Predicted unsaturated hydraulic conductivity of OS-CCR 2-4.

## 8.9 Summary

This chapter adopted two OS treatment protocols to evaluate the effect of water repellency on compacted CCR considering standard proctor compaction characteristics, WRC, and the relationship between water content and water repellency, and suction and water repellency. Also, breakthrough pressure and saturated hydraulic conductivity test were demonstrated using a flexible wall permeameter setup.

- Two OS treatment protocols, namely pretreatment, and precondition, were successfully implemented to treat CCR for varying degrees of water repellency considering practical implementation and reactivity of device components with residual OS.

- The presence of residual OS and salt influenced the performance of the OS treatment protocol adopted to treat CCRs for water repellency.
- OS treatment of CCR using pretreatment for water repellency reduced the maximum dry unit weight by 3% and 6%, and optimum water content by 8% and 10% for dosages 4 g OS/kg CCR and 8 g OS/kg CCR, respectively. In general, the compaction characteristics decreased with dry unit weight and water content.
- The performance of TC and WP4C with OS-treated CCR test specimens compared relatively well with corresponding untreated CCR test specimens.
- The parametric models had a good fit to the measured WRC of OS-treated CCR.
- The porosity of the OS-treated CCR increased when compared to the corresponding untreated CCR leading to higher values of saturated water contents but resulted in quick drainage due to less effect of capillary and adsorptive forces.
- The AEVs of the OS-treated CCR were found to be lower than the corresponding untreated CCR. However, considering the varying degree of water repellency, the AEV increased with increasing OS dosage instead of decreasing with increasing with OS dosage. This observation requires further investigation.
- No unique trend was observed for other fitting parameters with varying degrees of water repellency.
- In general, the OS-treated CCR had reduced water retention capacity due to a reduction in capillary and adsorptive forces.

# CHAPTER 9: SUMMARY, CONCLUSIONS, CONTRIBUTIONS, AND RECOMMENDATIONS FOR FUTURE WORK

## 9.1 Summary

Engineered water repellency has been identified as a potential alternative approach to control water infiltration and leachate generation in CCRs as it reduces water interaction with CCRs. The research motivation of this study derives from the potential of engineered water repellent CCR to contribute to the effective management of CCRs in engineered systems and to investigate whether OS-treated CCRs could be used in structural fills/embankment or liner and capping systems as an infiltration control system. Majority of these engineered systems mostly function in unsaturated conditions, however, their design framework was based on limiting conditions of saturation and residual properties. Also, the current protocol on engineered water repellency is limited in providing a comprehensive design framework for laboratory and field implementation. Therefore, it is important to gain insight into the effect of engineered water repellency on the unsaturated properties of compacted CCRs. The objectives of this doctoral research study were to: 1) correlate applicable engineering properties of CCRs to unsaturated functions of compacted CCRs; 2) investigate the influence of soluble salts on the engineering performance of a select compacted CCR; 3) implement batch sorption approach to better understand OS surface modification of CCRs and evaluate feasible standardized method suitable for practical implementation of engineered water repellency in the field; and 4) assess the effect of engineered water repellency on unsaturated functions of compacted CCRs.

Five CCRs were characterized for geotechnical engineering properties that define the engineering performance of CCRs in unsaturated conditions. These characterization tests include physical and index property tests, particle size distribution, compaction characteristics test, hydraulic and mechanical properties tests, and elemental and mineral compositions. The CCRs were classified as silty (ML) and silty sand (SM) with no plasticity. The dry unit weights were found to be relatively lower compared with typical geotechnical soils, making them suitable for fill works. The CCRs have unique chemical composition comprised of oxides such as silica, ferric oxide, aluminum oxide and minerals such as quartz, mullite, and gypsum. The following paragraphs provide a comprehensive but concise overview of the experimental research design for each objective of this study.

**Objective 1)** The test specimens for the WRC measurements were subcored from standard Proctor compacted CCRs. The axis translation methods, PPE and TC, and the UFA method were used to measure the desaturation cycle of the WRC of the compacted CCRs. The vG, vGM, vGB, and FX parametric models were fitted to the measured data to generate unsaturated functions of the compacted CCRs. Multiple test specimens were evaluated as independent measurements. The multiple test specimens of each test method were considered to analyze the test method repeatability and variability whereas all test specimens from all the test methods were considered to analyze each CCR behavior. The AEVs generated from the parametric models were compared to pore sizes estimated from theoretical grain packing, cubic and tetrahedral, using the $D_{50}$ obtained from the particle size distribution analysis. The osmotic suction was determined relative to the difference between the independent matric and total suctions of the compacted CCRs.

**Objective 2)** A leaching program was performed on a select CCR with significant salt contents using the US EPA method 1313 standard leaching protocol. The leached CCR was evaluated for selected engineering characteristics, including specific gravity, particle size distribution, and hydraulic conductivity and strength properties. The WRC of the compacted CCR was evaluated using suction measurement methods TC and WP4C, and parametric models vG, vGM, vGB, and FX. A comparison was made with the corresponding unleached CCR for the effect of soluble salts, the select engineering properties, suction behavior, and unsaturated functions. Chemical analysis was performed on the leachate generated per leaching cycle.

**Objective 3):** The five CCRs were treated to varying degrees of water repellency using a batch sorption approach while changing variables defined as independent, including material, OS dosage, reaction time, and drying conditions. The degree of water repellency was assessed using the SDM with a drop image analysis tool. The variables were evaluated using SAS to determine the effects and interactions for water repellency using the batch sorption approach. The supernatants of the batches were evaluated for EC and pH.

**Objective 4):** For laboratory and practical implementation of engineered water repellency of CCRs, two treatment protocols, namely pretreatment, and preconditioning, were developed. The CCR with high salt contents was selected for this part of the study. The pretreatment protocol was considered for the remolding of OS-treated CCR for standard geotechnical testing whereas the preconditioned protocol was selected for WRC measurements to eliminate the potential negative consequences of OS residual reacting with device components and compromising the results. The precondition was based on

the sorption concept of OS-treatment. The WRC test specimens where subcored from standard Proctor compaction and tested using TC and WP4C. Parametric models vG, vGM, vGB, and FX were fitted to the measured data. A comparison of results was made with the corresponding untreated CCR for the effect of engineered water repellency on the unsaturated functions. Breakthrough pressure and saturated hydraulic conductivity were demonstrated using a flexible wall permeameter.

## 9.2 Conclusions

The following conclusions were made from the findings of the experimental study conducted to address the research questions and objectives of this study.

1. In general, the suction measurement methods PPE, TC, UFA, and WP4C agree well with the trend observed for water retention characteristics of compacted CCRs and falls within acceptable variability and repeatability range.
2. Comparing the matric suction measurement methods in terms of equilibration, suction range, and duration of the test shows that the axis translation methods are valid for suctions < 100 kPa and have longer equilibration and test completion time due associated limitation detailed in literature. The UFA covered a more extensive range of matric suction and has the potential to extend into the residual zone of the WRC of the compacted CCRs.
3. The measurable suction range of the compacted CCRs is between 2 kPa to 130,000 kPa with the axis translation method having the least matric suction range 2 kPa – 300 kPa compared to UFA with 4 kPa – 425 kPa. The WP4C for total suction had a wide range from complimenting 70 kPa – 130,000 kPa.

4. The matric and total suction measurements of the WRC of the compacted CCRs are dominated by the physical characteristics and chemical compositions of the CCRs, respectively.
5. The repeatability and variability of the suction measurements validated the osmotic suction estimated from the independent measurements of matric and total suctions.
6. The soluble salts present in CCRs can be attributed to air emission control measures, which require the use of salt-based additives to control the release of NOx and SOx into the atmosphere, thereby increasing the salt contents of CCRs. The soluble salts present in CCRs has implications for the engineering performance of compacted CCRs such as leaching of heavy metals, infiltration, and compaction characteristics.
7. The results of suction measurement and parametric modeling of the compacted leached and unleached CCR show a general agreement in the matric suction component of the WRC, although both samples have different compaction characteristics. However, total suction measurements of the leached CCR showed that the presence of the soluble salts dominated the total suction in the unleached CCR as lower suction values were reported compared to the unleached for the same volumetric water content measured.
8. The batch sorption treatment of CCRs for water repellency showed that material type and OS dosage/concentration of OS solutions are the most significant variables effecting varying degrees of water repellency. Interactions between variables existed with negligible variance contribution to water repellency

treatment. The chemistry of the supernatant generated during the batching process provided optimal condition for the chemical reaction of OS solution to the CCR particles.

9. The chemical compositions, soluble salts, and residual OS influence the remolding of OS-treated CCRs as they affect the hydrolytic stability of the siloxane and –Si-O-metal bond, which gives the water repellency effect.
10. The suction measurement methods, TC and WP4C, are good devices and protocols to determine the WRC of the OS-treated CCR if the residual OS in the OS-treated sample are removed. The WRC trend of the OS-treated CCR compared well with the corresponding untreated CCR covering the saturation, transition, and residual zones.
11. Differences were noted in the desaturation rate with varying degrees of water repellency. The desaturation process of the OS-treated CCR test specimens were unique and higher than the corresponding untreated CCR test specimens. The volumetric water contents of the OS-treated CCR were found to be lower than the corresponding untreated CCR. However, the effect of the degree of water repellency on volumetric water content was not clearly defined.
12. The parametric models, vG, vGM, vGB, and FX, had good fit to measured WRC of the OS-treated CCR. The AEVs were found to be distinctly lower than the untreated CCR, implying more comparable to coarse-grained textured material rather than the silty class of the untreated CCRs.

## 9.3 Research Contributions

This dissertation research provides a laboratory base experimental approach to address the research questions and objectives on the unsaturated property functions of compacted untreated and OS-treated CCRs. The relevant contributions of this dissertation research are discussed in the following paragraphs.

- In Chapter 5, the research presented findings that contribute to the knowledge base of estimating the unsaturated functions of compacted CCRs which describes field relevant processes related to infiltration, shear strength, volume change, and contaminant transport in geotechnical and geoenvironmental engineering applications. Several traditional suction measurement methods were used to measure the WRC of the compacted untreated CCRs. The unsaturated functions were estimated based on fitting parametric models to the WRC measurements using several suction measurement methods. These unsaturated functions would serve as data input for numerical modeling.
- In Chapter 6, research findings provided insight on the possible source of soluble salts and selected effect on the performance of compacted CCR for long term design consideration. CCR 2 was used due to the relatively high amount of soluble salts. An extensive leaching protocol was implemented to reduce the amount of salts. The leached CCR was evalauted for selected physical properties and WRC. Also, the leachate generated was chemically analyzed. The soluble salts were found to contribute to the compaction charactreistics and the WRC. Air emission control measures were the likely source of the high amount of soluble salts in the CCR.

- In Chapter 7, the research presented findings that contribute to the knowledge base of OS chemical reaction with CCRs for geotechnical and geoenvironmental applications. The batch sorption approach was found to provide insight on the OS chemical reaction with CCRs using independent variables including CCR materials, OS dosage, reaction time, and drying conditions. With contact angle as the dependent variable, the study showed that engineered water repellency of CCRs is dependent on the CCR material and OS dosage with time and drying conditions having no significant effect. Therefore, the batch sorption approach provides a laboratory based test to understand factors to consider in the optimization of OS treatment for engineered water repellency of CCRs.
- Based on findings in Chapter 7, two OS treatment protocols namely pretreatment and precondition as described in section 4.6.2 were implemented to perform further geotechnical testing of OS treated CCRs considering practical laboratory implementation and the potential interaction of the residual OS with some components of standardized test devices, respectively. The research findings of both treatment protocols provided insight on the effect of residual OS and/or soluble salts on OS chemical reaction with CCRs. In addition, the preconditioned approach was found to be suitable for remolding of OS-treated CCRs for further geotechnical laboratory testing. Chapter 8 explains the effect on water repellency on the WRC of compacted OS-treated CCR.

## 9.4 Recommendations for Future Research

a. The study did not validate the laboratory-measured WRC of untreated and OS-treated CCRs for sensitivity analysis for field relevant parameters such as

infiltration and strength using finite element tools, HYDRUS – 2D, Slope/W and Seep/W.

b. The study was limited in independently measuring the osmotic suction of the CCRs. The setup of the matric suction measurement methods, TC and UFA, provide accessories to collect pore fluid extracts for chemical analysis such as EC, and ionic strength to correlate pore fluid chemistry with osmotic suction.
c. The study was limited in establishing the effective OS dosage required for optimum water repellency for practical implementation.
d. Prior to OS treatment of CCRs and soils in general, a comprehensive analysis of the elemental and mineral compositions of substrates and a leaching test under natural conditions to identify soluble salts are required to address the impact on hydrolytic stability of bond formation.
e. Assessing the thickness of the OS surface modification of the substrates.
f. Developing pedotransfer functions to correlate hydraulic properties of CCRs.

# REFERENCES


Abedi-Koupai, J., and Mehdizadeh, H. (2007). "Estimation of osmotic suction from electrical conductivity and water content measurements in unsaturated soils". *Geotechnical Testing Journal, 31*(2), 142-148.

Abhijit, D., and Sreedeep, S. (2014). *Evaluating the Utility of Tensiometers for Establishing Water Retention Characteristics Curves of Fly Ash.* Paper presented at the Geo-Congress 2014 Technical Papers@ sGeo-characterization and Modeling for Sustainability.

ACAA. (2018). 2017 Production and Use Survey Results News Release. <https://www.acaa-usa.org/Portals/9/Files/PDFs/Coal-Ash-Production-and-Use-2017.pdf>04/25/2019

Arkles, B. (1977). "Tailoring Surfaces with Silanes". *CHEMTECH, 7*(12), 766.

Arkles, B. (2003). "Silane coupling agents: connecting across boundaries". *Morrisville: Gelest, 2003*, 9-12.

Arkles, B. (2006). Hydrophobicity, Hydrophilicity and Silanes. <https://www.gelest.com/wp-content/uploads/HydrophobicityHydrophilicityandSilanes.pdf>December 6, 2018

Arkles, B., Steinmetz, J., Zazyczny, J., and Mehta, P. (1992). "Factors contributing to the stability of alkoxysilanes in aqueous solution". *Journal of Adhesion Science and Technology, 6*(1), 193-206.

Asokan, P., Saxena, M., and Asolekar, S. R. (2005). "Coal combustion residues—environmental implications and recycling potentials". *Resources, Conservation and Recycling, 43*(3), 239-262.

ASTM. (2002). Standard Test Methods for Determination of the Soil Water Characteristic Curve for Desorption Using Hanging Column, Pressure Extractor, Chilled Mirror Hygrometer, or Centrifuge *ASTM D6836-02*. West Conshohocken, PA: ASTM International

ASTM. (2007). Standard Test Method for Particle-Size Analysis of Soils *ASTM D422-63((2007)e2*. West Conshohocken, PA: ASTM International.

ASTM. (2008). Determining Unsaturated and Saturated Hydraulic Conductivity in Porous Media by Steady-State Centrifugation *D6527-00*. West Conshohocken, PA: ASTM International.

ASTM. (2010). Standard Test Methods for Measurement of Hydraulic Conductivity of Unsaturated Soils *ASTM D7664*. West Conshohocken, PA: ASTM International.

ASTM. (2011a). Standard Practice for Classification of Soils for Engineering Purposes (Unified Soil Classification System) *ASTM D2487-11*. West Conshohocken, PA: ASTM International.

ASTM. (2011b). Standard Test Method for Direct Shear Test of Soils Under Consolidated Drained Conditions *ASTM D3080*. West Conshohocken, PA: ASTM International.

ASTM. (2012). Standard Test Methods for Laboratory Compaction Characteristics of Soil Using Standard Effort (12 400 ft-lbf/ft3 (600 kN-m/m3)) *ASTM D698-12e2*. West Conshohocken, PA: ASTM International

ASTM. (2014). Standard Test Methods for Specific Gravity of Soil Solids by Water Pycnometer *ASTM D854-14*. West Conshohocken, PA: ASTM International.

ASTM. (2015a). Standard Specification for Coal Fly Ash and Raw or Calcined Natural Pozzolan for Use in Concrete *ASTM C618-15*. West Conshohocken, PA: ASTM International.

ASTM. (2015b). Standard Test Method for Unconsolidated-Undrained Triaxial Compression Test on Cohesive Soils *ASTM D2850-15*. West Conshohocken, PA: ASTM International.

ASTM. (2016a). Standard Test Methods for Maximum Index Density and Unit Weight of Soils Using a Vibratory Table *ASTM D4253-16*. West Conshohocken, PA: ASTM International.

ASTM. (2016b). Standard Test Methods for Measurement of Hydraulic Conductivity of Saturated Porous Materials Using a Flexible Wall Permeameter *ASTM D5084-16*. West Conshohocken, PA: ASTM International.

ASTM. (2016c). Standard Test Methods for Minimum Index Density and Unit Weight of Soils and Calculation of Relative Density *D4254-16*. West Conshohocken, PA: ASTM International.

ASTM. (2017). Standard Test Methods for Liquid Limit, Plastic Limit, and Plasticity Index of Soils *ASTM D4318-17e1*. West Conshohocken, PA: ASTM International

Bachmann, J., and van der Ploeg, R. R. (2002). "A review on recent developments in soil water retention theory: interfacial tension and temperature effects". *Journal of Plant Nutrition and Soil Science, 165*(4), 468-478.

Bachus, R., Terzariol, M., Pasten, C., Chong, S., Dai, S., Cha, M., Kim, S., Jang, J., Papadopoulos, E., and Roshankhah, S. (2019). "Characterization and Engineering Properties of Dry and Ponded Class-F Fly Ash". *Journal of Geotechnical and Geoenvironmental Engineering, 145*(3), 04019003.

Barbour, S. L. (1998). "Nineteenth Canadian Geotechnical Colloquium: The soil-water characteristic curve: a historical perspective". *Canadian Geotechnical Journal, 35*(5), 873-894.

Basheer, P. A. M., Basheer, L., Cleland, D. J., and Long, A. E. (1997). "Surface treatments for concrete: assessmentmethods and reported performance". *Construction and Building Materials, 11*(7), 413-429.

Bauters, T. W. J., Steenhuis, T. S., DiCarlo, D. A., Nieber, J. L., Dekker, L. W., Ritsema, C. J., Parlange, J. Y., and Haverkamp, R. (2000). "Physics of water repellent soils". *Journal of Hydrology, 231*, 233-243.

Bittelli, M., and Flury, M. (2009). "Errors in Water Retention Curves Determined with Pressure Plates". *Soil Science Society of America Journal, 73*(5), 1453-1460.

Boadu, F. K. (2000). "Hydraulic Conductivity of Soils from Grain-Size Distribution: New Models". *Journal of Geotechnical and Geoenvironmental Engineering, 126*(8), 739-746.

Boynton, S. S., and Daniel, D. E. (1985). "Hydraulic conductivity tests on compacted clay". *Journal of Geotechnical Engineering, 111*(4), 465-478.

Brinker, C. J. (1988). "Hydrolysis and condensation of silicates: Effects on structure". *Journal of Non-Crystalline Solids, 100*(1), 31-50.

Brochier Salon, M.-C., and Belgacem, M. N. (2011). "Hydrolysis-Condensation Kinetics of Different Silane Coupling Agents". *Phosphorus, Sulfur, and Silicon and the Related Elements, 186*(2), 240-254.

Brooks, R., and Corey, T. (1964). "Hydraulic Properties of Porous Media". *Hydrology Papers, Colorado State University, 24*, 37.

Brzoska, J., Azouz, I. B., and Rondelez, F. (1994). "Silanization of solid substrates: a step toward reproducibility". *Langmuir, 10*(11), 4367-4373.

Burdine, N. T. (1953). "Relative Permeability Calculations From Pore Size Distribution Data". *Journal of Petroleum Technology, 5*(3), 71 - 78.

Buser, A. (2013). *Siloxanes: Emissions, properties and environmental fate.* ETH Zurich.

Butalia, T. S., and Wolfe, W. E. (1999). "Evaluation of permeability characteristics of FGD materials". *Fuel, 78*(2), 149-152.

Byun, Y., Khoa Tran, M., Sup Yun, T., and Lee, J. (2012). "Strength and Stiffness Characteristics of Unsaturated Hydrophobic Granular Media". *Geotechnical Testing Journal, 35*(1), 1-8.

Cabalar, A. F., and Akbulut, N. (2016). "Evaluation of actual and estimated hydraulic conductivity of sands with different gradation and shape". *SpringerPlus, 5*(1), 820-820.

Caillahua, M. C., and Moura, F. J. (2018). "Technical feasibility for use of FGD gypsum as an additive setting time retarder for Portland cement". *Journal of Materials Research and Technology, 7*(2), 190-197.

Carrillo, M. L. K., Yates, S. R., and Letey, J. (1999). "Measurement of Initial Soil-Water Contact Angle of Water Repellent Soils". *Soil Science Society of America Journal, 63*(3), 433-436.

Chapuis, R. P., and Aubertin, M. (2003). "On the use of the Kozeny Carman equation to predict the hydraulic conductivity of soils". *Canadian Geotechnical Journal, 40*(3), 616-628.

Chesner, W. H., Collins, R. J., and MacKay, M. (1998). *User guidelines for waste and by-product materials in pavement construction* (No. FHWA-RD-97-148). Retrieved from <https://www.fhwa.dot.gov/publications/research/infrastructure/structures/97148/cfa54.cfm>

Choi, Y., Choo, H., Yun, T., Lee, C., and Lee, W. (2016). "Engineering Characteristics of Chemically Treated Water-Repellent Kaolin". *Materials, 9*(12), 978.

Conca, J., Levitt, D., Heller, P., Mockler, T., and Sully, M. (1997). *Direct UFA measurements of the unsaturated hydraulic conductivity: Comparisons to van Genuchten/Mualem estimations, and applications to recharge mapping in arid regions.* Paper presented at the Proc. Int. Worksh. on Characterization and Measurement of the Hydraulic Properties of Unsaturated Porous Media, Riverside, CA.

Conca, J. L., Apted, M., and Arthur, R. (1992). "Aqueous Diffusion in Repository and Backfill Environments". *MRS Proceedings, 294*, 294-395.

Conca, J. L., and Wright, J. (1992). "Diffusion And Flow In Gravel, Soil, And Whole Rock". *Applied Hydrogeology, 1*(1), 5-24.

Conca, J. L., and Wright, J. (1998). "The UFA method for rapid, direct measurements of unsaturated transport properties in soil, sediment, and rock". *Soil Research, 36*(2), 291-316.

Czachor, H., Doerr, S. H., and Lichner, L. (2010). "Water retention of repellent and subcritical repellent soils: New insights from model and experimental investigations". *Journal of Hydrology, 380*(1), 104-111.

Dai, J.-G., Akira, Y., Wittmann, F. H., Yokota, H., and Zhang, P. (2010). "Water repellent surface impregnation for extension of service life of reinforced concrete structures in marine environments: The role of cracks". *Cement and Concrete Composites, 32*(2), 101-109.

Daniels, J. L., and Hourani, M. S. (2009). Soil improvement with organo-silane *Advances in Ground Improvement: Research to Practice in the United States and China* (pp. 217-224).

Daniels, J. L., Hourani, M. S., and Harper, L. S. (2009a). *Organo-silane chemistry: A water repellent technology for coal ash and soils.* Paper presented at the Proceedings.

Daniels, J. L., Mehta, P., Vaden, M., Sweem, D., Mason, M. D., Zavareh, M., and Ogunro, V. (2009b). "Nano-scale organo-silane applications in geotechnical and geoenvironmental engineering". *Journal of Terraspace Science and Engineering, 1*(1), 21-30.

Daniels, J. L., Pando, M. A., Ogunro, V. O., Feyyisa, J. L., Dumenu, L., Moid, M. I., and Rodriguez, C. (2018). *Water Repellency for Ash Containment and Reuse*. Retrieved from <https://erefdn.org/water-repellency-for-ash-containment-and-reuse/>

Das, S. K., and Yudhbir. (2005). "Geotechnical characterization of some Indian fly ashes". *Journal of Materials in Civil Engineering, 17*(5), 544-552.

Decagon Devices Inc. (2015). Operator's Manual WP4C Dewpoint Potentiameter. Pullman, WA, USA.

Deetz, J. D., and Faller, R. (2015). "Reactive modeling of the initial stages of alkoxysilane polycondensation: effects of precursor molecule structure and solution composition". *Soft Matter, 11*(34), 6780-6789.

Deka, A. (2015). *A Study on the Water Retention and Contaminant Retention Behavior of Fly Ash, Bentonite and Its Mixes.*

Deonarine, A., Kolker, A., and Doughten, M. (2015). *Trace elements in coal ash*: US Department of the Interior, US Geological Survey.

Dillon, S. (2015). Investigation into beneficial uses of substandard fly ash. In L. K. Crouch, M. Allen, D. Badoe, B. Mohr, & K. Young (Eds.): ProQuest Dissertations Publishing.

Dourado Neto, D., de Jong van Lier, Q., Genuchten, M. T., Reichardt, K., Metselaar, K., and Nielsen, D. (2011). "Alternative Analytical Expressions for the General van

Genuchten–Mualem and van Genuchten–Burdine Hydraulic Conductivity Models". *Vadose Zone Journal, 10*(2), 618-623.

Drakonaki, S., Diamadopoulos, E., Vamvouka, D., and Lahaniatis, M. (1998). "Leaching behavior of lignite fly ash". *Journal of Environmental Science and Health, Part A, 33*(2), 237-248.

Dumenu, L., Pando, M. A., Ogunro, V. O., Daniels, J. L., Moid, M. I., and Rodriguez, C. (2017). Water Retention Characteristics of Compacted Coal Combustion Residuals *Geotechnical Frontiers 2017* (pp. 403-413).

Durner, W. (1994). "Hydraulic conductivity estimation for soils with heterogeneous pore structure". *Water Resources Research, 30*(2), 211-223.

Ebrahimi-Birang, N., and Fredlund, D. (2016). "Assessment of the WP4-T Device for Measuring Total Suction". *Geotechnical Testing Journal*.

Elgabu, H. (2013). Critical evaluation of some suction measurement techniques: ProQuest Dissertations Publishing.

EPA, A. (1995). "Compilation of Air Pollutant Emission Factors, Volume I Stationary Point and Area Sources". *Environmental Protection Agency*.

FDGProducts.org. (2016). Introduction to FDG Gypsum. <http://fgdproducts.org/FGDGypsumIntro.htm>1/12/2016

Federal Register. (2010). *Hazardous and Solid Waste Management System; Identification and Listing of Special Wastes; Disposal of Coal Combustion Residuals From Electric Utilities; Proposed Rule*. www.gpo.gov: Government Publishing Office Retrieved from https://www.gpo.gov/fdsys/pkg/FR-2010-06-21/html/2010-12286.htm.

Feyyisa, J. L. (2017). *Engineered Water Repellency for Infiltration Control in Coal Fly Ash.* (PhD Dissertation), Univeristy of North Carolina at Charlotte, ProQuest.

Feyyisa, J. L., and Daniels, J. L. (2016). A Dynamic Contact Angle Measurement Technique for Water-Repellent Coal Fly Ash (CFA) *Geo-Chicago 2016* (pp. 925-938).

Feyyisa, J. L., Daniels, J. L., and Pando, M. A. (2017). "Contact Angle Measurements for Use in Specifying Organosilane-Modified Coal Combustion Fly Ash". *Journal of Materials in Civil Engineering, 29*(9).

Feyyisa, J. L., Daniels, J. L., Pando, M. A., and Ogunro, V. O. (2019). "Relationship between breakthrough pressure and contact angle for organo-silane treated coal fly ash". *Environmental Technology & Innovation, 14*, 100332.

FHWA. (2016, 03/08/2016). User Guidelines for Waste and Byproduct Materials in Pavement Construction. <https://www.fhwa.dot.gov/publications/research/infrastructure/structures/97148/cfa54.cfm>08/20/2019

Fink, D. H. (1970). "Water repellency and infiltration resistance of organic-film-coated soils". *Proceedings - Soil Science Society of America, v. 34*(no. 2), pp. 189-194-1970 v.1934 no.1972.

Fink, D. H., and Myers, L. E. (1969). "Synthetic hydrophobic soils for harvesting precipitation".

Foncea, C., Acevedo, P., and Olguin, R. (2005). *Geotechnical characterization of saline soils.* Paper presented at the PROCEEDINGS OF THE INTERNATIONAL CONFERENCE ON SOIL MECHANICS AND GEOTECHNICAL ENGINEERING.

Fredlund, D. G. (2006). "Unsaturated Soil Mechanics in Engineering Practice". *Journal of Geotechnical and Geoenvironmental Engineering, 132*(3), 286-321.

Fredlund, D. G., and Xing, A. (1994). "Equations for the soil-water characteristic curve". *Canadian Geotechnical Journal, 31*(4), 521-532.

Gartley, K. L. (2011). "Recommended methods for measuring soluble salts in soils". *Recommended Soil Testing Procedures for the Northeastern United States. Northeastern Regional Publication, 493*, 1864-1862.

Global Silicon Council. (2019). *THE UNIQUE PHYSICO-CHEMICAL PROPERTIES OF SILOXANES*. Retrieved from www.sehsc.americanchemistry.com: <https://sehsc.americanchemistry.com/Resources/Siloxane-Fact-Sheet.pdf>

Gorakhki, M., and Bareither, C. (2016). "Effects of Salinity on the Geotechnical Characterization of Fine-Grained Soils and Mine Tailings". *Geotechnical Testing Journal, 39*(1), 45-58.

Gubiani, P. I., Reichert, J. M., Campbell, C., Reinert, D. J., and Gelain, N. S. (2013). "Assessing Errors and Accuracy in Dew-Point Potentiometer and Pressure Plate Extractor Meaurements". *Soil Science Society of America Journal, 77*(1), 19-24.

Halow, J. S., and Covey, J. N. (1982). *Challenge of change: sixth international ash-utilization symposium proceedings*: ; Department of Energy, Morgantown, WV (USA). Morgantown Energy Technology Center; National Ash Association, Washington, DC (USA).

Hao, R. X., and Guo, X. Y. (2012). *The properties of flue gas desulphurization (FGD) gypsum.* Paper presented at the Applied Mechanics and Materials.

Houston, W., Dye, H., Zapata, C., Perera, Y., and Harraz, A. (2006). *Determination of SWCC using one point suction measurement and standard curves.* Paper presented at the Unsaturated Soils 2006.

Huang, W.-H. (1990). "The use of bottom ash in highway embankments, subgrades, and subbases".

Issa, A. A., and Luyt, A. S. (2019). "Kinetics of Alkoxysilanes and Organoalkoxysilanes Polymerization: A Review". *Polymers, 11*(3), 537.

Izquierdo, M., and Querol, X. (2012). "Leaching behaviour of elements from coal combustion fly ash: An overview". *International Journal of Coal Geology, 94*, 54-66.

Jaafar, R., and Likos, W. J. (2014). "Pore-Scale Model for Estimating Saturated and Unsaturated Hydraulic Conductivity from Grain Size Distribution". *Journal of Geotechnical and Geoenvironmental Engineering, 140*(2), 04013012.

Jayaranjan, M. L. D., van Hullebusch, E. D., and Annachhatre, A. P. (2014). "Reuse options for coal fired power plant bottom ash and fly ash". *Reviews in Environmental Science and Bio/Technology, 13*(4), 467-486.

Jiang, H., Zheng, Z., Li, Z., and Wang, X. (2006). "Effects of Temperature and Solvent on the Hydrolysis of Alkoxysilane under Alkaline Conditions". *Industrial & Engineering Chemistry Research, 45*(25), 8617-8622.

Jirka, Š., and R., N. J. (2005). "Estimating soil hydraulic parameters from transient flow experiments in a centrifuge using parameter optimization technique". *Water Resources Research, 41*(4).

Jordan, C. S., Daniels, J. L., and Langley, W. (2015). "The effects of temperature and wet-dry cycling on water-repellent soils". *Environmental Geotechnics, 4*(4), 299-307.

Kairies, C. L., Schroeder, K. T., and Cardone, C. R. (2006). "Mercury in gypsum produced from flue gas desulfurization". *Fuel, 85*(17), 2530-2536.

Kaniraj, S. R., and Gayathri, V. (2003). "Geotechnical behavior of fly ash mixed with randomly oriented fiber inclusions". *Geotextiles and Geomembranes, 21*(3), 123-149.

Kaniraj, S. R., and Gayathri, V. (2004). "Permeability and Consolidation Characteristics of Compacted Fly Ash". *Journal of energy engineering, 130*(1), 18-43.

Kaniraj, S. R., and Havanagi, V. G. (2001). "Behavior of Cement-Stabilized Fiber-Reinforced Fly Ash-Soil Mixtures". *Journal of Geotechnical and Geoenvironmental Engineering, 127*(7), 574-584.

Karim, M. Z., Tucker-Kulesza, S. E., and Derby, M. M. (2018). *Synthesizing Hydrophobic Sand and Comparison of Shear Strength Properties with Hydrophilic Sand.* Paper presented at the IFCEE 2018.

Keatts, M. I., Daniels, J. L., Langley, W. G., Pando, M. A., and Ogunro, V. O. (2018). "Apparent Contact Angle and Water Entry Head Measurements for Organo-Silane Modified Sand and Coal Fly Ash". *Journal of Geotechnical and Geoenvironmental Engineering, 144*(6), 04018030.

Khanzadeh Moradllo, M., Sudbrink, B., and Ley, M. T. (2016). "Determining the effective service life of silane treatments in concrete bridge decks". *Construction and Building Materials, 116*, 121-127.

Kim, B. (2003). Properties of coal ash mixtures and their use in highway embankments. In R. Salgado (Ed.): ProQuest Dissertations Publishing.

Kim, B., and Prezzi, M. (2008a). "Compaction characteristics and corrosivity of Indiana class-F fly and bottom ash mixtures". *Construction and Building Materials, 22*(4), 694-702.

Kim, B., and Prezzi, M. (2008b). "Evaluation of the mechanical properties of class-F fly ash". *Waste Management, 28*(3), 649-659.

Kim, B., Prezzi, M., and Salgado, R. (2005). "Geotechnical properties of fly and bottom ash mixtures for use in highway embankments". *Journal of Geotechnical and Geoenvironmental Engineering, 131*(7), 914-924.

Kim, B., Yoon, S., Balunaini, U., and Salgado, R. (2006). "Determination of ash mixture properties and construction of test embankment-part A". *Joint Transportation Research Program*, 262.

Kim, D., Yang, H., Yun, T., Kim, B., Kato, S., Park, S., and Delage, P. (2013). *Characterization of geomechanical and hydraulic properties of non-wettable*

*sand.* Paper presented at the Proc. 18th International conference on soil mechanics and geotechnical engineering.

Kim, D. H., Yang, H. J., Kim, K. Y., and Yun, T. S. (2015). "Experimental Investigation of Evaporation and Drainage in Wettable and Water-Repellent Sands". *Sustainability, 7*(5), 5648-5663.

Kosugi, K. i., Hopmans, J. W., and Dane, J. H. (2002). 3.3.4 Parametric Models. In J. H. Dane & C. G. Topp (Eds.), *Methods of Soil Analysis: Part 4 Physical Methods* (pp. 728-757). Madison, WI: Soil Science Society of America.

Krahn, J., and Fredlund, D. (1972). "On total, matric and osmotic suction". *The Emergence of Unsaturated Soil Mechanics*, 35.

Krasnoslobodtsev, A. V., and Smirnov, S. N. (2002). "Effect of Water on Silanization of Silica by Trimethoxysilanes". *Langmuir, 18*(8), 3181-3184.

Kwok, D. Y., and Neumann, A. W. (1999). "Contact angle measurement and contact angle interpretation". *Advances in Colloid and Interface Science, 81*(3), 167-249.

Lee, C., Yang, H.-J., Yun, T. S., Choi, Y., and Yang, S. (2015). "Water-Entry Pressure and Friction Angle in an Artificially Synthesized Water-Repellent Silty Soil". *Vadose Zone Journal, 14*(4).

Lee, J. K., Shang, J. Q., Wang, H., and Zhao, C. (2014). "In-situ study of beneficial utilization of coal fly ash in reactive mine tailings". *Journal of Environmental Management, 135*, 73-80.

Leonards, G. A., and Bailey, B. (1982). "Pulverized coal ash as structural fill". *J. Geotech. Eng. Div., Am. Soc. Civ. Eng.;(United States), 108*.

Leong, E.-C., Tripathy, S., and Rahardjo, H. (2003). "Total suction measurement of unsaturated soils with a device using the chilled-mirror dew-point technique". *Geotechnique, 53*(2), 173-182.

Ley, M., Sudbrink, B., Kotha, H., Materer, N., and Apblett, A. (2012). "Expected life of silane water repellant treatments on bridge decks". *Research & Development Division Oklahoma Department of Transportation, No. FHWA/ODOT-2229*.

Ley, T., and Moradllo, M. K. (2015). "Expected Life of Silane Water Repellent Treatments on Bridge Decks, Phase 2". *Research & Development Division Oklahoma Department of Transportation. No. FHWA-OK-15-05/ODOT-2229*.

Licari, J. J., and Swanson, D. W. (2011). Chapter 7 - Test and Inspection Methods. In J. J. Licari & D. W. Swanson (Eds.), *Adhesives Technology for Electronic Applications (Second Edition)* (pp. 345-377). Oxford: William Andrew Publishing.

Liu, H., Ju, Z., Bachmann, J., Horton, R., and Ren, T. (2012). "Moisture-Dependent Wettability of Artificial Hydrophobic Soils and Its Relevance for Soil Water Desorption Curves". *Soil Science Society of America Journal, 76*(2), 342-349.

Lourenço, S., Jones, N., Morley, C., Doerr, S., and Bryant, R. (2015a). "Hysteresis in the soil water retention of a sand–clay mixture with contact angles lower than ninety degrees". *Vadose Zone Journal, 14*(7).

Lourenço, S., Jones, N., Morley, C., Doerr, S. H., and Bryant, R. (2015b). "Hysteresis in the Soil Water Retention of a Sand–Clay Mixture with Contact Angles Lower than Ninety Degrees". *Vadose Zone Journal, 14*(7).

Lu, N., and Likos, W. J. (2004). *Unsaturated soil mechanics*. Hoboken, New Jersey: John Wiley & Sons, Inc.

Malaya, C., and Sreedeep, S. (2010). *Evaluation of SWCC model and estimation procedure for soil and fly ash.* Paper presented at the World Environment and Water Resources Congress, ASCE, Providence, Rode Island.

Malaya, C., and Sreedeep, S. (2014). *Study of the Influence of Fly Ash Addition on Water Retention Characteristics of Soils.* Paper presented at the Geo-Congress 2014 Technical Papers@ sGeo-characterization and Modeling for Sustainability.

Marinho, F. A. M., Take, W. A., and Tarantino, A. (2009). Measurement of Matric Suction Using Tensiometric and Axis Translation Techniques. In A. Tarantino, E. Romero, & Y.-J. Cui (Eds.), *Laboratory and Field Testing of Unsaturated Soils* (pp. 3-19). Dordrecht: Springer Netherlands.

Martin, J. P., Collins, R. A., Browning, J. S., and Biehl, F. J. (1990). "Properties and use of fly ashes for embankments". *Journal of Energy Engineering, 116*(2), 71-86.

Menezes, G. B., Ward, A., and Moo-Young, H. K. (2011). "Unsaturated flow in anisotropic heterogeneous media: a centrifuge study". *International Journal of Hydrology Science and Technology, 1*(3-4), 147-163.

Miller, C. J., Yesiller, N., Yaldo, K., and Merayyan, S. (2002). "Impact of Soil Type and Compaction Conditions on Soil Water Characteristic". *Journal of Geotechnical and Geoenvironmental Engineering, 128*(9), 733-742.

Miller, D. (1996). *Osmotic suction as a valid stress state variable in unsaturated soils.* (Ph.D.), Colorado State University, ProQuest Dissertations Publishing. Retrieved from https://search.proquest.com/docview/304282350?pq-origsite=primo

Miller, D. J., and Nelson, J. D. (2006). Osmotic suction in unsaturated soil mechanics *Unsaturated Soils 2006* (pp. 1382-1393).

Mishra, M., and Karanam, U. M. R. (2006). "Geotechnical characterization of fly ash composites for backfilling mine voids". *Geotechnical & Geological Engineering, 24*(6), 1749-1765.

Mualem, Y. (1976). "A new model for predicting the hydraulic conductivity of unsaturated porous media". *Water Resources Research, 12*(3), 513-522.

Mudd, G. M. (2001). *Solute transport modelling of Latrobe Valley ash disposal sites.* Victoria University.

Mudd, G. M., Chakrabarti, S., and Kodikara, J. (2007). "Evaluation of engineering properties for the use of leached brown coal ash in soil covers". *Journal of Hazardous Materials, 139*(3), 409-412.

Nieber, J. L., Bauters, T. W. J., Steenhuis, T. S., and Parlange, J. Y. (2000). "Numerical simulation of experimental gravity-driven unstable flow in water repellent sand". *Journal of Hydrology, 231-232*, 295-307.

Nimmo, J. R., Rubin, J., and Hammermeister, D. P. (1987). "Unsaturated flow in a centrifugal field: Measurement of hydraulic conductivity and testing of Darcy's Law". *Water Resources Research, 23*(1), 124-134.

Padilla, J., Perera, Y., Houston, W., Perez, N., and Fredlund, D. (2006). Quantification of air diffusion through high air-entry ceramic disks *Unsaturated Soils 2006* (pp. 1852-1863).

Pal, S. K., and Ghosh, A. (2009). *Shear strength behaviour of Indian fly ashes.* Paper presented at the Indian Geotechnical conference, Guntur, India.

Palmer, B. G., Edil, T. B., and Benson, C. H. (2000). "Liners for waste containment constructed with class F and C fly ashes". *Journal of Hazardous Materials, 76*(2–3), 193-216.

Pan, H., Qing, Y., and Pei-yong, L. (2010). "Direct and indirect measurement of soil suction in the laboratory". *Electronic Journal of Geotechnical Engineering, 15*(3), 1-14.

Pandian, N. (2013). "Fly ash characterization with reference to geotechnical applications". *Journal of the Indian Institute of Science, 84*(6), 189.

Pantoja, M., Velasco, F., Broekema, D., Abenojar, J., and Real, J. C. d. (2010). "The Influence of pH on the Hydrolysis Process of γ-Methacryloxypropyltrimethoxysilane, Analyzed by FT-IR, and the Silanization of Electrogalvanized Steel". *Journal of Adhesion Science and Technology, 24*(6), 1131-1143.

Parker, J. (1989). "Multiphase flow and transport in porous media". *Reviews of Geophysics, 27*(3), 311-328.

Patrick, P., Olsen, H., and Higgins, J. (2007). "Comparison of Chilled-mirror Measurements and Filter Paper Estimates of Total Soil Suction". *Geotechnical Testing Journal, 30*(5), 1-8.

Pease, R. E., Rauch, A. F., and Ladwig, K. (2017a). *Geotechnical Properties of Flue-Gas Desulfurization (FGD) Sludge Material*. Paper presented at the World of Coal Ash, Lexington, KY. http://www.flyash.info/2017/032-Pease-woca2017p.pdf

Pease, R. E., Rauch, A. F., and LAdwig, K. (2017b). *Geotechnical Properties of Flue-Gas Desulfurization (FGD) Sludge Material.* Paper presented at the 2017 World of Coal Ash (WOCA).

Peroni, N., and Tarantino, A. (2005). Measurement of osmotic suction using the squeezing technique. In T. Schanz (Ed.), *Unsaturated Soils: Experimental Studies: Proceedings of the International Conference "From Experimental Evidence towards Numerical Modeling of Unsaturated Soils," Weimar, Germany, September 18–19, 2003 Volume I* (pp. 159-168). Berlin, Heidelberg: Springer Berlin Heidelberg.

Pflughoeft-Hassett, D., Hassett, D. J., and Eylands, K. (2007). "A comparison of properties of FGD and natural gypsum products". *Am. Coal Ash Assoc*, -.

Pflughoeft-Hassett, D., Ladwid, K., Hassett, D., Dockter, B., Heebink, L., Eylands, K., and Hoffarth, J. (2009). *Characteristics and performance of fly ash from sodium sorbent scrubbing of SO3 emissions from coal-based power plants.* Paper presented at the Proceedings of the 2009 World of Coal Ash Conference, Lexington, KY.

Rana, A. S. M. A. (1996). Evaluation of engineering properties of hydrated fly ash as a flexible base material: Texas Tech University.

Renew, J. E., Ellison, K. M., Hendershot, K., Rajterowski, J., and Hang, C.-H. (2015). *Impact of Salt on Metal Leaching from Coal Fly Ash*. Paper presented at the World of Coal Ash, Nashville, Tennesses. http://www.flyash.info/2015/063-renew-2015.pdf

Roy, W. R., Krapac, I. G., Chou, S. F. J., and Griffin, R. A. (1992). *Technical Resource Document: Batch-type procedures for estimating soil adsorption of chemicals* (Vol. 87): Office of Solid Waste and Emergency Response, US Environmental Protection Agency.

Santos, F., Li, L., Li, Y., and Amini, F. (2011). "Geotechnical properties of fly ash and soil mixtures for use in highway embankments". *Proceeding of world of coal ash (WOCA), May*, 9-12.

SAS Institute Inc. (2008). The GLM ProcedureSAS/STAT® 9.2 User's Guide (pp. 2429 - 2617). Cary, NC: SAS Institute Inc. Retrieved from https://support.sas.com/documentation/cdl/en/statugglm/61789/PDF/default/statuglm.pdf.

SAS Institute Inc. (2013). The VARCOMP ProcedureSAS/STAT® 13.1 User's Guide (pp. 8957 - 8983). Cary, NC. Retrieved from https://support.sas.com/documentation/onlinedoc/stat/131/varcomp.pdf.

Saulick, Y., Lourenço, S. D. N., Baudet, B. A., Woche, S. K., and Bachmann, J. (2018). "Physical properties controlling water repellency in synthesized granular solids". *European Journal of Soil Science, 69*(4), 698-709.

Sillers, W. S., and Fredlund, D. G. (2001). "Statistical assessment of soil-water characteristic curve models for geotechnical engineering". *Canadian Geotechnical Journal, 38*(6), 1297-1313.

Sindi, H. A. H. (2019). *Characterizing Unsaturated Hydraulic Properties of Compacted Coal Combustion By-Products (CCP) Using Steady-State Centrifugation (SSC) Unsaturated Flow Apparatus (UFA).* California State University, Los Angeles.

Soilmoisture Equipment Corp. (2015). Product Operating Instructions. <http://www.soilmoisture.com/resources/Product-Operating-instructions/>11/08/2015

Sreedeep, S., and Singh, D. N. (2006). "Methodology for determination of osmotic suction of soils". *Geotechnical & Geological Engineering, 24*(5), 1469-1479.

Sridharan, A., Pandian, N., and Srinivas, S. (2001). "Compaction behaviour of Indian coal ashes". *Proceedings of the Institution of Civil Engineers-Ground Improvement, 5*(1), 13-22.

Subedi, S., Kawamoto, K., Jayarathna, L., Vithanage, M., Moldrup, P., Wollesen de Jonge, L., and Komatsu, T. (2012a). "Characterizing Time-Dependent Contact Angles for Sands Hydrophobized with Oleic and Stearic Acids". *Vadose Zone Journal, 11*(1).

Subedi, S., Kawamoto, K., Jayarathna, L., Vithanage, M., Moldrup, P., Wollesen de Jonge, L., and Komatsu, T. (2012b). "Characterizing time-dependent contact angles for sands hydrophobized with oleic and stearic acids". *Vadose Zone Journal, 11*(1), 0-0.

Sun, M., Hou, J., Cheng, G., Baig, S. A., Tan, L., and Xu, X. (2014). "The relationship between speciation and release ability of mercury in flue gas desulfurization (FGD) gypsum". *Fuel, 125*, 66-72.

Taha, R. (1993). "Environmental and engineering properties of flue gas desulfurization gypsum". *Transportation research record*, 14-14.

Thomas, M. (2007). *Optimizing the use of fly ash in concrete* (Vol. 5420): Portland Cement Association Skokie, IL.

Thyagaraj, T., and Rao, S. M. (2010). "Influence of Osmotic Suction on the Soil-Water Characteristic Curves of Compacted Expansive Clay". *Journal of Geotechnical and Geoenvironmental Engineering, 136*(12), 1695-1702.

Tishmack, J. K., and Burns, P. E. (2004). "The chemistry and mineralogy of coal and coal combustion products". *Geological Society, London, Special Publications, 236*(1), 223-246.

Toth, P. S., Chan, H. T., and Cragg, C. B. (1988). "Coal ash as structural fill, with special reference to Ontario experience". *Canadian Geotechnical Journal, 25*(4), 694-704.

Trivedi, A., and Sud, V. (2004). "Collapse behavior of coal ash". *Journal of Geotechnical and Geoenvironmental Engineering, 130*(4), 403-415.

Trivedi, A., and Sud, V. K. (2002). "Grain characteristics and engineering properties of coal ash". *Granular Matter, 4*(3), 93-101.

Truong, Q. H., Lee, J.-S., Dong, Y., and Yun, T. S. (2011). "Capillary induced small-strain stiffness for hydrophilic and hydrophobic granular materials: Experimental and numerical studies". *Soils and Foundations, 51*(4), 713-721.

Twardowska, I., and Szczepanska, J. (2002). "Solid waste: terminological and long-term environmental risk assessment problems exemplified in a power plant fly ash study". *Science of The Total Environment, 285*(1), 29-51.

Ugwu, O. O., Arop, J. B., Nwoji, C. U., and Osadebe, N. N. (2013). "Nanotechnology as a Preventive Engineering Solution to Highway Infrastructure Failures". *Journal of Construction Engineering and Management, 139*(8), 987-993.

USEPA. (1994). Method 200.7, Revision 4.4: Determination of Metals and Trace Elements in Water and Wastes by Inductively CoupledPlasma-Atomic EmissionSpectrometry. www.epa.gov: US EPA.

USEPA. (2012). Method 1313: Liquid Solid Partitioning as a Function of Extract pH using a Parallel Batch Extraction Procedure: United States Environmental Protection Agency Washington, DC.

USEPA. (2019). Coal Ash Reuse. <https://www.epa.gov/coalash/coal-ash-reuse>08/20/2019

van den Berg, E. H., Perfect, E., Tu, C., Knappett, P. S. K., Leao, T. P., and Donat, R. W. (2009). "Unsaturated Hydraulic Conductivity Measurements with Centrifuges: A Review". *Vadose Zone Journal, 8*(3), 531-547.

van Genuchten, M. T. (1980). "A closed-form equation for predicting the hydraulic conductivity of unsaturated soils". *Soil Science Society of America Journal, 44*(5), 892-898.

Vanapalli, S. K., Nicotera, M. V., and Sharma, R. S. (2009). Axis Translation and Negative Water Column Techniques for Suction Control. In A. Tarantino, E. Romero, & Y.-J. Cui (Eds.), *Laboratory and Field Testing of Unsaturated Soils* (pp. 33-48). Dordrecht: Springer Netherlands.

Vargaftik, N., Volkov, B., and Voljak, L. (1983). "International tables of the surface tension of water". *Journal of Physical and Chemical Reference Data, 12*(3), 817-820.

Wang, Z., Wu, L., and Wu, Q. J. (2000). "Water-entry value as an alternative indicator of soil water-repellency and wettability". *Journal of Hydrology, 231-232*, 76-83.

Webb, R., Stormont, J., Stone, M., and Thomson, B. (2014). "Characterizing the unsaturated and saturated hydraulic properties of coal combustion by-products in landfills of Northwestern New Mexico". *J. Am. Soc. Min. Recla, 3*(1), 70-99.

Xenidis, A., Mylona, E., and Paspaliaris, I. (2002). "Potential use of lignite fly ash for the control of acid generation from sulphidic wastes". *Waste Management, 22*(6), 631-641.

Xiameter. (2009). *A Guide to Silane Solutions: The Basics of Silane Chemistry*. Retrieved from www.xiameter.com: <https://www.xiameter.com/en/ExploreSilicones/Documents/Silane%20Chemistry-1a-95-718-01-F2.pdf>

Xu, M., Yu, D., Yao, H., Liu, X., and Qiao, Y. (2011). "Coal combustion-generated aerosols: Formation and properties". *Proceedings of the Combustion Institute, 33*(1), 1681-1697.

Yao, Z. T., Ji, X. S., Sarker, P. K., Tang, J. H., Ge, L. Q., Xia, M. S., and Xi, Y. Q. (2015). "A comprehensive review on the applications of coal fly ash". *Earth-Science Reviews, 141*, 105-121.

Young, S. (1993). *Physical and hydraulic properties of fly ash and other by-products from coal combustion*: Electric Power Research Institute.

Zapata, C., Houston, W., Houston, S., and Walsh, K. (2000). Soil - Water Characteristic Curve Variability *Advances in Unsaturated Geotechnics* (pp. 84-124): American Society of Civil Engineers.

# APPENDIX A. SUCTION MEASUREMENT PROCEDURE

**PPE**: In this study, the 5-bar and 15-bar PPE were used with the 1-bar and 5-bar HAE ceramic disk, respectively. The test method begins with the saturation of the HAE disk. The HAE disk was saturated by filling the water compartment with deaired DI water and allowed to soak for at least 24 hours. The soaked HAE disk was subsequently flushed by applying the bubbling pressure of the HAE disk to eliminated trapped air within the pores of the disk. This process continued until no air bubble was noticed flowing through the outlet. The PPE specimens were prepared in fabricated stainless-steel specimen rings of approximate dimensions 10 mm x 50mm. In all triplicate samples were prepared for each selected CCR. The specimens were extruded from a standard Proctor compacted sample and trimmed to fit specimen rings with the initial masses logged. The compacted specimens were installed in an assembly as presented in Figure A-1 and saturated in a deaired DI water bath for at least 24 hours to achieve saturation of at least 95%. At the end of saturation, the saturation masses of the test specimens were logged. The saturated test specimens were then placed on the saturated HAE disk with a filter paper of medium permeability placed between the HAE disk and test specimen. This prevented the fine particle CCR from clogging the pores of the HAE disk. Using the air pressure assembly in Figure 4-8, the specified air pressure is applied with the PPE tightly sealed to prevent leakage.

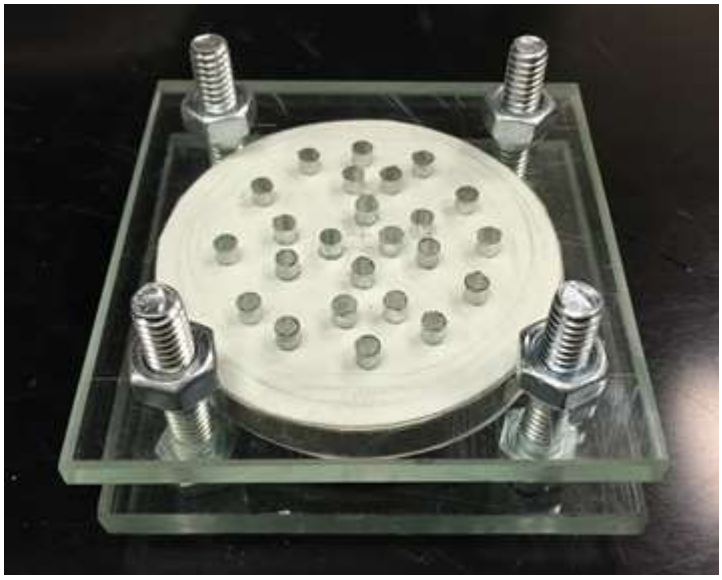

Figure A-1 Assembly used to contain PPE compacted specimen for saturation.

The test began with the 5-bar PPE with 1 bar HAE ceramic disk for air pressure 10 kPa, 20 kPa, 30 kPa, 40 kPa, and 50 kPa. The test specimens were transferred to the 15-bar PPE with previously saturated 5 bar HAE ceramic disk for air pressure 100 kPa, 300 kPa, and 500 kPa. For each air pressure applied starting from the lowest, the masses of the test specimens were logged at specific time interval until no apparent change in the masses of the test specimen wherein equilibration was attained. The next air pressure was applied until equilibration was attained. At the end of the last air pressure application, the test specimens were oven dried. The gravimetric water contents were back calculated for the saturation water content and for each equilibrated mass. The mass of the filter paper placed between the test specimens and the HAE ceramic disk was corrected using an independent filter paper placed in the PPE with the test specimen as described by Elgabu (2013)

**TC**: Similarly, the test method began with the saturation of the HAE disk. The HAE disk was placed in a deaired DI water bath for 24 hours to saturate. The saturated HAE ceramic disk was mounted into the bottom cap then the brace ring with O-rings installed. The bass ring was filled with deaired DI water then the top cap. The saturated HAE disk was subsequently flushed by applying the bubbling pressure of the HAE disk to eliminated trapped air within the pores of the disk. This process continued until no air bubble was noticed flowing through the outlet. Duplicate test specimens were prepared for each selected CCR. The specimens were subcored from a standard Proctor compacted sample and trimmed to fit specimen rings with the initial masses logged. The test specimens were installed with a saturated filter paper with medium permeability to prevent the fine particle CCR from clogging the pores of the HAE ceramic disk. Press firmly and twist gently to ensure good contact with HAE ceramic disk. Install the top cap then log the total mass prior to saturation. Place the complete setup in a water bath of deaired DI water bath for at least 24 hours. Ensure the TC setup is fully submerged but with top cap partly loose to prevent entrapped air from resisting the capillary rise of water during saturation. The degree of saturation was checked using measured parameters including bulk density, dry density, and specific gravity. The process of saturation continued until at least 95% degree of saturation achieved.

Using the air pressure assembly in Figure 4-9, the specified air pressure was applied with the TC tightly sealed to prevent leakage. The test began with air pressures 10 kPa, 20 kPa, 30 kPa, 40 kPa, 50 kPa, and 100 kPa. For each air pressure applied starting from the lowest, the masses of the test specimens were logged at specific time

interval until no apparent change in the masses of the test specimen wherein equilibration was attained. The next air pressure was applied until equilibration was attained. At the end of the last air pressure application, the TC set up was disassembled and test specimens were oven dried. The gravimetric water contents were back calculated for the saturation water content and for each equilibrated mass. The mass of the HAE ceramic disk and the filter paper placed between the test specimens and the HAE ceramic disk was corrected using a TC setup without test specimen.

**UFA:** Duplicate test speciemens were subcored from a standard Proctor compaction into special cylindrical cups with perforated bottom. Filter paper was installed at the bottom of the cylindrical cups to prevent the loss of CCR particles through the perforated bottom during testing. The filter paper was saturated to provide an apparent adhesion to the bottom of the cup thus preventing the filter paper from being displaced during the process. Note, the duplicate test specieman were subcored from one standard Proctor compaction. The test specimens were subsequently saturated by allowing infiltration at relatively lower rotation speed. It was observed that saturation by capillary action caused the infusion pumps to crash in the saturation zone of the test specimens. As indicated in section 4.5.1, hydraulic conductivity measurement was performed first followed by the WRC measurement.

**WP4C:** Triplicate test specimens were subcored from a standard Proctor compacted sample into a stainless steel of dimension 37mm x 8.5mm. The test specimens were saturated in a deaired DI water bath for at least 24 hours. The close bottom of the cup limits the flow of water during saturation due to the presence of entrapped air. The WP4C was calibrated was calibrated every 24 hours using 0.5M KCl solution provided

by Decagon and subsequently prepared in the UNC Charlotte Environmental Engineering research labs. The saturated test specimens were trimmed to almost half cup depth with initial moisture content measured. Due to limitations associated with saturation, few drops of deaired DI water was added to increase the saturation level. The sample cup with trimmed sample was sealed with a plastic cap and pama film and left for 24 hours to equilibrate. Readings were taken for an hour using the continuous mode for suction range 0 MPa – 2 MPa and an average value was determined. For suction ranges 2MPa – 40 MPa single readings are taken in precise and fast mode, respectively. Moisture content was measured for each reading over a period of 10 days.

# APPENDIX B. SUCTION EQUILIBRATION – TC

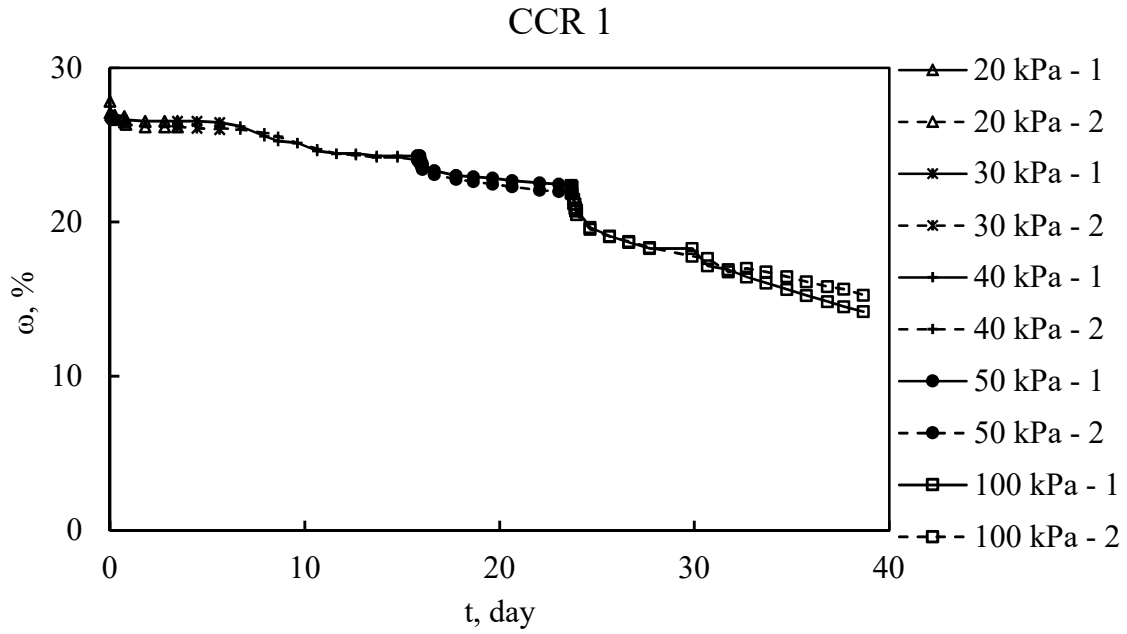


Figure B-1.TC suction equilibration plot for CCR 1.

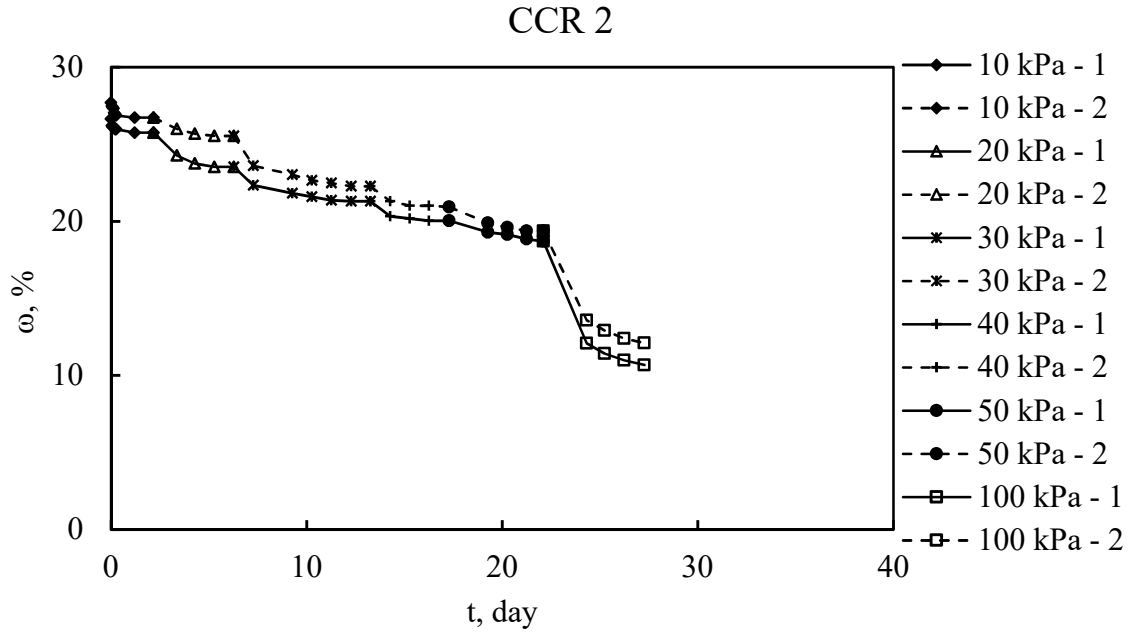


Figure B-2.TC suction equilibration plot for CCR 2.

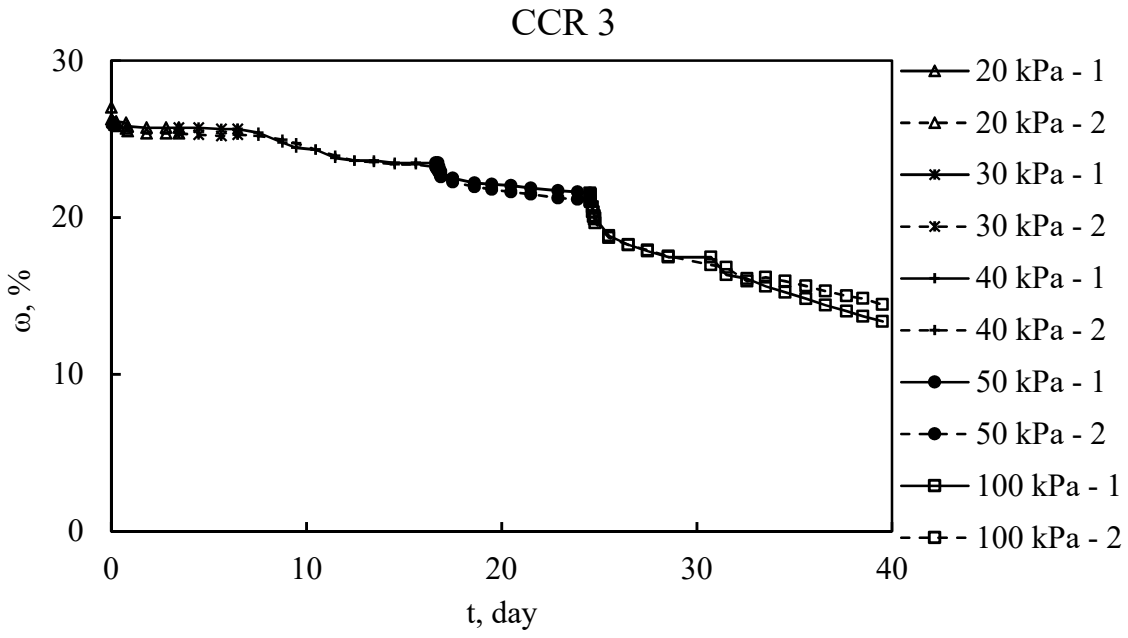


Figure B-3. TC suction equilibration plot for CCR 3.

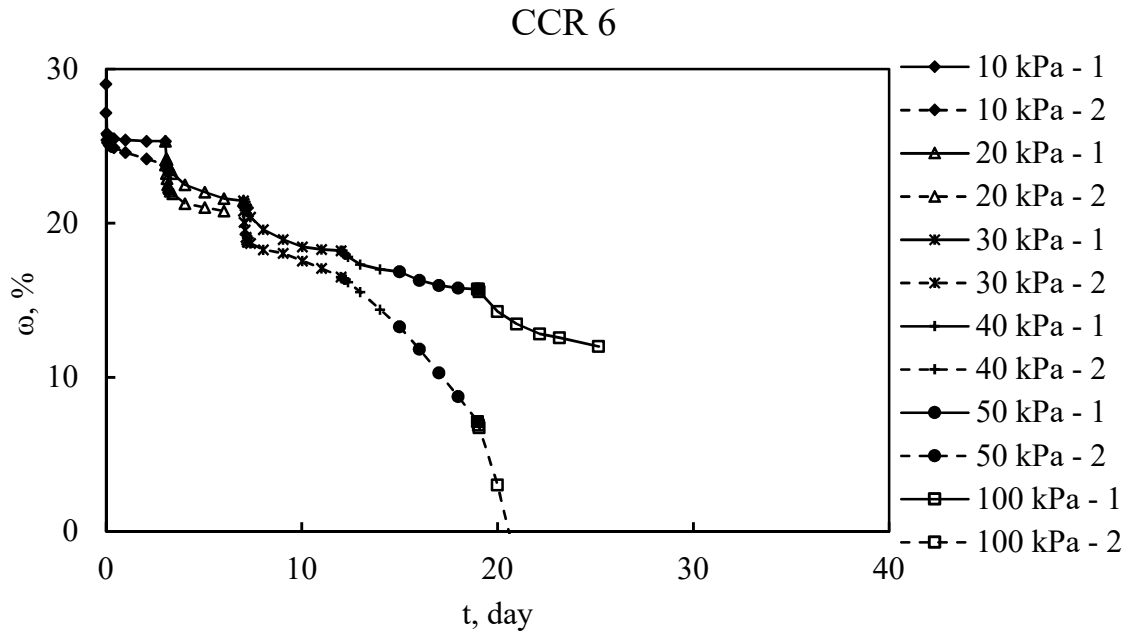


Figure B-4. TC suction equilibration plot for CCR 6.

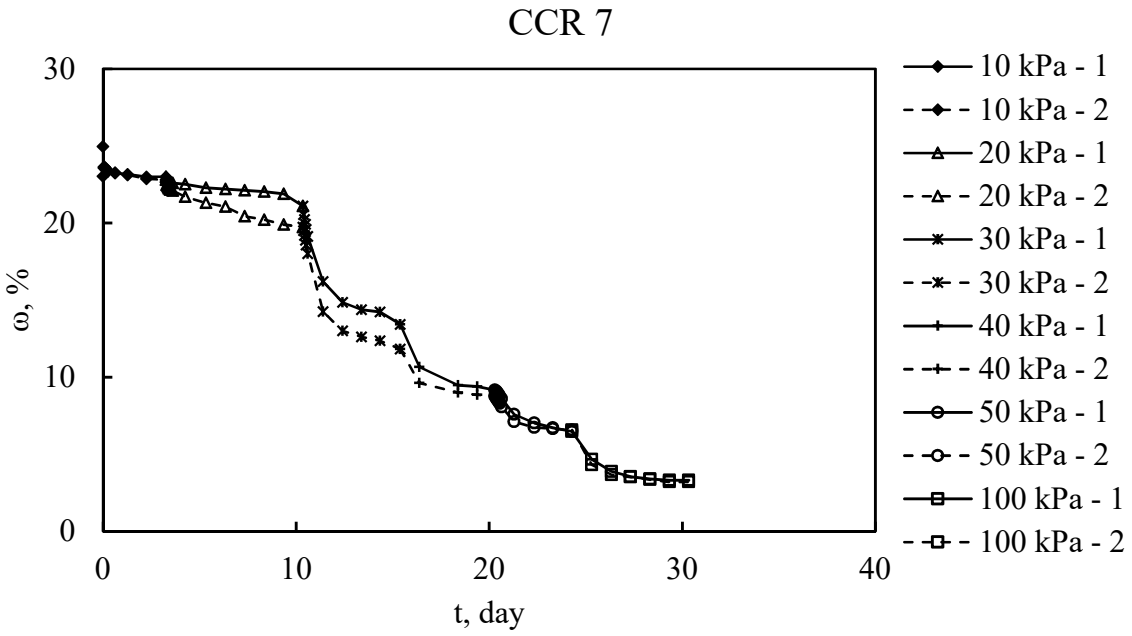


Figure B-5. TC suction equilibration plot for CCR 7.

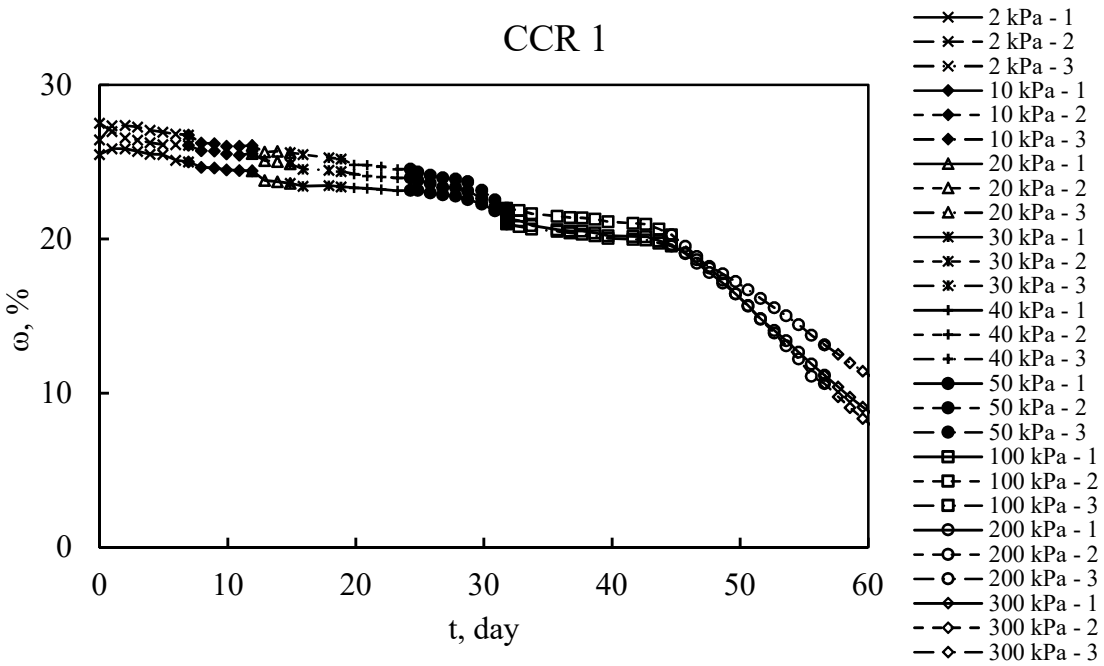


Figure C-1. PPE suction equilibration plot for CCR 1.

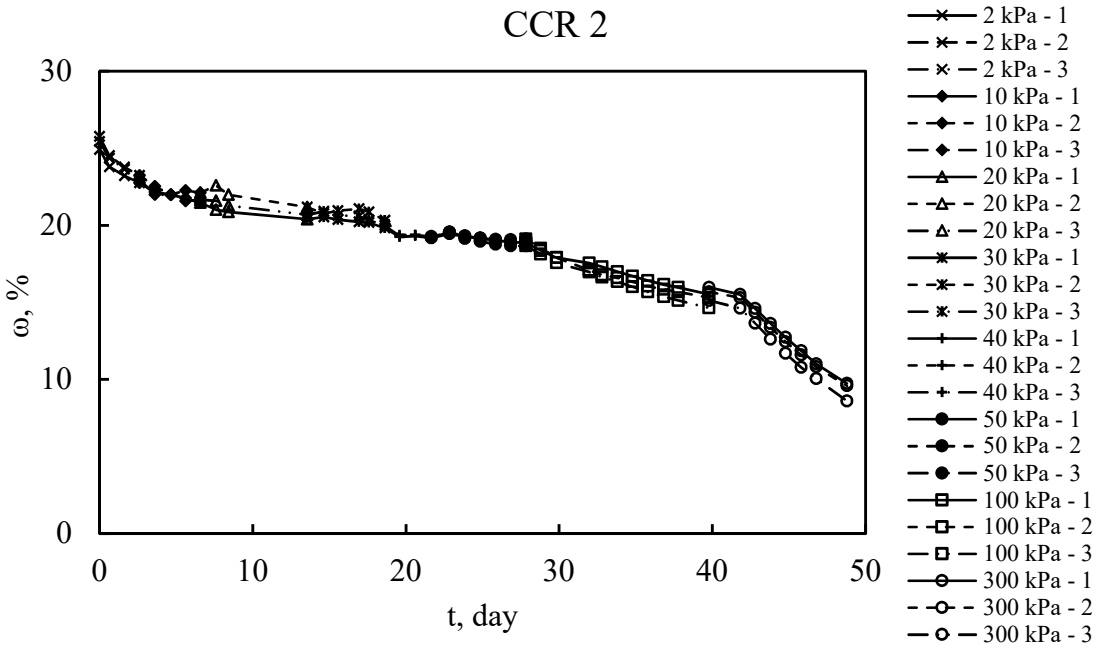


Figure C-2. PPE suction equilibration plot for CCR 2.

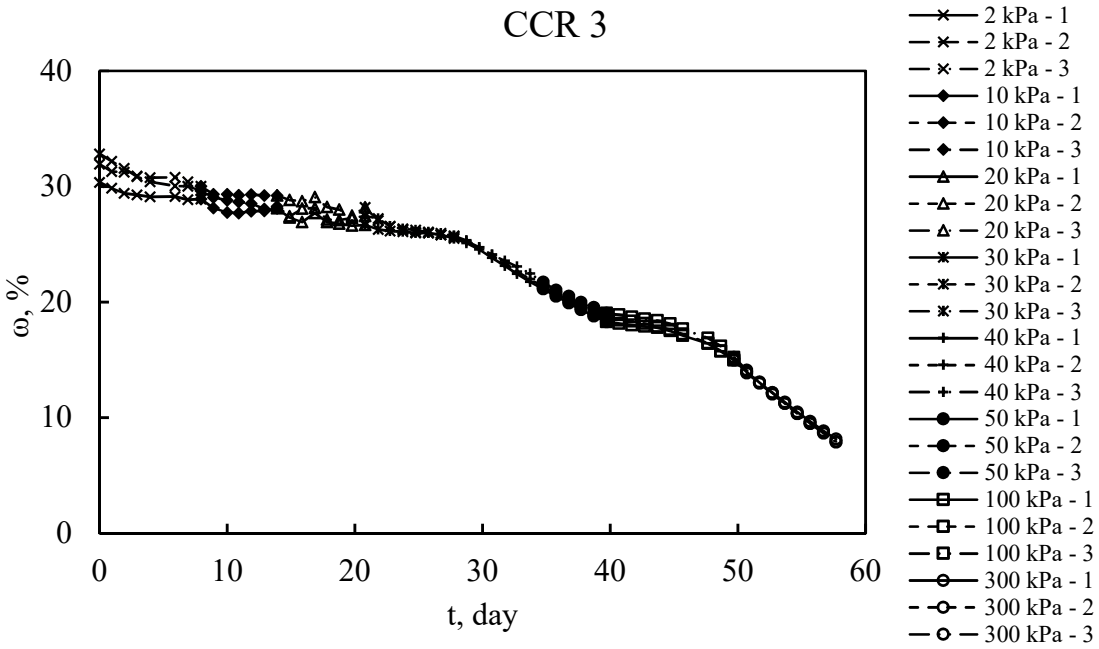


Figure C-3. PPE suction equilibration plot for CCR 3.

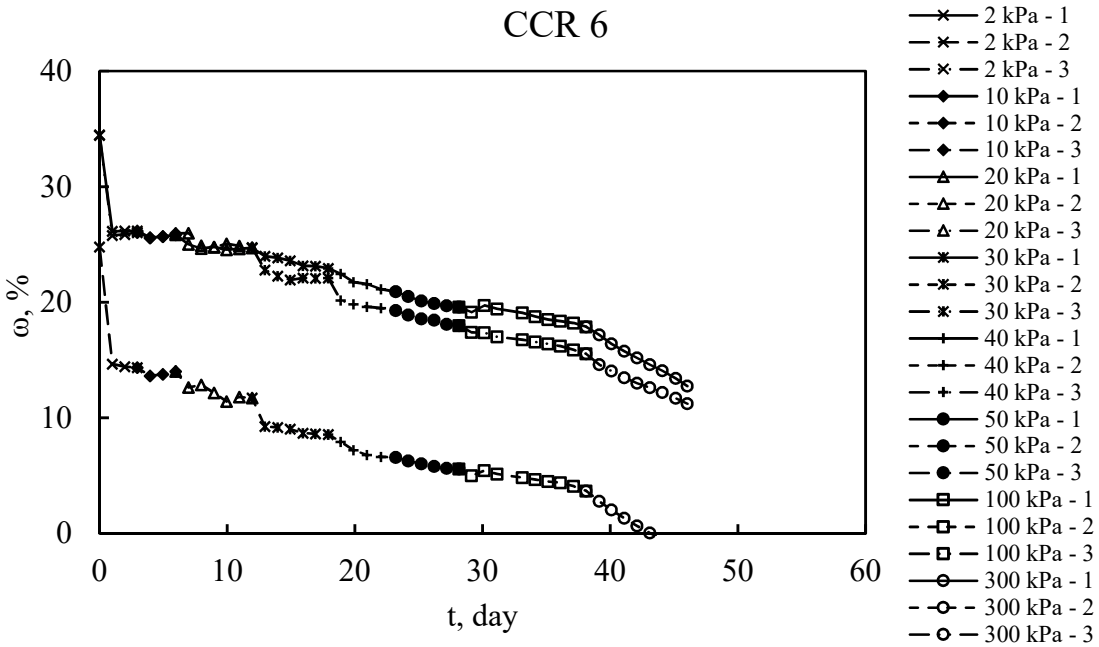


Figure C-4. PPE suction equilibration plot for CCR 6.

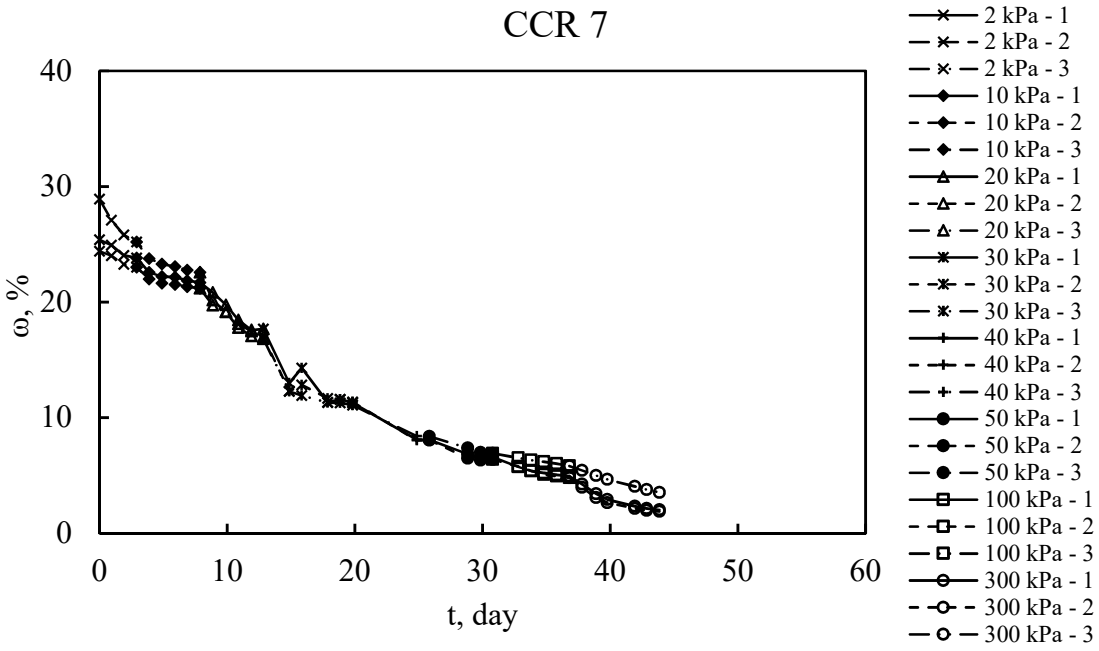


Figure C-5. PPE suction equilibration plot for CCR 7.

Table D-1. Summary of comprehensive parametric model parameters of compacted untreated CCRs.

| CCR | $D_{50}$, mm | Packing Pore Radii, mm | | Model | AEV Pore Radii, mm | | | | | | |
|---|---|---|---|---|---|---|---|---|---|---|---|
| | | | | | PPE | | | TC | | UFA | |
| | | Cubic | Tetrahedral | | 1 | 2 | 3 | 1 | 2 | 1 | 2 |
| 1 | 0.012 | 0.0025 | 0.0009 | vG | 0.0011 | 0.0006 | 0.0013 | 0.0043 | 0.0040 | 0.0013 | n/a |
| | | | | vGM | 0.0012 | 0.0015 | 0.0016 | 0.0022 | 0.0018 | 0.0011 | n/a |
| | | | | vGB | 0.0017 | 0.0021 | 0.0024 | 0.0031 | 0.0028 | 0.0015 | n/a |
| | | | | FX | 0.0011 | 0.0012 | 0.0010 | 0.0022 | 0.0019 | 0.0006 | n/a |
| 2 | 0.026 | 0.0053 | 0.0004 | vG | 0.0014 | 0.0019 | 0.0021 | 0.0044 | 0.0044 | 0.0033 | 0.0014 |
| | | | | vGM | 0.0050 | 0.0072 | 0.0061 | 0.0034 | 0.0027 | 0.0028 | 0.0040 |
| | | | | vGB | 0.0058 | 0.0079 | 0.0086 | 0.0039 | 0.0042 | 0.0035 | 0.0048 |
| | | | | FX | 0.0000 | 0.0000 | 0.0000 | 0.0023 | 0.0023 | 0.0020 | 0.0000 |
| 3 | 0.042 | 0.0086 | 0.0006 | vG | 0.0035 | 0.0031 | 0.0050 | 0.0023 | 0.0016 | 0.0004 | 0.0022 |
| | | | | vGM | 0.0046 | 0.0050 | 0.0039 | 0.0042 | 0.0048 | 0.0047 | 0.0019 |
| | | | | vGB | 0.0062 | 0.0067 | 0.0054 | 0.0056 | 0.0063 | 0.0063 | 0.0028 |
| | | | | FX | 0.0014 | 0.0010 | 0.0023 | 0.0019 | 0.0016 | 0.0008 | 0.0013 |
| 6 | 0.063 | 0.0129 | 0.0010 | vG | 0.0013 | 0.0050 | 0.0013 | 0.0157 | 0.0001 | 0.0033 | 0.0014 |
| | | | | vGM | 0.0014 | 0.0079 | 0.0014 | 0.0149 | 0.0067 | 0.0028 | 0.0040 |
| | | | | vGB | 0.0027 | 0.0095 | 0.0014 | 0.0126 | 0.0079 | 0.0035 | 0.0048 |
| | | | | FX | 0.0006 | 0.0020 | 0.0007 | 0.0055 | 0.0079 | 0.0020 | 0.0000 |
| 7 | 0.039 | 0.0080 | 0.0006 | vG | 0.0052 | 0.0011 | 0.0114 | 0.0069 | 0.0079 | 0.0000 | 0.0000 |
| | | | | vGM | 0.0095 | 0.0119 | 0.0087 | 0.0052 | 0.0057 | 0.0000 | 0.0000 |
| | | | | vGB | 0.0120 | 0.0149 | 0.0112 | 0.0061 | 0.0068 | 0.0335 | 0.0394 |
| | | | | FX | 0.0061 | 0.0029 | 0.0078 | 0.0057 | 0.0062 | 0.0000 | 0.0000 |

# APPENDIX E. THE VARCOMP PROCEDURE

Syntax

```
Data ContactAngle;
   Do Drying='Air','Drying';
      Do Material='1','2','3','6';
         Do Dosage='2','4','6','8';
            Do Time='0.25','6','12','24';
               Input ContactAngle forfor;
               Output;
            End;
         End;
      End;
   End;
Cards;
"DATA";
proc varcomp method=type1;
class Material Dosage Time Drying;
model ContactAngle = Material|Dosage|Time|Drying;
Run;
```

Table E-1. Summary of independent variables and interaction contribution to dependent variable variance.

| Item | Source | Sum of Squares | Percentage, % |
|---|---|---|---|
| 1 | Material | 4495 | 5.14 |
| 2 | Dosage | 66267 | 75.79 |
| 3 | Material*Dosage | 4394 | 5.03 |
| 4 | Reaction Time | 3892 | 4.45 |
| 5 | Material* Reaction Time | 1435 | 1.64 |
| 6 | Dosage*Time | 1785 | 2.04 |
| 7 | Material*Dosage*Reaction Time | 3468 | 3.97 |
| 8 | Drying | 95 | 0.11 |
| 9 | Material*Drying | 56 | 0.06 |
| 10 | Dosage*Drying | 187 | 0.21 |
| 11 | Material*Dosage*Drying | 247 | 0.28 |
| 12 | Time*Drying | 25 | 0.03 |
| 13 | Material*Reaction Time*Drying | 358 | 0.41 |
| 14 | Dosage* Reaction Time*Drying | 197 | 0.23 |
| 15 | Material*Dosage* Reaction Time*Drying | 536 | 0.61 |
| 16 | Error | 0.00 | 0.00 |
| | Corrected Total | 87438 | 100 |

Table F-1. Summary of comprehensive parametric model parameters of Leached CCR 2.

| Suction | Model | Sample | Parameters | | | | | | |
|---|---|---|---|---|---|---|---|---|---|
| | | | $\theta_s$, $m^3/m^3$ | $\theta_r$, $m^3/m^3$ | $\psi_{AEV}$, MPa | $\psi_r$, MPa | n | m | $R^2$ |
| Matric | vG | 1 | 0.4350 | 0.0124 | 0.046 | 16 | 2.3709 | 0.6656 | 0.9905 |
| | | 2 | 0.4171 | 0.0003 | 0.041 | >1000 | 2.3198 | 0.3832 | 0.9974 |
| | | Ave | 0.4260 | 0.0041 | 0.053 | >1000 | 2.0878 | 0.6787 | 0.9767 |
| | vGM | 1 | 0.4350 | 0.0123 | 0.043 | 30 | 2.4850 | 0.5976 | 0.9907 |
| | | 2 | 0.4171 | 0.0014 | 0.050 | >1000 | 2.0672 | 0.5162 | 0.9975 |
| | | Ave | 0.4260 | 0.0039 | 0.046 | >1000 | 2.2511 | 0.5558 | 0.9769 |
| | vGB | 1 | 0.4350 | 0.0118 | 0.043 | 30 | 2.4850 | 0.5976 | 0.9907 |
| | | 2 | 0.4171 | 0.0010 | 0.050 | >1000 | 2.0672 | 0.5162 | 0.9975 |
| | | Ave | 0.4260 | 0.0031 | 0.034 | >1000 | 2.9603 | 0.3244 | 0.9771 |
| | FX | 1 | 0.4350 | 0.0000 | 0.041 | >1000 | 2.5567 | 1.3206 | 0.9913 |
| | | 2 | 0.4171 | 0.0087 | 0.059 | >1000 | 1.4875 | 1.8970 | 0.9931 |
| | | Ave | 0.4260 | 0.0000 | 0.046 | >1000 | 2.2090 | 1.4133 | 0.9773 |
| Total | vG | 1 | 0.4291 | 0.0006 | 0.111 | 22 | 2.4546 | 0.7921 | 0.9913 |
| | | 2 | 0.4117 | 0.0119 | 0.088 | 50 | 3.5391 | 0.3844 | 0.9736 |
| | | Ave | 0.4204 | 0.0000 | 0.087 | 140 | 4.2476 | 0.2899 | 0.9742 |
| | vGM | 1 | 0.4291 | 0.0006 | 0.111 | 22 | 2.4546 | 0.7922 | 0.9982 |
| | | 2 | 0.4117 | 0.0108 | 0.082 | 350 | 3.9248 | 0.3017 | 0.9987 |
| | | Ave | 0.4204 | 0.0000 | 0.088 | 130 | 4.1335 | 0.4226 | 0.9949 |
| | vGB | 1 | 0.4291 | 0.0000 | 0.083 | 42 | 3.4640 | 0.4226 | 0.9828 |
| | | 2 | 0.4117 | 0.0122 | 0.090 | 74 | 3.4034 | 0.4123 | 0.9604 |
| | | Ave | 0.4204 | 0.0000 | 0.097 | 68 | 3.3826 | 0.4087 | 0.9540 |
| | FX | 1 | 0.4291 | 0.0000 | 0.107 | >1000 | 2.5005 | 1.8867 | 0.9830 |
| | | 2 | 0.4117 | 0.0052 | 0.098 | >1000 | 3.3277 | 1.2109 | 0.9663 |
| | | Ave | 0.4204 | 0.0000 | 0.101 | >1000 | 3.6313 | 1.0789 | 0.9566 |

Table G-1. Summary of comprehensive parametric model parameters of OS-CCR 2-4.

| Suction | Model | Sample ID | Parameters | | | | | | |
|---|---|---|---|---|---|---|---|---|---|
| | | | $\theta_s$, $m^3/m^3$ | $\theta_r$, $m^3/m^3$ | $\psi_{AEV}$, Mpa | $\psi_r$, Mpa | n | m | $R^2$ |
| Matric | vG | 1 | 0.4290 | 0.0273 | 237 | 1 | 0.9856 | 3.3995 | 0.9910 |
| | | 2 | 0.4237 | 0.0289 | 22 | 0.8 | 2.8978 | 0.4820 | 0.9822 |
| | | Ave | 0.4264 | 0.0289 | 23 | 0.8 | 2.8978 | 0.4820 | 0.9417 |
| | vGM | 1 | 0.4290 | 0.0200 | 25 | 860 | 1.9013 | 0.4741 | 0.9816 |
| | | 2 | 0.4237 | 0.0306 | 25 | 6.5 | 2.5703 | 0.6109 | 0.9826 |
| | | Ave | 0.4264 | 0.0197 | 22 | 180 | 2.0417 | 0.5102 | 0.9416 |
| | vGB | 1 | 0.4290 | 0.0183 | 18 | >1000 | 2.7713 | 0.5976 | 0.9906 |
| | | 2 | 0.4237 | 0.0276 | 20 | 16 | 3.2887 | 0.5162 | 0.9974 |
| | | Ave | 0.4264 | 0.0166 | 17 | >1000 | 2.8716 | 0.3244 | 0.9794 |
| | FX | 1 | 0.4290 | 0.0000 | 41 | >1000 | 0.9741 | 7.8694 | 0.9910 |
| | | 2 | 0.4237 | 0.0087 | 59 | >1000 | 2.5916 | 1.7016 | 0.9857 |
| | | Ave | 0.4264 | 0.0000 | 46 | >1000 | 1.6882 | 1.9544 | 0.9415 |
| Total | vG | 1 | 0.4565 | 0.0013 | 86 | >1000 | 3.5524 | 0.4903 | 0.9810 |
| | | 2 | 0.4537 | 0.0000 | 91 | >1000 | 2.5180 | 0.6968 | 0.9597 |
| | | Ave | 0.4551 | 0.0001 | 94 | >1000 | 2.7225 | 0.6765 | 0.9667 |
| | vGM | 1 | 0.4565 | 0.0028 | 98 | >1000 | 3.0030 | 0.6670 | 0.9803 |
| | | 2 | 0.4537 | 0.0000 | 86 | >1000 | 2.6509 | 0.6418 | 0.9596 |
| | | Ave | 0.4551 | 0.0000 | 91 | >1000 | 2.7919 | 0.4594 | 0.9667 |
| | vGB | 1 | 0.4565 | 0.0010 | 84 | >1000 | 3.6995 | 0.4594 | 0.9811 |
| | | 2 | 0.4537 | 0.0000 | 71 | >1000 | 3.3730 | 0.4071 | 0.9578 |
| | | Ave | 0.4551 | 0.0000 | 77 | >1000 | 3.5143 | 0.4309 | 0.9661 |
| | FX | 1 | 0.4565 | 0.0010 | 94 | >1000 | 3.2712 | 1.5411 | 0.9836 |
| | | 2 | 0.4537 | 0.0000 | 92 | >1000 | 2.5001 | 1.7962 | 0.9622 |
| | | Ave | 0.4551 | 0.0000 | 95 | >1000 | 2.7207 | 1.7535 | 0.9693 |

Table G-2. Summary of comprehensive parametric model parameters of OS-CCR 2-8.

| Suction | Model | Sample ID | Parameters | | | | | | |
|---|---|---|---|---|---|---|---|---|---|
| | | | $\theta_s$, $m^3/m^3$ | $\theta_r$, $m^3/m^3$ | $\psi_{AEV}$, Mpa | $\psi_r$, Mpa | n | m | $R^2$ |
| Matric | vG | 1 | 0.4289 | 0.0000 | 24 | >1000 | 2.7553 | 0.2024 | 0.9978 |
| | | 2 | 0.4237 | 0.0289 | 19 | >1000 | 4.6353 | 0.1214 | 0.9984 |
| | | Ave | 0.4216 | 0.0289 | 17 | >1000 | 4.6353 | 0.1214 | 0.9959 |
| | vGM | 1 | 0.4289 | 0.0000 | 37 | >1000 | 1.7298 | 0.4219 | 0.9962 |
| | | 2 | 0.4144 | 0.0000 | 35 | >1000 | 1.8718 | 0.4657 | 0.9937 |
| | | Ave | 0.4216 | 0.0000 | 36 | >1000 | 1.7956 | 0.4431 | 0.9895 |
| | vGB | 1 | 0.4289 | 0.0000 | 24 | >1000 | 2.5707 | 0.2220 | 0.9977 |
| | | 2 | 0.4144 | 0.0000 | 24 | >1000 | 2.6554 | 0.2468 | 0.9970 |
| | | Ave | 0.4216 | 0.0000 | 24 | >1000 | 2.5936 | 0.2289 | 0.9936 |
| | FX | 1 | 0.4289 | 0.0000 | 60 | >1000 | 1.4255 | 1.8275 | 0.9942 |
| | | 2 | 0.4144 | 0.0000 | 43 | >1000 | 1.7588 | 1.4904 | 0.9927 |
| | | Ave | 0.4216 | 0.0000 | 44 | >1000 | 1.6572 | 1.4425 | 0.9878 |
| Total | vG | 1 | 0.4338 | 0.0030 | 101 | >1000 | 6.2753 | 0.2443 | 0.9826 |
| | | 2 | 0.4457 | 0.0065 | 101 | >1000 | 6.2753 | 0.2443 | 0.9826 |
| | | Ave | 0.4398 | 0.0032 | 98 | >1000 | 8.0388 | 0.1603 | 0.9704 |
| | vGM | 1 | 0.4338 | 0.0108 | 98 | >1000 | 3.0030 | 0.6670 | 0.9803 |
| | | 2 | 0.4457 | 0.0195 | 86 | >1000 | 2.6509 | 0.6883 | 0.9596 |
| | | Ave | 0.4398 | 0.0130 | 145 | >1000 | 3.2083 | 0.4594 | 0.9656 |
| | vGB | 1 | 0.4338 | 0.0089 | 84 | >1000 | 3.6995 | 0.4594 | 0.9811 |
| | | 2 | 0.4457 | 0.0130 | 71 | >1000 | 3.3730 | 0.4071 | 0.9578 |
| | | Ave | 0.4398 | 0.0107 | 124 | >1000 | 3.7693 | 0.4694 | 0.9675 |
| | FX | 1 | 0.4338 | 0.0057 | 94 | >1000 | 3.2712 | 1.5411 | 0.9836 |
| | | 2 | 0.4457 | 0.0104 | 92 | >1000 | 2.5001 | 1.7962 | 0.9622 |
| | | Ave | 0.4398 | 0.0000 | 122 | >1000 | 4.4776 | 1.0785 | 0.9746 |